

DRILLING CARBON FIBER REINFORCED PLASTIC AND TITANIUM STACKS

By

Gabriel Castro

A thesis submitted in the partial fulfillment of
the requirements for the degree of

Masters of Science in Mechanical Engineering

WASHINGTON STATE UNIVERSITY
School of Engineering and Computer Science
May 2010

To the Faculty of Washington State University

The members of the Committee appointed to examine the thesis of
GABRIEL CASTRO find it satisfactory and recommend that it be accepted.

Dave (Dae-Wook) Kim, Ph.D, Chair

Linda (Xiaolin) Chen, Ph.D

Wei Xue, Ph.D

ACKNOWLEDGEMENTS

I wish to sincerely thank professor Dave (Dae-Wook) Kim for his guidance and encouragement throughout the entire research. Through him, I have gained a invaluable learning experience. I would also like to thank Jeff Lantrip, from The Boeing Company, for providing this enjoyable challenge. I am also honored to have been able to work in collaboration with Patrick Kwon and Kung-Hee Park from Michigan State University and M. Ramulu from University of Washington. Furthermore, I also wish to thank Troy Dunmire, Chad Swanson, and Matt Finlayson, all whom contributed to the learning experience and progression of the experiments. Lastly, I would like to thank Daniel Hennigan and Aaron Beal whose fixture design proved successful and to Jennifer Chang for her assistance; to all I wish success in all of their endeavors.

DRILLING CARBON FIBER REINFORCED PLASTIC AND TITANIUM STACKS

Abstract

By Gabriel Castro
Washington State University Vancouver
May 2010

Chair: Dave (Dae-Wook) Kim

An increasing trend can be seen in the implementation of advance composite/metal stack materials into airframes due to the high performance of their high strength to weight ratio. Advanced materials such as carbon fiber reinforced plastics (CFRP) and titanium (Ti) are popularly used as stack materials by the aerospace industry. However, CFRP and Ti are both difficult-to-cut materials due to their material properties. The vast differences in their material properties also increase the difficulty of drilling the materials together. Tool wear mechanisms and hole quality are two common concerns when drilling. Common tool wear mechanisms seen in drilling CFRP and titanium are abrasion, attrition, diffusion-dissolution, mechanical fatigue, and thermal fatigue. When drilling CFRP, common defects observed include and are not limited to: delamination, fiber pullout, fuzzing, and matrix melting. In titanium, burr formation is commonly found. Also, titanium hole walls can undergo phase transformation when subject to high temperatures. This study will include analysis of the effect of tool wear on hole quality on the drilling of CFRP/Ti stacks and other possible sources of damage.

TABLE OF CONTENTS

	PAGE
ACKNOWLEDGEMENTS.....	iii
ABSTRACT	iv
LIST OF FIGURES.....	viii
LIST OF TABLES	xiv
CHAPTER 1: INTRODUCTION.....	1
CHAPTER 2: LITERATURE SURVEY	4
2.1 THE CUTTING PROCESSES OF CFRP AND TITANIUM IN DRILLING.....	4
2.1.1 CARBON FIBER REINFORCED PLASTIC	4
2.1.2 TITANIUM	7
2.2 TOOL MATERIALS IN DRILLING.....	9
2.2.1 TUNGSTEN CARBIDE	9
2.2.2 COATED CARBIDE TOOLS.....	12
2.2.3 POLY-CRYSTALLINE DIAMOND	13
2.3 HOLE QUALITY.....	14
2.3.1 CARBONFIBER REINFORCED PLASTICS HOLES	14
2.3.2 TITANIUM HOLES	20
2.3.3 COMPOSITE/METAL HYBRID MATERIAL SYSTEMS.....	25
CHAPTER 3: OBJECTIVES.....	30
CHAPTER 4: EXPERIMENT DESIGN AND PROCEDURES.....	31
4.1 WORKPIECE MATERIALS.....	31

4.1.1 CARBON FIBER REINFORCED PLASTIC (CFRP).....	31
4.1.2 TITANIUM ALLOY.....	32
4.2 DRILL TYPES.....	33
4.2.1 TUNGSTEN CARBIDE (WC).....	33
4.2.2 POLY-CRYSTALLINE DIAMOND (PCD)	34
4.3 EXPERIMENT DESIGN.....	35
4.3.1 EXPERIMENT TYPE I	35
4.3.2 EXPERIMENT TYPE II	36
4.3.3 PARAMETERS	36
4.4 DRILLING EXPERIMENT SETUP.....	38
4.4.1 DRILLING EXPERIMENTAL SYSTEM SETUP.....	38
4.4.2 DRILLING FORCE DATA ACQUISITION SYSTEM SET UP.....	40
4.5 HOLE QUALITY MEASUREMENT METHODS	41
4.5.1 COORDINATED MEASURING MACHINE	41
4.5.2 OPTICAL MICROSCOPY	42
4.5.3 SCANNING ELECTRON MICROSCOPY.....	43
4.5.4 SURFACE PROFILOMETER	44
4.5.5 HEIGHT DIAL GAGE	46
CHAPTER 5: RESULTS AND DISCUSSION.....	47
5.1 THRUST & TORQUE ANALYSIS	47
5.2 TOOL WEAR	55
5.2.1 TUNGSTEN CARBIDE (WC).....	56
5.2.2 POLY-CRYSTALLINE DIAMOND (PCD)	66

5.3 HOLE QUALITY.....	71
5.3.1 HOLE SIZE AND ROUNDNESS.....	71
5.3.2 SURFACE ROUGHNESS	84
5.3.3 TITANIUM BURR HEIGHT.....	103
CHAPTER 6: CONCLUSION	107
BIBLIOGRAPHY	109
APPENDIX A: HOLE QUALITY SUMMARY	113
APPENDIX B: THRUST AND TORQUE	118
APPENDIX C: DIAMETER AND ROUNDNESS.....	139
APPENDIX D: SURFACE ROUGHNESS AND SURFACE PROFILES	151

LIST OF FIGURES

	PAGE
2.1.1-1: Cutting types schematics and dominant process characteristics in FRP orthogonal cutting.	5
2.1.1-2: Cutting signal forces at various fiber orientations in GFRP.	6
2.1.2-1: a) Typical cross-section of Ti-6Al-4V segmented chip and b) quick stop cross section of titanium with coated carbide tool adhered to chip underside.	7
2.1.2-2: Adhered workpiece material on to tool cutting edge.	9
2.2.1-2: Attrition at the a) rake face and b) flank face.	11
2.3.1-1: Composite implementation in aircraft over time.	15
2.3.1-2: FRP drilling quality criteria.	16
2.3.1-3: Circular composite plate drilling delamination model with twist drill.	17
2.3.2-1: Surface roughness of titanium holes under dry drilling conditions, using pressurized air (Tool I, pressurized air applied after every hole; Tool II, pressurized air applied every 8 holes).	20
2.3.2-2: Burr categories a) uniform burr, b) transient burr, and c) crown burr.	21
2.3.2-3: Burr height over cutting time (Tool I, pressurized air applied after every hole; Tool II, pressurized air applied every 8 holes).	22
2.3.2-4: polished and etched Ti-6Al-4V cross section under dry drilling (Exp. I) and wet drilling (Exp II, internal cutting fluid supply).	23
2.3.2-5: Nanoindentation hardness profile adjacent to the hole edge.	23

2.3.2-6: Two regions A and B contain different microstructures. Deformation in direction of drill movement found in region B grains in dry drilling.	24
2.3.3-1: Effect of speed and feed on thrust a) constant speed and b) constant feed for standard HSS drills; c) constant speed and d) feed for standard carbide drills (speed, 600rpm; feed, 0.00732mm/rev, drill diameter, 6.35mm).....	26
2.3.3-2: The effect of speed/feed parameters on surface roughness, Ra, Gr/bi a) constant feed and b) speed; Ti c) constant feed and d) speed (speed, 600rpm; feed, 0.00732mm/rev, drill diameter, 6.35mm).	27
2.3.3-3: The effect of speed/feed parameters on burr height, entrance a) constant feed and b) speed; exit c) constant feed and d) speed (speed, 600rpm; feed, 0.00732mm/rev, drill diameter, 6.35mm).	27
2.3.3-4: a) Gr/bi damage region, b) top view (drilled with HSS), c) side view, at 0.08mm/rev and 1750rpm with 6.35mm drill diameter.	28
2.3.3-5: Hole surface roughness in Al/CFRP/Ti stack.....	29
4.1.1: CFRP ply orientation	31
4.1.2-1: Titanium plate after alpha casing removal.	32
4.2-1: Drill types	33
4.2.1-1: WC micro grains a) 5000x and b) 10000x magnification.....	34
4.3.1-1: Experiment Type I cycle sequence.	35
4.3.2-1: Experiment Type II cycle sequence.	36
4.4-1: CNC setup with coolant mister.....	38
4.4-2: a) CFRP/Ti stack setup with positioning plate b) pre-drilled aluminum positioning plate (Solid Works Design) and c) fixture.	39

4.4.3-1: Thrust and torque signal capture setup.	41
4.5.1-1: Coordinated Measuring Machine (CMM) (Brown & Shape Manufacturing Company)	42
4.5.2-1: Optical microscope with camera and digital measurement readout.	43
4.5.3-1: Scanning Electron Microscope (SEM) (Aspex Instruments).	44
4.5.4-1: a) Surface profilometer with touch screen display (Mahr) b) close up of stylus.	45
4.5.4-2: Surface roughness profile example.	46
4.5.5-1: Height gage with dial (Brown & Shape).	46
5.1-1: Drilling force profile in drilling CFRP/Ti stacks (WC drill at low speed experiment type II, hole 1). Arrows indicate peak locations.	47
5.1-2: Drilling force profile in drilling CFRP/Ti stacks (PCD drill at low speed experiment type II, hole 1). Arrows indicate peak locations.	48
5.1-3: Max a) thrust and b) torque of each hole with high speed Experiment Type I.	50
5.1-4: Max a) thrust and b) torque of each hole with low speed Experiment Type I.	51
5.1-5: Max a) thrust and b) torque of each hole with high speed Experiment Type II.	52
5.1-6: Max a) thrust and b) torque of each hole with low speed Experiment Type II.	54
5.2-1: Drill cutting edges and faces.	56

5.2.1-1: Cutting edge corner at 500x magnification for DC Carbide with various cutting distances and parameters.....	57
5.2.1-2: SEM-EDX on high speed Type II WC (DC) after drilling hole 60.....	58
5.2.1-3: Cutting edge corner low speed Type I WC (DC, hole 60) a) 500x and b) 5000x magnification; ~5µm wide grind mark.	59
5.2.1-4: Cutting edge corner at 500x magnification for etched WC (DC) with various cutting distances and parameters with close up of high speed Type II.....	60
5.2.1-5: Cutting edge corner of etched WC (DC) for low speed Type II at hole 40 a) 500x and b) 5000x magnification; high speed Type II at hole 60 c) 100x and d) 1000x magnification.	61
5.2.1-6: Cutting edge corner SEM images for DC5 Carbide with various cutting distances and parameters. 500x magnification.....	63
5.2.1-7: Low speed Type II WC (DC5) at hole 80 a) 100x and b) 2500x magnification; high speed Type II WC (DC5) at hole 80 c) 100x and d) 2500x magnification.	64
5.2.1-8: Titanium built up edge (low speed Experiment Type II hole 80).	65
5.2.2-1: SEM images for PCD with various cutting distances and parameters. 500x magnification.....	67
5.2.2-2: SEM images at hole 80 of PCD Experiment Type I with a) high and b) low speeds at 250x magnification.	68
5.2.2-3: PCD low speed Type II hole 80 at 50x magnification.....	69
5.3.1-1: High speed Type I diameter a) CFRP and b) Titanium.	72
5.3.1-2: Low speed Type I diameter a) CFRP and b) Titanium.....	73

5.3.1-3: High speed Type II diameter a) CFRP and b) Titanium.	75
5.3.1-4: Low speed Type II diameter a) CFRP and b) Titanium.....	76
5.3.1-5: Hole profile across the entire stack at holes 1 and 60 for low speed Experiment Type II.	77
5.3.1-6: High speed Experiment Type I roundness a) CFRP and b) Titanium.	79
5.3.1-7: Low speed Experiment Type I roundness a) CFRP and b) Titanium.....	80
5.3.1-8: High speed Experiment Type II roundness a) CFRP and b) Titanium.	81
5.3.1-9: Low speed Experiment Type II roundness a) CFRP and b) Titanium.....	82
5.3.2-1: WC (DC) high speed Experiment Type I hole surface roughness for a) CFRP and b) titanium.....	85
5.3.2-2: WC (DC) drilled CFRP hole surface profile during high speed Experiment Type I at a) hole 20, b) hole 22, c) hole 41, and d) hole 51.....	86
5.3.2-3: WC (DC) high speed Experiment Type I CFRP hole surface SEM images at a) hole 1 and b-c) hole 29 at 100x magnification. Red locators indicate hole defects.	88
5.3.2-4: WC (DC) high speed Experiment Type II hole surface roughness for a) CFRP and b) titanium.....	89
5.3.2-5: WC (DC) drilled CFRP hole surface profiles from high speed Experiment Type II at a) hole 2, b) hole 5 and c) hole 80.....	90
5.3.2-6: WC (DC) drilled titanium hole surface profiles from high speed Experiment Type II at a) hole 2 and b) hole 5 and c) hole 80.....	91

5.3.2-7: WC (DC) low speed Experiment Type II hole surface roughness for a) CFRP and b) titanium.	93
5.3.2-8: WC (DC) drilled CFRP hole surface profiles for Experiment Type II at hole 60 with a) high speed and b) low speed conditions.	94
5.3.2-9: CFRP hole surface when drilling with WC (DC) at low speed Experiment Type II; a) hole 1 and b) hole 51.	95
5.3.2-10: WC (DC) drilled titanium hole surface profiles for Experiment Type II at hole 60 with a) high speed and b) low speed conditions.	96
5.3.2-11: PCD low speed Experiment Type II hole surface roughness for a) CFRP and b) titanium.	98
5.3.2-12: CFRP hole surface profile under low speed Experiment Type II conditions drilled with a) WC (DC) at hole 51 and b) PCD at hole 21.	99
5.3.2-13: Low speed Experiment Type II CFRP hole surface drilled by PCD; hole entry and exit at a,b) hole 1 and c,d) hole 51. 100x magnification.	100
5.3.2-14: Titanium hole surface profile under low speed Experiment Type II conditions at hole 47 drilled with a) WC (DC) and b) PCD tools.	101
5.3.2-15: CFRP hole surface profile under high speed Experiment Type I conditions at hole 47 drilled with a) WC (DC) and b) PCD tools.	102
5.3.3-1: a) Entry and b) exit burr height from Experiment Type II.	105
5.3.3-2: Burr height progression images of Experiment Type II series 4 holes.	106

LIST OF TABLES

4.2-1: Drill geometry	33
4.4.1-1: Assignment of drilling experiment types and speeds	37
5.2.1-1: Titanium built up edge and wear depth for WC (DC) at hole 80.....	66

CHAPTER 1: INTRODUCTION

Airframe industries are increasing the implementation of composite/metal stacks due to their high strength to weight ratio in order to increase fuel efficiency and cycle life. Among these materials, carbon fiber reinforced plastics (CFRP) and titanium (Ti) are increasing in popularity. For example, the structural weight of the Boeing 787 and the F-22 contains 14% and 39% titanium content, respectively. In terms of composites, the Boeing 787 has a 51% structural weight content while the F-22 has a 36% structural weight content. Structural components made from composites are generally attached to titanium rather than aluminum due to galvanic corrosion that occurs between composite/aluminum stacks [1]. Titanium alloys are also popular with various applications, which include and are not limited to biomedical implant materials and sporting goods (golf club heads, bicycle frames, etc.).

When it comes to machining for CFRP and titanium, both are difficult-to-cut materials. CFRP is highly abrasive (two- and three-body abrasion), requiring tools with high hardness to resist its abrasive nature. Its anisotropic properties submit the tool to various cutting loads (varying ply orientation combined by a matrix material). Temperature during machining must be kept minimal to prevent matrix melting. The tool edge must be kept sharp for higher quality. Titanium has a low thermal conductivity (6.7W/m-K), which leads to high temperature gradients localized on the cutting edge. With high temperatures, titanium is chemically reactive, leading to adhesion and diffusion, and

ultimately tool failure. Titanium undergoes work hardening and has a high hot hardness. Cyclic forces also occur due as drilling titanium produces segmented chips, which can lead to mechanical fatigue failure. In both CFRP and titanium, hole quality is important for fatigue life performance [1].

While drilling each material individually is well known to be difficult, drilling CFRP/Ti stacks is also challenging. When drilling CFRP, poly-crystalline diamond (PCD) has the best performance. However, PCD has low fracture toughness, resulting in pitting and the higher risk of premature brittle fracture when machining titanium. For high-speed titanium machining, tungsten carbide (WC) is the optimal tool material. However, when machining CFRP, WC tools undergo two- and three-body abrasion, resulting with spalling, as the cobalt binder is easily abraded by composite fibers and titanium [2]. When drilling titanium, the removal of tool material grains with the titanium adhesion, otherwise known as attrition, can occur. On top of these, drilling both materials together can lead to increased surface defects. High cutting temperatures can produce discoloration around the CFRP at the CFRP/Ti interface as the temperature passes the limit the matrix can withstand. A damage ring may also occur due to severe rounding of the tool cutting edge [3]. Stiff titanium chips at high feeds can produce surface damage to CFRP hole walls [4]. When drilling CFRP, the titanium adhesion from the previous hole acts as a cutting edge, producing more fiber pullout to occur when drilling CFRP in the next hole due to the lower sharpness of the acting titanium adhesion. Cutting speeds and feeds also affect hole surface roughness in both CFRP and titanium.

This thesis focuses on hole quality for the drilling of carbon fiber reinforced plastics and titanium stacks and lightly covers preliminary results in identifying tool wear mechanisms. There are six chapters in this thesis. Chapter 1, the Introduction, provides a glance at the motivation and problem this research is attempting to solve. The second chapter, the Literature Review, brings forth ample knowledge from past to present research vital to this report as well as to the continuation of this research. The third chapter, Objectives, identifies the motivation and goals for this research. Experiment Designs and Procedures, chapter 4, describes the experiments conducted in this study and introduces the equipment used for the experiment analysis. The fifth chapter presents the results collected throughout the experiments and provides a discussion of the results. The final chapter, chapter 6, is the conclusion ascertained by the results.

CHAPTER 2: LITERATURE SURVEY

2.1 THE CUTTING PROCESSES OF CFRP AND TITANIUM IN DRILLING

The incorporation of carbon fiber reinforced plastics (CFRP) and titanium stacks (CFRP/Ti) in aerospace structural applications have been increasing along side new advances in material technology. The difficulty of stack drilling lies in the dissimilarity of the workpiece materials. CFRP/Ti stacks appeal to the airframe industry because their increased incorporation into airframes lead to an increase in aircraft efficiency and reduction of lifecycle cost. However, the dissimilar properties of both hard-to-cut materials lead to even more difficulty when drilling combined stacks as their drilling parameters differ as well as their wear mechanisms [1, 3].

2.1.1 CARBON FIBER REINFORCED PLASTIC

CFRP is an appealing material to the aerospace industry as well as in sports due to its enhanced properties over conventional metals. These properties are: high specific stiffness, high specific strength, high damping, and low thermal expansion coefficient. CFRP constructed structures have a high natural frequency, increasing their use in rotating structures. Composites in general are lightweight materials.

Chip formation encountered when machining CFRP varies greatly from the continuous chip formation seen in metal. In general, CFRP machining produces discontinuous and dust type chips. D.H. Wang, M. Ramulu, and D. Arola [5] observed in a study on

orthogonal cutting mechanism in Gr/Ep at various fiber orientations and M. Ramulu, D. Kim, and G. Choi further characterize the chip formation process [6]. When drilling 0° unidirectional Gr/Ep, small, distinct fragmented chips would form through delamination until bending fracture occurs under cantilever loading resulting in a broken chip surface. As fiber orientation angle increases, the quantity of distinct chips would decrease as discontinuous dust chips form. In the 45° fiber orientation, fiber cutting occurs through micro fracture. On the machined surface and out of plane displacement ahead of the tool for 90° fiber orientation, cracks can be observed to form. The combination of forward and downward compressive forces encourages “brooming” or fuzzing to occur. In the case of orientations above 90° such as the 135° fiber orientation, macro fracture was observed. Figure 2.1.1-1 from M. Ramulu, D. Kim, and G. Choi shows four identified cutting type schematics.

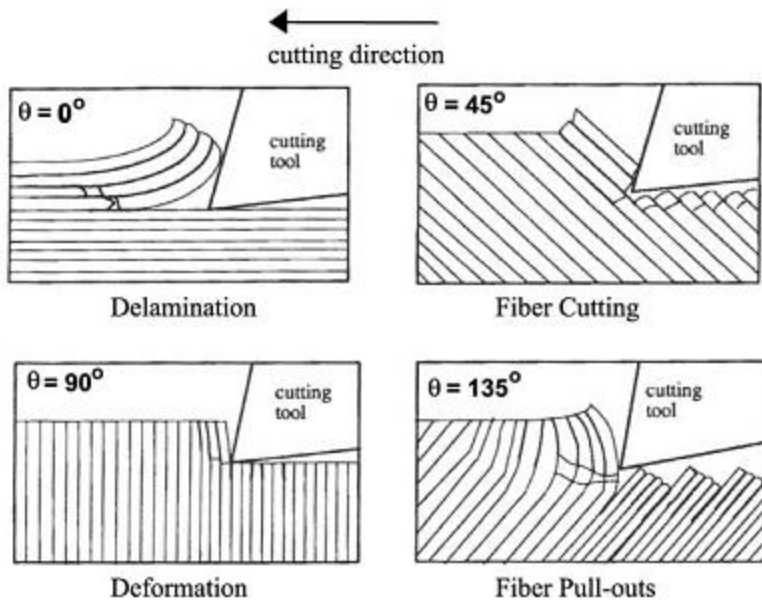


Figure 2.1.1-1: Cutting types schematics and dominant process characteristics in FRP orthogonal cutting [6].

M. Ramulu, D. Kim, and G. Choi also show distinctions in force when cutting the four types of fiber orientation (figure 2.1.1-2) [6]. In the 0° orientation, downward peaks in the force can indicate the occurrence of delamination of fiber from the matrix. In the 90° orientation, force levels decline over time as continued cutting results in finer grains; the finer grains are found to ease friction. For 135° orientations, a noticeable peak occurs in the force signal, which would indicate another cutting mechanism than found in 0° and 90° orientations. This is in agreement with the macro fracture observed by D.H. Wang, M. Ramulu, and D. Arola [5, 6].

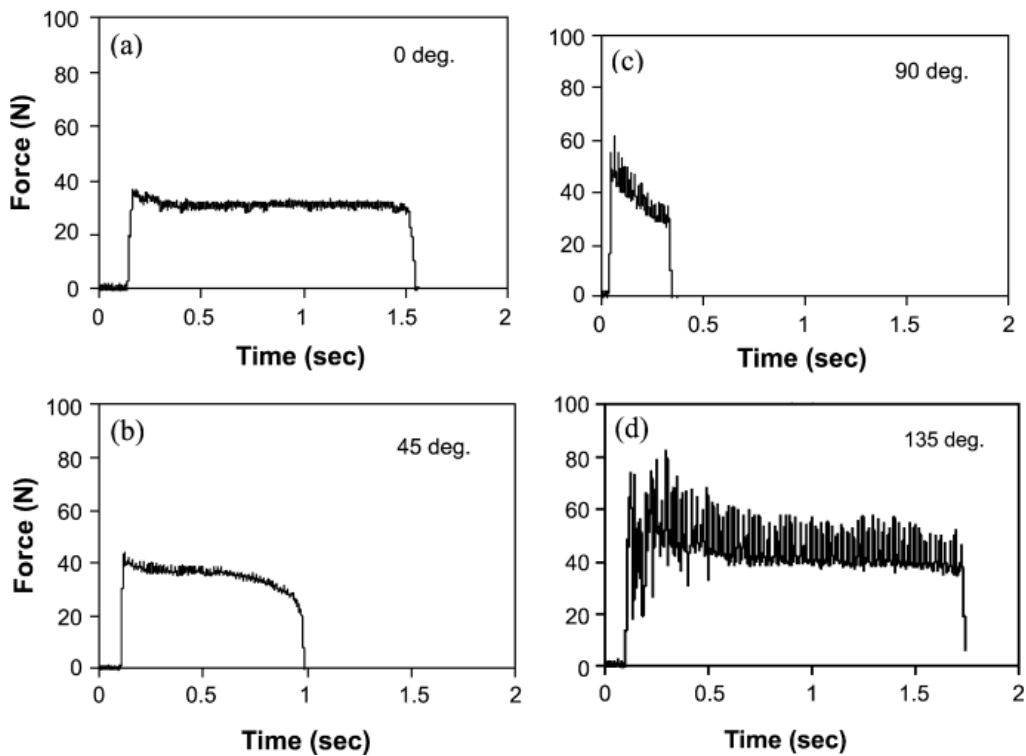
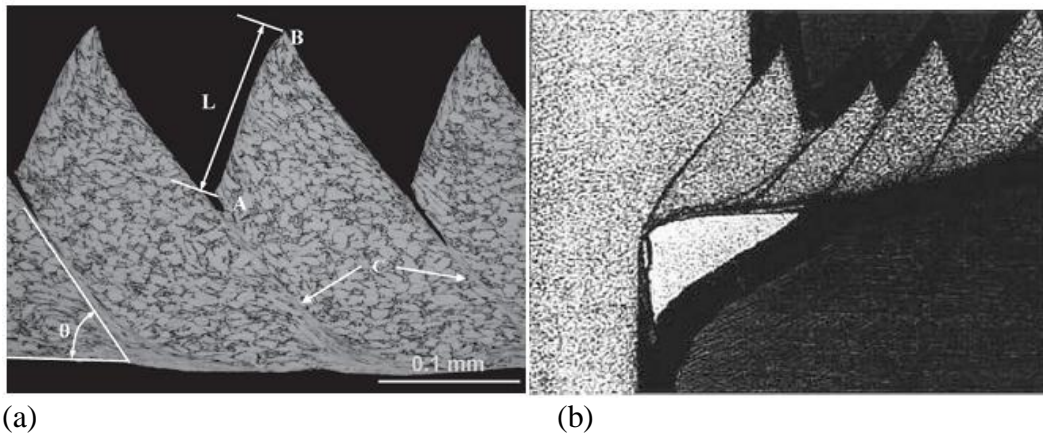


Figure 2.1.1-2: Cutting signal forces at various fiber orientations in GFRP [6].

2.1.2 TITANIUM

Titanium is the ninth most abundant element on earth, and the fourth most abundant structural metal. It is considered to be light metal, having half the specific weight of iron and nickel. Titanium exhibits high strength, corrosion resistance, and fatigue resistance along with low density and modulus, thus appealing to the aerospace industry for aeroengine and airframe applications.



(a) (b)
Figure 2.1.2-1: a) Typical cross-section of Ti-6Al-4V segmented chip [7] and b) quick stop cross section of titanium with coated carbide tool adhered to chip underside [8].

When cutting metal, the chip is formed by shear along the shear plane. Figure 2.1.2-1 shows the typical segmented chip cross-section seen in turning titanium alloys [7, 8]. Segmented chips are normally produced during titanium alloy machining. Segmentation is also found during when drilling titanium alloys, regardless of tool geometry. The causation of the segmentation is debatable between two ideas; the formation of segmented chips is due either to crack growth from the chip outer surface or adiabatic shear band formation from localized shear deformation. Shear deformation would result from the prevalence of thermal softening over strain hardening. However, studies have indicated temperatures to reach 100 to 200°C in the primary deformation zone, which is not enough for thermal softening to prevail over strain hardening. Observations through

quick-stop tests reveal the primary shear to occur as discrete bursts of “catastrophic shear” rather than being continuous. The occurrence of alpha to beta phase transformation within shear bands is also debatable. Chip segmentation is also seen to cause cyclic loading in thrust and cutting speed. Most literatures on chip formation are studies based on turning, which cutting conditions are constant along the tool cutting edge. Unlike turning, drilling provides a more complex cutting process as cutting speed and rake angle vary along cutting edge. The resulting chip morphology at various stages in drilling becomes more complex [7, 9, 10].

The difficulty with titanium alloys is the poor machinability of the material. Titanium has a high hot hardness and strength, which often leads to deformation of the cutting tool. During machining, the alloy exhibits a high dynamic shear stress, resulting in localization of shear stress. This produces abrasive saw-tooth edges, which promotes notching. Cutting tools experience localized temperature due to the low thermal diffusivity of titanium alloys leading to a high thermal gradient at the tool tip. Unstable built-up edge (BUE) is formed due to welding of the workpiece material, reducing hole quality. Titanium alloys are also classified as reactive metals; at elevated temperatures (500°C and above), the alloys will react with most tool materials [11].

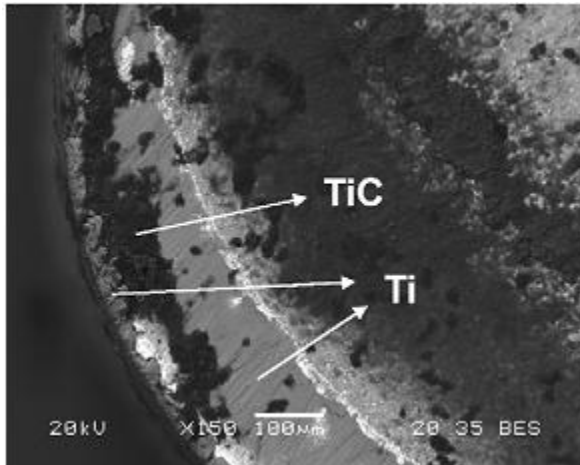


Figure 2.1.2-2: Adhered workpiece material on to tool cutting edge [12].

Workpiece material can be found to adhere to the tool cutting edge when machining titanium alloys, BUE, as depicted by Figure 2.1.2-2. BUE initially acts to protect the cutting edge from diffusion and rapid wear; however, prolonged drilling will result in the BUE to become unstable and break off. At high temperatures, the chemical reactivity of titanium results in strong bonding forces. As a result, attrition occurs, which is defined as the removal of tool particles along with the BUE [12], [13]

2.2 TOOL MATERIALS IN DRILLING

2.2.1 TUNGSTEN CARBIDE

Tungsten carbide (WC) tools consist of WC grains with a cobalt (Co) binder. Finer grain sizes and reduced amounts of Co binder in carbide tools will increase hardness, which in some cases can improve resistance to wear [14]; however, finer grain size carbides exhibit greater solubility when machining reactive alloys than coarser grain carbides due to the increased surface area resulting in WC removal from the rake face by the chip. WC tools with coarser grain sizes exhibit higher rate of grain loss; however contain higher fracture toughness [11].

When drilling carbon fiber composites with WC-Co drills, the dominant mechanism mentioned by S. Rawat and H. Attia is abrasion. Two forms of abrasion occur: soft abrasion and hard abrasion. Soft abrasion is the process in which the Co binder is removed through three-body abrasion. Removing small amounts of the Co binder by the abrasive composite particles leads to microscopic spalling through crack nucleation and propagation. Hard abrasion is the result of crack initiation and propagation within the WC grains due to the dynamic shear stresses generated by impacts with the broken fibers and powder-like chips. The removed grains then contribute to the three-body abrasion process. Another wear mechanism mentioned by S. Rawat and H. Attia is the process in which WC material is removed through shearing along the slip planes as the slip plane produces a hardness of 11 GPa (22 GPa hardness is observed perpendicular to the slip planes) [2, 15].

When drilling titanium alloys with WC tools at higher speeds, the high temperature gradient results in higher stresses in the tool nose. This leads to plastic deformation and subsequent tool failure. At temperatures above 500°C, the carbon from WC tools will diffuse into titanium, reacting to form a titanium carbide layer (TiC). The diffusion of carbon results in the embrittlement of carbide tools. However, this layer will also act as a protective layer, increasing crater wear resistance located on the rake face by reducing further diffusion. At higher temperatures at 740°C and above, adhesion may begin to occur [11, 16, 17]. The strong bond between the tool and chip from the TiC layer may lead the adherent material to break away from the tool. Loose WC grains may be

removed along with the adherent material. This tool wear mechanism is known as attrition wear [11, 13, 18, 19]. Figure 2.1.2-3 demonstrates attrition by identifying grains likely to be removed with the BUE.

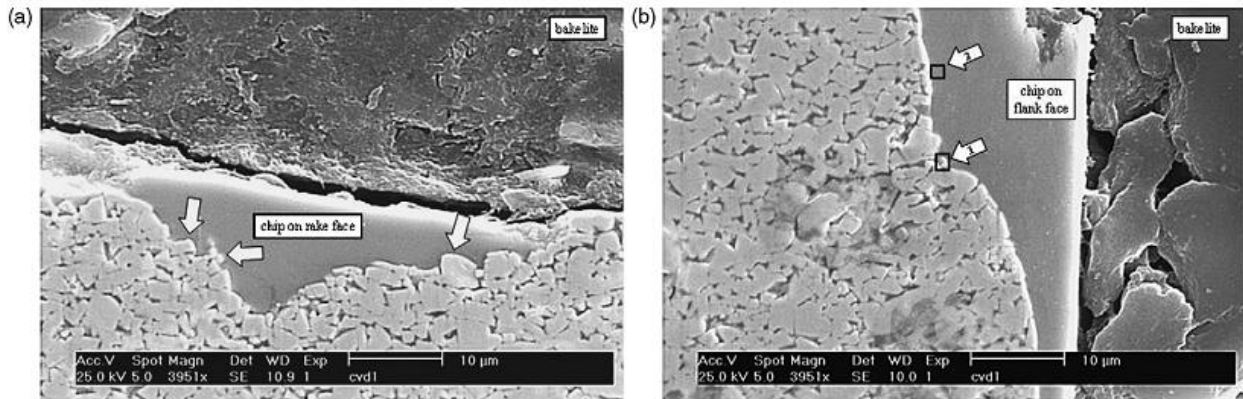


Figure 2.2.1-2: Attrition at the a) rake face and b) flank face [19].

At lower cutting speeds, chemical reactions become negligible. Tool wear from cutting titanium alloys then mainly occur due to mechanical and thermal fatigue along with micro-fractures through the tool wear mechanism known as abrasion. Two forms of abrasion may occur, soft abrasion and hard abrasion, as described by S. Rawat & H. Attia in carbon fiber composite drilling. However, whereas hard abrasion in carbon fiber composite drilling is described as a fracturing process of the WC grains as aforementioned, H. Saito et al. describes hard abrasion in WC during titanium drilling as material removal through plastic deformation [14]. In a study on dry drilling Ti-6Al-4V with WC, diffusion was observed to occur along the helical flute, cutting edge corner, and rake face. Carbon atoms from WC diffuse at a higher rate than metal atoms, forming a TiC layer. The reduced carbon content may lead to tool embrittlement along the affected tool subsurface region [18].

2.2.2 COATED CARBIDE TOOLS

Coated carbide tools are known to act as a thermal barrier and often reduce friction during machining at the tool-chip and tool-workpiece interfaces, lowering cutting temperature and forces. Coatings can also exhibit higher hardness, leading to better resistance to abrasion. The coating is seen to delay rapid tool wear [11, 20]. In composite machining, coated carbide tools display a similar wear pattern to uncoated carbide tools [21]. Drilling Ti-6Al-4V with TiAlN coated carbide showed better results than uncoated carbide as reported by Sharif and Rahim, whereas in milling and turning, uncoated carbides are reported to outperform coated carbides. It is suggested that a micro-thin oxide layer Al_2O_3 is formed through oxidation of the coating by the environment. This layer then acts to insulate the tool and to reduce friction as a solid lubricant. However, at a higher cutting speed of 55m/min, tool life of the coated tool became equivalent to uncoated carbide. The main wear mechanisms observed were attrition and diffusion [13, 22]. When machining titanium alloys, coated carbides are also seen to exhibit flaking (spalling), chipping, and plastic deformation. Delamination of the coating layer is said to be the main wear mode of coated carbide tools. It is debated whether the delamination process is due to chemical reaction or crack propagation at the surface interface. In either case, thermal activation is significant in initiating delamination [19].

2.2.3 POLY-CRYSTALLINE DIAMOND

Poly-crystalline diamond (PCD) exhibits great performance and is the preferred tool material in machining FRP. This tool material is shown to possess superior wear resistance and produce lower surface roughness values in machining CFRP and Ti materials separately.

When drilling CFRP with PCD, spalling, cracking and notching can be observed over time. The spalling process is due to thermal and mechanical oscillations and occurs on the rake face. Cracking occurs from low cycle fatigue and thermal fatigue as well as tool degradation at high temperatures. Notching is primarily caused by oxidation [23].

In a study by F. Nabhani, machining titanium alloy Ti-6Al-4V with PCD resulted with lower wear rates than coated WC and CBN tools. Diffusion leads to the development of a TiC interlayer, acting as a protective layer to further diffusion. Farhad Nabhani mentions in a study on titanium by A.D. McQuillan and M.K. McQuillan in 1956, that graphite crucibles were observed to withstand attack by liquid titanium through the formation of a stable TiC layer. The critical temperature for adhesion to occur in titanium drilling with PCD is at 760°C [8]. Micro failure due to attrition can also be observed in machining Ti-6Al-4V with PCD [24]. It is possible for graphitization to occur when drilling titanium with PCD. W. König and A. Neises report that during diffusion testing and machining at 110 m/min cutting speed of Ti-6Al-4V with PCD, diamond-to-graphite conversion could be observed and is dependent on the diamond grain size. With diamond grain size below 1 µm, this conversion was observed to occur

above 700°C; however, with a grain size of 8 to 10 μm , this conversion was not observed even at 800°C. Cracking due to thermal induced stress also occurs. The reduction in abrasion resistance due to graphitization is said to be much greater than that caused by thermal cracking [25].

Recent experimental study conducted by Richard Garrick shows that mechanical failure was observed through a chipping process when drilling titanium in CFRP/Ti stacks due to work hardening of the titanium and the low fracture toughness of the tool material [26].

2.3 HOLE QUALITY

Hole quality can be degraded by several factors including imperfections in drill angle, cutting tool vibration, workpiece vibration, and chip removal [27]. In both CFRP and Ti drilling, temperature can also contribute to poor hole quality.

2.3.1 CARBON FIBER REINFORCED PLASTIC HOLES

When drilling CFRP holes, to achieve high quality over a small number of holes, low feeds are to be used. However, for larger scale production with fair quality, higher feeds can be used. Drilling of CFRP is very widely used for joints in aerospace structures. The use of composites reduces the number of fasteners; however, the majority eliminated are small diameter fasteners, which can be made through automated processes. Holes remaining to be drilled have large diameters and are located on multi-stack materials such as CFRP/Ti. More composites are being implemented in the airframe industry. Figure 2.3.1-1 displays the trend in composite content overtime in aircraft designs [1].

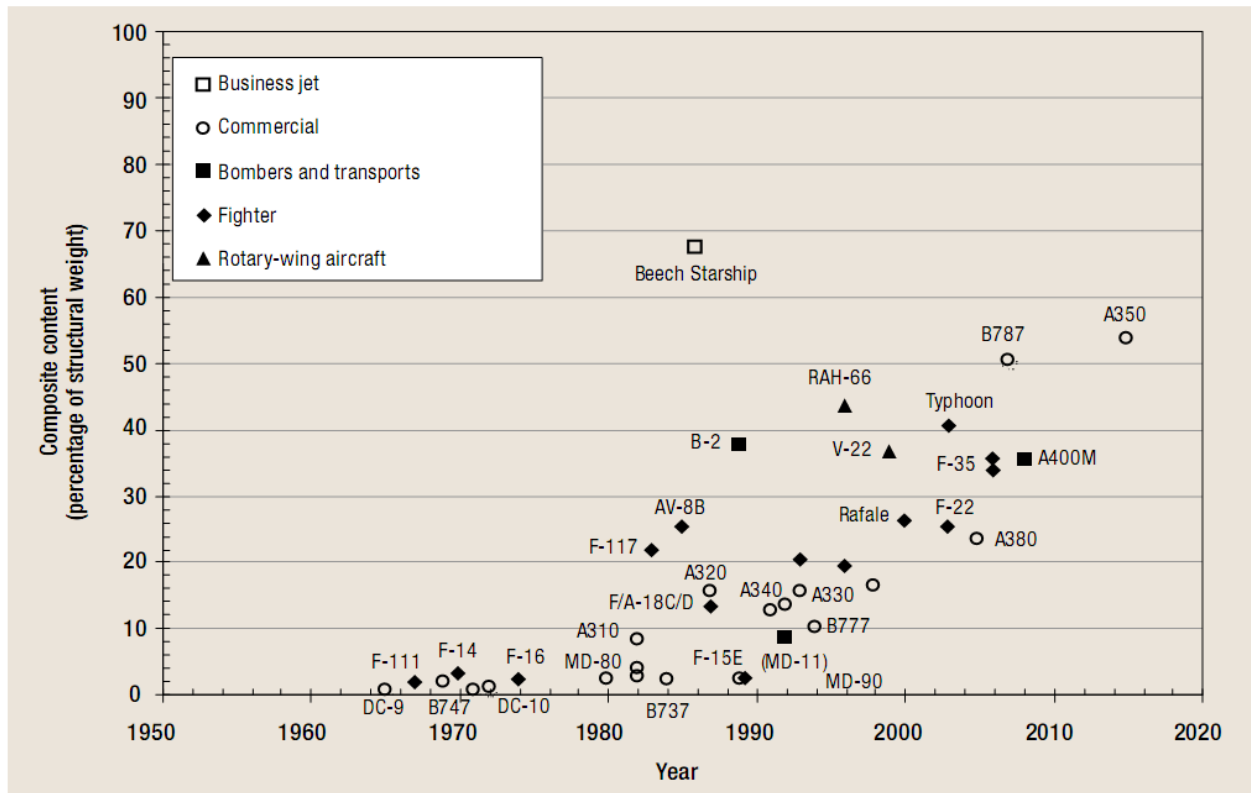


Figure 2.3.1-1: Composite implementation in aircraft over time [1].

Hole quality plays an important roll to ensure high quality performance of the composite materials used in airframes. Figure 2.3.1-2 defines various quality criteria used when drilling FRP materials. Quality assessments of geometrical deviations described by the figure are roundness and dimensional, where roundness error is defined as the deviation from an ideal circle and dimensional error is defined as deviation from the target diameter. Cylindricity through the wall thickness is also an important geometrical quality. Quality assessment of the hole surface is defined through standard roughness parameters. Quality assessment on material damage must also be taken account for. Edge chipping and spalling are very common defects, as well as fuzzing and delamination. Delamination refers to the separation of the surface layers at the entry and exit sides of the plate and is distinguished from the interlaminar cracks on the inner

layers. Fuzzing is defined as uncut fibers, which can be corrected by further machining [28].

Producing precise quality holes in CFRP are necessary in manufacturing reliable structures as defects formed in CFRP during the machining process will reduce fatigue strength of the workpiece material. Production of high quality holes in drilling as the prevention of delamination and fuzzing is very difficult due to the large variance between the carbon fiber and matrix materials [29].

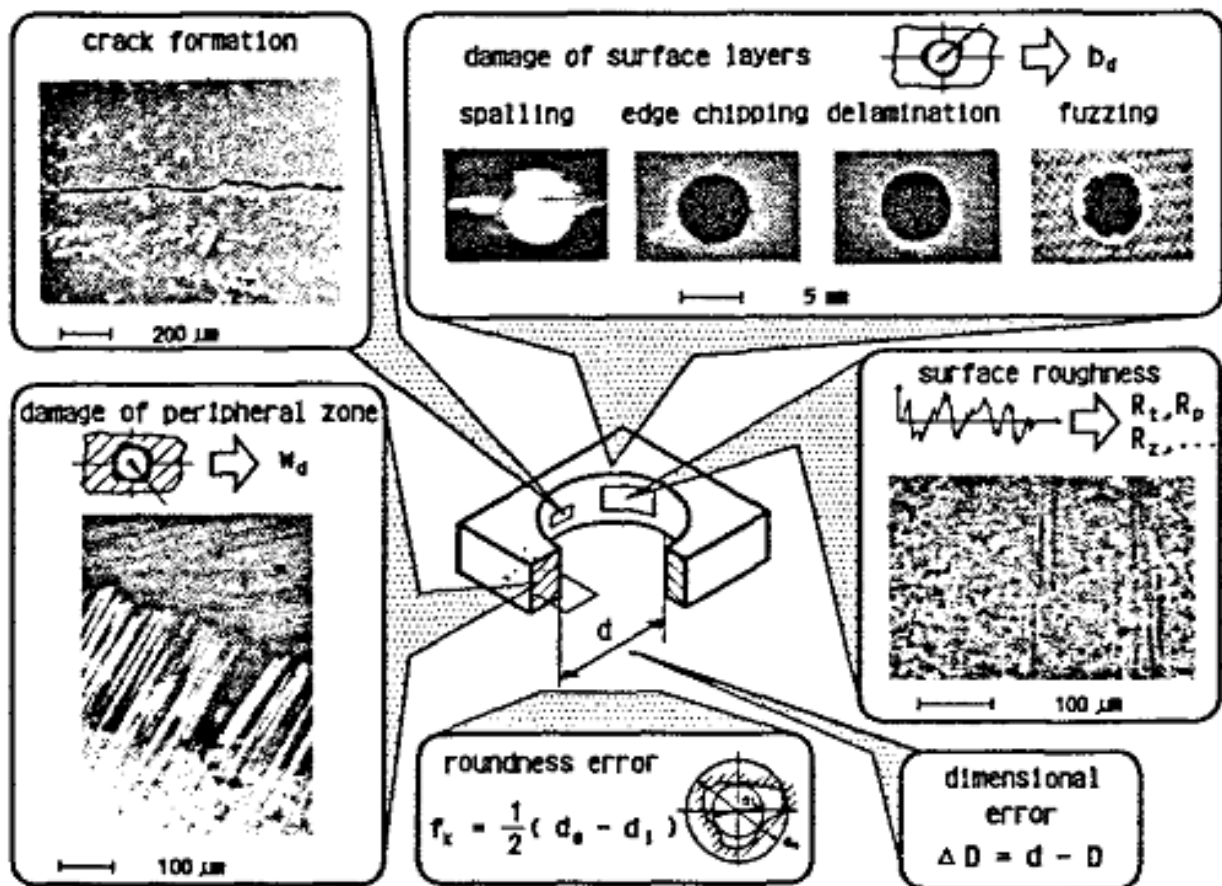


Figure 2.3.1-2: FRP drilling quality criteria [28].

The most common defect in drilling carbon fiber reinforced plastics is exit delamination. Delamination is the most problematic hole defect, approximately 60% of the components

produced in the aircraft industry is rejected owing to delamination. Entry side delamination may also occur; however, it is not as common. The occurrence of delamination is due to the heterogeneous nature of the fiber and matrix combination and is related to thrust force. More specifically, entry delamination is affected distinctly by feed, whereas exit delamination is affected significantly by cutting speed. Entry delamination is also dependent on the fibrous characteristic of the workpiece material and drill geometry. Delamination is regarded as the most critical in comparison to other hole defects in CFRP drilling as it can severely impair component performance [30], [31], [32].

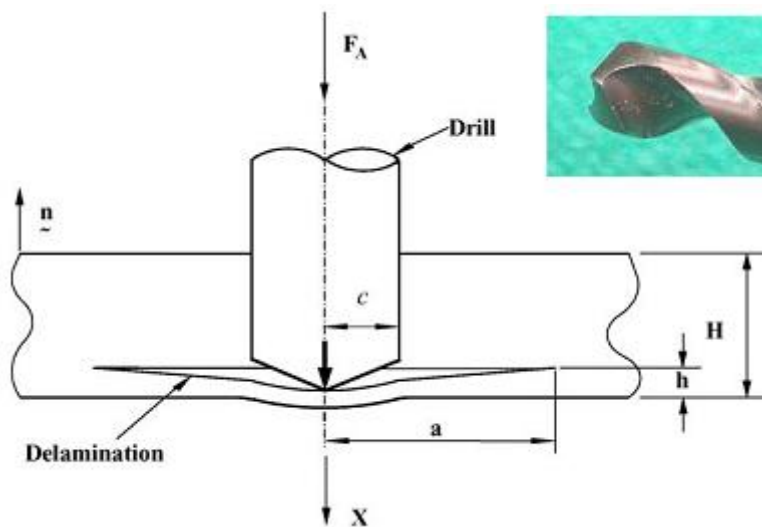


Figure 2.3.1-3: Circular composite plate drilling delamination model with twist drill [33].

Figure 2.3.1-3 displays the model of delamination formation in drilling composite materials as depicted by H. Hocheng and C.C. Tsao (2005) [33]. H. Hocheng and C.C. Tsao (2005) provide an energy balance equation to model delamination,

$$G_{IC}dA = F_A dX - dU \quad (1)$$

where dX is the drill movement at the propagation of delamination associated with the thrust force, F_A . G_{IC} is the mode I critical crack propagation energy per unit area. For

pure laminate bending and isotropic behavior, dA , the change in delamination crack area is defined by the equation:

$$dA = \pi \left(a + da \right) \left(a + da \right) - \pi a^2 \quad (2)$$

The infinitesimal strain energy is notated by dU . For circular plates clamped at the end, the stored strain energy, U , is defined as:

$$U = \frac{8\pi M X^2}{a^2} \quad (3)$$

where M is the stiffness per unit width

$$M = \frac{Eh^3}{12(1-\nu^2)} \quad (4)$$

E is the modulus of elasticity, ν is Poison's ration, and X is the displacement related to the thrust.

$$X = \frac{F_A a^2}{16\pi M} \quad (5)$$

The thrust force at crack propagation is:

$$F_A = \pi \sqrt{32G_{IC}M} = \pi \left[\frac{8G_{IC}Eh^3}{3(1-\nu^2)} \right]^{1/2} \quad (6)$$

M. Ramulu, T. Branson, and D. Kim reported that severe fiber pull out was observed at the fiber ply 135° from the cutting direction due to intermittent fracture across the fiber direction [3]. Matrix damage can also increases the chances of fiber pullout; thus, increasing surface roughness defects (Rv). Surface roughness in composite drilling is significantly affected by feed rate and increased thrust force [30, 32]. L.M.P Durão et al. show for twist drills, increase in feed rate lead to an increase in surface roughness when

drilling CFRP [34]. D. Kim and M. Ramulu also display the relationship of fiber pull out depth with feed and speed [35].

Composite materials exhibit a wide difference in thermal properties of fiber and matrix and poor thermal conductivity. Its heat insulating and abrasive nature exposes cutting tools to a hazardous environment and thermal wear processes. Unlike metals, FRP materials are anisotropic and inhomogeneous. Machining CFRP is related with plowing, cutting, and cracking, whereas metal machining displays plastic deformation and shearing [23].

Thermal damage in the matrix can be observed to appear on the hole wall when temperatures reach 300-400°C. A major contributing factor to thermal damage is the low thermal conductivity of FRP composites. At lower temperature, damage can be associated with the onset of plastic deformation. Fiber/matrix cracking, porosity formation, and layer separation can also be observed [36]. Thermal damage can even occur in fibers. G. Caprino and V. Tagliaferri map out damage in drilling GFRP in [37].

Roundness defects can correlate to the angle between the fiber orientation of the ply and the direction of the cutting edge. Over time, hole diameter can be seen to decrease and roundness can be seen to increase as tool wear increases under various cutting parameters [32, 38].

2.3.2 TITANIUM HOLES

As in composite drilling, geometrical defect titanium drilled holes include roundness and dimensional error as well as cylindricity, verticality, and surface roughness. Other common defects found in titanium drilling include entry burrs, exit burrs, and metallurgical changes.

In a study on dry drilling titanium alloy Ti-6Al-4V by J.L. Cantero, M.M. Tardío, J.A. canteli, M. Marcos, and M.H. Miguélez [18], hole roughness (Ra) was found to be constant with cutting time at the beginning during what was described as an initial wear, followed by a slight increase during what was described as medium wear, then a sharp increase in roundness occurs in the tool as the tool enters a final wear period, nearing the end of the tool life (Figure 2.3.2-1).

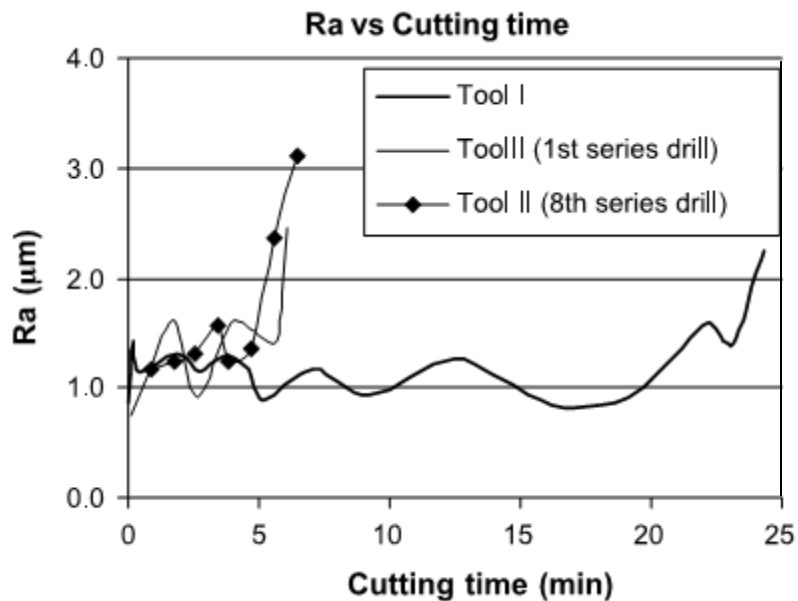


Figure 2.3.2-1: Surface roughness of titanium holes under dry drilling conditions, using pressurized air (Tool I, pressurized air applied after every hole; Tool II, pressurized air applied every 8 holes) [18].

When drilling metal alloys, burr formation occurs on both entry and exit surfaces. Burr height on the exit side is much larger than that found on the entry side. Entry burrs form through plastic flow. Burrs can be classified into three different shapes: uniform, transient, and crown (Figure 2.3.2-2). Different burr types are dependent on drill geometry, drill diameter, length/diameter ration, feed, speed, and material hardness. Exit burr formation occurs through the plastic deformation as the of the workpiece material as the drill transitions from cutting to bending, then fracture of the workpiece material. In uniformed burr, this results in the formation of what is called a drill cap [39].

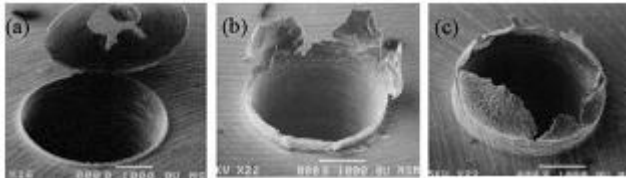


Figure 2.3.2-2: Burr categories a) uniform burr, b) transient burr, and c) crown burr [39].

When drilling titanium, temperature may also be taken accounted for in burr formation. As temperature increases along the bottom surface, the workpiece material experiences increase ductility. Thrust force also seen to be directly proportional to burr height. Thrust and temperature also increase as wear increases [3]. Figure 2.3.2-3 displays burr height increase over time under dry drilling conditions in an experiment by [18].

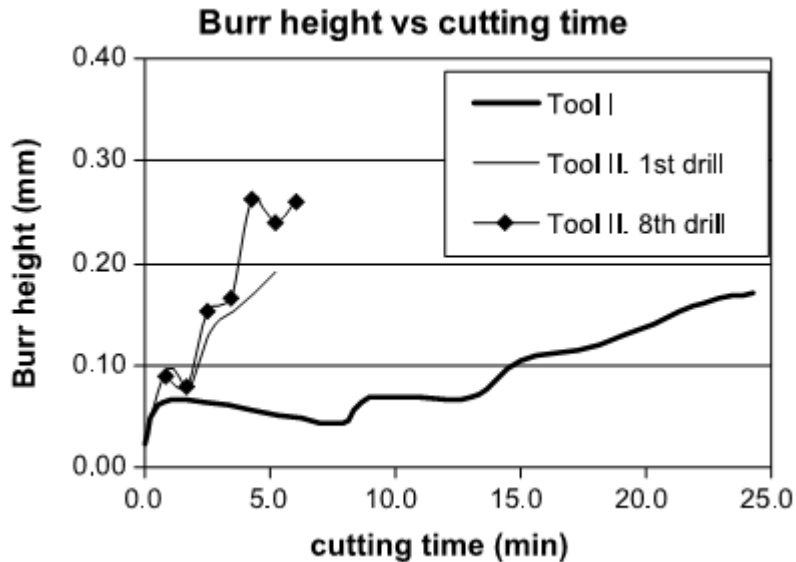


Figure 2.3.2-3: Burr height over cutting time (Tool I, pressurized air applied after every hole; Tool II, pressurized air applied every 8 holes) [18].

During drilling, the hole subsurface can undergo a combination of phase transformation, thermal softening, and strain hardening. In a study by R. Li et al., exposure of Ti-6Al-4V to high temperatures followed by cooling during drilling was shown cause transformation of the β -phase to α -phase along the hole surface (Figure 2.3.2-4). This α -phase is known as an “alpha case.” Alpha case is observed to form during dry drilling; however, for wet drilling, minute amounts of $\beta \rightarrow \alpha$ transformation occur, if any, due to superior heat evacuation [40].

In micro and nanoindentation tests performed by J. L. Cantero et al. and E. Brinksmeier and R. Janssen [18, 40], higher hardness values were found at locations closer to the hole surface in all conditions, which demonstrates the effect of plastic deformation on hardness exceeds the effect of thermal softening (Figure 2.3.2-5 and Figure 2.3.2-6). Figure 2.3.2-6 displays deformation of the α - β grains in region B in the drilling direction.

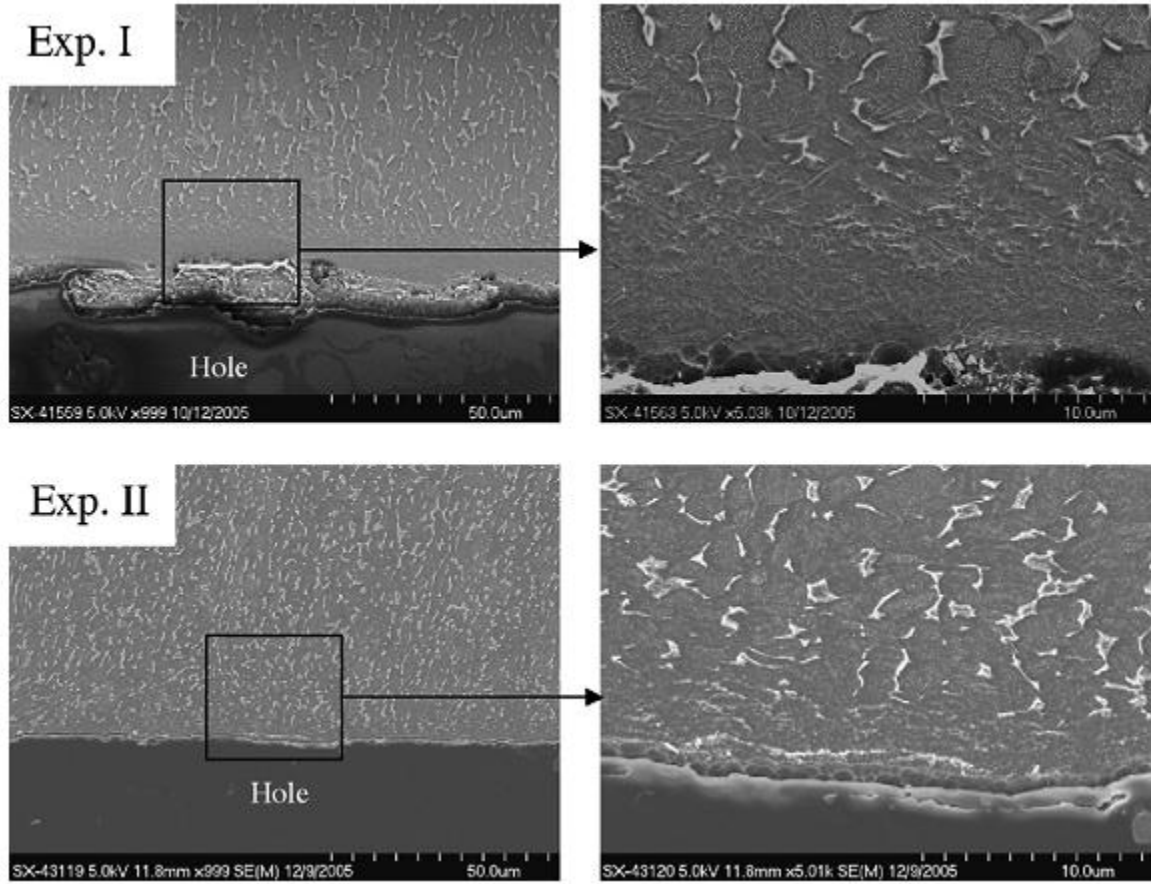


Figure 2.3.2-4: polished and etched Ti-6Al-4V cross section under dry drilling (Exp. I) and wet drilling (Exp II, internal cutting fluid supply) [40].

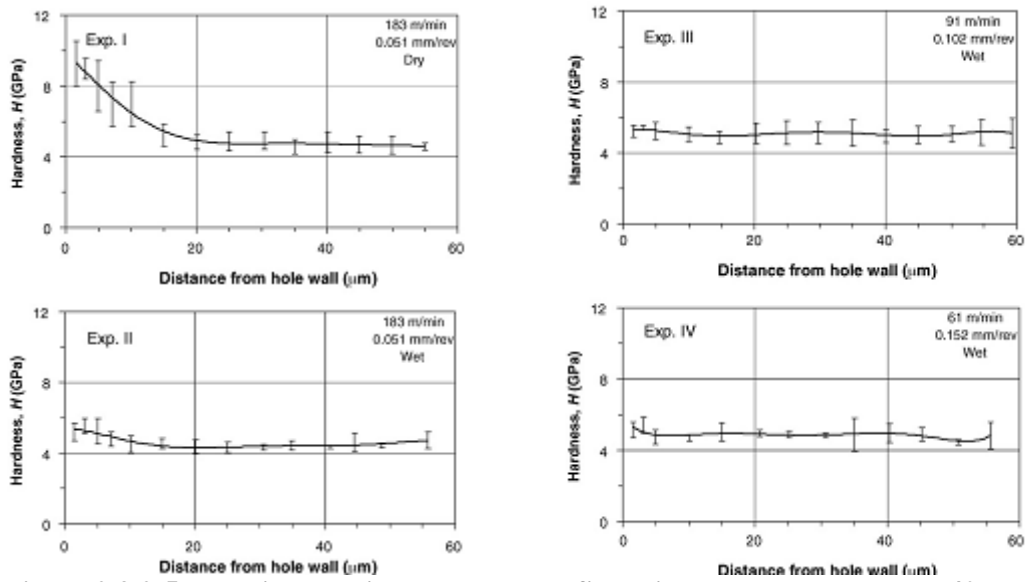


Figure 2.3.2-5: Nanoindentation hardness profile adjacent to the hole edge [40].

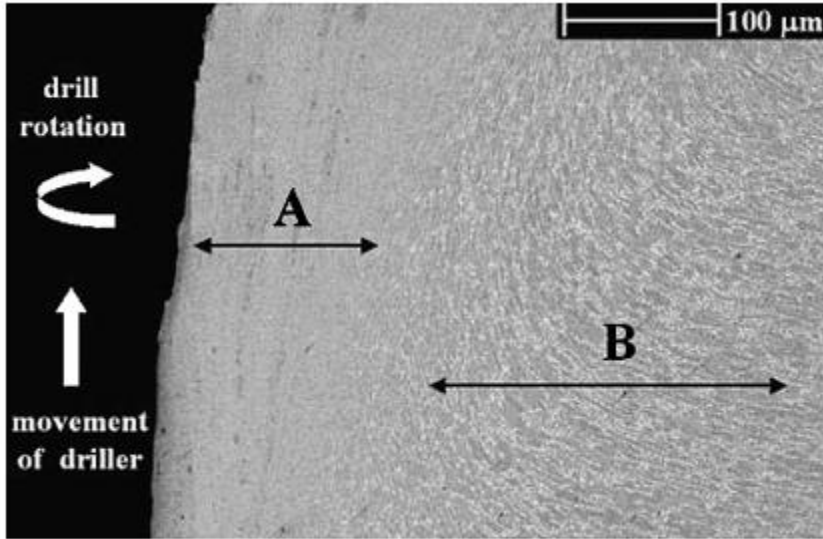


Figure 2.3.2-6: Two regions A and B contain different microstructures. Deformation in direction of drill movement found in region B grains in dry drilling [18].

2.3.3 COMPOSITE/METAL HYBRID MATERIAL SYSTEMS

Implementing composite/metal stacks into aircrafts bring in new machining challenges. As the previous sections showed well-known difficulties known in machining CFRP and titanium individually, there are very few literatures on drilling composite metal/stacks such as CFRP/Ti, carbon fiber reinforced plastic/aluminum (CFRP/Al) or Al/CFRP/Ti. Difficulties in drilling composite/metal stacks begin with the differences in machining properties. Drilling composites require low feeds and high speeds for optimal performance whereas drilling titanium optimally requires positive feed and low speeds [35]. Figure 2.3.3-1 displays the effect of feed and speed on thrust at different regions when drilling Gr/Bi-Ti stacks and reveals thrust forces in drilling each material are most heavily dependent upon feed with slight variations due to speed.

The next difficulty lies within the wear mechanisms. Due to their wear mechanisms, it is clear that tools for machining composite/metal stacks are required to have high hardness, as increased hardness produces enhanced performance over three-body abrasion in composite drilling, while maintaining a low chemical reactivity to resist diffusion and adhesion in titanium drilling [1].

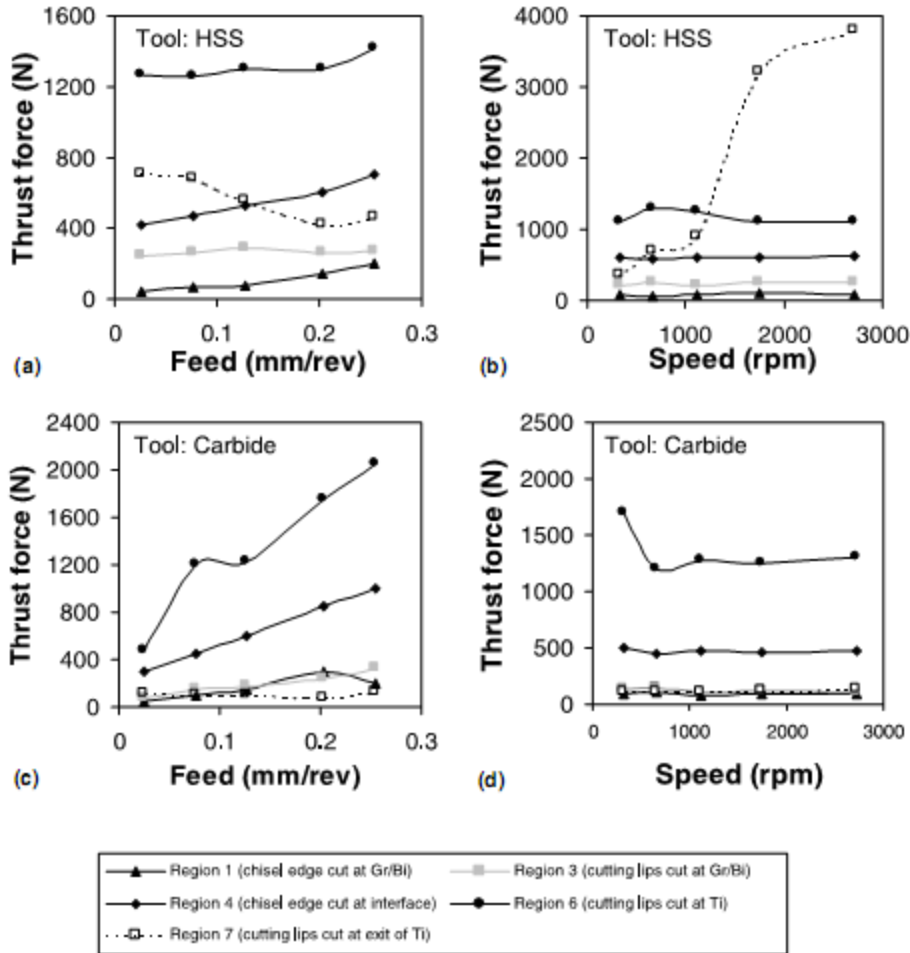


Figure 2.3.3-1: Effect of speed and feed on thrust a) constant speed and b) constant feed for standard HSS drills; c) constant speed and d) feed for standard carbide drills (speed, 600 rpm; feed, 0.00732 mm/rev, drill diameter, 6.35 mm) [3].

The third problem in machining composite/metal stacks is hole quality. Different feed and speed parameters produce different surface roughness values as well as exit burr heights. Figure 2.3.3-2 shows the effect of speed and feed on the hole surface roughness value, Ra, while Figure 2.3.3-3 displays the effect of speed and feed on titanium burr height [3]. Hole quality is seen to be dependent upon speed and feed as well as tool material.

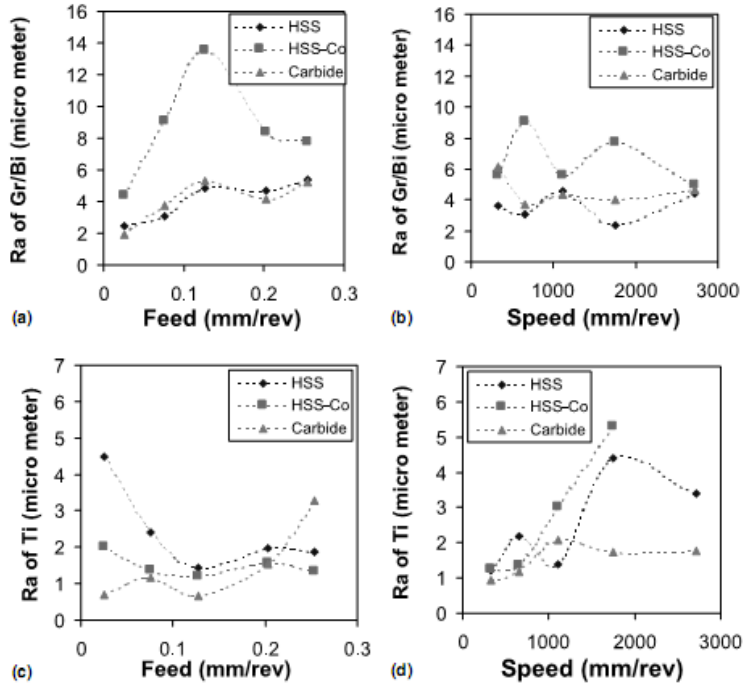


Figure 2.3.3-2: The effect of speed/feed parameters on surface roughness, Ra, Gr/bi a) constant feed and b) speed; Ti c) constant feed and d) speed (speed, 600 rpm; feed, 0.00732 mm/rev, drill diameter, 6.35 mm) [3].

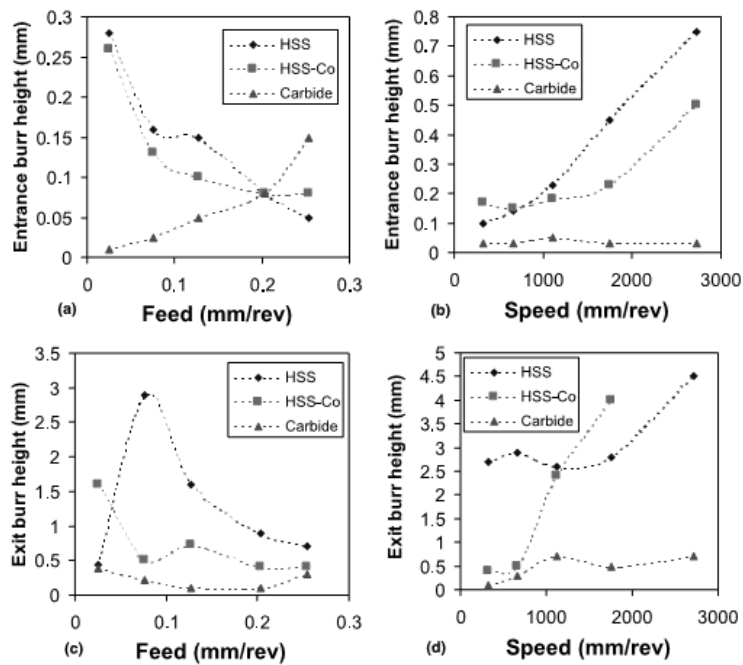
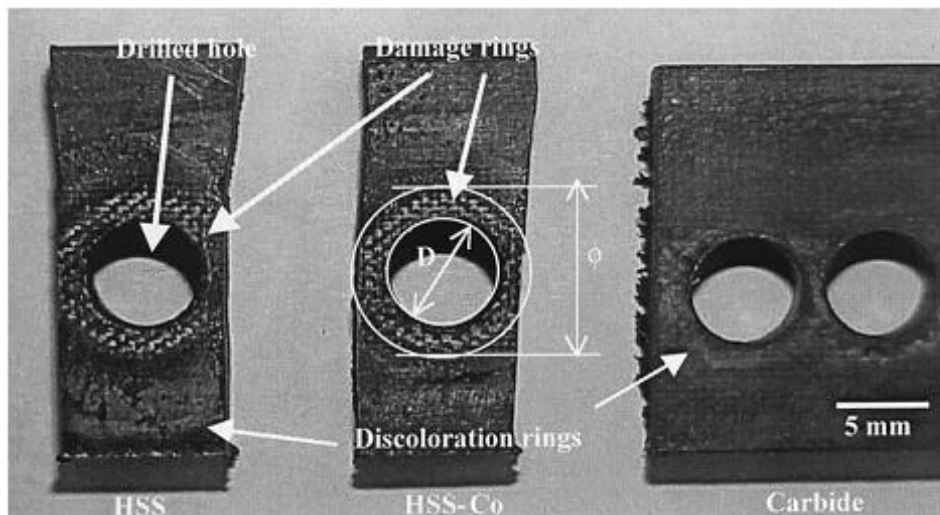
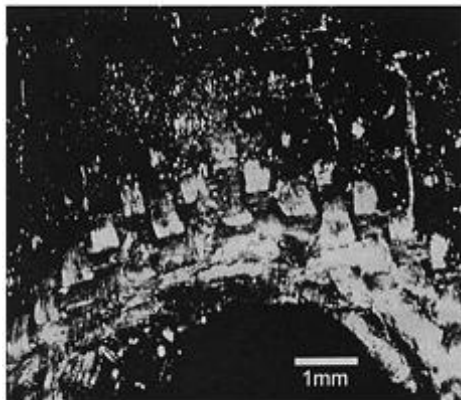


Figure 2.3.3-3: The effect of speed/feed parameters on burr height, entrance a) constant feed and b) speed; exit c) constant feed and d) speed (speed, 600 rpm; feed, 0.00732 mm/rev, drill diameter, 6.35 mm) [3].

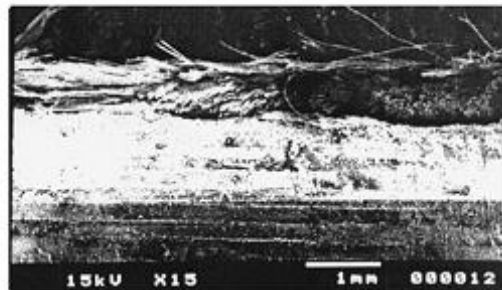
M. Ramulu, T. Branson, and D. Kim [3] reported two types of material damage at located at the Gr/bi-Ti interface on the Gr/bi exit side. The first being the discoloration ring and the second being the damage ring (Figure 2.3.3-4). Discoloration at the Gr/bi exit side is the result of the matrix overheating. Carbide drills were found to produce less damage due to the high hot hardness of the tool material in comparison to high speed steel (HSS). With a higher hot hardness, the tool cutting edge remained sharper in carbide drills when compared to HSS, thus cutting with higher efficiency with lower heat generation.



(a)



(b)



(c)

Figure 2.3.3-4: a) Gr/bi damage region, b) top view (drilled with HSS), c) side view, at 0.08 mm/rev and 1750 rpm with 6.35 mm drill diameter [3].

R. Zitoune, V. Krishnaraj and F. Collmet found, when drilling CFRP/Al, stiffer aluminum chips produced at higher feeds can damage the composite hole wall as the chips pass through [4]. This could contribute the increasing Gr/bi surface roughness found in Figure 2.3.3-2. However, the depth of fiber pullout is also dependent on feed [3].

E. Brinkmeier and R. Janssen [40] also found damage to the CFRP hole during Al/CFRP/Ti drilling. Figure 2.3.3-5 displays the surface roughness profile throughout the A/CFRP/Ti stack, revealing erosion along the CFRP layer at the CFRP/Titanium interface due to the hot titanium chips.

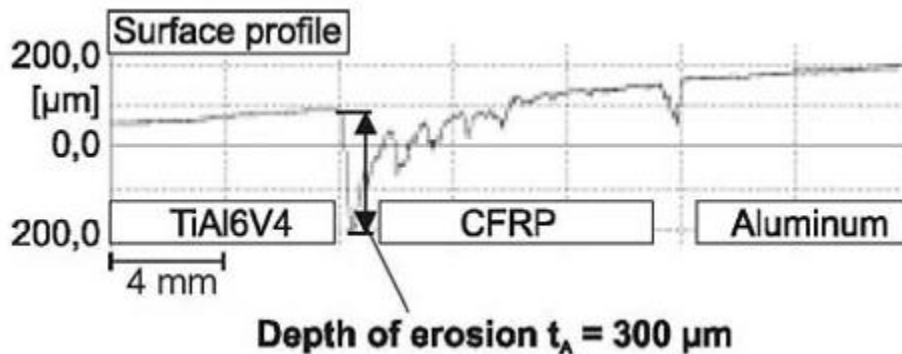


Figure 2.3.3-5: Hole surface roughness in Al/CFRP/Ti stack [40].

CHAPTER 3: OBJECTIVES

The purpose for the research is to evaluate machining performance when drilling carbon fiber reinforced plastic and titanium (CFRP/Ti) stacks in a single-shot rather than using individual drills for each material. In order to reduce cycle time, the aerospace industry sought to eliminate tool change; therefore, it is a necessity to identify tool wear mechanisms and to assess hole quality of each tool material under investigation when drilling CFRP/Ti stacks. The effect of drilling titanium in CFRP/Ti stacks on the CFRP hole quality must also be investigated in order to verify results. Two drilling experiments will be used to identify differences in CFRP hole quality and tool wear brought on by drilling CFRP only and CFRP/Ti stack. Two speed conditions will be used in the experiment to identify the effect of speed on tool wear and hole quality. Various inspection technologies will be used to identify tool wear mechanism and to assess hole quality.

The objectives of the study are summarized as the following:

- Investigate tool wear mechanism when drilling CFRP and Ti with poly-crystalline diamond (PCD) and tungsten carbide (WC).
- Investigate hole defects in drilling CFRP and Ti separately and in stacks.
- Investigate the effect of speed on hole quality and tool wear.

CHAPTER FOUR: EXPERIMENT DESIGN AND PROCEDURES

4.1 WORKPIECE MATERIALS

4.1.1 CARBON FIBER REINFORCED PLASTIC (CFRP)

The CFRP laminate acquired from The Boeing Company were multidirectional graphite epoxy composites consisting of graphite fibers and an epoxy matrix with a quasi-isotropic ply orientation of $[(90^\circ/-45^\circ/0^\circ/45^\circ)_4/0^\circ/90^\circ/0^\circ/90^\circ]_s$. The CFRP laminate had a thickness of 7.43 mm with a ply thickness of 0.1141 mm.



Figure 4.1.1: CFRP ply orientation.

4.1.2 TITANIUM ALLOY

The Ti-6Al-4V is the alloy used in this experiment. Titanium alloy, Ti-6Al-4V, is a two-phase α - β alloy, where V is used as the β phase stabilizing element. In these alloys, the alpha phase forms hexagonal close-packed (HCP) crystal structure while the beta phase forms a Body-centered cubic (BCC) crystal structure. The α - β alloys have higher strength than near- α alloys and higher corrosive resistance compared to aluminum and steel; however, the higher β stabilizer content also increases hardenability [11, 12]. The Ti alloy plate thickness used is 6.73 mm with an average surface roughness of 1.07 μm Ra (with an exception of two plates yet to be used in the experiment of 2.84 μm and 4.98 μm Ra), a flatness of 0.1016 μm . The plates provided by The Boeing Company had an alpha casing, which needed to be removed before the experiment commencement. Before removing the alpha casing, the lengths of each plate were divided by two. The alpha casing was then removed, 0.762 mm from each side, through fly cutting with WC tools, which speed and feed are 300 RPM and 0.0762 meters per minute. The plates after removing the alpha casing are shown in Figure 4.1.2-1.



Figure 4.1.2-1: Titanium plate after alpha casing removal.

4.2 DRILL TYPES

Fullerton Tool Company (WC) and Iijin Diamond (PCD) manufactured the drills used in this study. The Boeing Company provided the tools. Table 4.2-1 shows the drill geometry. The drills have a diameter of 9.525 mm and point angle of 135°. The helix, lip relief, and chisel edge angles are 28°, 72°, and 45°, respectively.

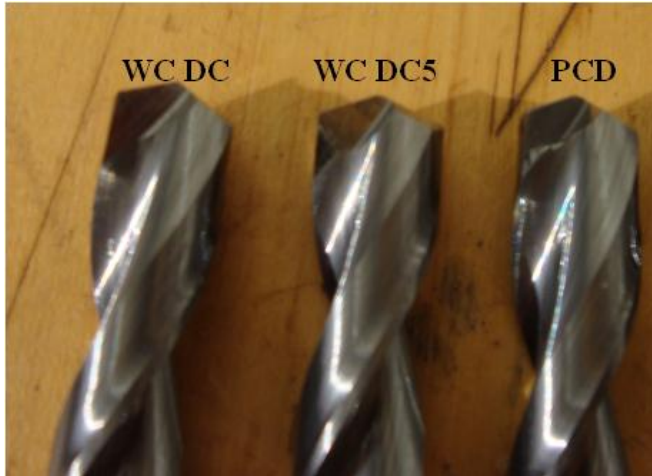


Figure 4.2-1: Drill types

Table 4.2-1: Drill geometry

	DC & DC5 CARBIDE	PCD
DRILL DIAMETER (mm)	9.525	9.525
FLUTE LENGTH (mm)	49.15	50.04
OVERALL LENGTH (mm)	100.3	100.6
WEB THICKNESS (mm)	0.853	0.953
CUTTING LIP LENGTH (mm)	5.115	5.115
POINT ANGLE (DEG.)	135	135
HELIX ANGLE (DEG.)	28	28
LIP RELIEF ANGLE (DEG.)	72	72
CHISEL EDGE ANGLE (DEG.)	45	45

4.2.1 TUNGSTEN CARBIDE (WC)

Two uncoated WC drill types were used: DC (DuraCarb) and DC5 (DuraCarb V). WC tools are commonly used in titanium machining due to their higher MRR over HSS, as aforementioned in Chapter 2. WC drills also have higher fracture toughness over PCD.

Figure 4.2.1-1 shows an SEM image of the micrograin structure of the WC used in this study.

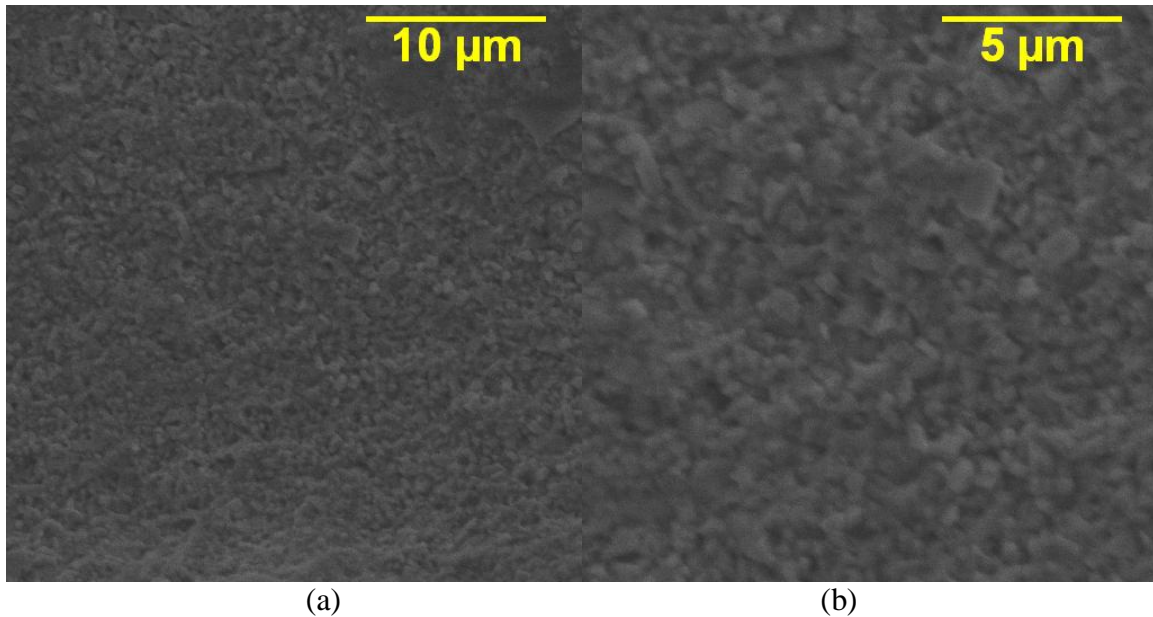


Figure 4.2.1-1: WC micro grains a) 5000x and b) 10000x magnification.

4.2.2 POLY-CRYSTALLINE DIAMOND (PCD)

Poly-crystalline diamond (PCD) is the preferred tool for machining CFRP owing to its high resistance to abrasion. This high resistance to the abrasive nature of CFRP machining is due to the hardness of the tool material. However, due to its low fracture toughness, it has not been often considered for drilling titanium in the past. The PCD drills used in this experiment consist of a carbide drill with brazed PCD inserts. Future testing may include PCD coated carbides.

4.3 EXPERIMENT DESIGN

Two experiment types are used in this study. In each experiment, two series of tools will be used, each series consisting of all tool types. The series also represent the drilling speed parameters used, denoted as High or Low, and experiment type. After drilling twenty holes for each tool in a series, tool wear is examined.

4.3.1 EXPERIMENT TYPE I

Figure 4.3.1-1 shows the general testing sequence for Experiment Type I. The sequence alternates every twenty holes for drilling CFRP then CFRP/Ti stacks. The purpose of this sequence is to exaggerate the tool wear caused by machining CFRP. Doing so, the effects of drilling CFRP and Ti can be differentiated through understanding the interaction between tool wear from CFRP drilling and stack drilling. Series 1 and 2 drills will be used in this sequence.

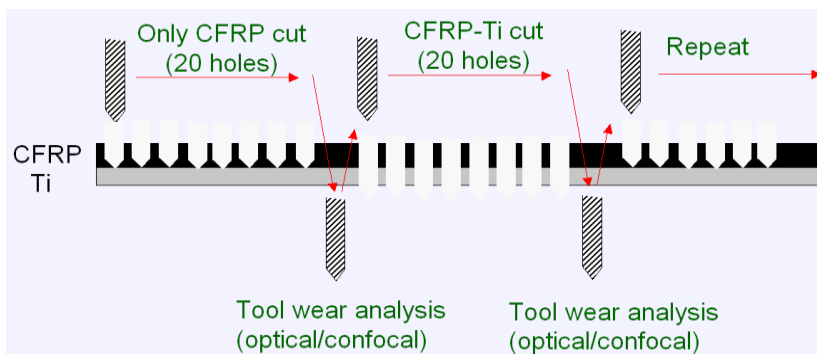


Figure 4.3.1-1: Series 1 & 2 experiment sequence (Experiment Type 1).

4.3.2 EXPERIMENT TYPE II

Whereas in Experiment Type I, drilling CFRP and CFRP/Ti stacks alternated, drilling for Experiment Type II occurs through CFRP/Ti stacks for every hole. This experiment type serves as a control and focuses on tool wear during CFRP/Ti stack Drilling. Series 3 & 4 are assigned to this experiment type.

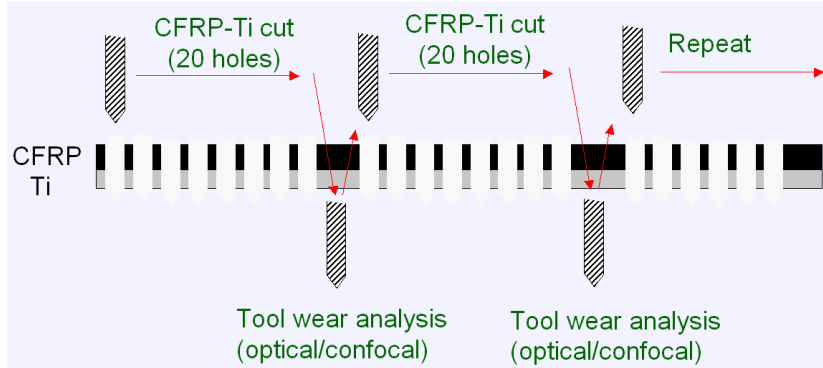


Figure 4.3.2-1: Series 3 & 4 experiment sequence (Experiment Type II).

4.3.3 PARAMETERS

Two speed settings (high and low) were used with one speed for each workpiece material, shown in Table 4.4.1-1, due to their dissimilar characteristics. For CFRP, a high-speed setting of 6000 rpm and low-speed setting of 2000 rpm were used. The speed setting used when drilling titanium is dependent on the drill type. That is, PCD and BAM speeds were set lower in comparison with carbide and BAM coated carbide drills in attempt to prevent premature failure due to their lower fracture toughness. For drilling titanium with carbide and coated carbide tools, the high-speed setting of 800 rpm and low-speed setting of 400 rpm while, whereas for PCD and BAM, the high- and low-speed settings are 500 rpm and 300 rpm, respectively. Two feeds are used, each one designated for the specific workpiece material under drilling: 0.0762 mm/rev and 0.0508 mm/rev for

CFRP and Ti, respectively. When drilling through CFRP/Ti stacks, the shift in speed parameter from CFRP to Ti drilling speeds is programmed to occur 0.0254 mm above the Ti plate in order to avoid damaging the drill point. Table 4.4.1-1 displays the drilling experiment conditions and spindle speed parameters assigned to each tool.

Table 4.4.1-1: Assignment of drilling experiment types and speeds

Drill type		Drilling Experiment Conditions				Drilling Speeds	
		Series 1	Series 2	Series 3	Series 4	High Speed (RPM)	Low Speed (RPM)
DC	Drill #	E1	E2	E3	E4	CFRP: 6000 Ti: 800	CFRP: 2000 Ti: 400
	Type	Type 1	Type 1	Type 2	Type 2		
	Speed	High	Low	High	Low		
DC 5	Drill #	F	F2	F3	F4	CFRP: 6000 Ti: 800	CFRP: 2000 Ti: 400
	Type	Type 1	Type 1	Type 2	Type 2		
	Speed	High	Low	High	Low		
PCD	Drill #	G1	G2	G3	G4	CFRP: 6000 Ti: 500	CFRP: 2000 Ti: 300
	Type	Type 1	Type 1	Type 2	Type 2		
	Speed	High	Low	High	Low		
Feed: 0.0762 mm/rev (CFRP) and 0.0508 mm/rev (Ti)							
Coolant: Water-soluble cutting fluid, Mist coolant flow rate at 16 mL/min.							

4.4 DRILLING EXPERIMENT SETUP

4.4.1 DRILLING EXPERIMENTAL SYSTEM SETUP

The experiments were conducted on a commercial 3-axis CNC mill (MiniMill, HASS, USA) with water-soluble coolant discharged through a coolant mister. A container was designed to reduce the amounts of carbon fiber dust circulating through the lubricant system (Figure 4.4-1). A vacuum hose is inserted through the right side of the container during the drilling process to support carbon fiber dust capture.

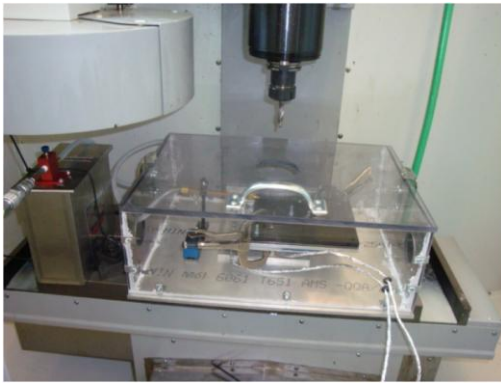


Figure 4.4-1: CNC setup with coolant mister.

Drilling was decided to commence from the CFRP side of the stack. The workpiece materials are bound together through six bolts and to a pre-drilled aluminum plate with 12.7mm inch diameter holes. The plates were then clamped to a fixture system, which consisted of four parts: a top fixture, fencing, dynamometer, and bottom fixture. The pre-drilled holes in the aluminum plate allowed for locating the plate into position on the fixture without disturbing burr height and hole quality with a positioning pin as shown in Figure 4.4-2. This is designed to allow spacing between each hole.

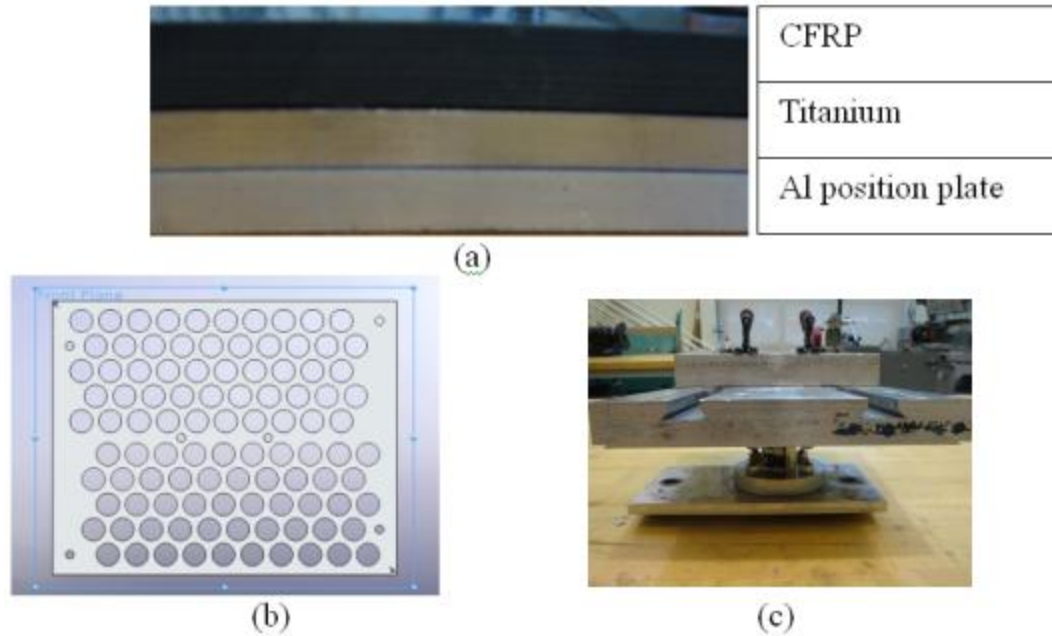


Figure 4.4-2: a) CFRP/Ti stack setup with positioning plate b) pre-drilled aluminum positioning plate (Solid Works Design) and c) fixture.

A water-soluble cutting fluid was used as a mist coolant throughout the operation with a flow rate of 16 mL/min. The coolant mister nozzle, set on a movable magnetic-base, was placed a distance equivalent to 1.75 times the size of the drilling diameter in order to keep an approximate average distance and spray diameter.

As aforementioned, the fixture configuration consists of four parts. At the top, an aluminum fixture is machined to locate the position of each hole through the use of two different location pins. The first location pin is used to locate the side of the pre-drilled aluminum plate; this is used to locate the first hole to be drilled in each row (Figure 4.4-2b left). Two sites on the top plate fixture are used to alternate the location of this pin in order to follow the alternating pattern seen on the pre-drilled aluminum plate, thus allowing a 100-hole capacity per sample. The second location pin is inserted into the pre-drilled aluminum holes to continue following the hole pattern through the rest of the row

(Figure 4.4-2b right). The second part of the fixture is a movable fence, which serves to properly align the plate; thus keeping each row in proper order. The function for the fence to move along the fixture through the use of locator pins and guides allows the plate to be shifted to begin the next row. The fence is bolted down to two guides inserted into the top fixture to keep rigidity. The third and fourth part of the fixture system consists of a dynamometer, which is bolted to the top fixture plate, and a bottom fixture plate. The bottom fixture plate is bolted down directly to the CNC stage.

4.4.2 DRILLING FORCE DATA ACQUISITION SYSTEM SET UP

To measure thrust and torque during the drilling operation, a commercially available dynamometer (TRS-1K-OPT-THR, Transducer Techniques, USA) was implemented into the fixture system as aforementioned. The analog voltage signals from the dynamometer input into two amplifiers; each one is calibrated to receive and amplify either thrust or torque. The signals then go through a Signal Conditioning Connector (SC-2345, National Instruments, USA), which conditions the voltage signals, allowing them to be routed to the DAQ module (USB-6251, National Instruments, USA). The DAQ module then takes the conditioned signal and converts it to a digital signal. The signal is then captured onto data acquisition software (LabView 7.1, National Instruments, USA) with a program designed and calibrated to fit the signal into an appropriate unit system and record the signal at a frequency of 100 data points per second. The data can then be compiled and processed. Figure 4.4.3-1 shows the thrust and torque capture setup that connects to the dynamometer.



Figure 4.4.3-1: Thrust and torque signal capture setup.

4.5 HOLE QUALITY MEASUREMENT METHODS

In both CFRP and Ti, hole quality is evaluated in terms of hole diameter, roundness, and roughness. Hole quality in Ti alloys is also evaluated through entry and exit burr heights, whereas in CFRP, delamination and fiber pullout are used to further quantify hole quality.

4.5.1 COORDINATED MEASURING MACHINE

Hole diameter and roundness are measured with the RefleX Coordinated Measuring System, manufactured by Brown & Shape Manufacturing Company (Figure 4.5.1-1). The system consists of a Coordinate Measuring Machine (CMM) mounted with a 1 mm Renishaw ruby tipped spherical probe and a control console. Hole size is the measure of the hole diameter, which defined the hole size tolerance. Hole roundness is defines a tolerance zone through two concentric circles. At for each hole, 8 points were measured to obtain the least square diameter and roundness. Both diameter and roundness of every

3 holes for every 20 hole cycle were measured at the midsection of each plate, and for every 10 holes at five locations 1 mm to 1.3 mm apart on each plate of the stack hole.

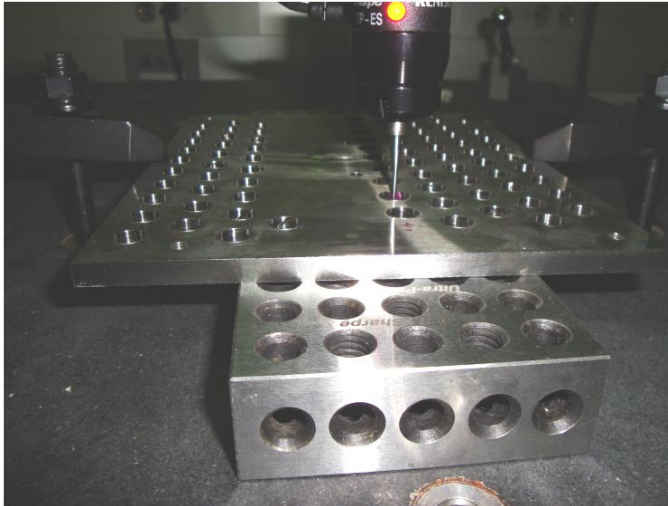


Figure 4.5.1-1: Coordinated Measuring Machine (CMM) (Brown & Shape Manufacturing Company).

4.5.2 OPTICAL MICROSCOPY

The optical microscope with camera and digital display shown in Figure 4.5.2-1 is used for various purposes throughout the experiment. This includes: measuring ply thickness, identifying ply orientation, locating fiber pullout, measuring scratch thickness (on CFRP holes from titanium chips), displaying scratch angle, and measuring titanium adhesion thickness.

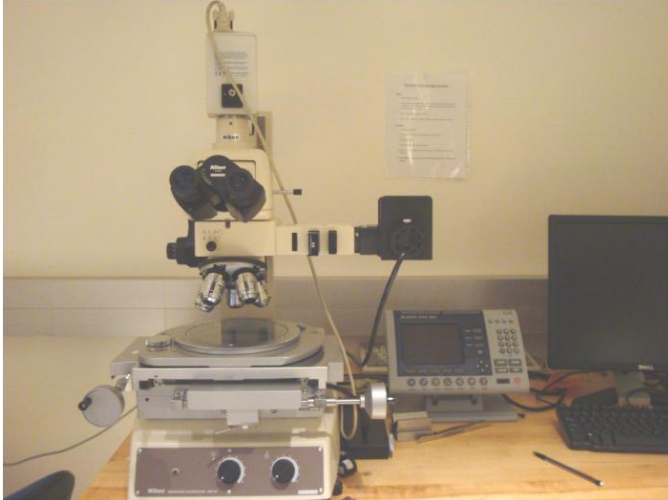


Figure 4.5.2-1: Optical microscope with camera and digital measurement readout.

4.5.3 SCANNING ELECTRON MICROSCOPY

The scanning electron microscope (SEM) manufactured by Aspex Instruments, was used to identify fiber orientations where fiber pullout occurs in the CFRP coupons as with the optical microscope. It is also extensively used investigate wear mechanisms by displaying the drill condition after every 20-hole cycle. The machine can also utilize EDX to identify adhesion of Ti workpiece material to the tool, removal of tool coating, and mixtures of Ti and WC on the tool cutting edge.



Figure 4.5.3-1: Scanning Electron Microscope (SEM) (Aspex Instruments).

4.5.4 SURFACE PROFILOMETER

The profilometer manufactured by Mahr is used to measure the surface roughness across the CFRP and Ti hole depth (Figure 4.5.4-1). For CFRP, the surface roughness profile was measured over a length of 5.6 mm with a velocity of 0.50mm/s, measuring from end to end of the hole. The surface roughness profile for titanium was measured over a length of 1.75 mm with a speed of 10 mm/s, measuring from the middle of the plate towards the exit side.

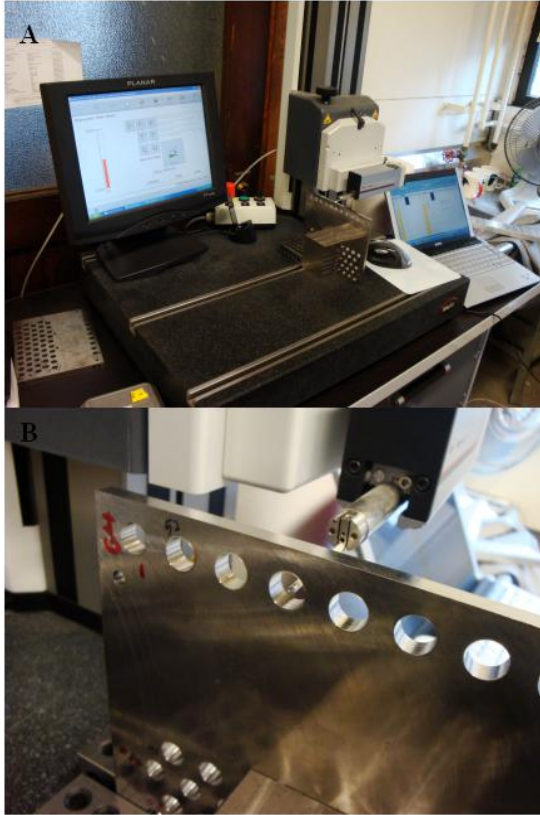


Figure 4.5.4-1: a) Surface profilometer with touch screen display (Mahr) b) close up of stylus.

There are several definitions for roughness. Roughness values used or shown in this report are R_a , R_q , R_z , R_t , R_p , and R_v . R_a is defined as the average of all the peak and valley heights compared to the mean line. R_q is described as the mean deviation from the mean line found through integrating the area under the curve of a sine wave equivalent to the profile. R_z averages the five highest peaks and five lowest valleys. R_t measures the highest peak to the lowest valley. R_p is the highest peak above the mean line, and R_v is the lowest valley beneath the mean line. In this report, R_a , R_v , and R_t will be the most significant. Figure 4.5.4-2 displays an example of a surface profile with R_p and R_v measures from the mean line

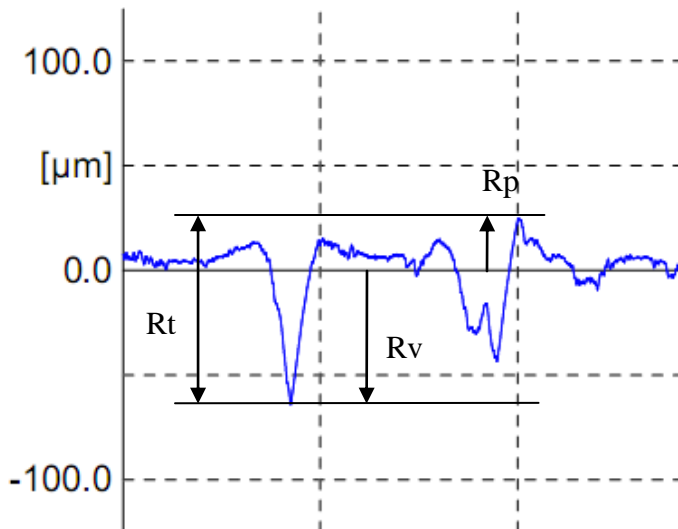


Figure 4.5.4-2: Surface roughness profile example.

4.5.5 HEIGHT DIAL GAGE

Figure 4.5-1 shows the height probe with dial used to measure titanium entry and exit burr heights. The probe is taken across the burr along the circumference of the hole and the measurement at the highest location found from the burr is recorded.

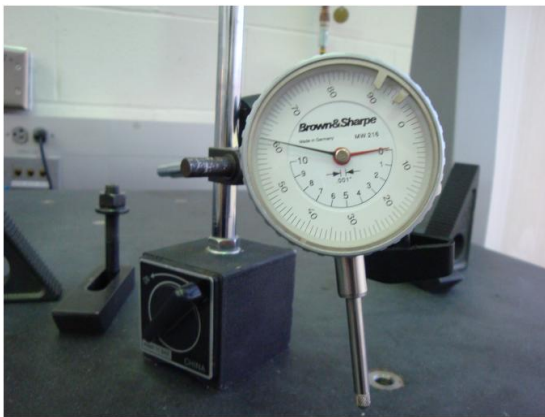


Figure 4.5.5-1: Height gage with dial (Brown & Shape).

CHAPTER 5: RESULTS AND DISCUSSION

5.1 THRUST & TORQUE ANALYSIS

Thrust and torque profiles typically vary with cutting time. During stack drilling, it is clear that there will be two major regions in the drilling force profiles as depicted by the force and thrust profile in Figure 5.1-1 and Figure 5.1-2. The first region is where the drill fully engages the CFRP plate. During CFRP drilling, the force profile drops almost to zero due to the change in spindle speed during the drilling process. The second region is where the drill fully engages the Ti plate. As the tool begins to penetrate the Ti plate, the thrust value increases rapidly while the torque value increases gradually. As the drill passes through the Ti plate, the drilling forces ebb.

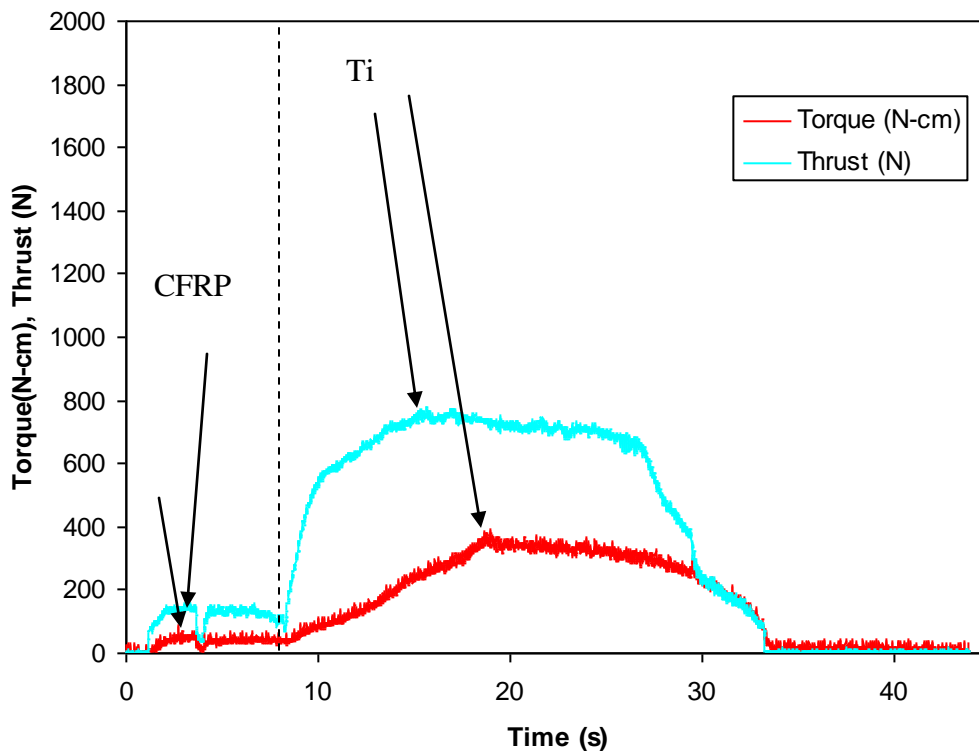


Figure 5.1-1: Drilling force profile in drilling CFRP/Ti stacks (WC drill at low speed experiment type II, hole 1). Arrows indicate peak locations.

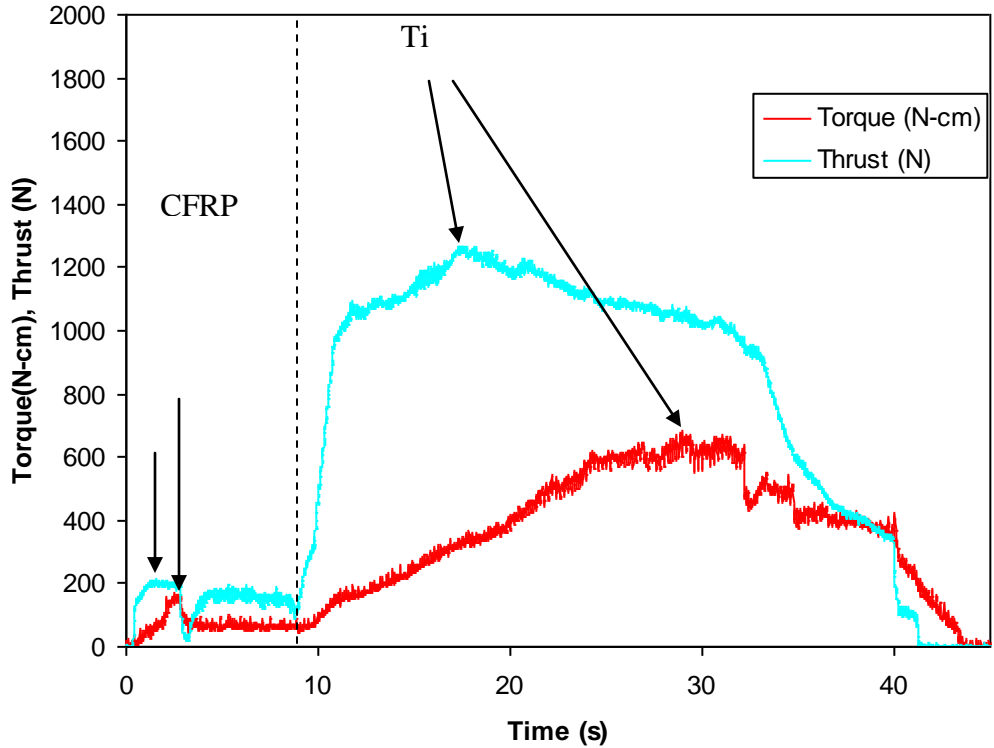


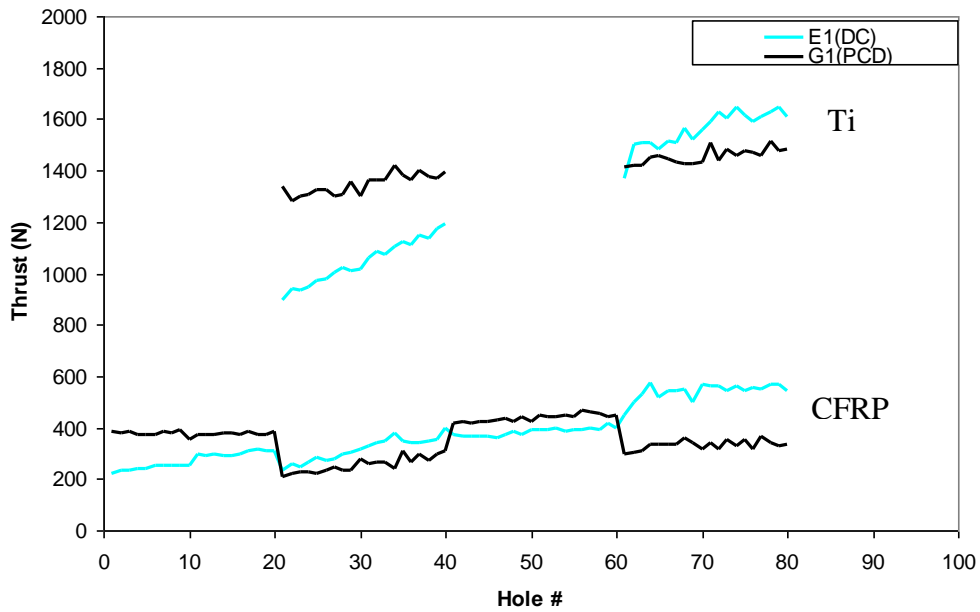
Figure 5.1-2: Drilling force profile in drilling CFRP/Ti stacks (PCD drill at low speed experiment type II, hole 1). Arrows indicate peak locations.

Figure 5.1-1 and 5.1-2 show the thrust profiles for low speed Experiment Type II at the first hole for WC and PCD, respectively.

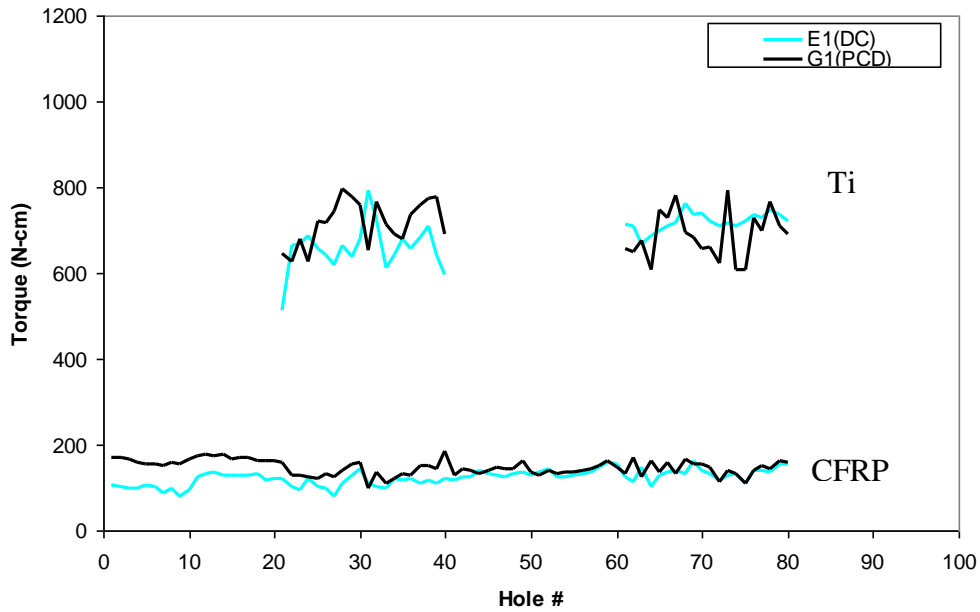
Figures 5.1-3 through 5.1-6 show the maximum thrust and torque values recorded when drilling each hole for each plate. Each series shows a general trend in thrust. Thrust and torque requirements for drilling through CFRP are much lower than those for drilling Ti. PCD begins with a higher thrust force compared to other tool materials; however, the rate in which thrust increases is the lowest with PCD tools. WC thrust values starts off with the lowest thrust values, yet WC yields the highest rate of thrust increase, with DC and DC5 both following equivalent trends. In low speed Experiment Type I (Figure 5.1-4),

the trend in torque values increases while drilling through the Ti plate, whereas the torque trend remains constant while drilling CFRP. In Experiment Type II (Figure 5.1-5 and Figure 5.1-6), the trend in torque values can be seen to increase during both Ti and CFRP regions.

The different thrust values at the beginning of the experiment are due to the differences in tool geometry between WC and PCD tools (refer to table 4.2-1) and/or due to the possibility of initial pitting at the first hole with PCD. The rate at which thrust increases can be correlated to speed and tool wear. Comparing thrust values from high speed to low speed in Experiment Type I, the rate of thrust increase for WC tools is higher under high speed conditions than under low speed conditions. In the case of PCD, the max thrust increase rate when drilling with PCD is higher in at low speed than in high speed. Comparing the SEM photos in Figure 5.2.2-2, wear on the PCD tool in low speed Experiment Type I is noticeably more severe than in high speed Experiment Type I. For Experiment Type II, Figures 5.1-5 and 5.1-6 reveal that using WC drills at the high speed setting have a higher max thrust increase rate. As shown in Figure 5.1-6, thrust increase between hole 1 and 80 is 447 N for WC and 161 N for PCD when drilling CFRP, whereas the thrust increase is 346 N for WC and 332 N for PCD when drilling titanium.



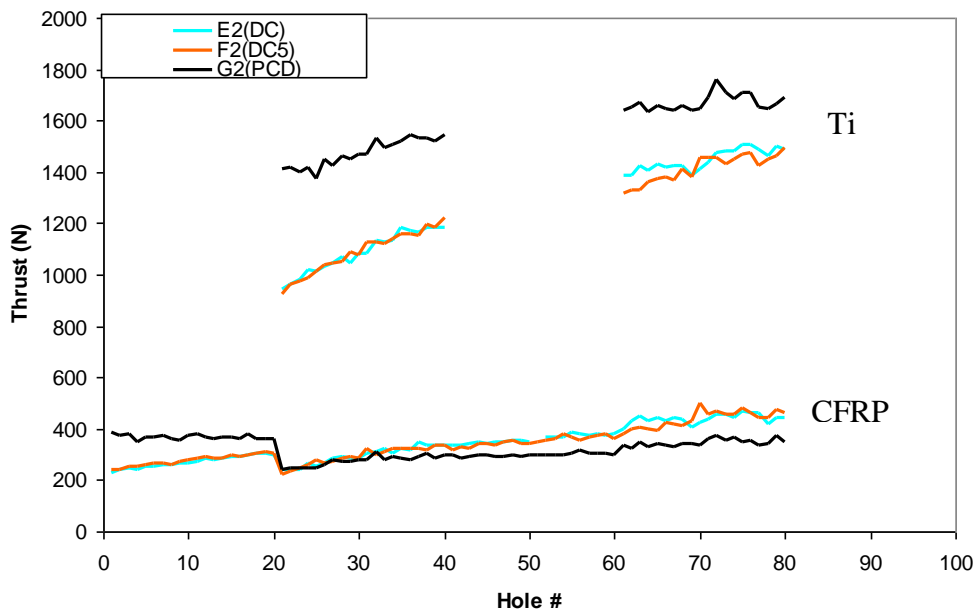
(a) Thrust force



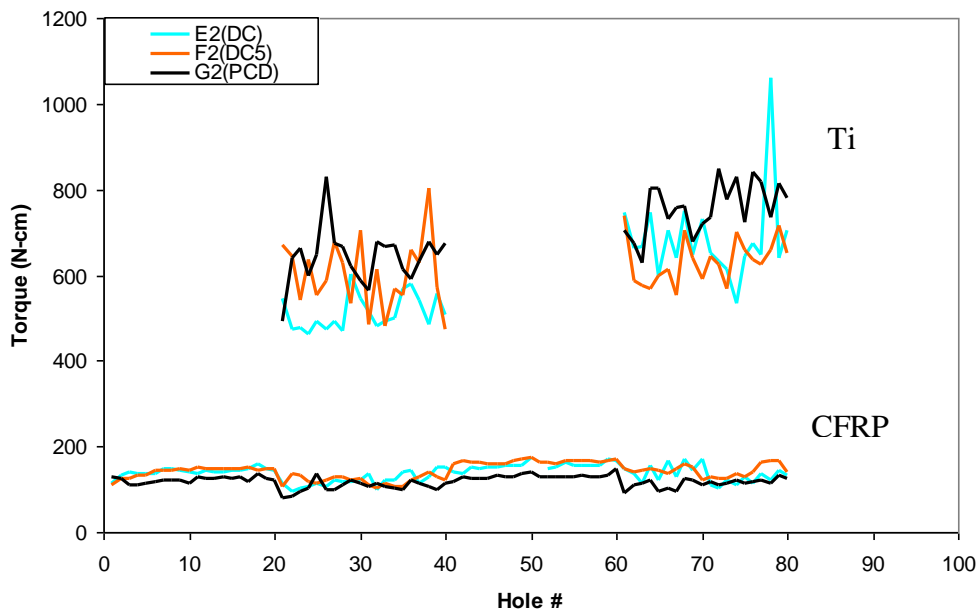
(b) Torque

Figure 5.1-3: Max a) thrust and b) torque of each hole with high speed Experiment Type I.

During high speed Experiment Type I drilling, WC DC5 failed prematurely at hole 28 due to operator error, thus being omitted from the graph.



(a) Thrust force

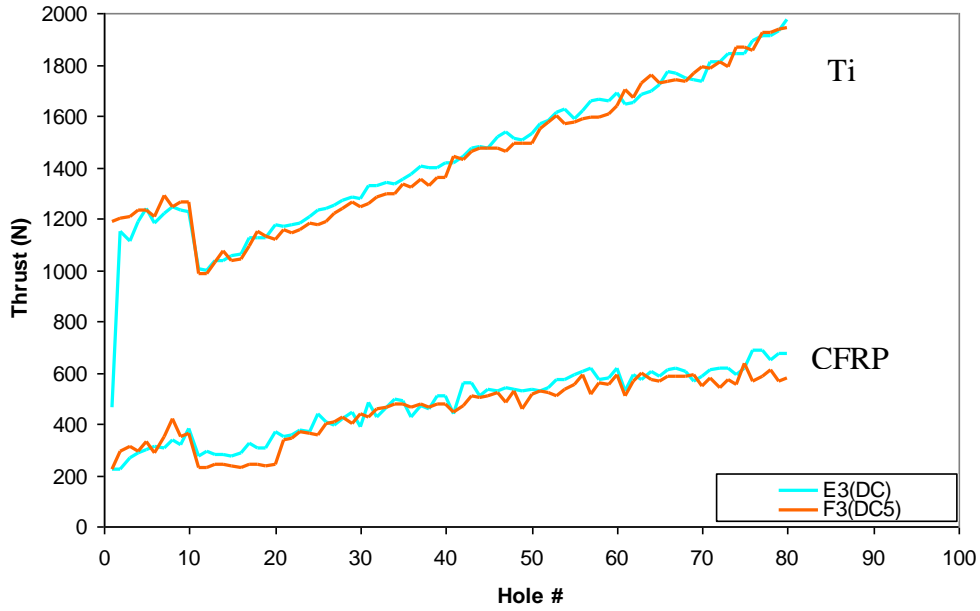


(b) Torque

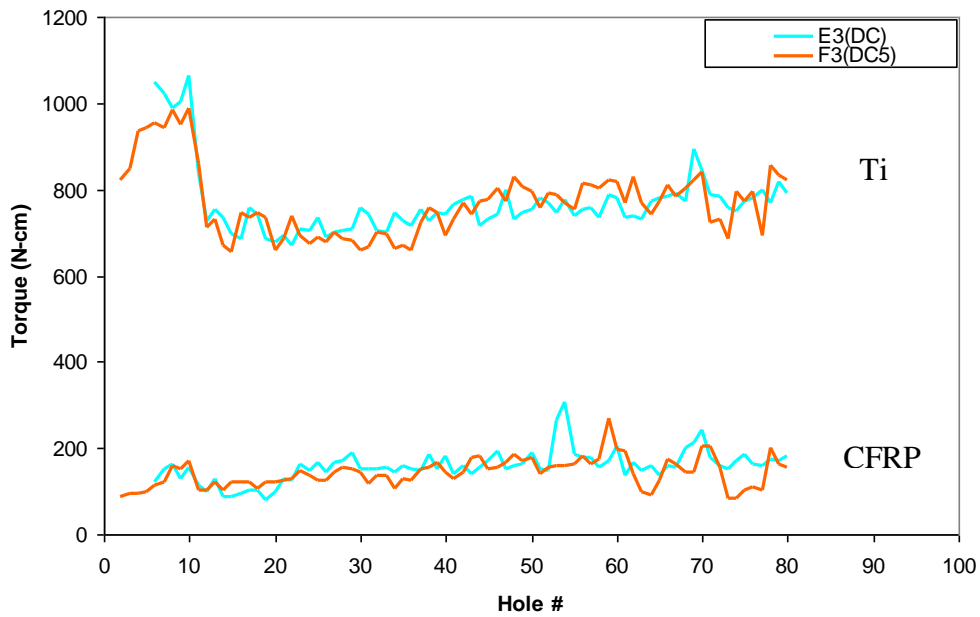
Figure 5.1-4: Max a) thrust and b) torque of each hole with low speed Experiment Type I.

During Experiment Type I (Figure 5.1-2 and 5.1-3), miscommunication on the definition of feed between the machinist and sponsor lead to using twice the wanted feed during the

first 20 holes in CFRP only drilling and in the first 10 holes during Experiment Type II at high speed.



(a) Thrust force



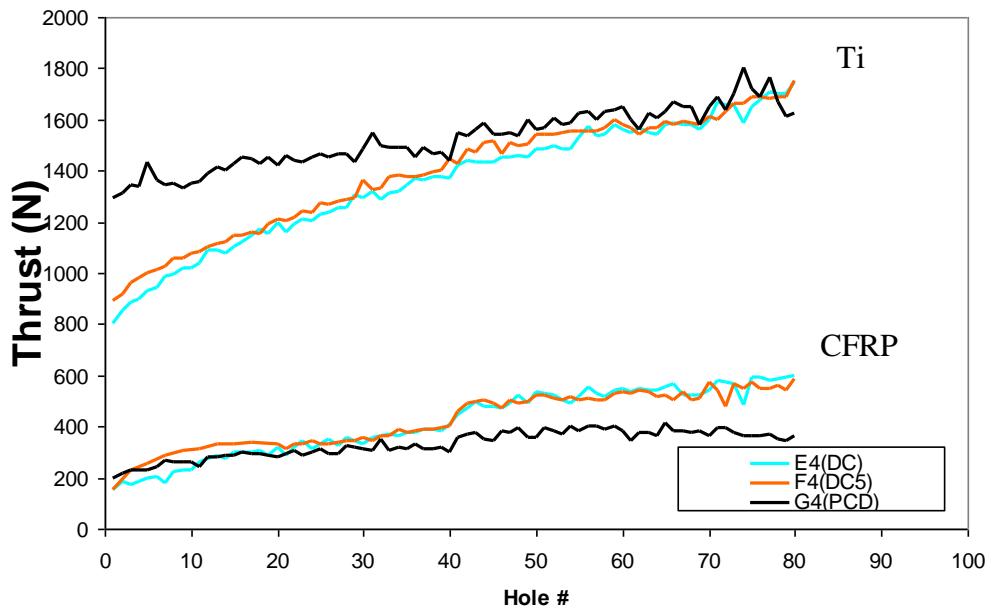
(b) Torque

Figure 5.1-5: Max a) thrust and b) torque of each hole with high speed Experiment Type II.

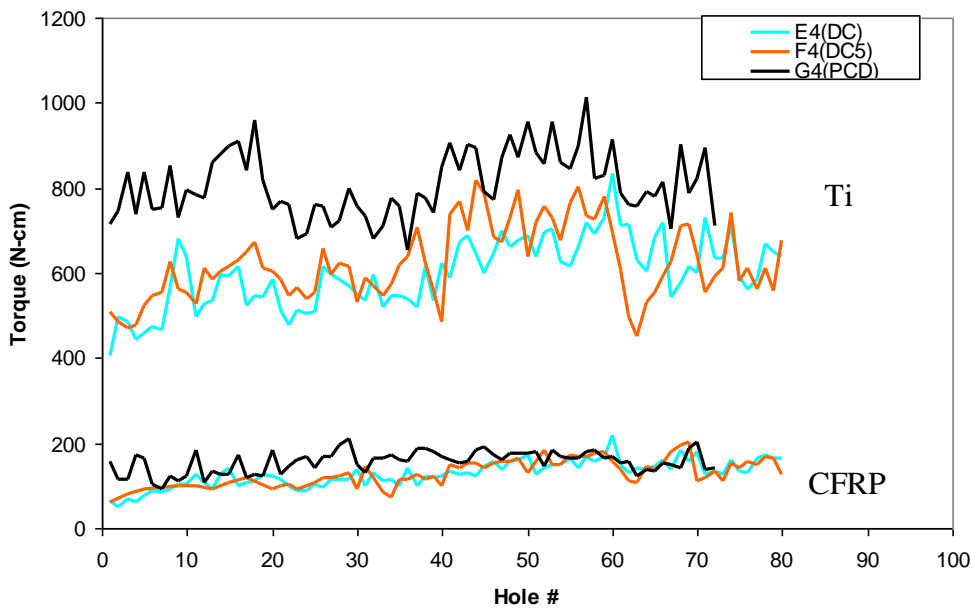
While drilling at high speed in Experiment Type II, PCD failed prematurely at hole 3, and is thus excluded from the graph. As a result, RPM was reduced in further stack drilling with PCD drills to prevent the reoccurrence of premature failure of the PCD drills.

At the initiation of stack drilling, the experiment was originally to be conducted under dry conditions in order to expose the tools to the worst possible conditions. The first CFRP/Ti stack hole drilled by WC at high speed Experiment Type II was conducted under dry conditions. However, drilling under dry conditions resulted in a fire during our drilling process. As the titanium chips burned, it would cause the CFRP powder like chips to smolder. The CFRP powder like chips were being evacuated into a vacuum during the drilling process in order to prevent or reduce the accumulation of these powder like chip into the coolant system and various parts of the CNC mill. The vacuum caught fire in response to the smoldering dust. Drilling was conducted henceforth under wet conditions rather than dry to prevent further fire damage.

Low speed Experiment Type II thrust force and torque values reveal a trend proportional to the number of holes drilled. After hole 73, a large portion of tool material fractured occurred in PCD during low speed Experiment Type II. The max thrust force seen during titanium drilling can be seen to increase sharply after tool the fracture (See Figure 5.2.2-3 for PCD fracture image).



(a) Thrust force



(b) Torque

Figure 5.1-6: Max a) thrust and b) torque of each hole with low speed Experiment Type II.

The maximum thrust values at each hole during both experiments increases as tool wear increases. The rates at which the thrust values increase reveal that PCD wears down at a lower rate than the WC tools. Whereas PCD displays a higher thrust increase rate at low

speed than at high speed in Experiment Type I, the opposite holds true for WC. DC5 is also shown to have a slightly lower thrust increase rate than DC; however, they are nearly identical. Overall, PCD tools produce a lower increase rate in maximum thrust values with hole number than WC tools, which may reflect a lower wear rate.

5.2 TOOL WEAR

Figure 5.2-1 defines the faces and cutting edges of the drill. SEM images of each tool were taken every 20 holes in order to observe the tool wear progression at the cutting edge corner throughout the experiment. As aforementioned, the increase of tool wear could directly correlate to the increase in thrust and torque values. After drilling hole 40, a removal process of the titanium adhesion in Experiment Type II through etching was executed in order for the Michigan State University (MSU) team to conduct analysis of tool wear volume through utilization of confocal microscopy and to allow the Washington State University Vancouver (WSUV) team to observe the tool wear which occurs under the adhesive layer. This titanium adhesion removal process was then conducted in Experiment Type II after every 20-hole cycle.

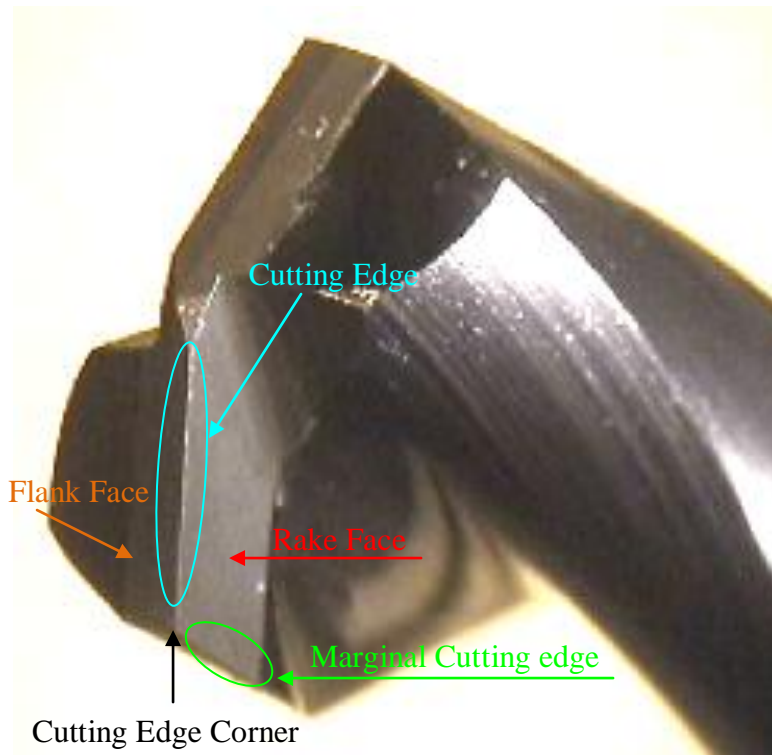


Figure 5.2-1: Drill cutting edges and faces.

5.2.1 TUNGSTEN CARBIDE (WC)

Figure 5.2.1-1 shows the SEM images of the cutting edge corner taken every 20 holes for WC (DC). During stack drilling, titanium adhesion is noticeable all each series. The chemical reactivity of titanium alloys, which increase with temperature, leads to titanium adhesion to form a built-up edge (BUE). The SEM image shows, at hole 60 (the end of the CFRP only drilling cycle) during Experiment Type I, the titanium adhesion has been removed by the CFRP.

Hole No.	Type I, High speed	Type I, Low speed	Type II, High speed	Type II, Low speed
0				
20				
40			Not available	
60				
80				

Figure 5.2.1-1: Cutting edge corner at 500x magnification for DC Carbide with various cutting distances and parameters.

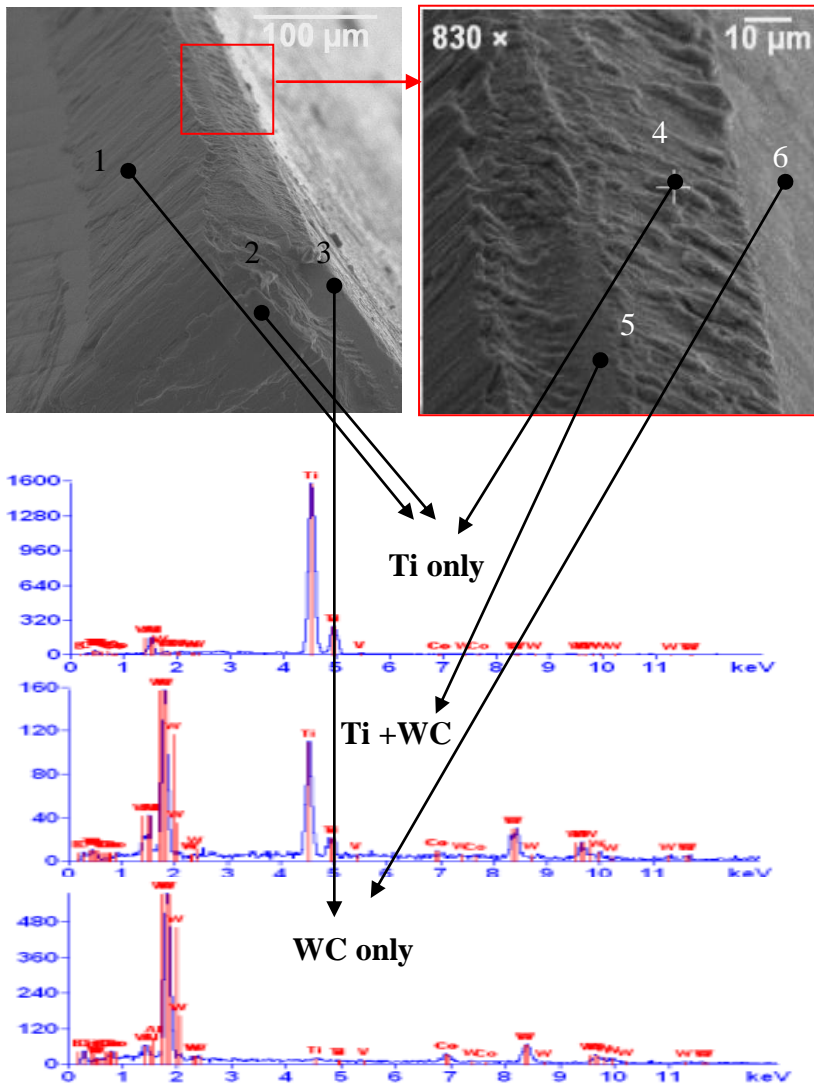


Figure 5.2.1-2: SEM-EDX on high speed Type II WC (DC) after drilling hole 60.

Definite proof on the occurrence of titanium adhesion can be identified through SEM-energy-dispersive X-ray spectroscopy analysis (EDX). Figure 5.2.1-2 illustrates the EDX analysis conducted at several locations. From Figure 5.2.1-2, adhesion is found to be prevalent on the cutting edge and the helical flute near the cutting edge corner.

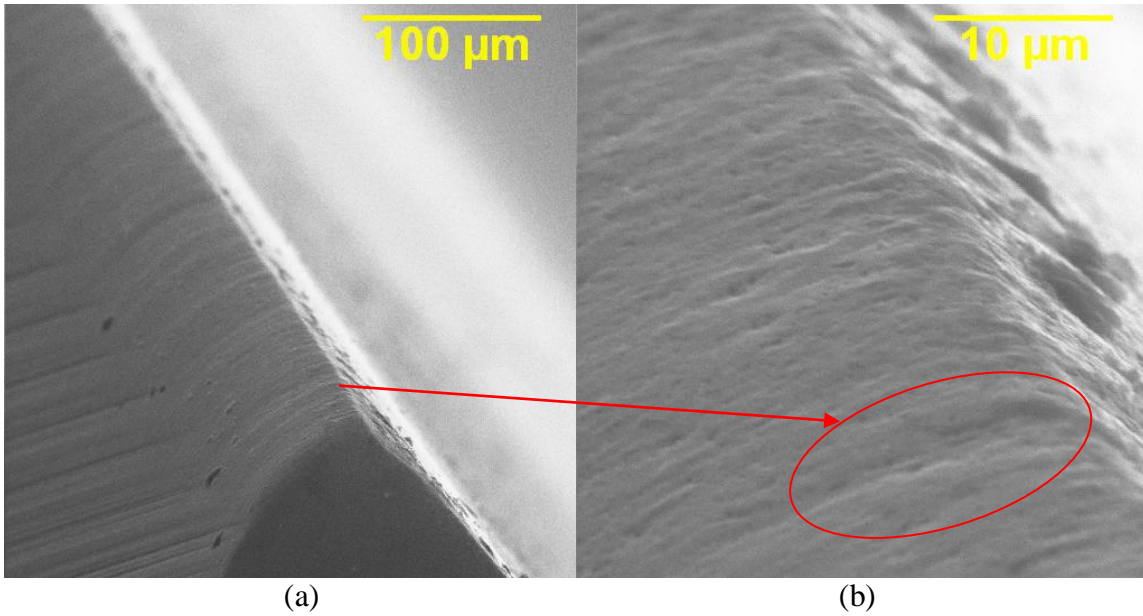


Figure 5.2.1-3: Cutting edge corner low speed Type I WC (DC, hole 60) a) 500x and b) 5000x magnification; ~5 μ m wide grind mark.

During the CFRP only cycles, smooth wear marks can be seen as an indication to the abrasive nature of CFRP. Figure 5.2.1-3b highlights one of many grind marks with widths equivalent to the 5 μ m fiber diameter found at hole 60 of the low speed Experiment Type I WC (DC) drill.

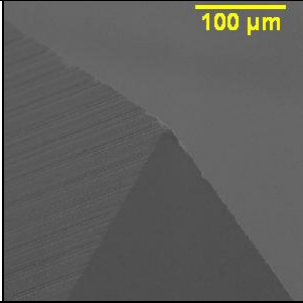
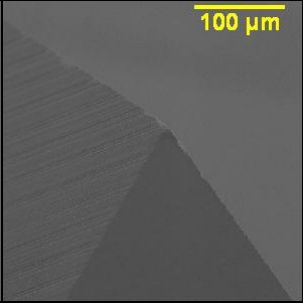
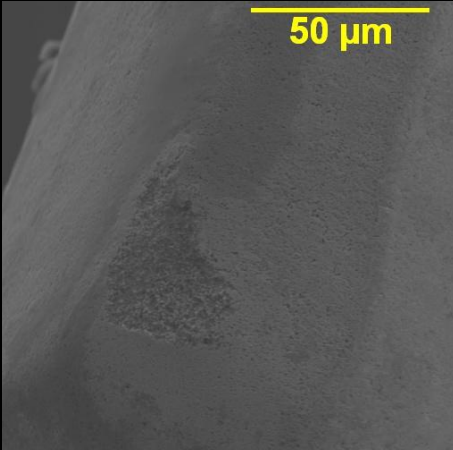
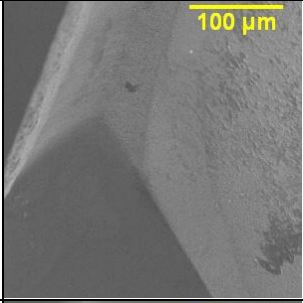
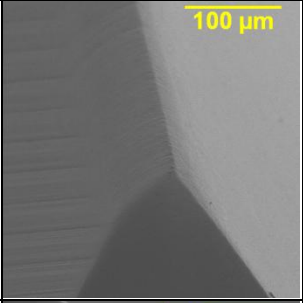
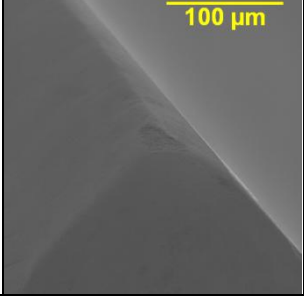
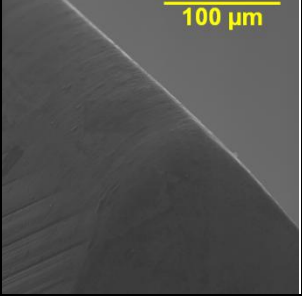
Hole No.	Type II, High speed	Type II, Low speed	
Hole 0			
40			Type II, High speed, hole no. 60 1000x magnification etched
60			

Figure 5.2.1-4: Cutting edge corner at 500x magnification for etched WC (DC) with various cutting distances and parameters with close up of high speed Type II.

Experiment Type II WC DC drills can be seen after etching in Figure 5.2.1-4 at 500x magnification. The close up of the WC tool after hole 60 under the high-speed parameter focuses on the manifestation of a rough surface on the tool cutting edge corner. Rounding occurs on both tools at the cutting edge corner and along the cutting edge.

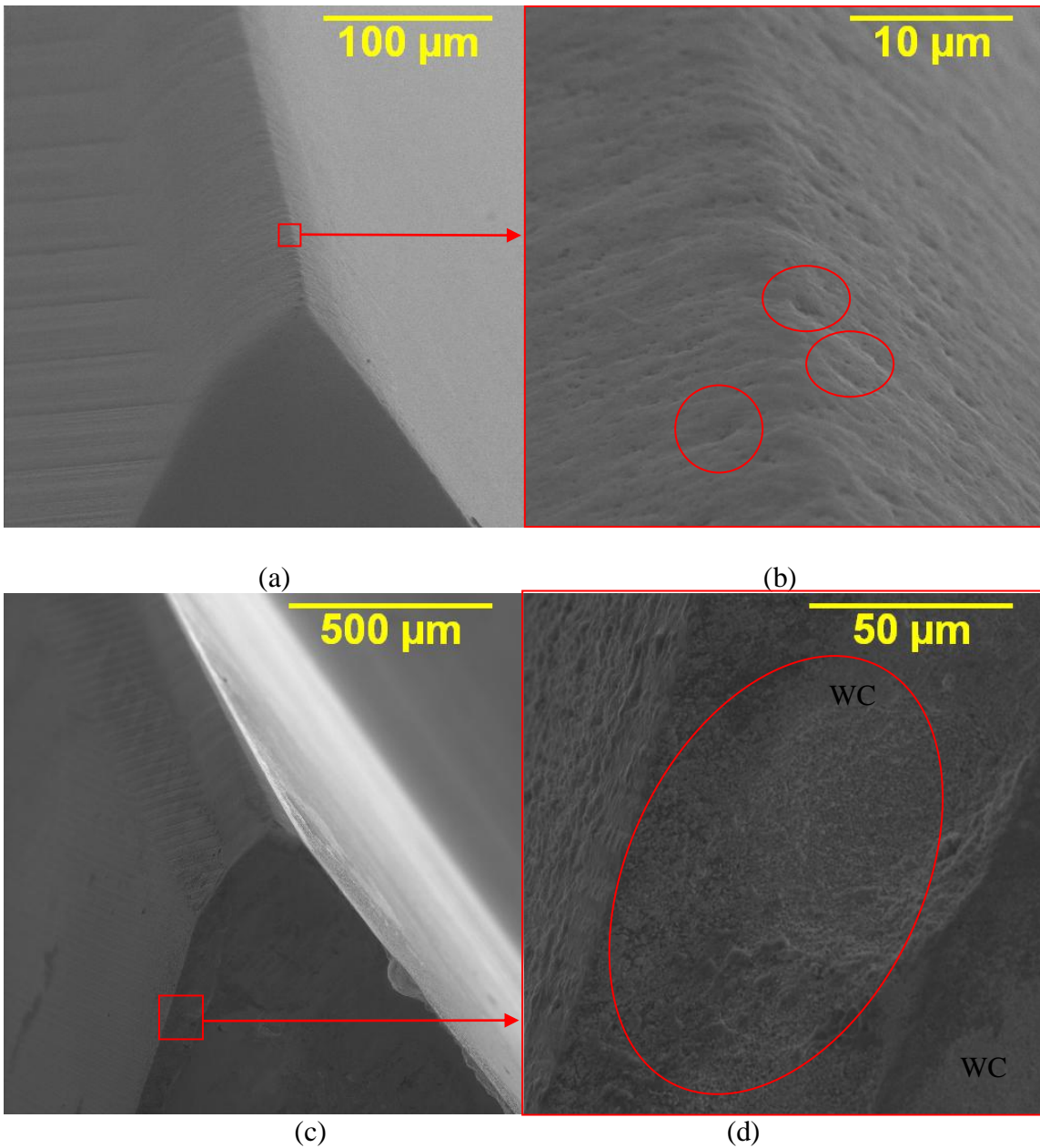


Figure 5.2.1-5: Cutting edge corner of etched WC (DC) for low speed Type II at hole 40 a) 500x and b) 5000x magnification; high speed Type II at hole 60 c) 100x and d) 10000x magnification.

Figure 5.2.1-5 shows the WC (DC) Experiment Type II drills at hole 40 and 60 for low speed and high speed, respectively, after etching away the titanium adhesion. Evidence of microscopic spalling and/or attrition can be found at the cutting edge corner in Figure 5.2.1-4 under high speed conditions and, under low speed conditions, along the cutting

edge in Figure 5.2.1-5b. In Figure 5.2.1-5d, the attrition wear mechanism is more evident as the exposed surface at helical flute near the flank face reveals a large volume of tool material under the high-speed condition. This large volume of attrition along the helical flute is not evident under the low-speed cutting condition. Spalling is defined as the removal of the carbide grains as the Co binder is removed by abrasive particles. Recall this form of abrasion is often referred to soft abrasion as defined in the section 2.2.1 of the literature review. In section 2.2.1, attrition was also defined as the removal of grains along with the adherent material due to the strong bond between the tool and chip.

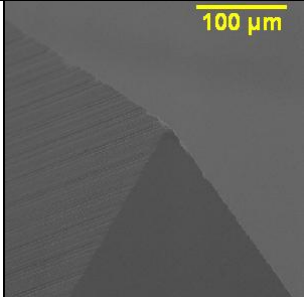
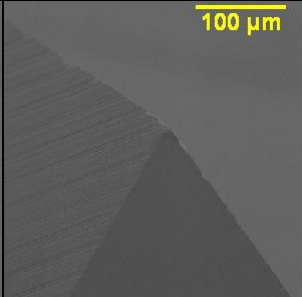
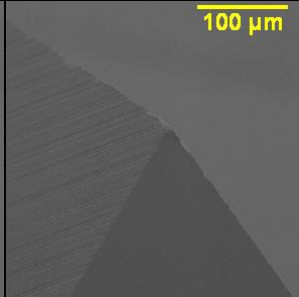
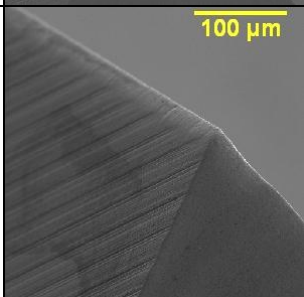
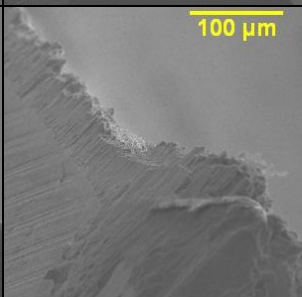
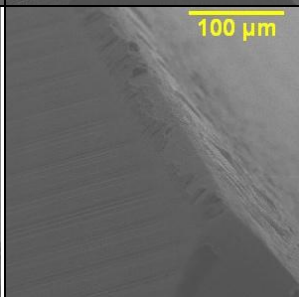
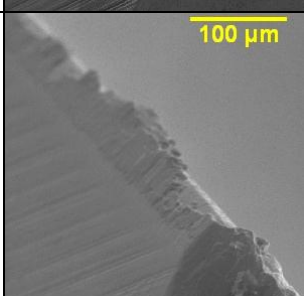
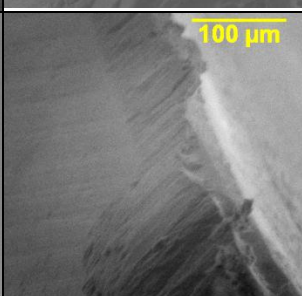
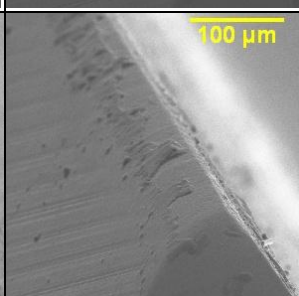
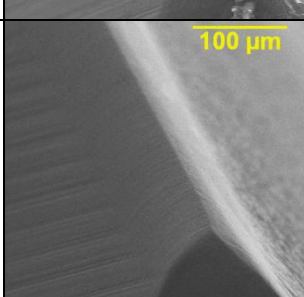
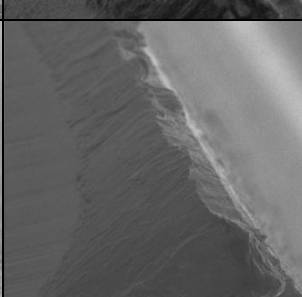
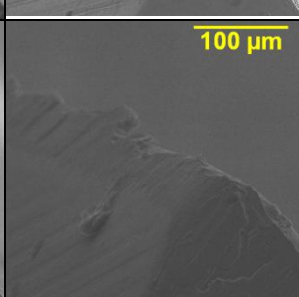
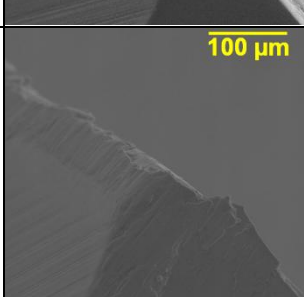
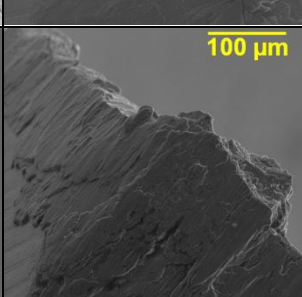
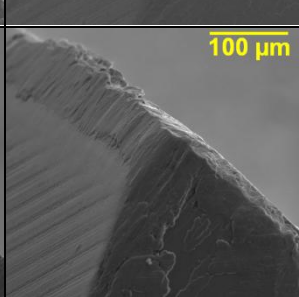
Hole No.	Type I, Low speed	Type II, High speed	Type II, Low speed
0			
20			
40			
60			
80			

Figure 5.2.1-6: Cutting edge corner SEM images for DC5 Carbide with various cutting distances and parameters. 500x magnification.

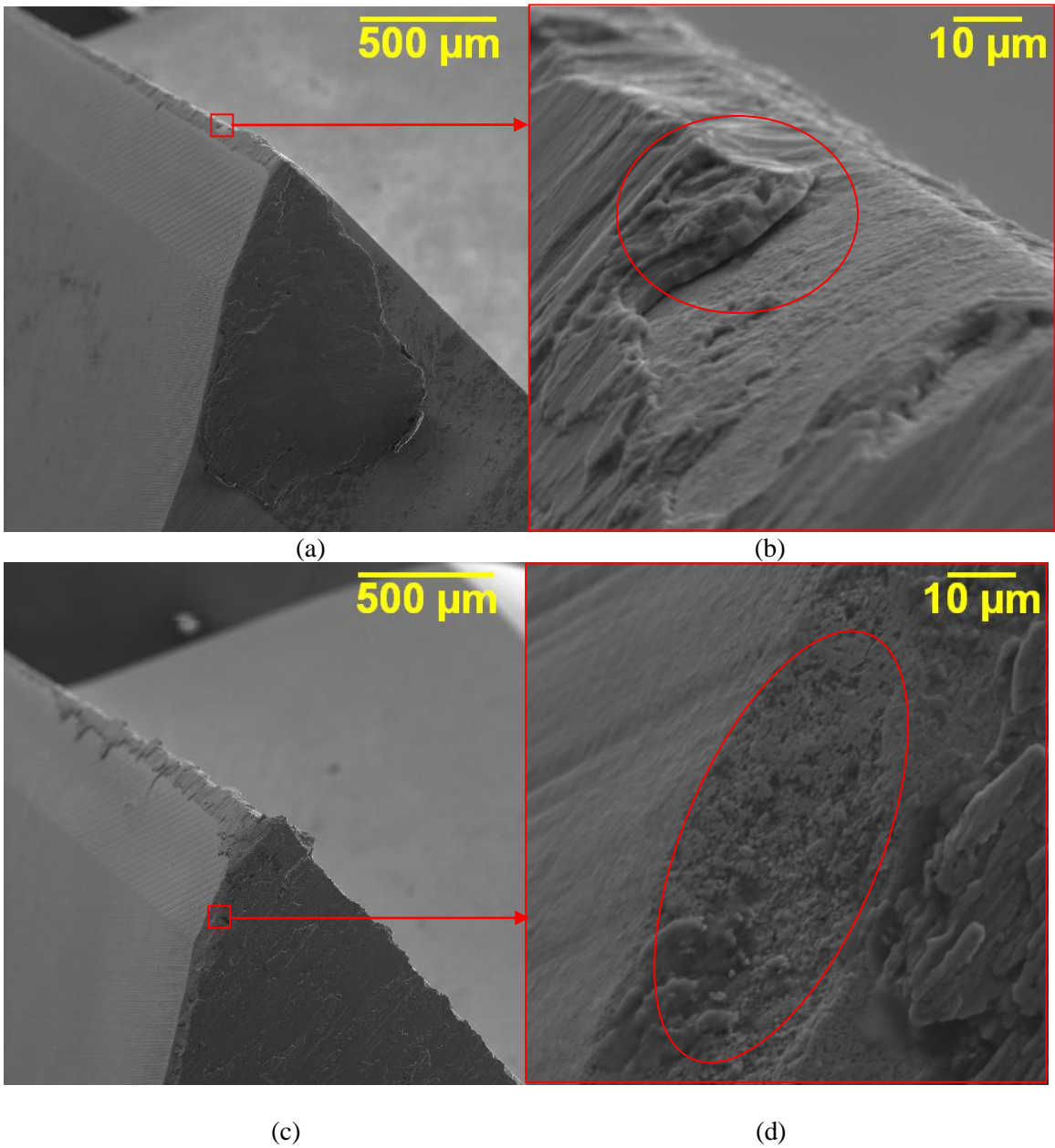


Figure 5.2.1-7: Low speed Type II WC (DC5) at hole 80 a) 100x and b) 2500x magnification; high speed Type II WC (DC5) at hole 80 c) 100x and d) 2500x magnification.

SEM images of WC (DC5) after every 20 holes can be seen in Figure 5.2.1-6. As with DC, titanium adhesion during the CFRP only cycle as indicated in low speed Experiment Type I for DC5.

Figure 5.2.1-7 displays WC (DC5) during Experiment Type II at hole 80 for low- and high-speed conditions. Figure 5.2.1-7a show that for low speed conditions, BUE often covers helical flute near the cutting edge; however, for high speed, it is apparent from Figure 5.2.1.7c that the BUE is removed near the flank surface. Figure 5.2.1-7d reveals in that region some titanium adhesion remains and several WC grains have been removed through the attrition mechanism, as with WC (DC). In Figure 5.2.1-7b, the titanium adhesion can be seen in mid action of separating from the WC tool.

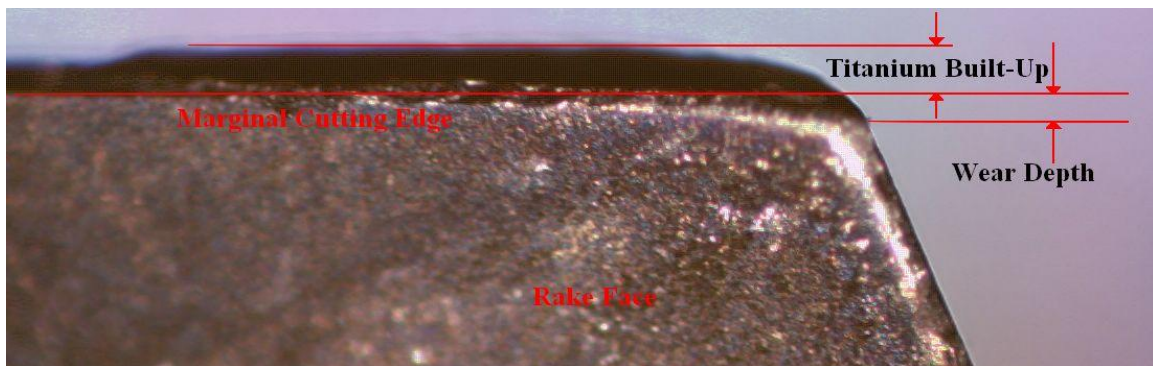


Figure 5.2.1-8: Titanium built up edge (low speed Experiment Type II hole 80).

Figure 5.2.1-8 the titanium built up edge on the marginal cutting edge viewed normal to the rake face. The Figure defines how the thickness value for the built up edge is measured along with a measured wear depth. The titanium BUE is measured from the outer diameter of the drill to the maximum height produced by the BUE. The wear depth in this instance is measured from the outer diameter to the maximum depth of wear found along the cutting edge normal to the drill circumference and marginal cutting edge. Note that this wear depth should not be confused with the averaged flank wear depth, which is more commonly used. Table 5.2.1-1 lists the recorded titanium BUE and wear depths along the marginal cutting edge for WC DC and DC5.

Table 5.2.1-1: Titanium built up edge and wear depth for WC (DC) at hole 80

WC (DC)	Experiment Type I		Experiment Type II	
	High speed	Low speed	High speed	Low speed
Ti BUE (μm)	85	44	34	18
Wear depth (μm)	27	48	58	51

From Table 5.2.1-1, it is clear that titanium BUE have higher average thickness values during high speed parameters in comparison to low speed parameters. In Experiment Type I, the low speed parameter produced larger wear depth whereas the high speed setting in Experiment Type II produced higher wear depths.

5.2.2 POLY-CRYSTALLINE DIAMOND (PCD)

The SEM images of the PCD drills in Figure 5.2.2-1 reveals pitting at the cutting edge corner occurs after drilling CFRP/Ti stacks. The fracture that results in the pitting may be due to mechanical fatigue. It is unlikely for graphitization to occur in this experiment [25]. Adhesion also occurs along the cutting edge and fills the pitting zone in minute amounts as compared to the WC drills; save for high speed Experiment Type I hole 80. During the CFRP only cycle, under both high and low speed settings, hole 60 shows titanium adhesion remaining along the pitting location at the cutting edge corner and along the cutting edge. Under high speed Experiment Type I conditions at hole 80 with the PCD drills, titanium adhesion fills the pitting zone and resembles the removed PCD tool material volume. Pitting can be seen to occur somewhere between hole 1 and hole 20. Afterwards, the wear

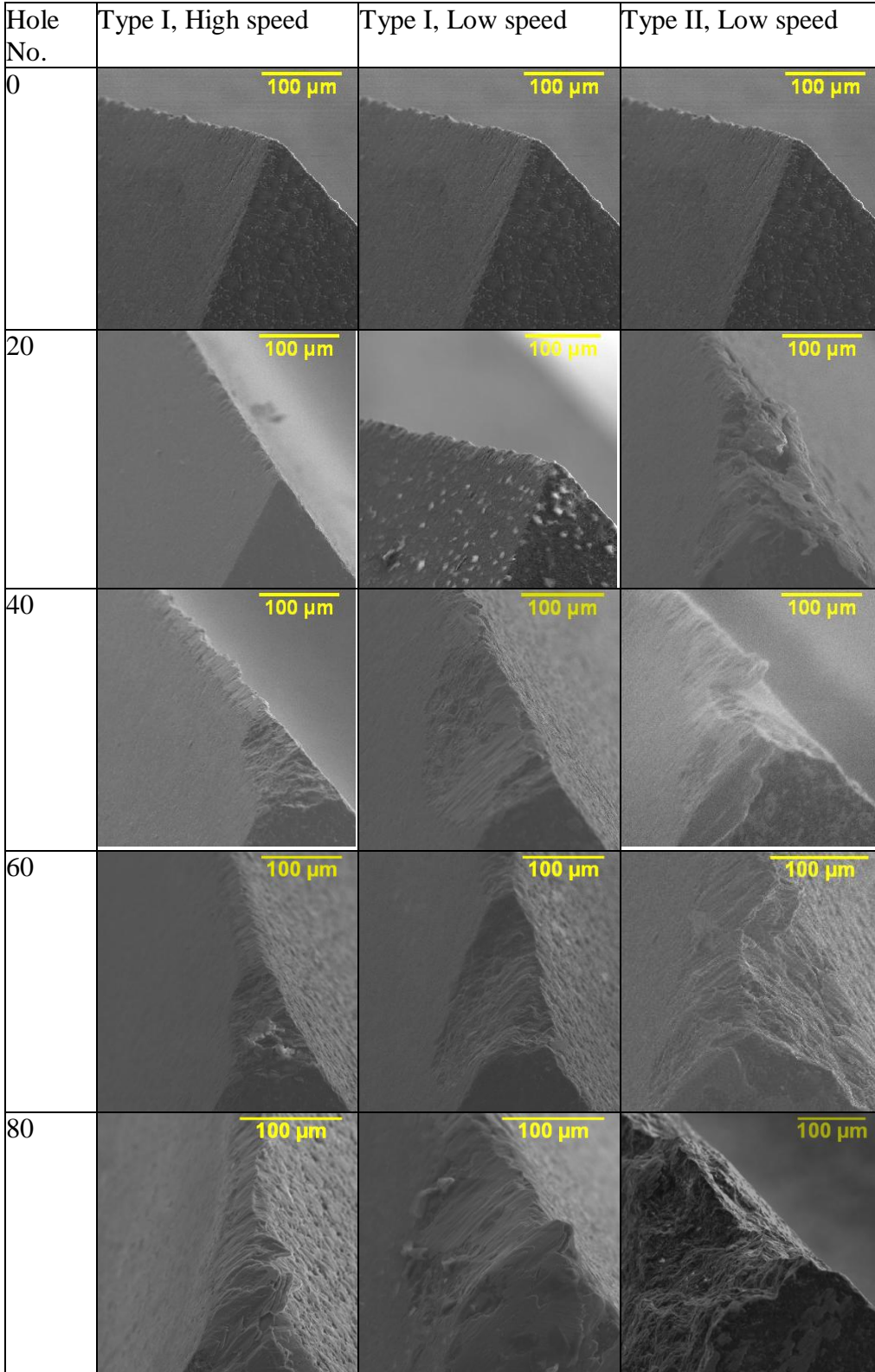
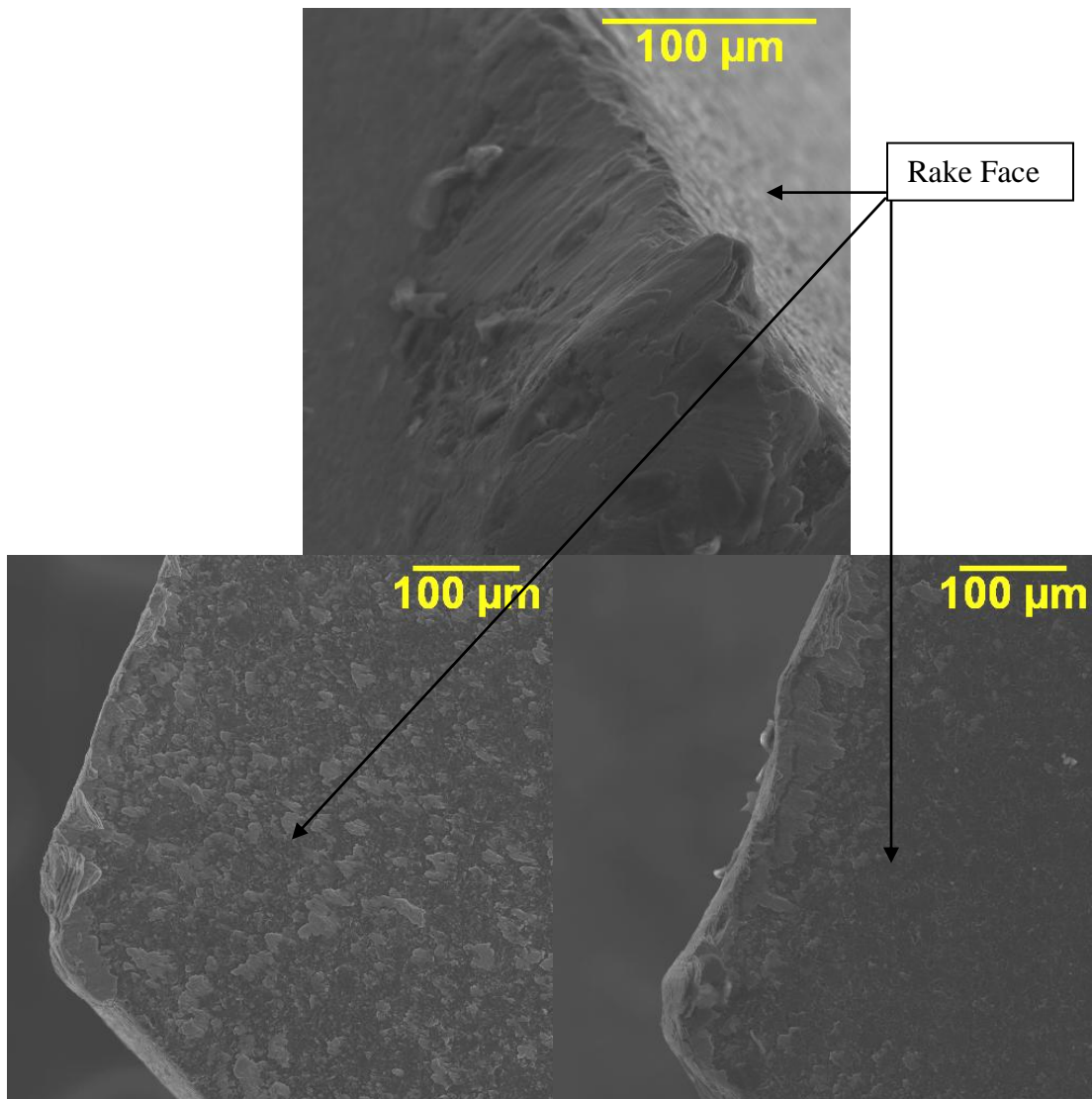


Figure 5.2.2-1: SEM images for PCD with various cutting distances and parameters. 500x magnification.



(a) G1 hole 80

(b) G2 hole 80

Figure 5.2.2-2: SEM images at hole 80 of PCD Experiment Type I with a) high and b) low speeds at 250x magnification.

Figure 5.2.2-2 shows a rake face view at the cutting edge corner for Experiment Type I PCD drills at hole 80. The PCD drill with the low speed setting shows a larger amount of tool material has been removed in comparison to the high speed setting at hole 80. As aforementioned in section 5.1, this can correlate to the rate at which the maximum thrust force is seen to increase.

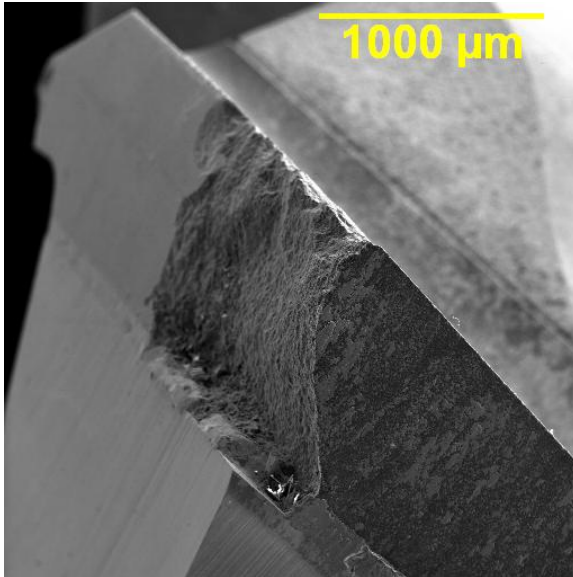


Figure 5.2.2-3: PCD low speed Type II hole 80 at 50x magnification.

Figure 5.2.2-3 shows the PCD drill used for low speed Type II after 80 holes. Different chips were produced after hole 73, which suggest the time of fracture. The effect of tool failure can also be seen in other trends such as force, hole diameter, and titanium burr heights.

For WC (DC) and (DC5), during CFRP only cycles, smooth wear marks with equivalent size as the carbon fibers are seen along the cutting edge as the tool undergoes abrasion. During stack drilling, titanium adhesion was prevalent on WC tools, whereas PCD was subject to trace amounts of titanium adhesion during low speed operations. However, in high speed Experiment Type I, PCD showed trace amounts of titanium adhesion until after the fourth drilling cycle (hole 61 to 80), where SEM images clearly show titanium adhesion replaced the removed PCD volume at the cutting edge corner. With carbide tools, the loss of tool material grains with the removal of titanium built up edge, otherwise known as attrition, can be observed in under both low speed and high speed

settings during stack drilling. However, attrition is more aggressive during high speed drilling, especially along the helical flute near the cutting edge corner. At the cutting edge corner, attrition is also more noticeable at high speeds. This is due to the higher chemical reactivity of titanium associated with the higher temperatures.

When drilling CFRP/Ti stacks with PCD, pitting is observed at the cutting edge corner possibly due to thermal and physical fatigue. In Experiment Type I, the PCD tool under the low speed setting exhibited more tool wear compared to the high speed setting. The higher wear rate in the low speed setting is reflected by the higher max thrust increase rate.

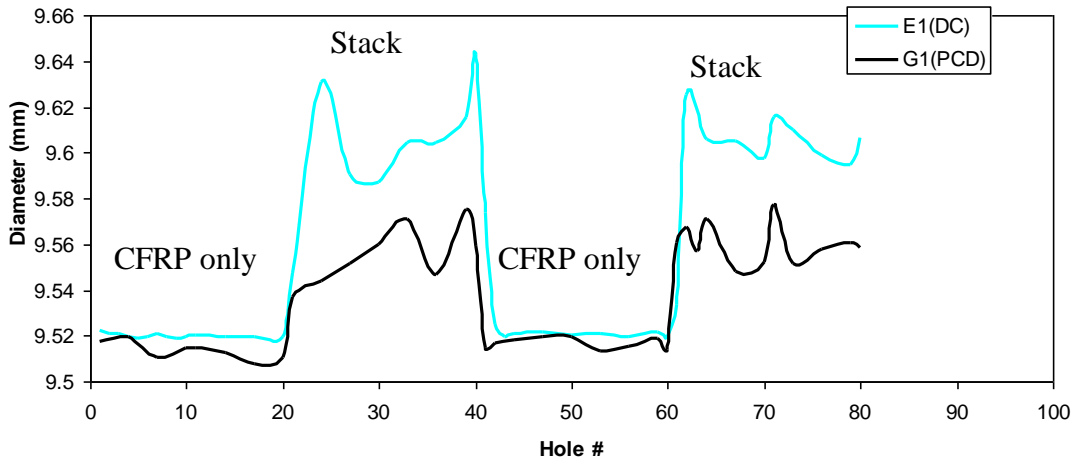
5.3 HOLE QUALITY

5.3.1 HOLE SIZE AND ROUNDNESS

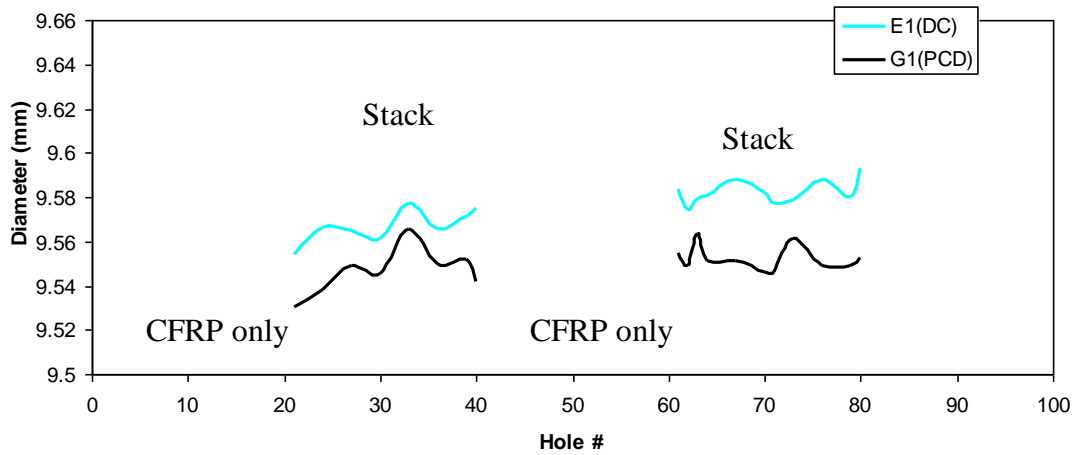
Hole size and roundness are measured with a CMM by taking at least eight points. Hole size is the measure of the hole diameter, which defines the size tolerance. Hole roundness specifies a tolerance zone bounded by two concentric circles. The importance to hole roundness lies within fatigue life as lower roundness values lead to longer fatigue life [41].

The hole diameter for high speed Experiment Type I is displayed in Figure 5.3.1-1. During the transition from CFRP only to stack drilling, a large discrepancy in diameter could be observed. When drilling with WC (DC), this large discrepancy in diameter is 28 μm between hole 20 and 21 and 14 μm between hole 60 and 61. For WC, the average difference between diameters when drilling CFRP only and stacks is approximately 78 μm , which is roughly equivalent to the 85 μm titanium adhesion averaged measurement along the outer surface of the marginal cutting edge, otherwise known as the helical flute, near the cutting edge corner (Figure 5.2-1) at hole 80. However, the titanium adhesion observed on the marginal cutting edge of PCD drills were seen as negligible. Figure 5.3.1-1 shows for PCD that a 26 μm diameter increase is observed in CFRP during stack drilling between holes 21 and 21 while holes 60 and 61 show a difference of 47 μm . The average difference between diameters when drilling CFRP only and stacks with PCD is approximately 43 μm . That is, titanium adhesion along the helical flute contributes to the increase in diameter seen in CFRP during stack drilling. Further observation of Figure

5.3.1-1 reveals an increase in diameter proportional to the hole number during stack drilling in both CFRP and titanium plates.

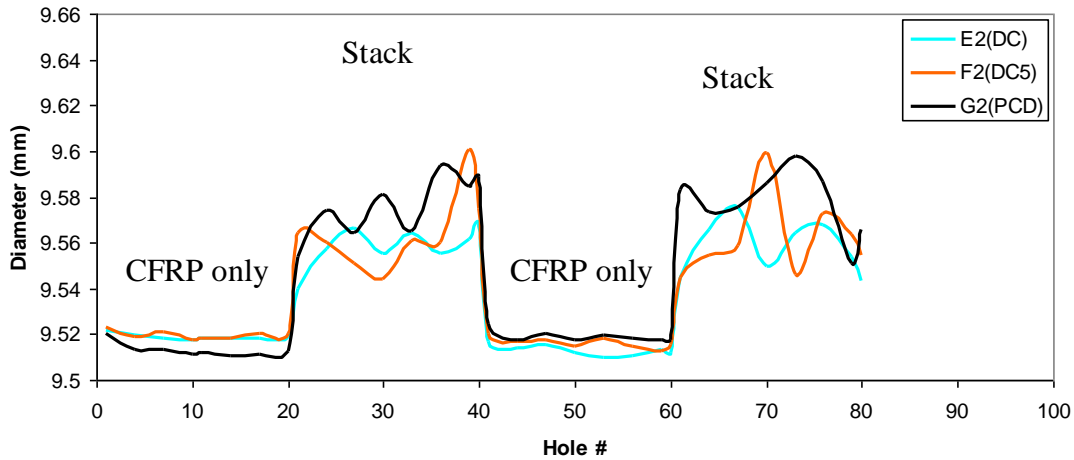


(a) CFRP hole diameter

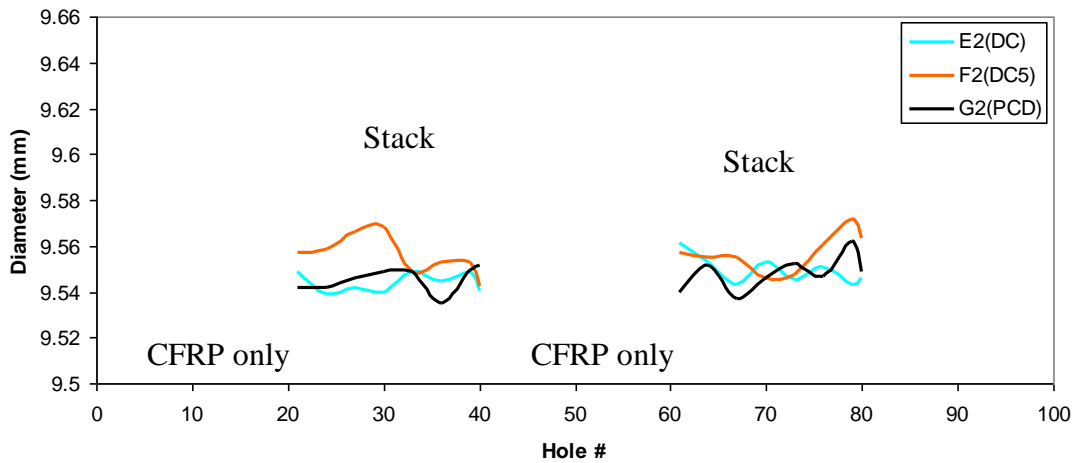


(b) Ti hole diameter

Figure 5.3.1-1: High speed Type I diameter a) CFRP and b) Titanium.



(a) CFRP hole diameter



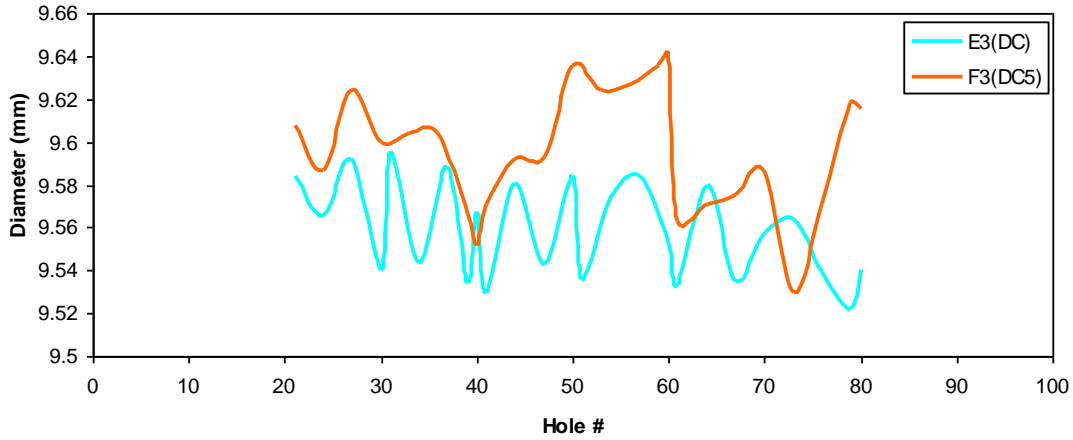
(b) Ti hole diameter

Figure 5.3.1-2: Low speed Type I diameter a) CFRP and b) Titanium.

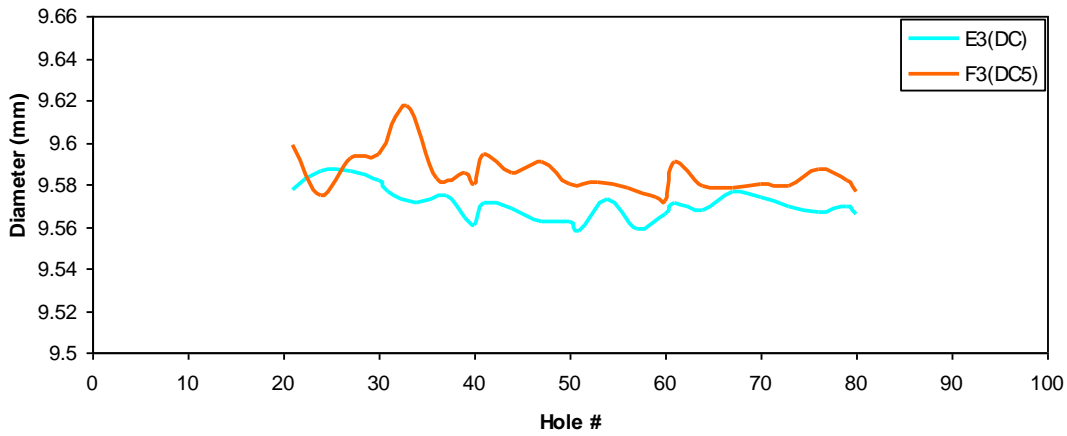
Figure 5.3.1-2 shows low speed Experiment Type I hole diameters. This Figure reveals the same trend in diameter as with high speed Experiment Type I; however, diameters during stack drilling are nearly the same between WC and PCD in low speed whereas in high speed, WC diameters were larger. When drilling with WC (DC), the large discrepancy in CFRP diameter shown by Figure 5.3.1-2 is 21 μm between hole 20 and 21 and 33 μm between hole 60 and 61. For WC, the average difference between diameters when drilling CFRP only and stacks is approximately 45 μm , which is equivalent to the average of 44 μm titanium adhesion measured along the outer surface of the marginal

cutting edge at hole 80. The titanium adhesion observed on the marginal cutting edge of PCD drills were again seen as negligible. Figure 5.3.1-2 shows for PCD that a 63 μm diameter increase is observed in CFRP during stack drilling between holes 21 and 21 while holes 60 and 61 show a difference of 59 μm . The average difference between diameters when drilling CFRP only and stacks with PCD is approximately 61 μm .

The diameter enlargement in accordance to speed agrees well for WC drills with the findings of D. Kim & M. Ramulu in [35]. However, for PCD, Figure 5.3.1-1 and Figure 5.3.1-2 show CFRP hole diameters are larger at the low speed parameter during stack drilling. This could be due to the excessive pitting seen in Section 5.2.2, which also correlates to the higher thrust increase rate seen in Section 5.1. The larger non-uniform wear would result in higher unbalanced forces in the radial direction. This observation by comparing results from Section 5.1 and 5.2 also agrees with the CFRP hole diameters observed when drilling with WC. That is, vibration increases with tool wear.



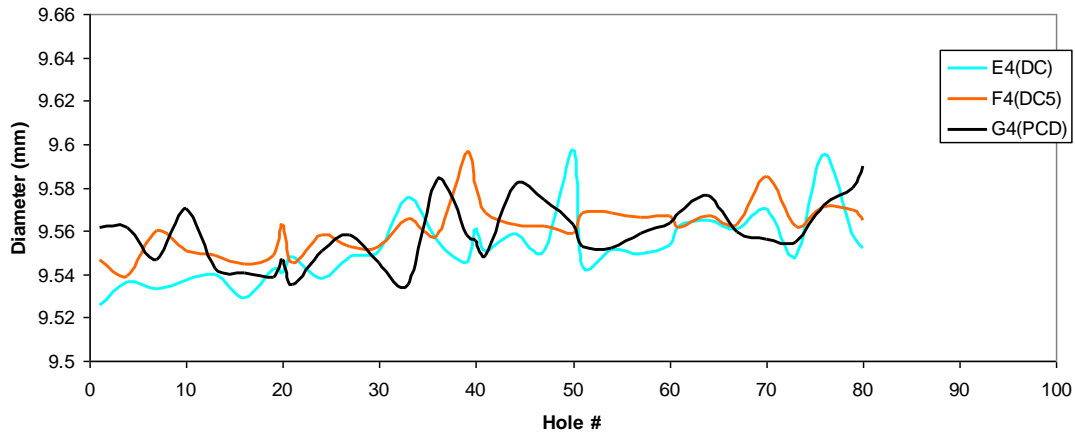
(a) CFRP hole diameter



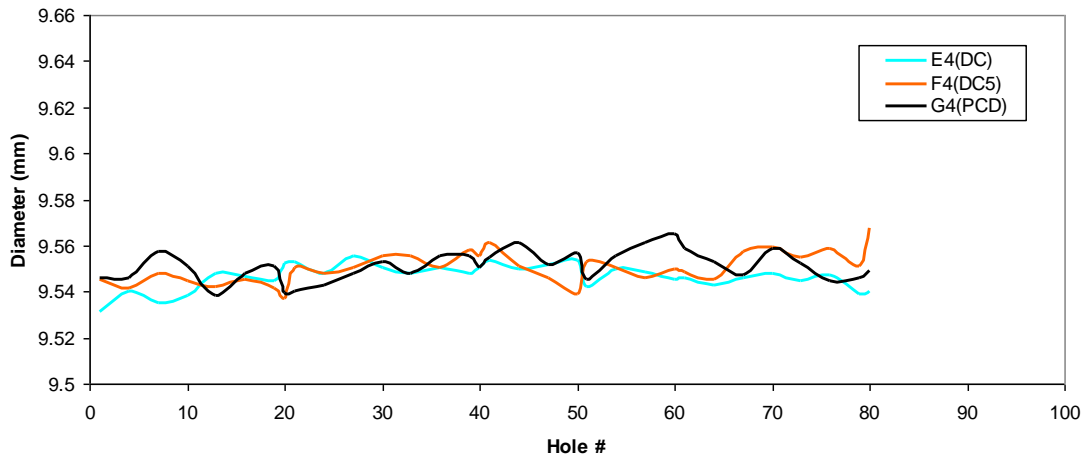
(b) Ti hole diameter

Figure 5.3.1-3: High speed Type II diameter a) CFRP and b) Titanium.

Figure 5.3.1-3 reveals a decreasing trend in hole diameters in both CFRP and titanium during high speed Experiment Type II. When drilling with WC DC5, Figure 5.3.1-3a shows a sharp decrease in CFRP hole diameters occur at holes 41 and 61, due to the prior etching at holes 40 and 60, followed by a diameter increase with the addition of a new layer of titanium adhesion. In Figure 5.3.1-3b, small increases in diameters occur at holes 41 and 61 when drilling with WC DC5 can be observed as new titanium adhesion layers are reformed onto the tool helical flute near the cutting edge corner and along the cutting edge.



(a) CFRP hole diameter



(b) Ti hole diameter

Figure 5.3.1-4: Low speed Type II diameter a) CFRP and b) Titanium.

Figure 5.3.1-4 shows low speed Experiment Type II CFRP and titanium hole diameters. Figure 5.3.1-4a shows WC drills produces a steady increase in hole diameter up to hole 40 when drilling CFRP. After hole 40, WC drilled holes begins to approach a constant diameter of 9.56 μm . PCD drilled holes in CFRP have a consistent diameter up to hole 40. After hole 40, PCD drilled holes begin to increase.

Figure 5.3.1-4b shows hole diameters drilled into the titanium plates. WC drilled holes in titanium increase at the beginning. When drilling with WC, diameters in the titanium

plates begin to approach a constant diameter after hole 20 and decrease in diameter after hole 50. PCD produced consistent hole diameters in titanium for the first 24 holes, after which a shift of 0.007 μm occurs. From hole 27 onward, the diameter once again remains constant; however, after hole 50, the range in diameter noticeably increases.

The trend seen in low speed Experiment Type II suggest the increase in BUE on WC tools increase the diameter in stack drilling up to a certain point after which the reduction of drill diameter due to tool wear becomes larger in magnitude than the BUE that forms on the tool surface. Recall in Figure 5.2.1-4, rounding at the cutting edge corner is observed.

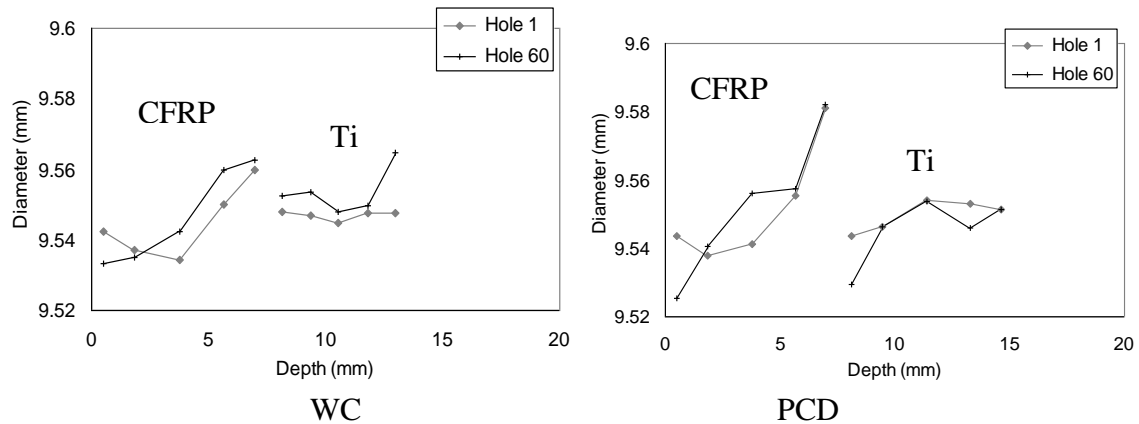
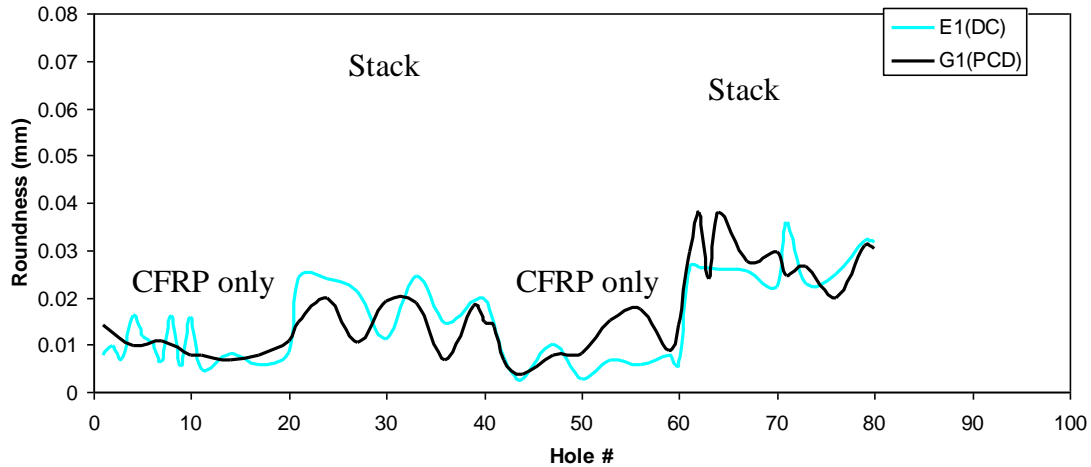


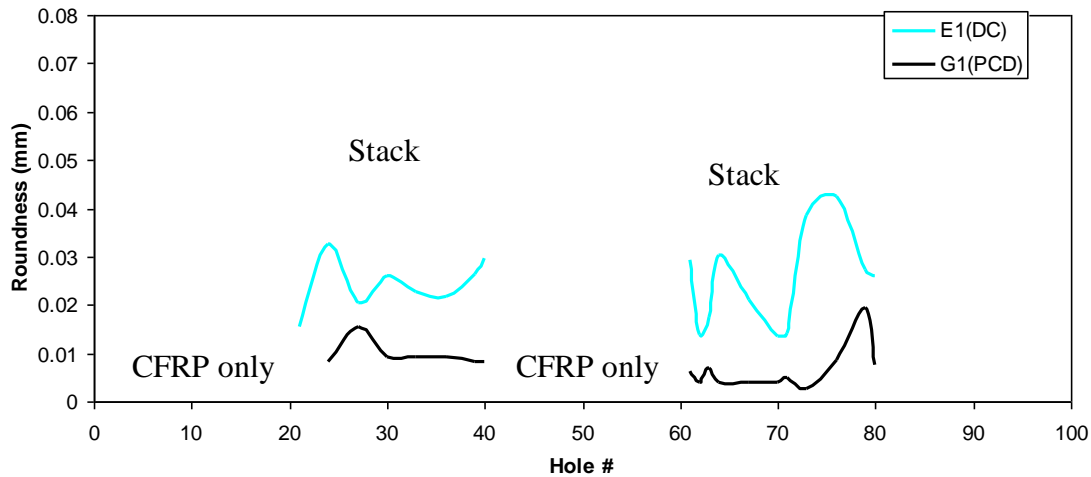
Figure 5.3.1-5: Hole profile across the entire stack at holes 1 and 60 for low speed Experiment Type II.

Figure 5.3.1-5 shows the hole profiles through the entire stack when drilling with WC and PCD for low speed Experiment Type II at holes 1 and 60. The holes drilled by WC and PCD are both tapered and increase with depth for both the 1st and 60th hole. With WC, an increase in diameter from hole 1 to hole 60 can be seen. However, multiple

points along 1st and 60th holes drilled by PCD match with the diameter through the overall profile. This may indicate relatively little change has occurred. A known cause for diameter and cylindricity errors in drilling is due to thermal distortion of the drill in dry and near-dry drilling. In a model by M. Bono and J. Ni, it was found that the final shape of a hole was determined by the contraction of the workpiece and the expansion of the drill [42]. Also, whereas in low speed drilling cutting fluid reduces heat generation and removes heat, cutting fluid in high speed drilling is limited only to heat removal [43].



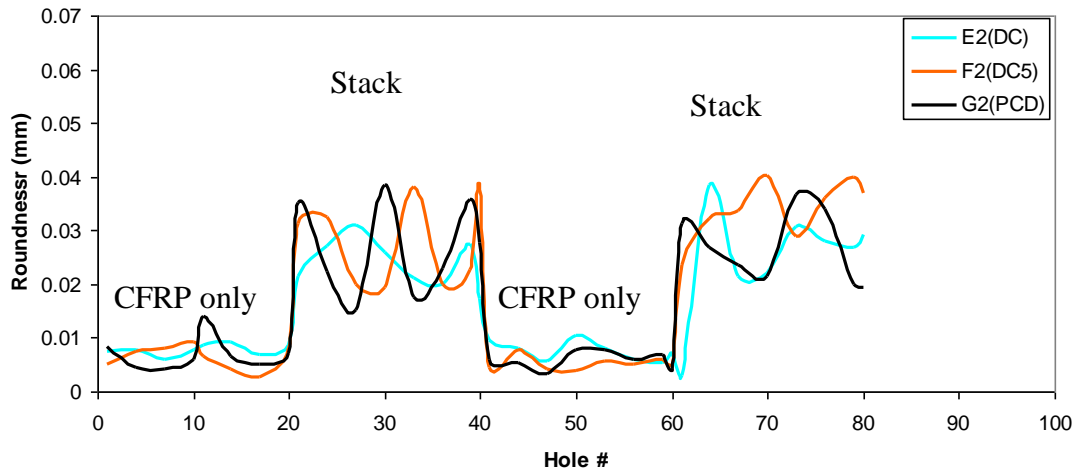
(a) CFRP hole roundness



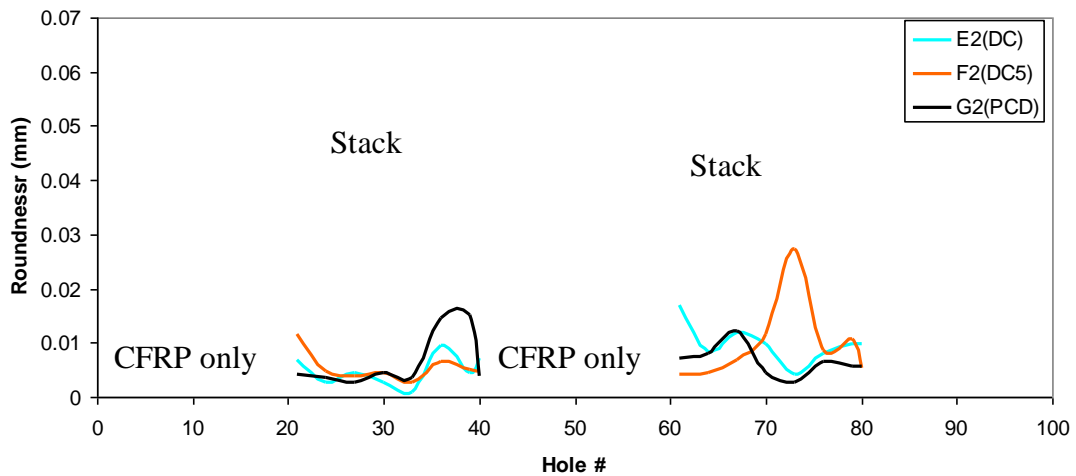
(b) Ti hole roundness

Figure 5.3.1-6: High speed Experiment Type I roundness a) CFRP and b) Titanium.

Figure 5.3.1-6 shows hole roundness for CFRP and titanium during Experiment Type I at high speeds when drilling with WC and PCD. In CFRP, roundness is seen to increase during stack drilling as with the diameter. Also, CFRP hole roundness values between PCD and WC are nearly equivalent, whereas in titanium, PCD show lower roundness values. The lower roundness in titanium produced by PCD tools may be due to the lower speed.



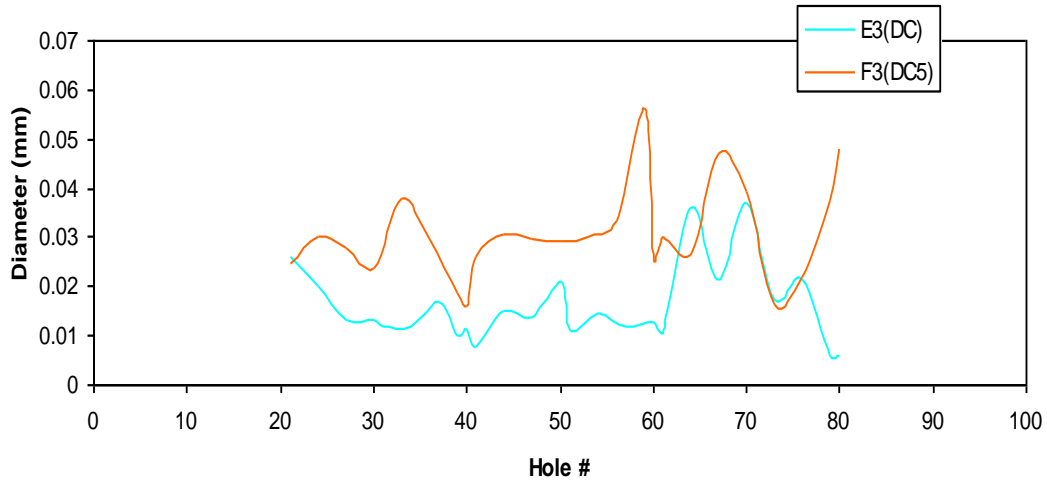
(a) CFRP hole roundness



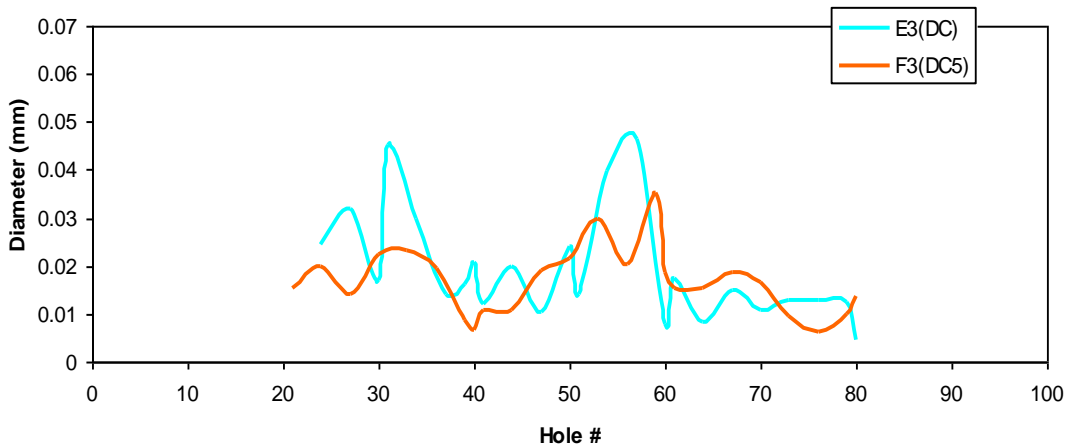
(b) Ti hole roundness

Figure 5.3.1-7: Low speed Experiment Type I roundness a) CFRP and b) Titanium.

Roundness values for low speed Experiment Type I can be found in Figure 5.3.1-7. As in for high speed Experiment Type I, we can observe roundness values in the titanium plate are generally lower than the counterpart roundness found in CFRP during stack drilling. In CFRP/Ti stack drilling, roundness in CFRP holes increase in comparison to the CFRP only cycle.



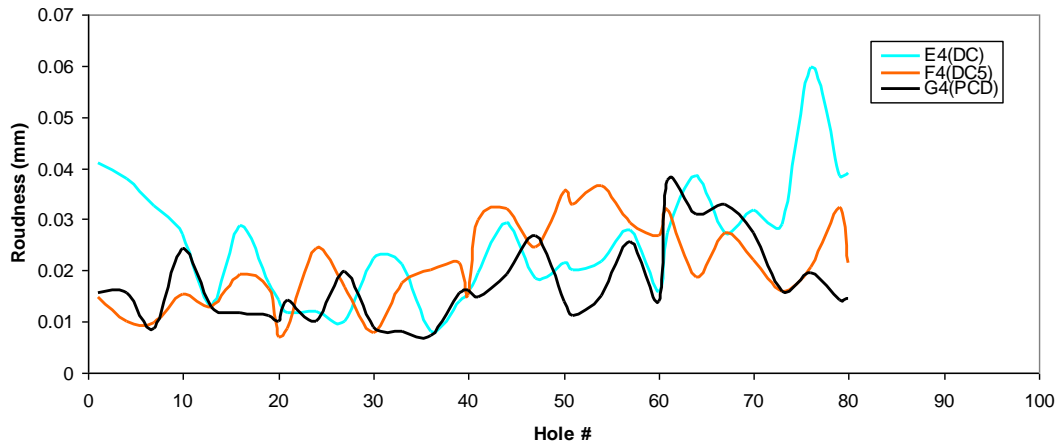
(a) CFRP hole roundness



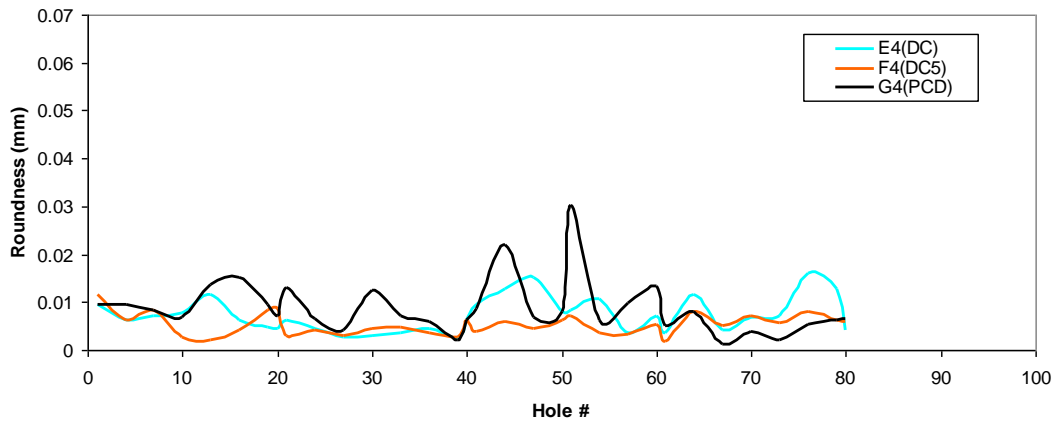
(b) Ti hole roundness

Figure 5.3.1-8: High speed Experiment Type II roundness a) CFRP and b) Titanium.

Roundness values found in holes from the titanium plate during high speed Experiment Type II decrease with hole number. However, with the removal of titanium adhesion at hole 40 and reapplication of titanium adhesion at hole 41, a noticeable increase in roundness values occur. In CFRP, Figure 5.3.1-8a shows a large increase in roundness at hole 61 after the titanium adhesion was etched from the tool at hole 60. Values from holes 1 through 20 were omitted because of the increased feed rate from holes 1 through 10 greatly affected the titanium adhesion thickness in that region.



(a) CFRP hole roundness



(b) Ti hole roundness

Figure 5.3.1-9: Low speed Experiment Type II roundness a) CFRP and b) Titanium.

Figure 5.3.1-9 shows the hole roundness in CFRP and titanium when drilling with WC and PCD during Experiment Type II at low speed. In CFRP, hole roundness decreases during the first 40 holes then increases during the last 40 holes when drilling with both WC and PCD. Hole roundness in titanium also decreases during the first 40 holes with WC and PCD; however, the roundness shifts after hole 40. For WC, the roundness continues to be nearly constant in the last 40 holes whereas PCD drilled holes reveal a

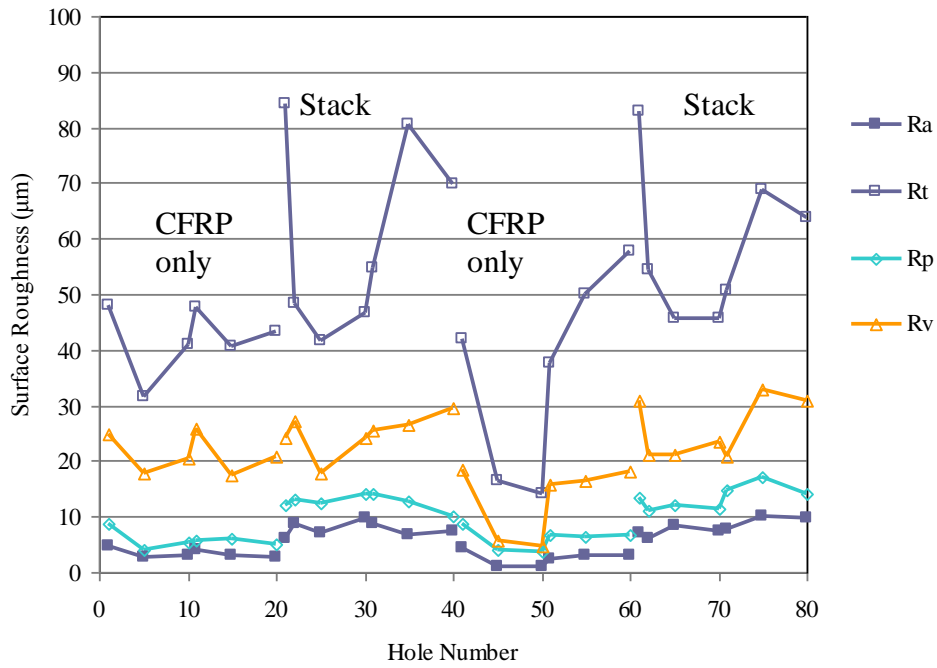
decreasing trend until reaching hole 73 where a noticeable increase begins. In both CFRP and titanium, large increases in roundness directly at holes 41 and 61 can be observed. It is highly likely the result of the removal of titanium adhesion at holes 40 and 60.

From Experiment Type I, hole diameter and roundness in CFRP are seen to be higher during stack drilling compared to CFRP only drilling. This difference in diameter is equivalent to the thickness of the titanium adhesion found along the helical flute near the cutting edge corner. The sharp decrease in hole diameter and roundness directly after etching followed by a large increase as a new layer of titanium adhesion forms seen in Experiment Type II supports the possibility that the titanium adhesion effects hole diameter and roundness. Not only does it seem to affect hole diameter and roundness values from CFRP drilling, but also it affects the diameter and roundness values found in titanium drilling. As the titanium adhesion thickness increases, hole diameter increases. Hole diameter becomes constant as the titanium thickness approaches a limit and as tool wear increases, where it then begins to decrease as the increase in tool wear becomes greater. PCD hole diameters are found to be more consistent because of the lower levels of titanium adhesion. Also, thermal distortion can also be observed through the thickness of the stack plates for holes drilled by both WC and PCD as hole diameter increases with depth.

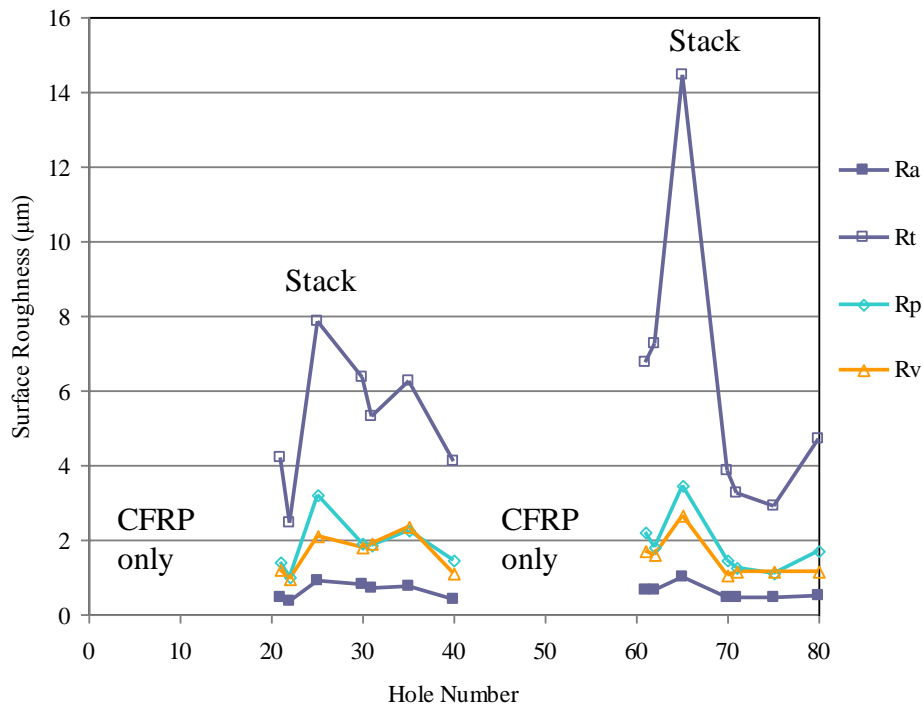
5.3.2 SURFACE ROUGHNESS

Surface roughness is an important quality in applications where components undergo fatigue. There are several definitions used in measuring surface roughness, some which are defined in Section 4.5.4. Lower surface roughness values in open holes show to have increased fatigue life in [41]. Surface roughness parameters used in this study include Ra, Rt, Rv, and Rp where Ra is defined as the average of all the peak and valley heights compared to the mean line, Rt measures the highest peak to the lowest valley, the highest peak above the mean line is defined as Rp, and the lowest valley beneath the mean line is defined as Rv.

Figure 5.3.2-1 shows the hole surface roughness values for both CFRP and titanium plates for WC (DC) high speed Experiment Type I. Three observations can be made from this figure: first, stack drilling enlarges CFRP hole surface roughness; second, titanium roughness values are significantly lower than those in CFRP; and third, surface roughness is nearly constant for each individual cycle on holes measured in both CFRP and titanium. However, when comparing each cycle to each other in CFRP, there is a decrease in Ra between the first and second CFRP only drilling cycles while an increase in Ra between the first and second stack drilling cycles can be seen.

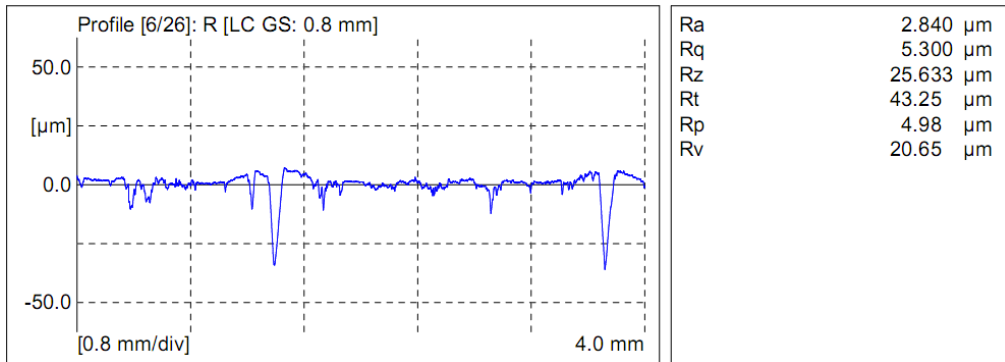


(a) CFRP hole surface roughness

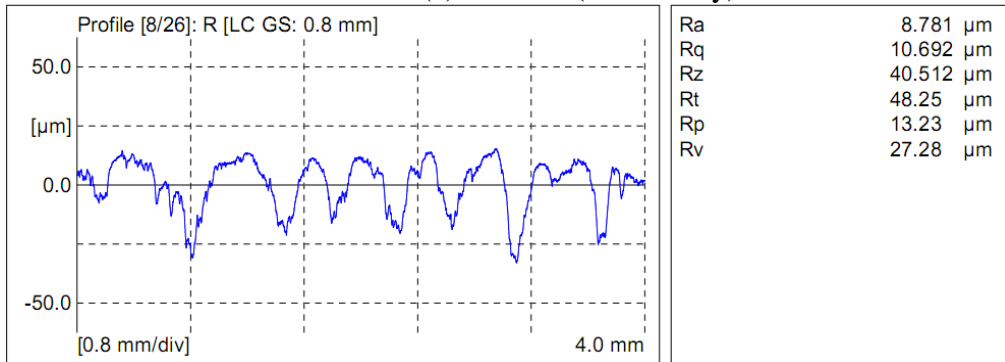


(b) Titanium hole surface roughness

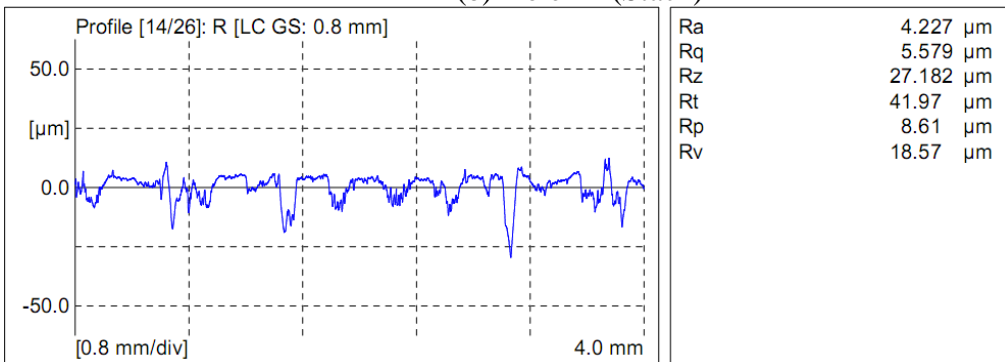
Figure 5.3.2-1: WC (DC) high speed Experiment Type I hole surface roughness for a) CFRP and b) titanium.



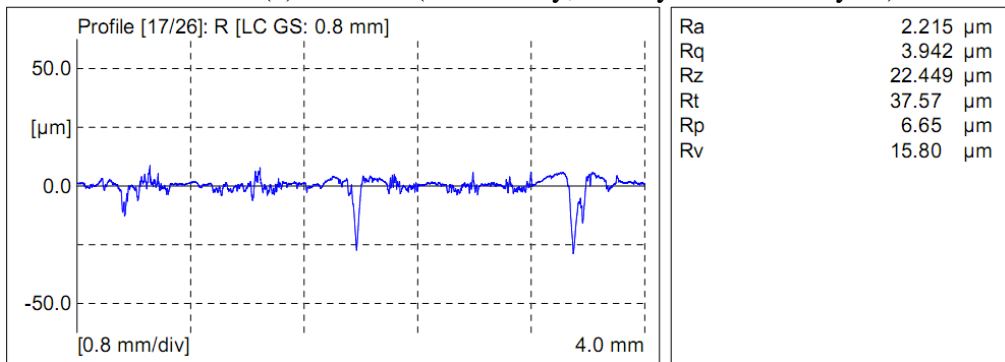
(a) Hole 20 (CFRP only)



(b) Hole 22 (Stack)



(c) Hole 41 (CFRP only, shortly after stack cycle)

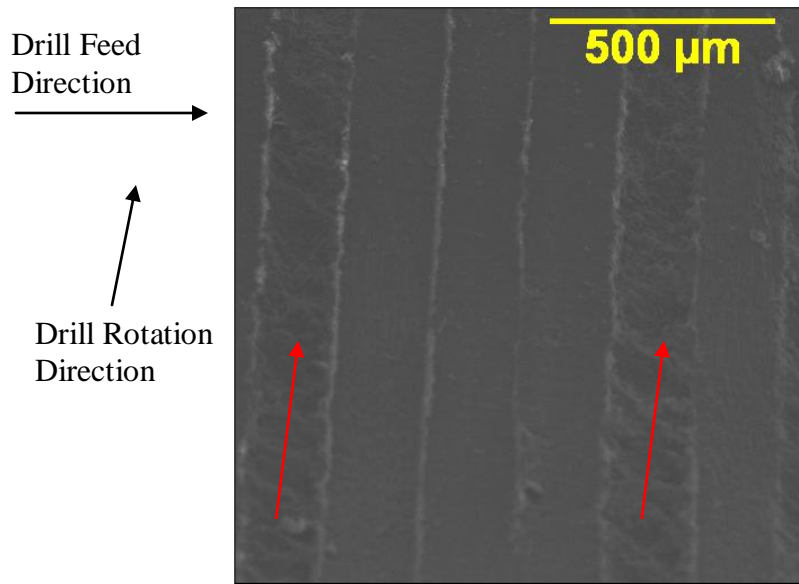


(d) Hole 51 (CFRP only)

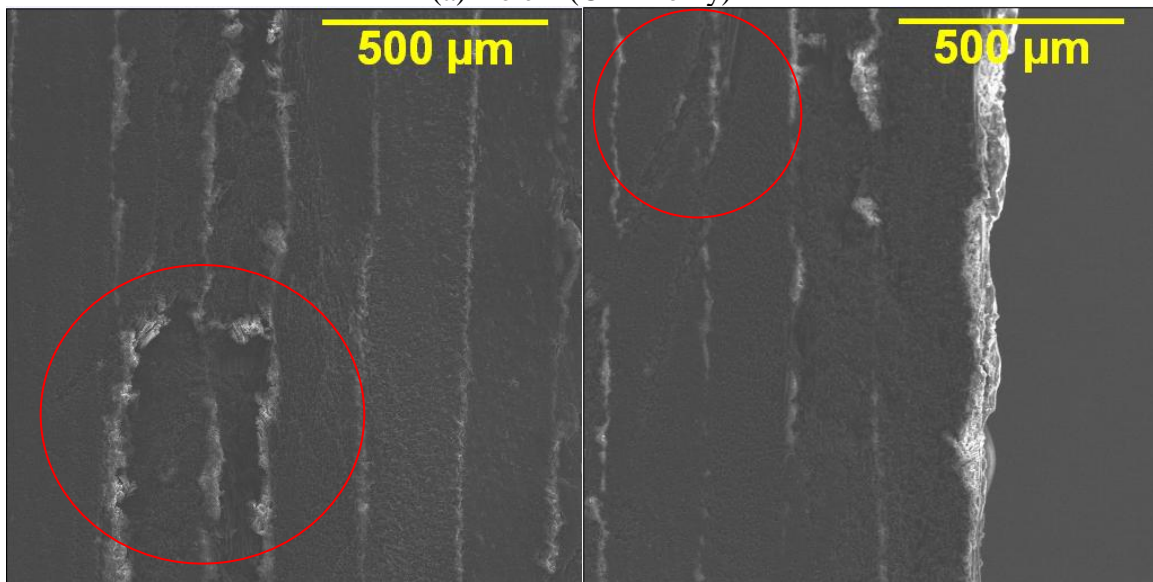
Figure 5.3.2-2: WC (DC) drilled CFRP hole surface profile during high speed Experiment Type I at a) hole 20, b) hole 22, c) hole 41, and d) hole 51.

Figure 5.3.2-2 displays the surface roughness profile for CFRP during CFRP only and stack drilling cycles. Valleys measured from the mean line indicate fiber pullout. During the first CFRP only drilling cycle (Figure 5.3.2-2a), fiber pullout occurs; however, the occurrence of fiber pull out in the first cycle is less frequent in comparison to the stack cycles (Figure 5.3.2-2b). Shortly after the stack drilling cycle (Figure 5.3.2-2c), fiber pullout still occurs frequently as titanium adhesion continues to interfere with the hole quality; however, Ra values are lower than during stack drilling. Figure 5.3.2-2d reveals after drilling 10 holes in the second CFRP only cycle (hole 51), the occurrence of severe fiber pullout becomes less frequent as with the first cycle; after hole 51, the Ra values in the second CFRP only cycle also return to the same magnitudes as found in the first cycle.

Figure 5.3.2-3 shows SEM images taken of the CFRP hole surface during CFRP only drilling (Figure 5.3.2-3a, hole 1) and stack drilling (Figure 5.3.2-3b-c, hole 29). In Figure 5.3.2-3a, the arrows indicate fiber pullout located along plies at 135° orientations. In Figure 5.3.2-3b, severe fiber pullout is found along plies at 90 and 135° degree orientations. 5.3.2-3c shows scratches on the CFRP hole surface with equivalent widths to the titanium chips.



(a) Hole 1 (CFRP only)

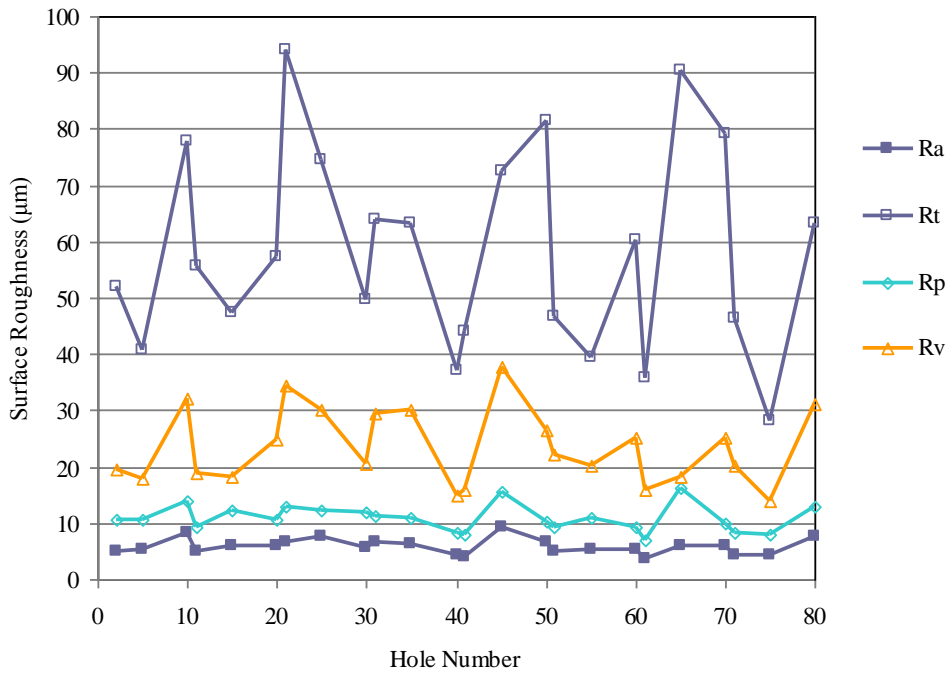


(b) Hole 29 (stack)

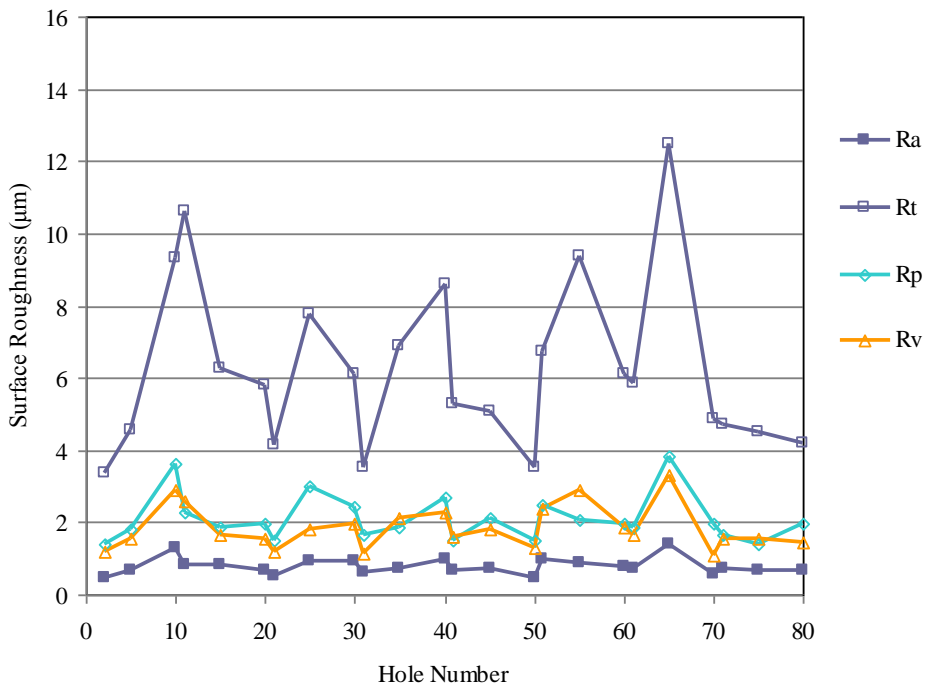
(c) Hole 29 (stack)

Figure 5.3.2-3: WC (DC) high speed Experiment Type I CFRP hole surface SEM images at a) hole 1 and b-c) hole 29 at 100x magnification. Red locators indicate hole defects.

Figure 5.3.2-4 displays the CFRP and titanium holes surface roughness under high speed Experiment Type II. Surface roughness values during high speed Experiment Type II are relatively constant with hole number when drilling with WC (DC).

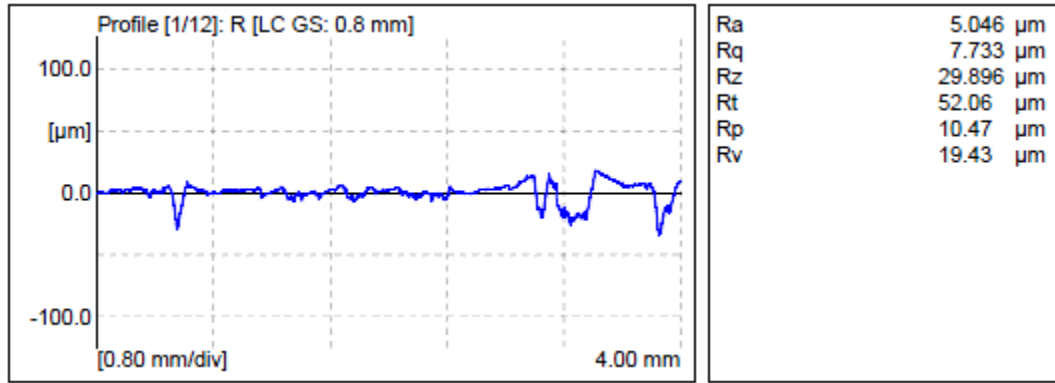


(a) CFRP hole surface roughness

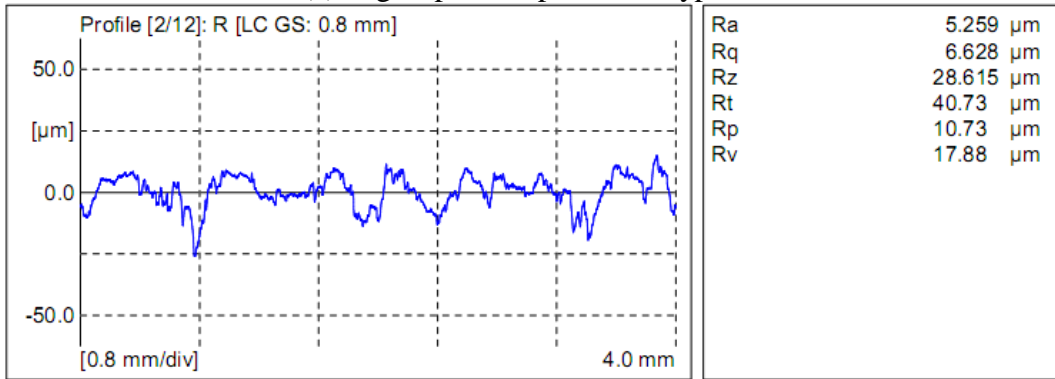


(b) Titanium hole surface roughness

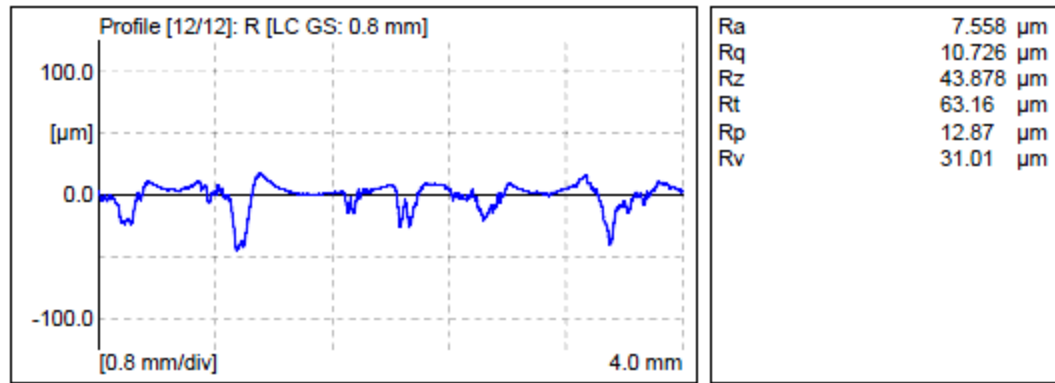
Figure 5.3.2-4: WC (DC) high speed Experiment Type II hole surface roughness for a) CFRP and b) titanium.



(a) High Speed Experiment Type II, Hole 2



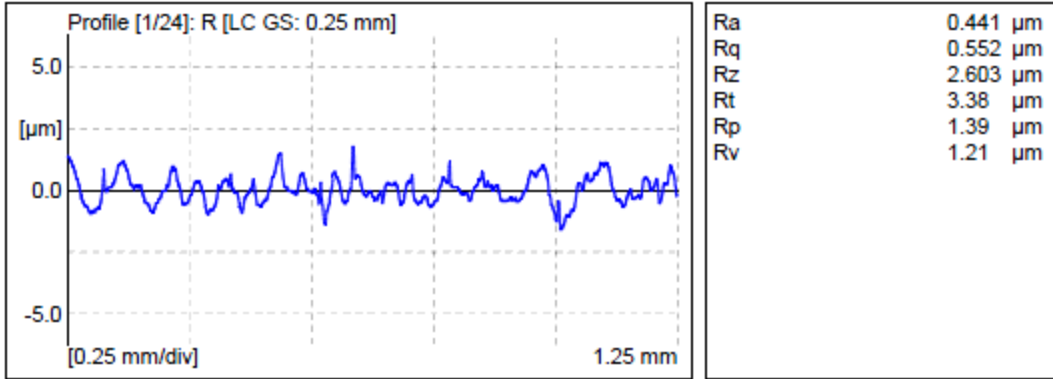
(b) High Speed Experiment Type II, Hole 5



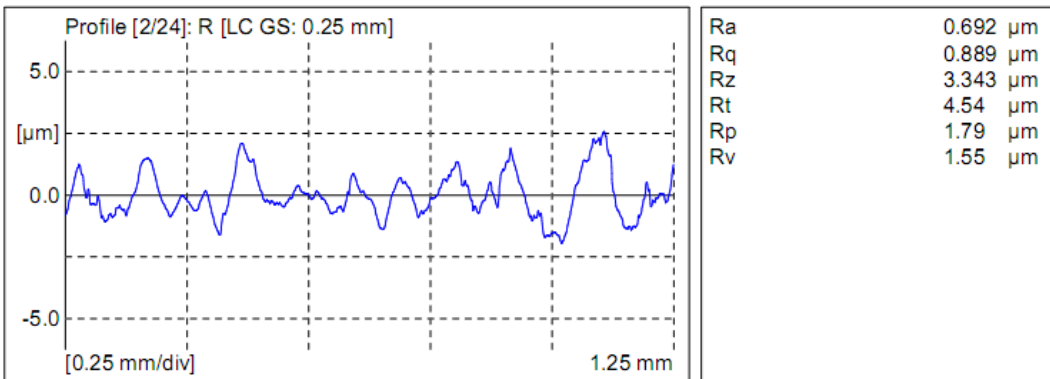
(c) High Speed Experiment Type II, Hole 80

Figure 5.3.2-5: WC (DC) drilled CFRP hole surface profiles from high speed Experiment Type II at a) hole 2, b) hole 5 and c) hole 80.

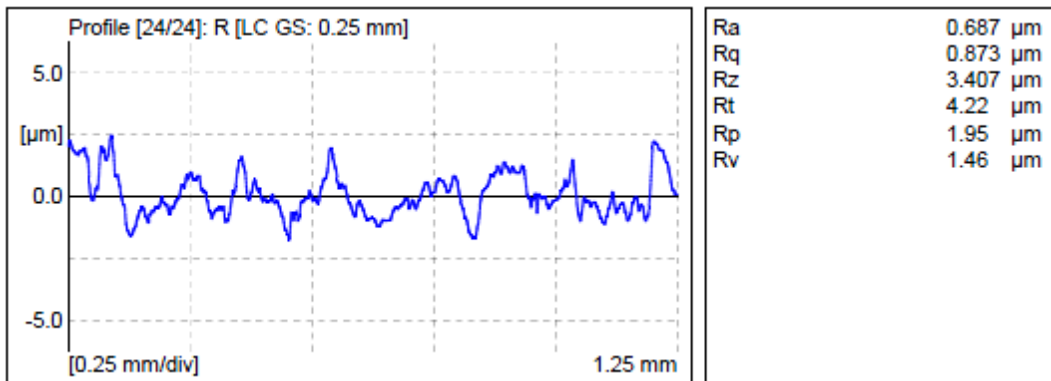
Figure 5.3.2-5 shows the CFRP hole surface roughness drilled by WC (DC) under high speed conditions in Experiment Type II at holes 2, 5 and 80. After hole 2, fiber pullout can be seen to occur more often.



(a) High Speed Experiment Type II, Hole 2



(b) High Speed Experiment Type II, Hole 5



(c) High Speed Experiment Type II, Hole 80

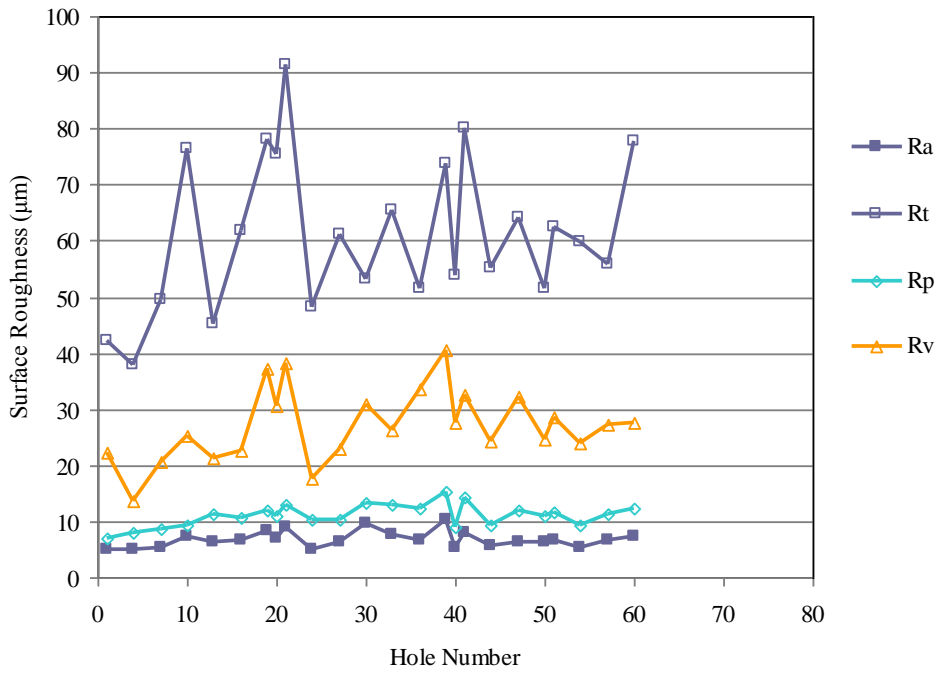
Figure 5.3.2-6: WC (DC) drilled titanium hole surface profiles from high speed Experiment Type II at a) hole 2 and b) hole 5 and c) hole 80.

Figure 5.3.2-6 shows the titanium hole surface roughness profiles drilled by WC (DC) under high speed Experiment Type II at hole 2, 5 and 80. All Ra values starting from

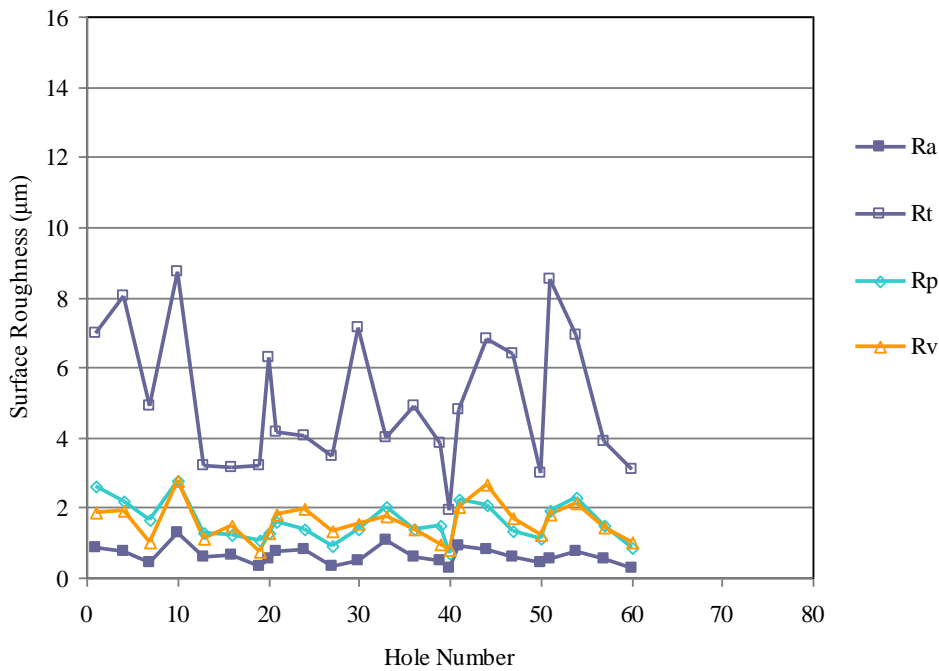
hole 5 and above are higher than at hole 2 in titanium holes under these conditions. However, as seen in figure 5.3.2-4b, roughness values become constant after hole 5.

Figure 5.3.2-7 displays CFRP and titanium surface roughness at low speed Experiment Type II conditions drilled by WC (DC). Surface roughness during low speed drilling with WC (DC) is seen to increase when machining CFRP (Figure 5.3.2-7a) and to decrease when machining titanium (Figure 5.3.2-7b).

When comparing surface roughness in CFRP holes between high speed (Figure 5.3.2-4a) and low speed (Figure 5.3.2-7a), drilling under the high speed condition can be seen to produce lower surface roughness on average with an average Ra of 5.832 μm and average Rv of 23.5 μm . Drilling under the low speed condition produced an average Ra of 6.808 μm and average Rv of 27.17 μm . However, surface roughnesses in titanium holes show the opposite response, with low speed producing lower surface roughness values. With the high speed condition (Figure 5.3.2-4b), the average Ra value for titanium hole surfaces is 0.78 μm whereas the average Ra value under the low speed condition is 0.614. For CFRP, the lower roughness at higher feeds may be due to matrix smearing similarly found by M. Ramulu et al. [3]. Higher surface roughness for titanium at high speeds may correlate to temperature and possibly thermal softening of the tool.

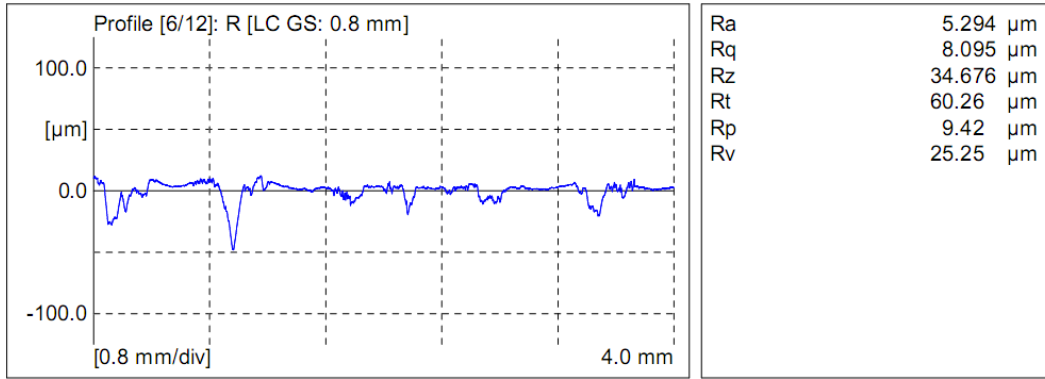


(a) CFRP surface roughness

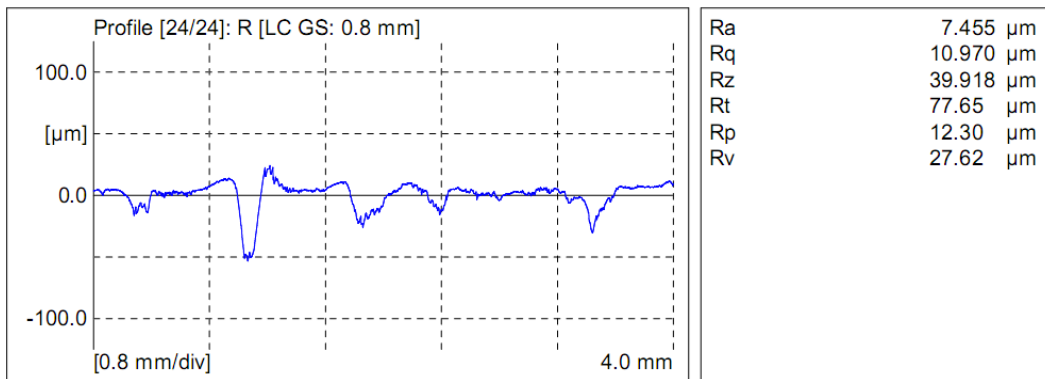


(b) Titanium surface roughness

Figure 5.3.2-7: WC (DC) low speed Experiment Type II hole surface roughness for a) CFRP and b) titanium.



(a) High Speed Experiment Type II, Hole 60



(b) Low Speed Experiment Type II, Hole 60

Figure 5.3.2-8: WC (DC) drilled CFRP hole surface profiles for Experiment Type II at hole 60 with a) high speed and b) low speed conditions.

Figure 5.3.2-8 shows CFRP hole surface roughness profiles in Experiment Type II with high speed and low speed conditions after drilling hole 60 with WC (DC). The depth of fiber pullout is more severe during the low speed condition as aforementioned when comparing Figures 5.3.2-4 and 5.3.2-7.

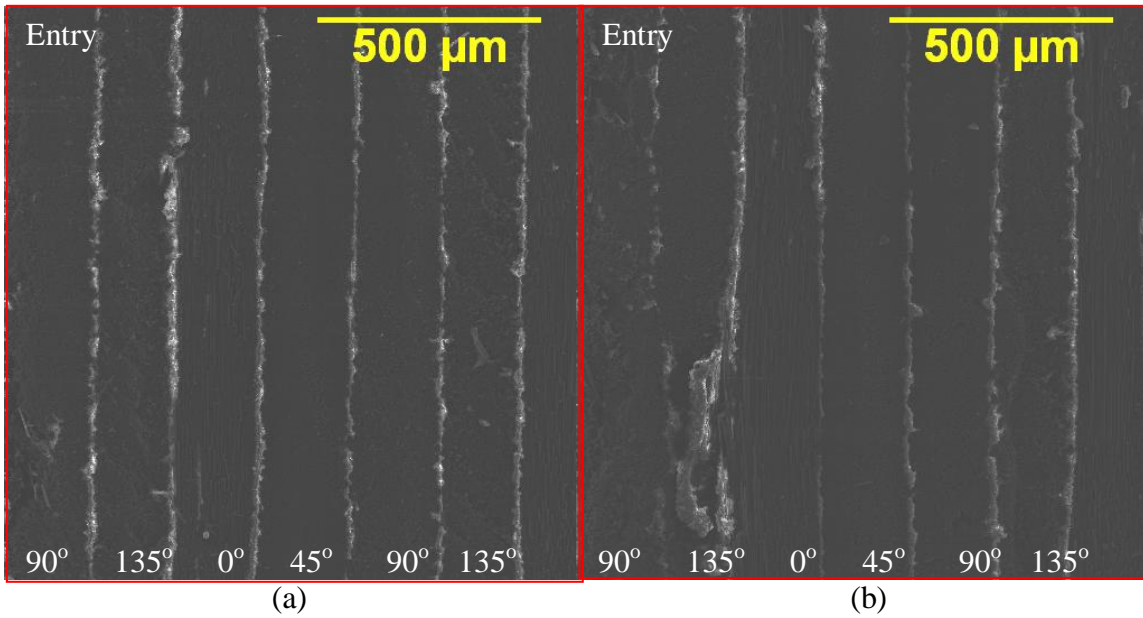
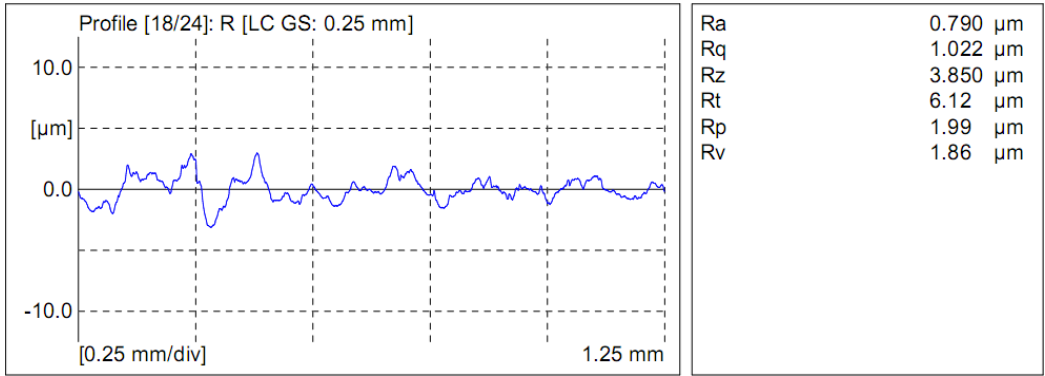
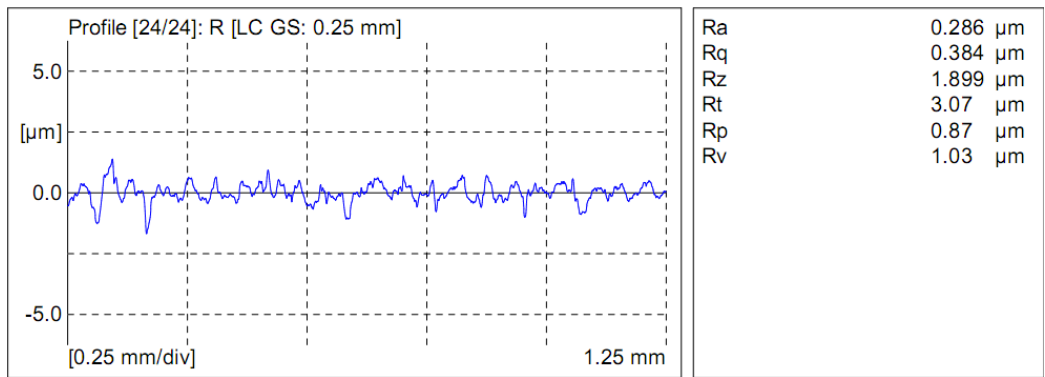


Figure 5.3.2-9: CFRP hole surface when drilling with WC (DC) at low speed Experiment Type II; a) hole 1 and b) hole 51.

Figure 5.3.2-9 shows the CFRP hole surface at hole 1 and 51 when drilling with WC (DC) under the low speed condition during Experiment Type II. At 135° and 90° orientation, fiber pullout is shown to become more severe after hole 1, especially in the 135° orientations. Long fibers are exposed in the 0° orientations due to the cutting mechanism of 0° orientation plies, which involve delamination of the fibers and bending fracture.



(a) High Speed Experiment Type II, Hole 60



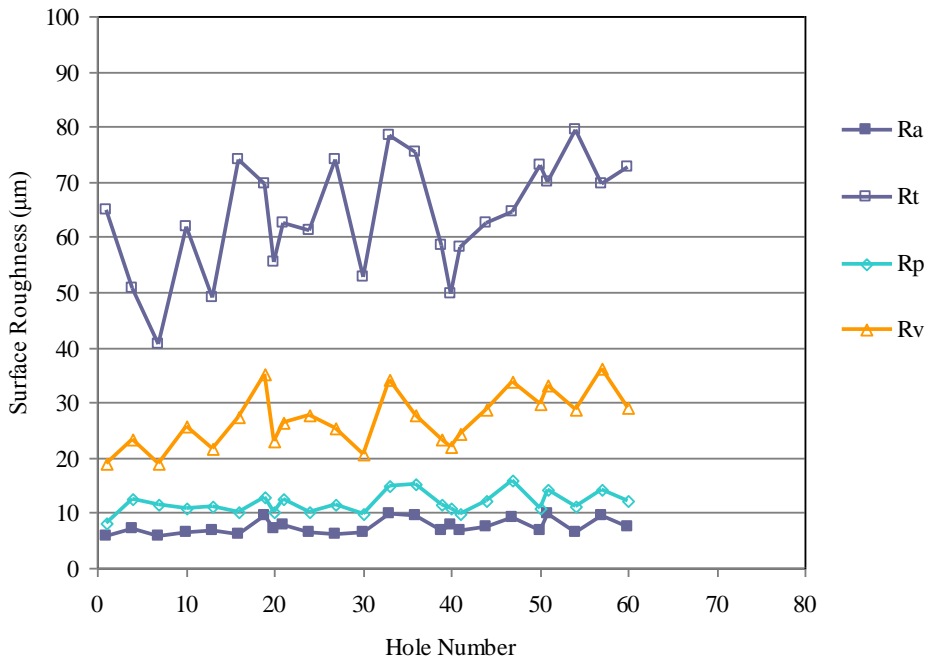
(b) High Speed Experiment Type II, Hole 60

Figure 5.3.2-10: WC (DC) drilled titanium hole surface profiles for Experiment Type II at hole 60 with a) high speed and b) low speed conditions.

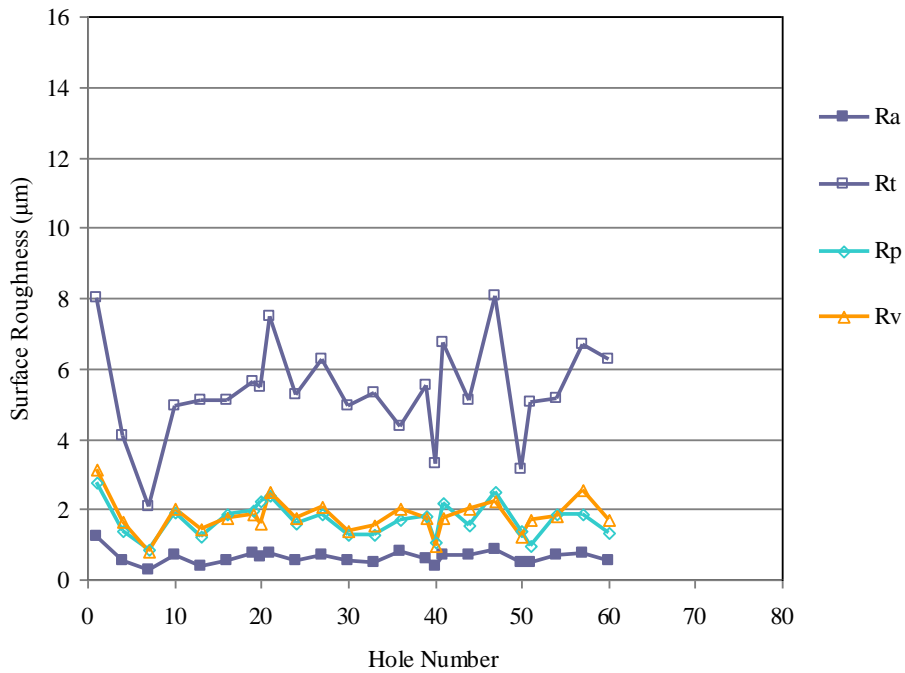
Figure 5.3.2-10 displays Ti hole surface roughness profiles in Experiment Type II with high speed and low speed conditions at hole 60 after drilling with WC (DC). Lower cutting speeds provide lower surface roughness as cutting temperatures are lower.

Figure 5.3.2-11 shows the CFRP and titanium hole surface roughness when drilling with PCD at the low speed condition during Experiment Type II. CFRP hole surface roughness values are seen to increase with hole number while titanium hole surface roughness values remain constant. When comparing CFRP hole surface roughness produced by WC to PCD (Figure 5.3.2-7a and Figure 5.3.2-11a), PCD produces lower Rv surface roughness values compared to WC (DC). For WC (DC), the average Rv value is 27.17 μm . For PCD, average Rv value is 26.84 μm . The lower average Rv value produced in PCD drilled CFRP holes reveal that fiber pullout is slightly less severe compare to WC (DC). The standard deviation in CFRP surface roughness values is also lower for PCD, revealing a more consistent trend. When viewing the surface roughness values in Experiment Type I for CFRP, we find PCD produces lower Ra and Rv values (see Appendix C).

When comparing titanium hole surface roughness drilled by WC (DC) to PCD, Figure 5.3.2-7b and Figure 5.3.2-11b show average Ra values for PCD to be nearly the same (0.613 μm) as with WC (0.614 μm).

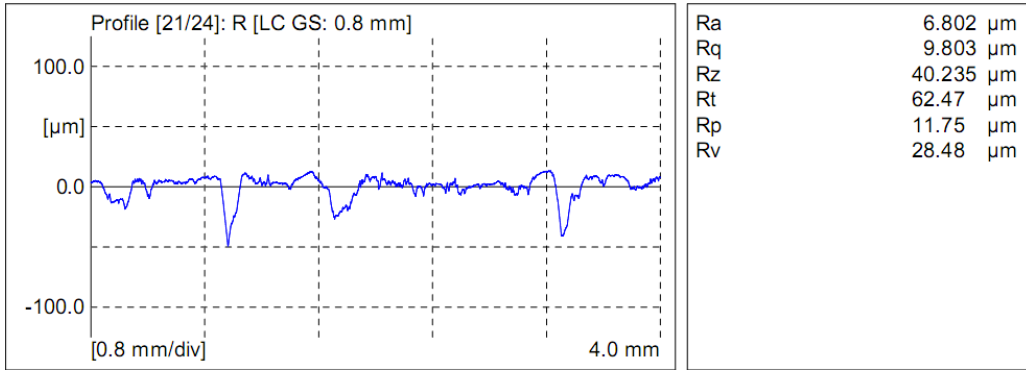


(a) CFRP hole surface roughness

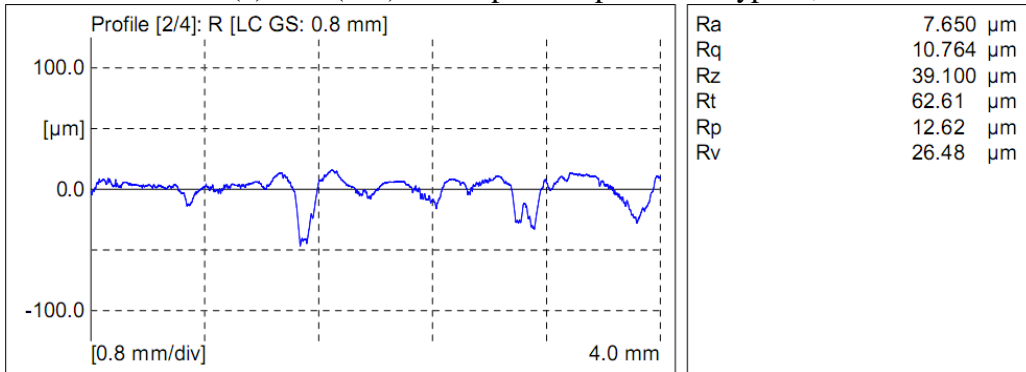


(b) Titanium hole surface roughness

Figure 5.3.2-11: PCD low speed Experiment Type II hole surface roughness for a) CFRP and b) titanium.



(a) WC (DC) Low Speed Experiment Type II, Hole 51



(b) PCD Low Speed Experiment Type II, Hole 21

Figure 5.3.2-12: CFRP hole surface profile under low speed Experiment Type II conditions drilled with a) WC (DC) at hole 51 and b) PCD at hole 21.

Figure 5.3.2-12 compares CFRP hole profiles drilled by WC (DC) and PCD under low speed Experiment Type II conditions with Ra and Rv values close to their respective averages. The surface profiles show layers near fiber pullout sites have higher peaks. That is, when drilling, fibers in plies neighboring a fiber pullout site will flow in the direction of the fiber pullout due to the lack of compressive force that would otherwise prevent them. As a result, near by fibers may be longer as seen in Figures 5.3.2-3b, 5.3.2-9b, and 5.3.2-13d. While fiber pullout in PCD drilled CFRP holes was slightly less severe when comparing Rv values.

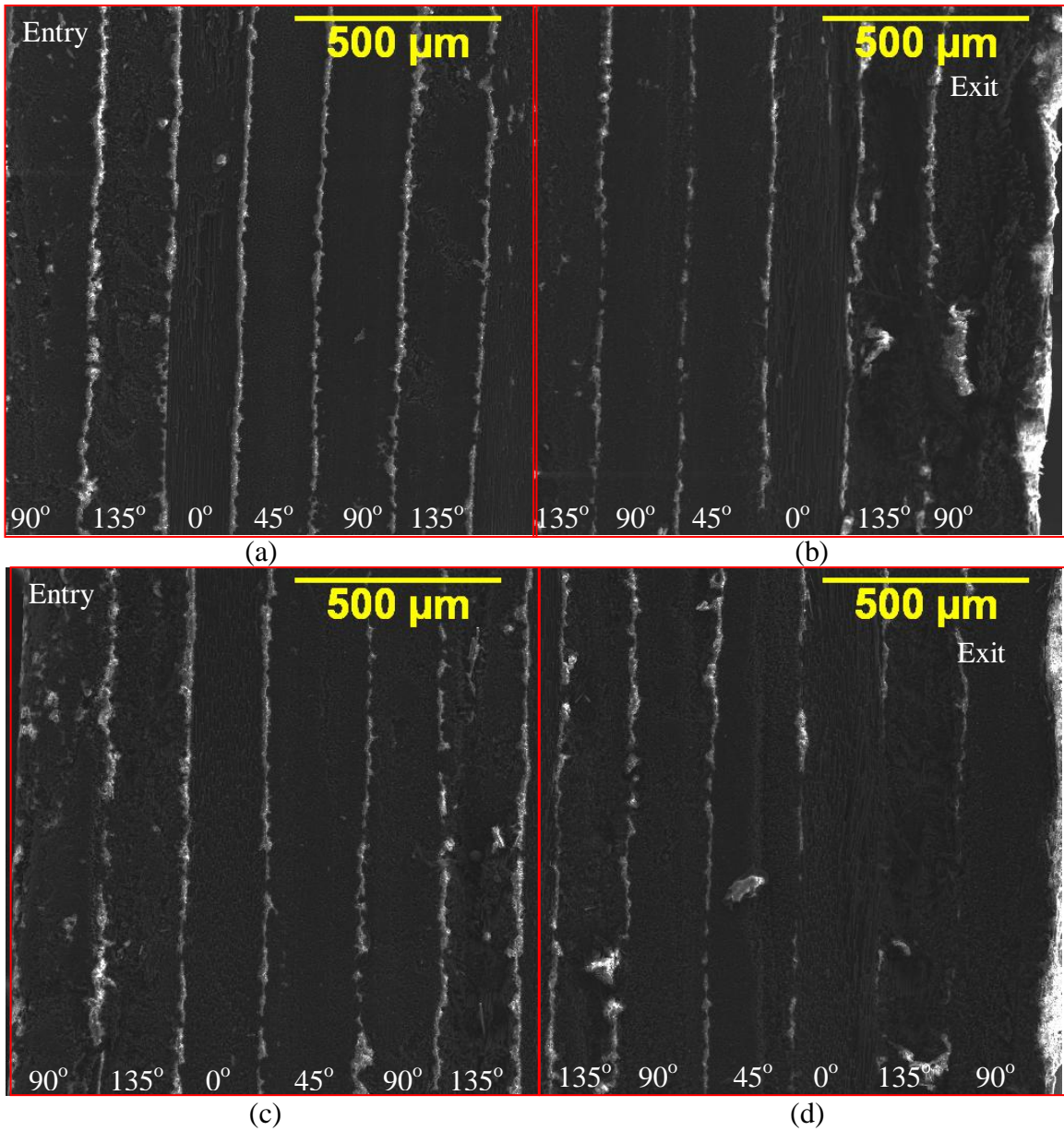
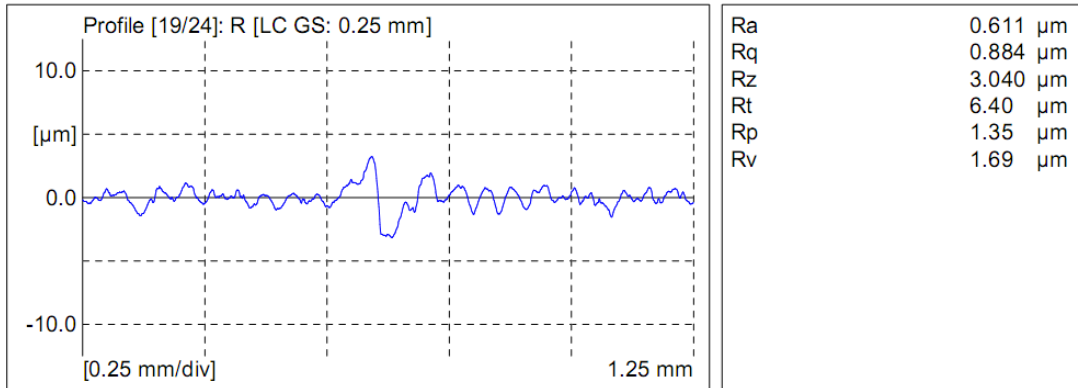


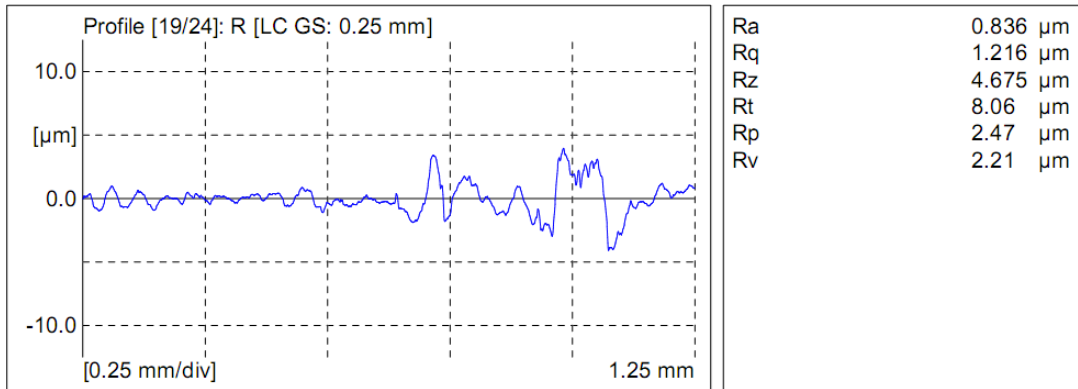
Figure 5.3.2-13: Low speed Experiment Type II CFRP hole surface drilled by PCD; hole entry and exit at a,b) hole 1 and c,d) hole 51. 100x magnification.

Figure 5.3.2-13 visually compares PCD drilled CFRP surfaces between hole 1 and 51 at the hole entry and exit. At hole 1, a relatively low amount of fiber pullout is observed at the hole entry and exit. At hole 1, a relatively low amount of fiber pullout is observed at the 135° ply orientation near the entry side. However, more severe fiber pullout is found on the 135° ply orientation along exit side. In hole 1, fuzzing is found to occur at the 90°

oriented ply. In hole 51, severe fiber pullout also occurs at the 135°-oriented plies. At the exit side, fuzzing is seen in a 0° oriented ply neighboring a 135° ply.



(a) WC (DC) Low Speed Experiment Type II, Hole 47



(b) PCD Low Speed Experiment Type II, Hole 47

Figure 5.3.2-14: Titanium hole surface profile under low speed Experiment Type II conditions at hole 47 drilled with a) WC (DC) and b) PCD tools.

Figure 5.3.2-14 displays the titanium hole surface profile under the low speed condition during Experiment Type II drilled by WC and PCD at hole 47. WC (DC) titanium hole surface roughness profiles show lower deviation than those produced by PCD. This is reflected in the Rq values, which is defined as the mean deviation from the mean line found through integrating the area under the curve of a sine wave equivalent to the profile. Average Rq values for titanium holes drilled by WC and PCD are 0.805μm and 0.825μm respectively. However, average Ra values from both tools are nearly equivalent. Average Ra values for WC and PCD are respectively 0.614μm and 0.613μm.

Titanium adhesion during stack drilling increases surface roughness in CFRP due the increase occurrence of fiber pullout. The increase occurrence of fiber pullout is due to the reduced fiber cutting efficiency brought on by the titanium adhesive layer compared to the actual sharper tool edge. Titanium chips during stack drilling can also produce scratches on the CFRP hole surface.

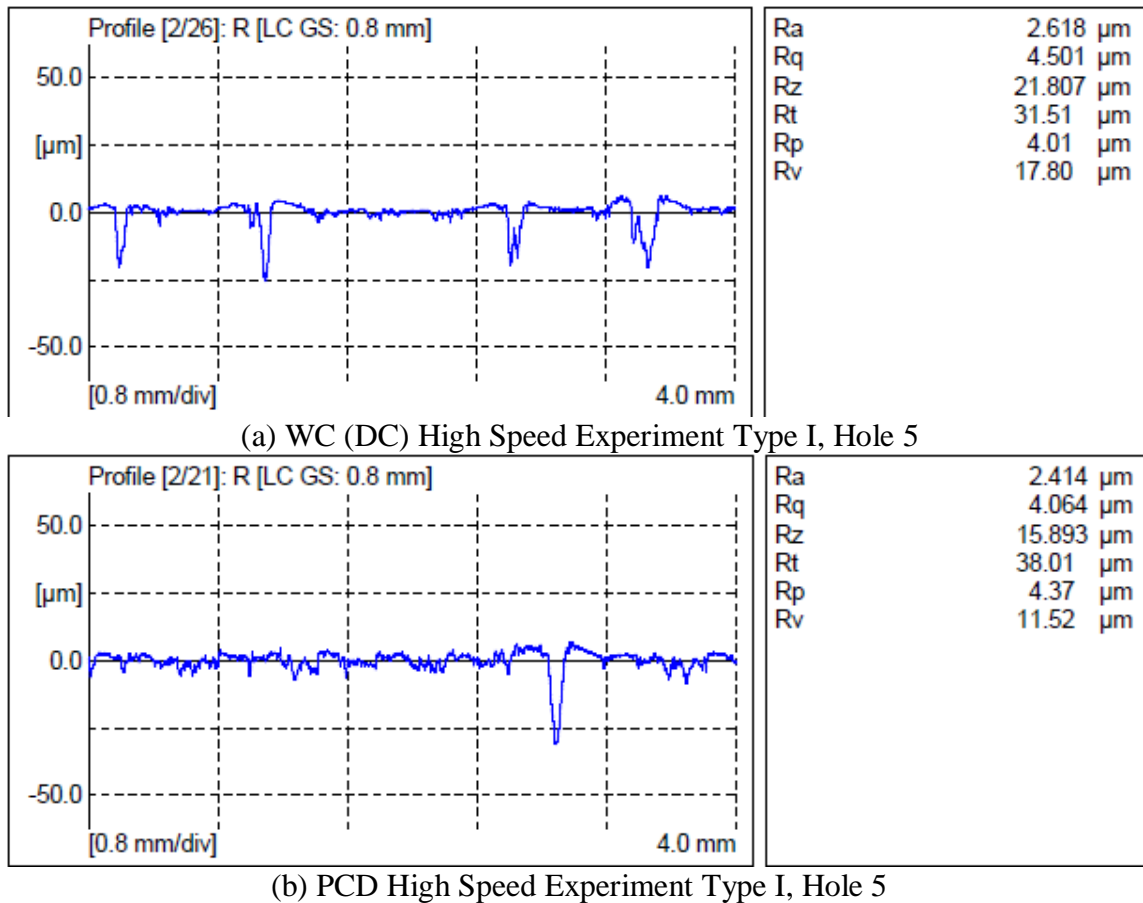


Figure 5.3.2-15: CFRP hole surface profile under high speed Experiment Type I conditions at hole 47 drilled with a) WC (DC) and b) PCD tools.

Figure 5.3.2-15 shows the CFRP surface profiles during high speed Experiment Type I at hole 5 drilled by WC and PCD. As aforementioned, average Ra and Rv values drilled by PCD during Experiment Type I are lower than WC (DC).

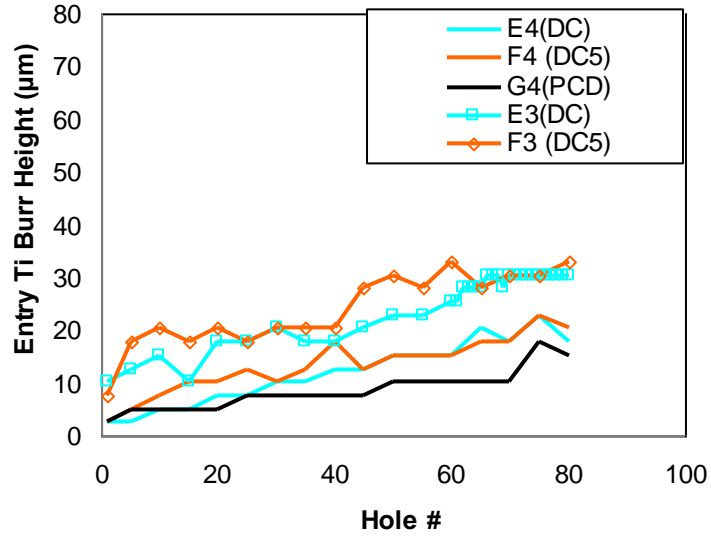
Speed also affects the surface roughness. Under the high speed setting, CFRP hole surfaces had lower Ra and Rv values than with the low speed setting. However, the low speed setting produced better hole surface roughness when drilling titanium. This is due to the increased chemical reactivity at high temperatures associated with higher speeds. Also at high speed, WC is observed to produce constant surface roughness values after initial testing. At the low speed setting, roughness values during CFRP drilling are seen to increase for both WC and PCD tools; however, WC produced decreasing roughness values in titanium for the low speed setting whereas PCD produced constant values in titanium. PCD produced slightly lower Rv values on average. However, PCD roughness values have a lower standard deviation. When comparing hole surface roughness values of those drilled by PCD to those drilled by WC, multiple tests with each tool under the same condition would better improve the understanding of how drilling stack materials affect hole quality in terms of surface roughness.

5.3.3 TITANIUM BURR HEIGHT

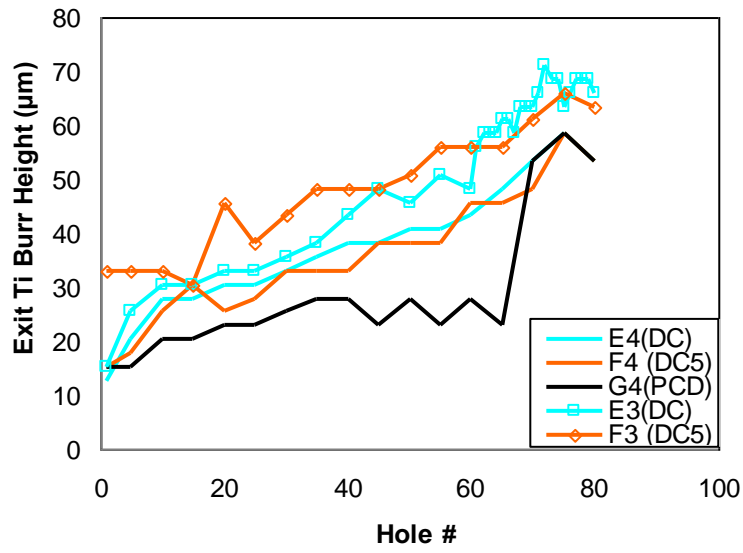
The burr formation and growth increases as the number of holes increase. Figure 5.3.3-1 shows both entry and exit Ti burr height up to 80 holes for Experiment Type II. Figure 5.3.3-2 shows entry and exit burr photos at holes 1, 60, and 80 of the titanium plates from low speed Experiment Type II. In Figure 5.3.3-1a, the entry burr formation is seen to be minimal by drilling with both WC and PCD tools. The progression shows a steady increase in entry burr height by both tools; however, WC shows a higher rate of increase in entry burr size than PCD, as WC drilled holes reach an entry burr height of 15 μm and PCD reaches 10 μm by hole 60. This same trend is seen in exit burr formation (Figure

5.3.3-1b), where both burr height progressions increase with WC increasing at a higher rate than PCD. The percent difference between exit and entry burrs at hole 60 for WC and PCD were 65% and 64%, respectively, with the exit burrs being of higher magnitude in height. By hole 70, the titanium burrs have already increased just before the onset of the tool fracture to values equivalent in height to those of WC.

It is clear that heat generation during drilling has a major influence on the entry/exit burr heights. Due to the low thermal conductivity of titanium, the titanium plate will heat up rapidly during drilling and not dissipate the heat quickly, thus forcing the heat to be localized at the tool cutting edge. PCD might produce less heat during titanium drilling, when compared with WC, due to the superior frictional characteristics and thermal conductivity of PCD. However, it must be kept in mind that PCD speed is reduced to prevent premature failure, in response to the fracture of G3. With constant feeds, increasing speeds will increase burr height, [3], as shown in Figure 5.3.3-1 when comparing burrs formed at high speeds and low speeds when using WC drills.











(a)



(b)

Figure 5.3.3-1: a) Entry and b) exit burr height from Experiment Type II.

Drill type	Hole 1		Hole 60	
	Entry	Exit	Entry	Exit
WC				
	2.54 microns	12.7 microns	15.24 microns	43.18 microns
PCD				
	2.54 microns	15.24 microns	10.16 microns	27.94 microns





		Hole 80	
		Entry	Exit
WC			
		17.78	53.34
PCD			
		15.24	53.34

Figure 5.3.3-2: Burr height progression images of low speed Experiment Type II.

Figure 5.3.3-2 shows photos of the titanium burrs at holes 1, 60 and 80. Titanium burrs produced by the PCD drill at hole 73, where a large volume of fracture occurred, through hole 80 can be seen to differ drastically from prior burrs. Burrs seen in holes 1 and 60 for both tools are uniform whereas the exit burr at holes 73 through hole 80 drilled by PCD at low speed is non-uniformed.

Entry burr heights are found to be significantly smaller than exit burr heights. Both entry and exit burrs increase in height with increase in tool wear. Higher speeds also produce higher burr heights due to the higher thrust values and temperature. After tool failure seen in PCD, burr heights increased significantly.

CHAPTER 6: CONCLUSIONS

The experimental study on machining performance evaluation of drilling carbon fiber reinforced plastic and titanium (CFRP/Ti) stacks was conducted. Effects of tool material and drilling speed on tool wear and hole quality of CFRP/Ti stacks were investigated. Based on the experimental results, some conclusions can be made.

- 1) The maximum thrust values at each hole during both experiments increases as tool wear increases. The rates at which the thrust values increase reveal that PCD wears down at a lower rate than the WC tools. The micrograin % has minimal effects on machining performance because the results from DC and DC5 WC drills are nearly identical.
- 2) During CFRP only cycles, smooth wear marks with equivalent size as the carbon fibers are seen along the cutting edge as the WC (DC and DC5) drills undergoes abrasion.
- 3) Titanium adhesion was prevalent on WC tools, whereas PCD was subject to trace amounts of titanium adhesion during low speed operations.
- 4) Attrition is more aggressive on WC tools at high speeds at the cutting edge corner and along the helical flute.
- 5) The main wear mechanism seen in PCD was pitting, possibly due to thermal and mechanical fatigue.
- 6) The titanium adhesion affects hole diameter, roundness, and roughness by acting as a less efficient cutting edge.
- 7) Hole diameters produced by PCD tools were more consistent than those produced by WC.

8) Surface roughness for both CFRP and titanium are affected by speed and tool type.

9) WC tools produce less surface roughness under most surface roughness definitions in this instance; however, PCD produced slightly lower Rv values.

10) Entry and exit burr heights increase with tool wear and with speed. PCD produce smaller entry and exit burrs until fracture.

Overall, PCD produced slightly better hole quality results in terms of diameter, roundness, fiber pullout, and burr height. However, WC drills produced surface roughness with better Ra values in CFRP.

BIBLIOGRAPHY

- [1] Lantrip, J., "New Tools Needed" *Cutting Tool Engineering*, Vol. 60 No. 8, 8 pages, 2008. <http://www.ctemag.com/pdf/2008/0808-Holemaking.pdf>
- [2] Rawat, S. and H. Attia, "Wear mechanisms and tool life management of WC-Co drills during dry high speed drilling of woven carbon fibre composites." *Wear*, Vol.267, No.5-8, pp.1022-1030, 2009.
- [3] Ramulu, M., T. Branson and D. Kim, "A Study on the Drilling of Composite and Titanium Stacks," *Composite Structures*, Vol. 54, pp. 67-77, 2001.
- [4] Zitoune, R., Krihnaraj, V., Collombet, F., "Studying of drilling composite material and aluminium stack, *Composite Structures*," Vol. 92, pp. 1246-1255, 2010.
- [5] D.H. Wang, M. Ramulu, D. Arola, "Orthogonal cutting mechanisms of graphite epoxy composite. Part I: Unidirectional laminate," *International Journal of Machine Tools & Manufacture*, Vol. 35, No. 12, 1623-1638, 1995.
- [6] Ramulu, M., Kim, D., and Choi, G., "Frequency analysis and characterization in orthogonal cutting of glass fiber reinforced composites," *Composites: Part A*, Vol. 34, pp. 949-962, 2003.
- [7] Sun, S., Brandt, M., Dargusch, M.S., "Characteristics of cutting forces and chip formation in machining of titanium alloys," *International Journal of Machine Tools & Manufacture*, Vol. 49, pp. 561-568, 2009.
- [8] Nabhani, F., "Wear mechanisms of ultra-hard cutting tools materials," *Journal of Materials Processing Technology*, Vol. 115, pp. 402-412, 2001.
- [9] Hua, J. and R. Shivpuri, "Prediction of chip morphology and segmentation during the machining of titanium alloys," *Journal of Materials Processing Technology*, Vol. 150, pp. 124-133, 2004
- [10] Li, R., Riester, L., Watkins, T.R., Blau, P.J., Shih, A.J., "Metallurgical analysis and Nanoindentation characterization of Ti-6Al-4V workpiece and chips in high throughput drilling," *Material Science and Engineering A*, Vol. 472, pp. 115-124, 2008.
- [11] Ezugqu, E. O., Bonney, J., Yamane, Y., "An overview of the machinability of aeroengine alloys, *Journal of Materials Processing Technology*," Vol. 134, pp 233-253, 2003.

- [12] Arrazola, P.-J., Garay, A., Iriarte, L.-M., Armendia, M., Marya, S., Le Maître, F., Machinability of titanium alloys (Ti6Al4V and Ti555.3), *Journal of Materials Processing Technology*, Vol. 209, No. 5, pp. 2223-2230, 2008.
- [13] Rahim, E.A., and S. Sharif, "Tool failure modes and wear mechanism of coated carbide tools when drilling Ti-6Al-4V," *International Journal of Precision Technology*, Vol. 1, No. 1, pp. 30-39, 2007.
- [14] Saito, H. iwabuchi, A., Shimizu, T., "Effects of Co content and WC grain size on wear of WC cemented carbide," *Wear*, Vol. 261, pp. 126-132, 2006.
- [15] Jia, K. & T.E. Fischer, "Sliding wear of conventional and nanostructured cemented carbides," *Wear*, Vol. 203-204, pp. 310-318, 1997.
- [16] Bhat, D.G., Bedekar, V.A, Batzer, S.A., "A Preliminary Study of Chemical Solubility of ultra-Hard Ceramic AlMgB₁₄ in Titanium: Reconciliation of Model with Experiment," *Machine Science and Technology*, Vol. 8 no. 3 pp. 341-355, 2004.
- [17] Stephenson, D.A. and J.S. Agapiou, (1997). Metal Cutting Theory and Practice, Second Edition, Taylor & Francis.
- [18] Cantero, J.L., Tardío, M.M., Canteli, J.A., Marcos, M., Miguélez, M.H., "Dry drilling of alloy Ti-6Al-4V," *International Journal of Machine Tools & Manufacture*, Vol. 45, pp. 1246-1255, 2005.
- [19] Abdel-Aal, H.A., Nouari, M., El Mansori, M., "Tribo-energetic correlation of tool thermal properties to wear of WC-Co inserts in high speed dry machining of aeronautical grade titanium alloys," *Wear*, Vol. 266, 432-443, 2009.
- [20] Nabhani, F. "Machining of Aerospace Titanium Alloys," *Robotics and Computer Integrated Manufacturing*, Vol. 17, pp. 99-106, 2001.
- [21] Faria, P.E., Campos, R.F., Abaro, A.M., Godoy, G.C.D., Davim, J.P., "Thrust Force and Wear Assessment When Drilling Glass Fiber-Reinforced Polymeric Composite," *Journal of Composite Materials*, Vol. 42, No. 14, pp 1401-1414, 2008.
- [22] Sharif, S. and E.A. Rahim, "Performance of coated-and uncoated-carbide tools when drilling titanium alloy-Ti-6Al4V." *Journal of Materials Processing Technology*, Vol.185, No.1-3, pp.72-76, 2007.
- [23] Sreejith, P.S., Krishnamurthy, R., Malhotra, S.K., Narayanasamy, K., "Evaluation of PCD tool performance during machining of carbon/phenolic ablative composites," *Journal of Materials Processing Technology*, Vol. 104, pp.53-58, 2000.

- [24] Nurul Amin, A.K.M., Ismail, A.F., Nor Khairusshima, M.K., "Effectiveness of uncoated WC-Co and PCD inserts in end milling of titanium alloy – Ti-6Al-4V," *Journal of Materials Processing Technology*, Vol. 192-193, pp. 147-158, 2007.
- [25] König, W. and A. Neises, "Wear mechanisms of ultrahard, non-metallic cutting materials," *Wear*, Vol. 162-164, pp 12-21, 1993.
- [26] Garrick, R. "Drilling Advanced Aircraft structures with PCD(Poly-Crystalline Diamond) Drills." *Society of Automotive Engineers International*, Technical Paper 2007-01-3893, 2007.
- [27] Ralph, W.C., Johnson, W.S., Toivonen, P., Makeev, A., Newman Jr., J.C., "Effects of various aircraft production drilling procedures on hole quality," *International Journal of Fatigue*, Vol. 28, No. 8, pp. 943-950, 2006.
- [28] König, W. & P. Graß, "Quality Definition and Assessment in Drilling of Fibre Reinforced Thermosets," *CIRP Annals-Manufacturing Technology*, Vol. 38, no. 1, pp. 119-124, 1989.
- [29] Park, K.Y., Choi, J.H., and Lee, D.G., "Delamination-Free and High Efficiency Drilling of Carbon Fiber Reinforced Plastics," *Journal of Composite Materials*, Vol. 29, No. 15, pp. 1988-2002, 1995.
- [30] Abrão, A.M., Faria, P.E., Campos Rubio, J.C., Reis, P., Paulo Davim, J., "Drilling of fiber reinforced plastics: A review," *Journal of Materials Processing Technology*, Vol. 186, pp. 1-7, 2007.
- [31] Tsao, C.C., "Experimental study of drilling composite materials with step-core drill," *Materials & Design*, Vol. 29, No. 9, pp. 1740-1744, 2008.
- [32] Lachaud, F., Piquet, R., Collmet, F., Surcin, L., "Drilling of composite structures." *Composite Structures*. Vol. 52. pp. 511-516, 2001.
- [33] Hocheng, H. and C.C. Tsao, "The path towards delamination-free drilling of composite materials," *Journal of Materials Processing Technology*, Vol. 167, No. 2-3, pp. 251-264, 2005.
- [34] Durão, L.M.P., Gonçalves, D.J.S., Travares, J.M.R.S., de Albuquerque, V.H.C., Vieira, A.A., Marques, A.T., "Drilling tool geometry evaluation for reinforced composite laminates," *Structures*, Vol. 92, no. 7, pp. 1545-1550, 2010.
- [35] Kim, D., and M. Ramulu, "Drilling process optimization for graphite/bismaleimide- titanium alloy stacks," *Composite Structures*, Vol. 63, pp. 101-114, 2004.

- [36] Shyha, I.S., Aspinwall, D.K., Soo, S.L., Bradley, S., “Drill geometry and operating effects when cutting small diameter holes in CFRP,” *International Journal of Machine Tools & Manufacture*, Vol. 49, No 12-13, pp. 1008-1014, 2009.
- [37] Caprino, G. and V. Taliaferri, “Damage development in drilling glass fibre reinforced plastics,” *International Journal of Machine Tools & Manufacture*, Vol. 35, No. 6, pp. 817-829, 1995.
- [38] Faria, P.E., Campos Rubio, J.C., Abaro, A.M., Davim, J.P., Dimensional and Geometric Deviations Induced by Drilling of Polymeric Composite, *Journal of Reinforced Plastics and Composites*, Vol. 28, No. 19, pp. 2353-2363, 2008.
- [39] Min, S., Kim, J., Dornfeld, D.A., “Development of a drilling burr control chart for low alloy steel AISI 4118,” *Journal of Materials Processing Technology*, Vol. 113, pp. 4-9, 2001.
- [40] Brinksmeier, E. and R. Janssen, “Drilling of Multi-Layer Composite Materials consisting of Carbon Fiber Reinforced Plastics (CFRP), Titanium, and Aluminum Alloys,” *CIRP Annals-Manufacturing Technology*, Vol. 51, No. 1, pp. 87-90, 2002.
- [41] Liu, J., Shao, X.J., Liu, Y.J., Liu, Y.S., Yue, Z.F., “The effect of holes quality on fatigue life of open hole.” *Materials Science and Engineering A*, Vol. 467, 8-14, 2007.
- [42] Bono, M. and J. Ni, “The effects of thermal distortions on the diameter and cylindricity of dry drilled holes,” *International Journal of Machine Tools & Manufacture*, Vol. 41, pp. 2261-2270, 2001.
- [43] Haan, D.M., Datzner, S.A., Olson, W.W., Sutherland, J.W., “An experimental study of cutting fluid effects in drilling,” *Journal of Materials Processing Technology*, Vol. 71, pp. 305-313, 1997.

APPENDIX

APPENDIX A: Hole Quality Summary

APPENDIX B: Thrust and Torque

APPENDIX C: Diameter and Roundness

APPENDIX D: Surface Roughness and Surface Profiles

APPENDIX A

APPENDIX A

Hole Quality Summary Tables:

Hole Size and Roundness: Experiment Type I

Low Speed Experiment Type I	Hole Size (Microns)	Hole Size (Microns)	Roundness (Microns)	Roundness (Microns)
WC (DC)	CFRP	Ti	CFRP	Ti
Range	0.0658	0.0224	0.0353	0.0160
Average	9.5371	9.5467	0.0160	0.0074
WC (DC5)	CFRP	Ti	CFRP	Ti
Range	0.0881	0.0292	0.0373	0.0246
Average	9.5405	9.5564	0.0184	0.0077
PCD	CFRP	Ti	CFRP	Ti
Range	0.0871	0.0269	0.0351	0.0124
Average	9.5630	9.5466	0.0166	0.0065

High Speed Experiment Type I	Hole Size (Microns)	Hole Size (Microns)	Roundness (Microns)	Roundness (Microns)
WC (DC)	CFRP	Ti	CFRP	Ti
Range	0.1240	0.0391	0.0328	0.0290
Average	9.5561	9.5757	0.0151	0.0251
PCD	CFRP	Ti	CFRP	Ti
Range	0.0696	0.0356	0.0343	0.0668
Average	9.5378	9.5498	0.0170	0.0110

APPENDIX A

Hole Size and Roundness: Experiment Type II

Low Speed Experiment Type II	Hole Size (mm)	Hole Size (mm)	Roundness (mm)	Roundness (mm)
WC (DC)	CFRP	Ti	CFRP	Ti
Range	0.0714	0.0244	0.0516	0.0137
Average	9.5522	9.5464	0.0248	0.0072
Standard Deviation	0.0161	0.0057	0.0113	0.0037
WC (DC5)	CFRP	Ti	CFRP	Ti
Range	0.0572	0.0302	0.0297	0.0097
Average	9.5617	9.5502	0.0211	0.0054
Standard Deviation	0.0120	0.0069	0.0085	0.0023
PCD	CFRP	Ti	CFRP	Ti
Range	0.0546	0.0272	0.0305	0.0290
Average	9.5587	9.5509	0.0170	0.0087
Standard Deviation	0.0144	0.0066	0.0076	0.0057

High Speed Experiment Type II	Hole Size (mm)	Hole Size (mm)	Roundness (mm)	Roundness (mm)
WC (DC)	CFRP	Ti	CFRP	Ti
Range	0.2700	0.0351	0.1872	0.0640
Average	9.5686	9.5727	0.0280	0.0229
Standard Deviation	0.0444	0.0089	0.0348	0.0156
WC (DC5)	CFRP	Ti	CFRP	Ti
Range	0.3249	0.0632	0.2461	0.0371
Average	9.6101	9.5846	0.0419	0.0203
Standard Deviation	0.0606	0.0120	0.0465	0.0101

APPENDIX A

Hole Surface Roughness: Experiment Type I

High Speed Experiment Type I	Surface Roughness (Ra) (Microns)	Surface Roughness (Rv) (Microns)	Surface Roughness (Ra) (Microns)
WC (DC)	CFRP	CFRP	Ti
Range	9.23	28.09	0.66
Average	5.59	21.64	0.61
PCD	CFRP	CFRP	Ti
Range	7.63	16.08	N/A
Average	4.34	18.23	N/A

Hole Surface Roughness and Ti burrs: Experiment Type II

Low Speed Experiment Type II	Surface Roughness (Ra) (Microns)	Surface Roughness (Rv) (Microns)	Surface Roughness (Ra) (Microns)	Entry Burr Height (Microns)	Exit Burr Height (Microns)
WC (DC)	CFRP	CFRP	Ti	Ti	Ti
Range	5.33	26.79	1.01	20.32	40.64
Average	6.81	27.17	0.61		
Standard Deviation	1.44	6.50	0.25		
WC (DC5)	CFRP	CFRP	Ti	Ti	Ti
Range				25.40	35.56
Average					
Standard Deviation					
PCD	CFRP	CFRP	Ti	Ti	Ti
Range	4.20	17.34	0.95	7.62	12.70
Average	7.42	26.84	0.61		
Standard Deviation	1.31	5.03	0.19		
High Speed Experiment Type II	Surface Roughness (Ra) (Microns)	Surface Roughness (Rv) (Microns)	Surface Roughness (Ra) (Microns)	Entry Burr Height (Microns)	Exit Burr Height (Microns)
WC (DC)	CFRP	CFRP	Ti	Ti	Ti
Range	5.62	23.87	0.94	20.32	55.88
Average	5.83	23.47	0.78		
Standard Deviation	1.40	6.70	0.23		
WC (DC5)	CFRP	CFRP	Ti	Ti	Ti
Range				20.32	43.18
Average					
Standard Deviation					

APPENDIX B

APPENDIX B

Thrust and Torque Tables:

High Speed Experiment Type I WC (DC) Thrust and Torque

Hole #	CFRP		Ti	
	Max Torque (N*cm)	Max Thrust (N)	Max Torque (N*cm)	Max Thrust (N)
1	106.931	219.822		
2	103.107	232.807		
3	98.744	234.060		
4	99.733	239.597		
5	107.291	238.608		
6	100.453	253.966		
7	85.113	255.350		
8	97.754	255.284		
9	79.985	255.416		
10	93.435	255.416		
11	125.645	298.589		
12	130.999	288.439		
13	134.642	295.360		
14	129.604	287.846		
15	126.545	293.053		
16	127.220	297.139		
17	129.874	311.772		
18	133.878	315.595		
19	115.613	312.234		
20	122.046	308.477		
21	120.118	231.308	514.985	893.133
22	100.507	257.997	664.228	942.898
23	95.604	244.652	669.641	933.011
24	122.570	266.893	686.677	948.106
25	100.507	284.686	658.283	973.614
26	98.056	271.342	640.183	978.228
27	80.896	280.238	617.823	1002.682
28	107.861	298.031	665.825	1019.622
29	129.924	302.479	639.473	1009.669
30	144.632	315.824	678.425	1017.909
31	107.861	329.168	792.619	1060.028
32	100.507	338.065	722.878	1086.196
33	98.056	346.961	613.120	1069.651
34	122.570	378.099	642.490	1102.740
35	117.667	346.961	677.626	1120.076
36	122.570	342.513	658.017	1111.968
37	110.313	338.065	682.151	1149.012
38	115.215	346.961	710.722	1137.609
39	110.313	355.858	641.159	1170.566
40	122.570	400.340	596.972	1191.791

APPENDIX B

High Speed Experiment Type I WC (DC) Thrust and Torque

		CFRP		
Hole #	Max Torque (N*cm)	Max Thrust (N)		
41	115.259	370.040		
42	125.463	364.965		
43	125.995	363.844		
44	141.345	367.865		
45	131.940	366.151		
46	127.592	361.603		
47	126.084	374.720		
48	133.449	384.212		
49	134.336	374.259		
50	129.899	390.342		
51	135.401	389.748		
52	144.362	391.132		
53	123.067	398.119		
54	122.801	387.969		
55	130.166	392.055		
56	131.851	389.616		
57	134.336	395.285		
58	146.314	394.165		
59	158.115	414.400	Ti	
60	153.768	399.306	Max Torque (N*cm)	Max Thrust (N)
61	124.246	446.497	714.273	1369.299
62	112.534	499.162	709.836	1500.996
63	146.073	529.416	669.020	1505.544
64	102.330	575.952	685.435	1510.225
65	129.747	516.893	696.615	1481.354
66	135.426	544.972	710.989	1516.552
67	139.773	539.567	715.426	1508.774
68	133.651	550.707	761.211	1567.439
69	160.802	500.019	736.632	1523.210
70	138.886	565.010	738.851	1556.892
71	131.876	561.516	722.436	1588.927
72	117.502	560.725	709.747	1627.224
73	129.570	541.940	717.378	1599.803
74	133.562	562.703	710.013	1643.637
75	107.831	542.797	721.903	1615.623
76	140.749	556.837	736.278	1589.125
77	139.773	549.454	729.889	1608.504
78	136.313	570.481	746.215	1625.048
79	153.083	568.635	734.439	1647.324
80	155.390	544.181	719.888	1611.071

APPENDIX B

High Speed Experiment Type I PCD Thrust and Torque

Hole #	CFRP		Ti	
	Max Torque (N*cm)	Max Thrust (N)	Max Torque (N*cm)	Max Thrust (N)
1	170.001	382.102		
2	168.832	377.291		
3	167.842	385.134		
4	158.305	369.645		
5	154.346	371.622		
6	156.101	374.390		
7	150.522	383.618		
8	157.180	376.895		
9	153.266	390.407		
10	166.493	350.793		
11	172.431	369.447		
12	176.389	372.677		
13	175.040	369.579		
14	177.289	377.159		
15	164.378	376.500		
16	168.742	369.974		
17	171.306	384.541		
18	163.793	369.842		
19	161.544	372.743		
20	160.689	384.409	645.152	1338.253
21	159.340	209.066	627.406	1281.764
22	127.472	222.411	680.732	1302.527
23	129.924	226.859	625.543	1304.439
24	125.021	226.859	722.435	1324.872
25	122.570	222.411	716.313	1324.740
26	132.375	235.756	741.601	1299.561
27	125.021	244.652	796.703	1308.855
28	139.729	235.756	777.980	1357.895
29	154.438	231.308	758.371	1299.165
30	159.340	280.238	651.984	1362.839
31	98.056	257.997	764.849	1362.114
32	137.278	266.893	712.409	1361.521
33	107.861	262.445	691.646	1419.921
34	120.118	240.204	677.893	1381.625
35	132.375	306.927	735.656	1365.871
36	127.472	266.893	757.484	1402.849
37	149.535	298.031	774.077	1378.329
38	149.535	271.342	777.892	1367.980
39	142.181	298.031	690.404	1396.192
40	183.854	311.376		

APPENDIX B

High Speed Experiment Type I PCD Thrust and Torque

Hole #	CFRP		Ti	
	Max Torque (N*cm)	Max Thrust (N)	Max Torque (N*cm)	Max Thrust (N)
41	127.681	417.366		
42	143.830	424.814		
43	140.281	416.773		
44	133.892	420.596		
45	140.015	420.003		
46	145.959	426.660		
47	144.096	436.218		
48	144.007	424.551		
49	160.866	441.688		
50	137.708	425.539		
51	129.456	446.368		
52	138.506	439.909		
53	132.473	440.568		
54	137.441	450.125		
55	135.578	438.854		
56	139.127	465.022		
57	141.967	460.078		
58	152.614	452.037		
59	160.866	441.688		
60	148.799	447.093		
61	131.585	295.030	655.533	1410.298
62	169.206	304.390	649.056	1417.285
63	125.197	309.070	676.917	1417.614
64	163.262	335.238	607.264	1448.594
65	135.933	336.819	747.280	1455.713
66	158.204	337.017	727.405	1445.496
67	133.626	331.810	779.755	1429.479
68	164.326	360.351	693.687	1424.403
69	153.324	337.545	684.814	1427.501
70	155.631	316.782	656.775	1433.829
71	146.847	338.467	659.082	1509.631
72	113.218	315.397	624.212	1436.730
73	141.257	350.925	793.331	1480.695
74	132.029	330.294	608.950	1456.636
75	111.089	350.925	606.643	1477.597
76	138.861	315.727	726.695	1468.698
77	149.686	365.492	697.680	1456.833
78	142.144	343.213	765.204	1513.520
79	160.600	329.239	711.167	1478.915
80	156.873	332.140	689.251	1483.529

APPENDIX B

Low Speed Experiment Type I WC (DC) Thrust and Torque

CFRP		Ti		
Hole #	Max Torque (N*cm)	Max Thrust (N)	Max Torque (N*cm)	Max Thrust (N)
1	111.880	224.832		
2	134.238	241.574		
3	139.231	244.079		
4	136.757	240.651		
5	134.642	251.066		
6	136.577	255.482		
7	146.024	256.932		
8	146.204	261.348		
9	143.685	266.028		
10	141.120	263.062		
11	137.881	272.290		
12	142.605	282.243		
13	138.826	278.024		
14	141.885	285.011		
15	142.155	290.350		
16	142.425	292.064		
17	148.498	296.019		
18	158.620	300.699		
19	149.038	303.335		
20	143.730	296.678		
21	114.284	237.846	544.798	944.283
22	93.790	237.935	472.306	960.761
23	102.468	241.538	476.121	982.381
24	107.861	266.893	460.328	1017.381
25	115.215	253.549	493.513	1015.404
26	105.410	266.893	473.548	1031.355
27	120.118	284.686	491.117	1042.165
28	117.667	293.583	468.668	1069.717
29	117.667	284.686	600.963	1044.011
30	120.118	284.686	545.596	1082.571
31	134.827	306.927	516.227	1082.900
32	98.056	311.376	480.824	1130.886
33	122.570	320.272	493.601	1129.436
34	120.118	302.479	498.126	1134.511
35	139.729	324.720	566.005	1182.167
36	142.181	315.824	577.540	1168.325
37	112.764	346.961	540.096	1161.602
38	129.924	338.065	484.906	1181.245
39	151.986	333.617	557.132	1181.838
40	151.986	333.617	506.467	1186.386

APPENDIX B

Low Speed Experiment Type I WC (DC) Thrust and Torque

Hole #	CFRP		Ti	
	Max Torque (N*cm)	Max Thrust (N)	Max Torque (N*cm)	Max Thrust (N)
41	141.878	333.656		
42	135.401	336.490		
43	152.082	340.181		
44	147.202	350.925		
45	151.904	342.884		
46	153.235	346.311		
47	153.945	351.255		
48	155.542	351.452		
49	156.429	353.364		
50	172.578	345.982		
51				
52	148.444	367.667		
53	149.775	366.547		
54	162.286	367.403		
55	155.099	385.793		
56	155.720	377.884		
57	154.655	373.006		
58	156.518	378.873		
59	172.135	371.358		
60	167.521	379.202		
61	149.001	397.720	746.836	1383.470
62	135.781	432.457	662.099	1384.789
63	114.219	447.288	664.406	1420.976
64	154.059	427.843	746.393	1402.124
65	121.406	440.630	598.480	1431.390
66	166.215	428.041	705.843	1415.505
67	127.617	441.817	641.070	1425.458
68	170.917	435.489	749.676	1421.042
69	142.879	405.432	648.257	1384.195
70	170.474	421.977	729.534	1412.605
71	110.138	436.148	650.387	1436.730
72	101.531	453.681	631.399	1471.994
73	119.454	456.186	611.967	1480.695
74	110.404	444.585	535.482	1481.354
75	128.860	466.073	644.442	1503.962
76	111.824	460.998	673.545	1508.906
77	135.958	462.711	647.725	1488.209
78	122.294	418.154	1058.990	1459.931
79	145.186	440.433	641.514	1498.623
80	131.522	445.772	704.778	1488.077

APPENDIX B

Low Speed Experiment Type I WC (DC5) Thrust and Torque

Hole #	CFRP		Ti	
	Max Torque (N*cm)	Max Thrust (N)	Max Torque (N*cm)	Max Thrust (N)
1	108.281	238.410		
2	126.005	237.487		
3	124.655	250.868		
4	131.403	256.141		
5	134.238	257.723		
6	142.245	265.171		
7	143.280	265.830		
8	143.145	262.271		
9	148.138	271.169		
10	144.719	276.311		
11	151.512	282.177		
12	147.104	289.889		
13	148.318	282.177		
14	149.218	287.714		
15	149.218	294.832		
16	149.173	290.416		
17	151.242	296.546		
18	143.460	304.851		
19	146.654	311.047		
20	146.384	301.094		
21	105.410	222.411	668.843	924.179
22	134.827	231.308	642.934	962.936
23	132.375	249.100	541.604	977.635
24	117.667	257.997	637.610	988.709
25	115.215	275.790	553.494	1015.140
26	122.570	266.893	587.566	1039.990
27	127.472	271.342	676.473	1043.352
28	129.924	284.686	629.802	1051.130
29	122.570	289.134	532.021	1087.646
30	125.021	284.686	705.399	1078.286
31	110.313	320.272	485.793	1125.679
32	102.958	298.031	614.185	1128.183
33	112.764	311.376	479.582	1119.483
34	105.410	324.720	566.182	1140.971
35	107.861	324.720	551.631	1155.801
36	122.570	320.272	657.308	1157.449
37	127.472	320.272	627.317	1150.924
38	139.729	315.824	803.091	1194.230
39	127.472	333.617	573.369	1186.188
40	120.118	333.617	471.508	1218.750

APPENDIX B

Low Speed Experiment Type I WC (DC5) Thrust and Torque

Hole #	CFRP		Ti	
	Max Torque (N*cm)	Max Thrust (N)	Max Torque (N*cm)	Max Thrust (N)
41	159.890	317.045		
42	165.835	328.910		
43	163.350	323.834		
44	162.108	339.456		
45	159.624	343.147		
46	157.938	337.149		
47	160.777	350.464		
48	166.811	353.562		
49	172.223	343.938		
50	174.442	340.906		
51	161.043	347.893		
52	161.398	352.902		
53	158.382	359.428		
54	166.811	378.411		
55	167.609	363.976		
56	164.681	352.111		
57	165.036	365.953		
58	164.326	371.622		
59	164.859	379.532		
60	170.271	359.362		
61	149.242	380.718	739.294	1316.831
62	138.772	399.767	586.679	1327.970
63	145.250	402.601	575.676	1329.948
64	148.444	396.010	567.336	1363.169
65	143.386	393.703	599.456	1371.276
66	134.957	426.660	612.677	1376.747
67	149.420	417.959	554.204	1368.574
68	159.091	414.532	704.867	1412.077
69	149.775	431.735	639.562	1380.966
70	119.252	498.045	588.808	1458.481
71	129.988	455.860	642.756	1455.317
72	126.439	469.438	624.478	1453.142
73	124.753	455.135	568.312	1431.852
74	135.046	453.091	700.519	1450.835
75	128.746	478.139	658.461	1470.610
76	139.926	464.495	637.610	1474.367
77	162.463	445.643	626.164	1425.326
78	167.964	443.600	657.574	1450.506
79	167.166	472.141	716.757	1462.766
80	141.878	459.551	651.008	1494.866

APPENDIX B

Low Speed Experiment Type I PCD Thrust and Torque

		CFRP			
Hole #	Max Torque (N*cm)	Max Thrust (N)			
1	127.625	383.091			
2	125.060	371.688			
3	111.385	379.663			
4	108.955	350.266			
5	115.433	364.503			
6	116.468	365.887			
7	121.372	371.622			
8	119.797	361.999			
9	121.551	355.803			
10	115.433	370.897			
11	130.009	376.631			
12	124.026	367.074			
13	124.566	360.614			
14	129.199	369.315			
15	125.960	369.117			
16	129.649	362.262			
17	118.987	377.093			
18	135.542	362.130			
19	124.476	358.835	Ti		
			Max Torque (N*cm)	Max Thrust (N)	
20	120.382	363.844			
21	78.445	240.204	490.318	1411.550	
22	83.347	249.100	639.118	1416.757	
23	95.604	249.100	663.430	1401.465	
24	102.958	244.652	597.948	1414.648	
25	134.827	244.652	647.814	1374.110	
26	98.056	257.997	830.775	1446.946	
27	98.056	275.790	675.409	1426.710	
28	110.313	271.342	664.495	1460.525	
29	122.570	271.342	620.929	1449.451	
30	112.764	275.790	588.099	1470.741	
31	105.410	275.790	562.722	1469.357	
32	115.215	311.376	678.603	1532.372	
33	107.861	280.238	666.270	1496.778	
34	102.958	293.583	669.730	1505.017	
35	98.056	284.686	614.185	1517.607	
36	122.570	280.238	589.341	1544.962	
37	115.215	289.134	630.689	1532.438	
38	105.410	302.479	678.692	1531.383	
39	98.056	284.686	647.636	1521.364	
40	112.764	298.031	672.214	1546.543	

APPENDIX B

Low Speed Experiment Type I PCD Thrust and Torque

Hole #	CFRP		Ti	
	Max Torque (N*cm)	Max Thrust (N)	Max Torque (N*cm)	Max Thrust (N)
41	117.389	300.105		
42	129.811	284.879		
43	123.511	291.669		
44	125.552	297.930		
45	125.463	294.898		
46	133.094	290.350		
47	128.835	289.032		
48	129.633	297.469		
49	137.885	292.657		
50	140.369	297.469		
51	128.657	296.085		
52	130.343	297.008		
53	129.988	299.380		
54	129.722	298.194		
55	126.883	304.588		
56	134.070	319.023		
57	130.343	304.719		
58	129.811	302.281		
59	132.029	303.335		
60	147.823	295.953	703.802	1638.297
61	92.303	334.245	673.812	1652.864
62	109.960	322.645	627.406	1673.496
63	113.510	345.187	801.051	1635.858
64	121.052	330.159	802.204	1657.347
65	93.812	343.539	730.599	1647.328
66	101.797	337.343	755.887	1639.154
67	94.788	330.686	762.275	1659.588
68	124.512	344.660	679.490	1641.132
69	119.454	340.969	719.685	1644.032
70	109.605	334.839	733.616	1690.898
71	116.793	359.622	846.924	1760.174
72	111.380	370.959	777.803	1706.585
73	113.421	355.931	827.315	1685.690
74	122.649	367.927	721.815	1709.947
75	112.977	350.197	839.648	1711.002
76	117.147	355.404	817.377	1654.842
77	121.052	335.498	733.261	1643.636
78	113.155	341.694	814.981	1663.345
79	132.941	374.255	779.933	1691.688
80	123.802	350.328		

APPENDIX B

High Speed Experiment Type II WC (DC) Thrust and Torque

Hole #	CFRP		Ti	
	Max Torque (N*cm)	Max Thrust (N)	Max Torque (N*cm)	Max Thrust (N)
1		222.411		464.363
2		222.411		1150.990
3		266.893		1113.221
4		286.910		1189.088
5		296.252		1238.920
6	122.570	311.376	1048.341	1179.728
7	151.986	306.927	1020.215	1218.816
8	161.792	333.617	989.425	1241.952
9	129.924	320.272	1002.113	1234.569
10	154.438	378.099	1063.425	1225.868
11	112.764	275.790	838.139	1000.046
12	98.056	293.583	728.114	996.157
13	129.924	280.238	751.982	1037.024
14	88.250	280.238	733.349	1033.530
15	88.250	275.790	696.704	1055.941
16	93.153	284.686	686.944	1060.951
17	102.958	324.720	758.104	1125.151
18	102.958	302.479	741.423	1125.019
19	78.445	302.479	686.766	1124.690
20	98.056	369.202	676.474	1174.126
21	130.077	346.772	691.646	1169.182
22	125.374	352.639	668.754	1175.971
23	162.108	376.368	708.328	1183.749
24	149.065	366.151	703.714	1205.303
25	168.319	436.152	732.729	1230.351
26	144.983	407.215	690.759	1237.338
27	166.456	391.396	701.850	1249.334
28	170.981	420.332	703.448	1267.988
29	191.123	446.236	709.304	1284.005
30	152.969	384.212	757.040	1273.063
31	151.816	481.434	743.376	1329.420
32	150.928	424.683	705.488	1324.872
33	156.430	461.858	699.987	1342.669
34	145.161	496.595	746.304	1331.991
35	160.245	488.949	728.292	1354.600
36	150.307	423.298	717.112	1373.319
37	148.799	468.845	751.717	1403.376
38	185.976	459.287	728.470	1395.928
39	151.904	510.041	746.215	1397.708
40	180.919	509.052	741.956	1415.768

APPENDIX B

High Speed Experiment Type II WC (DC) Thrust and Torque

Hole #	CFRP		Ti	
	Max Torque (N*cm)	Max Thrust (N)	Max Torque (N*cm)	Max Thrust (N)
41	140.724	436.086	763.252	1413.857
42	160.866	556.972	774.964	1441.541
43	141.700	557.829	783.394	1475.026
44	156.430	507.866	715.160	1479.706
45	168.674	534.100	729.357	1471.928
46	192.454	527.640	741.957	1519.518
47	151.372	537.132	800.163	1533.624
48	157.760	536.143	730.244	1509.961
49	162.729	529.749	745.506	1506.665
50	188.372	530.343	753.403	1529.604
51	150.218	525.729	778.602	1567.768
52	145.782	542.668	769.108	1583.588
53	266.188	571.868	745.949	1610.020
54	307.979	569.693	777.360	1624.653
55	184.734	592.433	738.585	1588.729
56	179.765	603.902	751.806	1621.291
57	177.192	615.174	755.355	1658.138
58	156.075	569.627	735.657	1662.818
59	170.715	576.153	787.653	1657.808
60	203.811	616.360	779.134	1690.304
61	135.756	526.783	734.148	1642.318
62	165.657	593.488	738.585	1649.635
63	149.154	570.945	728.824	1683.317
64	158.914	605.155	770.350	1693.007
65	136.554	582.810	778.868	1720.560
66	158.736	610.296	785.168	1773.226
67	155.187	617.613	791.734	1763.536
68	199.197	601.793	770.971	1748.310
69	211.619	563.761	895.105	1736.907
70	241.521	584.128	845.505	1734.995
71	178.079	612.669	788.540	1811.523
72	157.406	615.635	784.991	1811.325
73	151.017	616.360	757.041	1838.219
74	171.070	590.061	751.184	1838.680
75	185.000	614.844	771.060	1843.689
76	163.528	686.229	779.401	1892.137
77	157.228	685.899	797.945	1912.769
78	174.175	646.483	767.688	1910.659
79	171.070	673.573	816.224	1930.105
80	181.629	675.485	790.758	1976.377

APPENDIX B

High Speed Experiment Type II WC (DC5) Thrust and Torque

Hole #	CFRP		TI	
	Max Torque (N*cm)	Max Thrust (N)	Max Torque (N*cm)	Max Thrust (N)
1		222.411		1189.747
2	88.250	293.583	822.079	1198.778
3	93.153	311.376	849.408	1209.456
4	93.153	293.583	935.831	1228.966
5	98.056	329.168	943.107	1228.637
6	112.764	284.686	955.263	1204.842
7	122.570	346.961	943.817	1286.312
8	159.340	418.133	982.592	1246.763
9	151.986	351.410	950.383	1264.890
10	171.597	360.306	987.916	1266.208
11	102.958	226.859	858.990	987.127
12	102.958	231.308	712.586	986.863
13	120.118	240.204	729.977	1029.707
14	102.958	240.204	669.819	1075.452
15	120.118	235.756	655.533	1034.980
16	120.118	231.308	747.014	1039.792
17	120.118	240.204	733.793	1092.260
18	105.410	240.204	745.506	1149.276
19	120.118	235.756	734.857	1133.061
20	120.118	240.204	660.059	1120.405
21	126.528	338.863	684.814	1155.142
22	127.326	344.663	738.585	1143.212
23	146.847	368.985	691.469	1155.340
24	137.708	359.032	674.344	1183.881
25	124.221	355.078	689.251	1176.762
26	123.600	403.063	675.853	1187.045
27	143.209	405.040	700.963	1220.398
28	156.252	425.605	684.637	1236.678
29	149.775	400.163	681.797	1262.187
30	144.806	436.283	658.728	1244.852
31	116.324	428.506	667.956	1254.409
32	135.401	455.992	702.205	1279.589
33	134.957	464.824	695.462	1292.508
34	106.652	474.448	661.833	1295.936
35	129.633	474.184	669.641	1333.507
36	123.600	465.022	657.929	1322.236
37	153.147	475.436	724.920	1349.458
38	156.252	460.474	755.621	1326.718
39	165.125	478.271	747.014	1360.532
40	142.588	478.468	693.155	1356.709

APPENDIX B

High Speed Experiment Type II WC (DC5) Thrust and Torque

Hole #	CFRP		TI	
	Max Torque (N*cm)	Max Thrust (N)	Max Torque (N*cm)	Max Thrust (N)
41	130.254	447.027	730.865	1442.596
42	144.451	472.602	767.600	1427.238
43	178.079	508.591	741.247	1461.118
44	182.960	503.713	771.415	1470.676
45	151.461	508.986	774.520	1473.971
46	156.430	518.939	801.051	1471.467
47	168.231	483.478	773.101	1463.359
48	183.847	527.376	828.291	1489.989
49	169.384	459.881	805.576	1489.593
50	178.967	515.776	795.195	1493.746
51	139.571	524.806	758.283	1551.421
52	155.010	522.762	792.355	1574.096
53	159.535	507.273	786.410	1598.880
54	159.269	532.913	767.333	1567.373
55	162.641	549.589	752.338	1572.976
56	181.008	589.138	813.384	1588.993
57	163.350	513.337	811.432	1596.573
58	175.151	561.190	802.825	1594.068
59	267.874	550.644	822.257	1607.845
60	198.310	591.840	818.442	1635.990
61	194.626	510.391	766.605	1703.910
62	138.362	564.706	830.162	1671.292
63	97.334	594.163	768.912	1727.835
64	92.507	569.879	740.074	1759.232
65	125.541	562.910	772.603	1725.752
66	175.167	586.116	809.976	1733.870
67	164.156	582.883	782.984	1737.103
68	145.603	586.332	802.132	1733.942
69	144.999	588.559	820.357	1763.400
70	203.827	545.092	841.466	1788.331
71	205.184	575.842	724.041	1785.888
72	154.200	541.859	729.693	1807.298
73	82.552	571.675	686.091	1793.432
74	83.909	552.636	794.750	1868.656
75	102.462	637.558	772.603	1868.513
76	111.211	566.862	793.481	1855.652
77	102.462	583.674	692.897	1922.183
78	199.452	610.329	854.962	1925.416
79	161.139	567.293	831.431	1937.127
80	157.066	580.081	819.896	1945.102

APPENDIX B

Low Speed Experiment Type II WC (DC) Thrust and Torque

Hole #	CFRP		Ti	
	Max Torque (N*cm)	Max Thrust (N)	Max Torque (N*cm)	Max Thrust (N)
1	63.736	151.240	405.227	801.578
2	49.028	186.825	497.594	853.453
3	68.639	173.481	483.752	887.201
4	61.285	182.377	444.268	900.977
5	75.993	195.722	459.618	927.804
6	88.250	204.618	472.750	945.337
7	85.799	177.929	467.338	990.159
8	93.153	222.411	566.981	996.355
9	102.958	226.859	681.264	1016.590
10	102.958	231.308	639.117	1017.250
11	125.021	262.445	498.215	1036.826
12	107.861	271.342	526.343	1091.008
13	90.702	284.686	536.014	1086.460
14	125.021	271.342	597.060	1077.166
15	139.729	302.479	594.221	1101.092
16	100.507	298.031	613.387	1123.569
17	107.861	298.031	523.770	1148.814
18	110.313	306.927	545.775	1170.039
19	127.472	284.686	544.177	1153.099
20	122.570	315.824	585.880	1199.700
21	115.215	284.686	510.371	1162.327
22	98.056	315.824	476.920	1191.857
23	88.250	342.513	512.412	1210.708
24	88.250	311.376	505.314	1204.051
25	102.958	333.617	507.532	1232.196
26	95.604	351.410	615.605	1233.778
27	112.764	324.720	595.286	1254.871
28	112.764	355.858	586.147	1253.355
29	112.764	346.961	570.619	1303.714
30	137.278	333.617	548.614	1293.365
31	100.507	355.858	533.441	1316.171
32	129.924	364.754	595.641	1284.071
33	110.313	369.202	519.599	1315.249
34	112.764	360.306	546.396	1318.544
35	98.056	373.651	544.887	1343.131
36	139.729	373.651	539.386	1368.310
37	98.056	391.444	518.002	1361.916
38	122.570	391.444	614.629	1374.835
39	120.118	382.547	535.127	1378.790
40	122.570	404.788	624.833	1368.573

APPENDIX B

Low Speed Experiment Type II WC (DC) Thrust and Torque

Hole #	CFRP		Ti	
	Max Torque (N*cm)	Max Thrust (N)	Max Torque (N*cm)	Max Thrust (N)
41	132.739	443.139	589.962	1417.482
42	127.326	473.195	670.972	1442.003
43	131.497	499.824	686.855	1434.422
44	122.358	479.062	646.838	1434.225
45	145.782	479.325	601.586	1435.279
46	155.897	472.602	644.797	1449.319
47	138.151	490.662	699.366	1450.176
48	157.760	519.994	659.349	1457.624
49	160.156	492.838	675.498	1450.440
50	173.377	537.923	687.121	1483.331
51	127.060	525.531	638.941	1485.704
52	142.410	521.510	693.954	1498.689
53	150.928	506.152	702.294	1484.518
54	149.686	487.960	627.140	1483.595
55	165.480	516.764	615.073	1528.878
56	139.748	552.621	662.011	1572.316
57	169.561	529.090	718.709	1535.470
58	154.832	514.985	689.961	1541.600
59	167.343	539.109	728.470	1580.292
60	219.072	548.996	832.195	1559.661
61	150.840	534.100	712.232	1548.192
62	129.545	549.721	714.539	1568.823
63	143.120	540.691	632.020	1546.741
64	138.950	541.152	602.118	1540.941
65	146.048	556.840	684.903	1580.226
66	159.801	569.759	718.975	1585.170
67	137.264	520.851	542.758	1582.401
68	184.291	521.840	578.871	1581.610
69	158.470	521.971	614.540	1561.902
70	180.919	540.559	599.456	1599.803
71	124.576	579.185	728.470	1671.848
72	134.868	571.802	635.658	1658.336
73	124.664	566.793	634.061	1657.215
74	159.091	482.159	710.635	1587.741
75	134.247	594.675	593.068	1652.008
76	130.343	593.422	562.278	1675.474
77	165.746	582.283	586.502	1707.640
78	171.247	583.733	669.553	1700.785
79	164.593	590.061	651.452	1697.687
80	164.238	597.772	637.078	1747.848

APPENDIX B

Low Speed Experiment Type II WC (DC5) Thrust and Torque

CFRP			Ti		
Hole #	Max Torque (N*cm)	Max Thrust (N)	Hole #	Max Torque (N*cm)	Max Thrust (N)
1	61.285	155.688	1	506.733	891.353
3	78.445	231.308	2	487.124	914.819
5	93.153	253.549	3	470.177	960.959
7	95.604	289.134	4	477.009	981.326
9	98.056	306.927	5	524.568	1001.892
11	100.507	311.376	6	546.928	1009.669
13	90.702	333.617	7	552.429	1023.775
15	105.410	329.168	8	625.365	1058.973
17	120.118	338.065	9	560.859	1056.205
20	93.153	329.168	10	552.518	1075.452
21	100.507	311.376	11	529.093	1080.198
22	102.958	333.617	12	609.571	1099.313
23	90.702	333.617	13	586.147	1112.693
24	100.507	342.513	14	604.425	1119.021
25	105.410	329.168	15	614.984	1148.617
26	120.118	333.617	16	631.488	1146.310
27	120.118	338.065	17	647.903	1158.108
28	122.570	346.961	18	674.167	1154.747
29	129.924	346.961	19	610.636	1188.759
30	90.702	355.858	20	603.893	1207.676
31	144.632	346.961	21	585.171	1203.655
32	117.667	364.754	22	547.815	1216.970
33	85.799	364.754	23	567.070	1242.677
34	73.542	386.995	24	540.451	1236.415
35	115.215	373.651	25	553.849	1270.954
36	112.764	382.547	26	655.977	1270.097
37	127.472	391.444	27	596.705	1281.105
38	115.215	386.995	28	621.905	1288.026
39	122.570	395.892	29	616.492	1295.276
40	98.056	400.340	30	531.578	1365.937
			31	590.228	1323.092
			32	569.465	1332.914
			33	544.976	1377.142
			34	574.434	1382.020
			35	617.557	1374.704
			36	636.368	1377.142
			37	708.683	1380.504
			38	624.655	1397.774
			39	557.664	1399.422
			40	484.551	1445.628

APPENDIX B

Low Speed Experiment Type II WC (DC5) Thrust and Torque

Hole #	CFRP		Ti	
	Max Torque (N*cm)	Max Thrust (N)	Max Torque (N*cm)	Max Thrust (N)
41	148.799	460.606	737.520	1429.611
42	142.144	487.894	769.552	1486.891
43	153.235	493.826	699.277	1470.148
44	151.549	505.163	818.442	1506.599
45	141.878	491.651	786.765	1516.816
46	151.283	468.647	682.330	1467.841
47	155.010	502.659	671.061	1508.774
48	156.962	490.728	730.865	1495.855
49	165.125	493.826	793.686	1500.996
50	128.835	519.730	637.255	1539.557
51	158.204	519.994	719.685	1543.643
52	184.912	510.568	756.952	1540.018
53	150.041	504.372	728.558	1549.444
54	147.645	518.478	675.143	1551.355
55	171.602	504.636	763.962	1555.113
56	168.940	512.414	804.423	1551.421
57	167.077	503.779	732.196	1554.256
58	177.370	500.286	724.654	1569.680
59	177.902	529.947	777.804	1596.441
60	156.075	534.297	696.172	1579.897
61	90.770	525.531	529.715	1566.911
62	72.847	538.252	430.515	1542.061
63	70.451	533.111	392.805	1566.779
64	97.336	514.325	461.925	1567.109
65	91.391	520.258	481.801	1589.652
66	102.482	503.845	516.139	1581.281
67	120.139	532.584	545.065	1595.123
68	129.633	504.109	616.847	1583.983
69	134.247	507.339	621.639	1579.501
70	74.710	573.582	556.688	1612.986
71	78.969	542.668	483.131	1601.055
72	88.197	476.425	513.654	1631.508
73	75.065	565.277	532.554	1660.709
74	101.240	545.239	646.306	1662.620
75	94.230	573.450	506.467	1691.029
76	103.636	550.842	531.400	1685.624
77	98.844	545.766	487.568	1678.835
78	111.799	561.256	530.691	1686.943
79	108.427	544.382	485.705	1684.768
80	84.736	584.656	587.123	1749.628

APPENDIX B

Low Speed Experiment Type II PCD Thrust and Torque

Hole #	CFRP		Ti	
	Max Torque (N*cm)	Max Thrust (N)	Max Torque (N*cm)	Max Thrust (N)
1	156.889	200.170	713.651	1293.167
2	115.215	217.963	745.151	1310.041
3	115.215	226.859	837.608	1342.142
4	171.597	231.308	738.940	1339.176
5	164.243	231.308	836.543	1431.258
6	102.958	244.652	747.901	1361.916
7	93.153	266.893	751.539	1342.142
8	122.570	257.997	851.716	1351.040
9	110.313	257.997	731.752	1328.563
10	122.570	262.445	794.573	1349.326
11	183.854	244.652	783.837	1358.620
12	107.861	280.238	775.497	1390.919
13	132.375	280.238	858.814	1412.736
14	127.472	289.134	879.222	1402.454
15	125.021	284.686	897.767	1429.083
16	171.597	298.031	907.882	1451.890
17	117.667	293.583	842.488	1446.880
18	126.996	294.371	958.991	1427.172
19	123.092	288.702	816.490	1450.176
20	183.517	282.836	748.079	1421.899
21	126.173	290.812	768.664	1461.777
22	145.782	302.808	761.388	1437.125
23	158.736	288.043	680.200	1431.456
24	167.964	297.271	691.025	1455.317
25	142.499	313.354	762.364	1466.720
26	168.674	289.955	755.887	1453.604
27	166.900	294.437	705.133	1463.689
28	193.962	327.855	721.371	1468.039
29	209.312	317.177	800.252	1430.929
30	147.468	311.706	755.443	1486.627
31	131.497	307.488	734.769	1550.762
32	165.125	350.002	679.224	1494.866
33	164.504	305.840	711.699	1490.780
34	173.199	318.166	773.899	1488.275
35	158.825	313.947	755.354	1490.450
36	158.027	334.117	655.267	1451.824
37	187.840	309.004	786.943	1491.175
38	185.533	312.959	777.448	1462.107
39	181.274	320.209	740.803	1469.753
40	169.739	300.105	846.658	1442.596

APPENDIX B

Low Speed Experiment Type II PCD Thrust and Torque

Hole #	CFRP		Ti	
	Max Torque (N*cm)	Max Thrust (N)	Max Torque (N*cm)	Max Thrust (N)
41	159.091	354.550	903.978	1549.642
42	154.477	370.633	840.624	1534.415
43	157.849	375.511	903.268	1561.440
44	182.338	349.936	894.306	1588.927
45	191.832	345.652	792.887	1543.907
46	173.820	382.564	770.705	1544.039
47	160.600	378.543	869.905	1544.962
48	174.974	393.571	925.184	1535.074
49	177.370	353.562	870.970	1597.034
50	174.885	355.473	955.264	1560.715
51	179.322	395.615	884.013	1567.504
52	144.717	382.168	854.555	1603.560
53	183.048	369.381	956.417	1579.501
54	168.497	401.349	861.476	1587.147
55	163.350	384.212	843.109	1626.037
56	163.794	401.283	899.186	1628.146
57	178.434	403.063	1012.672	1596.969
58	181.895	387.507	821.015	1628.015
59	166.101	404.315	829.977	1635.792
60	169.473	380.784	912.052	1646.537
61	152.969	345.125	788.806	1600.001
62	156.784	375.379	759.614	1558.079
63	123.067	372.743	755.355	1627.092
64	136.554	362.064	791.202	1606.460
65	132.739	415.718	780.732	1633.617
66	152.259	379.202	814.538	1670.859
67	149.154	382.696	705.045	1651.942
68	142.677	373.402	902.470	1652.205
69	185.799	383.289	787.475	1578.249
70	201.415	364.371	820.483	1649.503
71	138.329	394.362	894.661	1687.075
72	140.103	395.087	711.788	1639.682
73	126.617	374.259	785.346	1701.971
74	144.806	363.251	759.969	1800.449
75	171.780	361.010	724.477	1717.791
76	150.928	361.274	859.702	1686.284
77	138.772	371.820	891.911	1765.250
78	151.106	347.959	912.674	1670.134
79	146.403	342.884	857.306	1614.304
80	158.470	360.812	790.847	1625.576

APPENDIX C

APPENDIX C

Hole Diameter and Roundness Tables

High Speed Experiment Type I WC (DC) Diameter and Roundness

CFRP				
Hole #	Diameter (mm)	Roundness (mm)		
1	9.5225	0.0079		
2	9.5212	0.0099		
3	9.5212	0.0071		
4	9.5192	0.0160		
5	9.5189	0.0117		
6	9.5197	0.0104		
7	9.5207	0.0064		
8	9.5194	0.0160		
9	9.5189	0.0053		
10	9.5192	0.0157		
11	9.5202	0.0046		
14	9.5197	0.0081		
17	9.5194	0.0056	Ti	
20	9.5197	0.0084	Diameter (mm)	Roundness (mm)
21	9.5474	0.0241	9.5542	0.0155
24	9.6309	0.0239	9.5667	0.0325
27	9.5905	0.0211	9.5651	0.0203
30	9.5870	0.0112	9.5613	0.0262
33	9.6042	0.0244	9.5768	0.0229
36	9.6045	0.0145	9.5659	0.0218
39	9.6157	0.0193	9.5712	0.0264
40	9.6429	0.0196	9.5750	0.0297

APPENDIX C

High Speed Experiment Type I WC (DC) Diameter and Roundness

CFRP				
Hole #	Diameter (mm)	Roundness (mm)		
41	9.5740	0.0145		
42	9.5250	0.0074		
43	9.5197	0.0038		
44	9.5209	0.0028		
47	9.5217	0.0102		
50	9.5199	0.0028		
53	9.5207	0.0069		
56	9.5197	0.0056		
59	9.5217	0.0076	Ti	
60	9.5192	0.0058	Diameter (mm)	Roundness (mm)
61	9.5336	0.0267	9.5834	0.0292
62	9.6251	0.0262	9.5745	0.0137
64	9.6060	0.0259	9.5809	0.0302
67	9.6048	0.0257	9.5882	0.0211
70	9.5974	0.0224	9.5824	0.0135
71	9.6152	0.0356	9.5773	0.0142
73	9.6101	0.0229	9.5783	0.0386
76	9.5987	0.0249	9.5877	0.0424
79	9.5943	0.0320	9.5801	0.0272
80	9.6063	0.0318	9.5933	0.0262

APPENDIX C

High Speed Experiment Type I PCD Diameter and Roundness

CFRP				
Hole #	Diameter (mm)	Roundness (mm)		
1	9.5174	0.0140		
4	9.5194	0.0099		
7	9.5108	0.0109		
10	9.5146	0.0076		
11	9.5146	0.0076		
14	9.5123	0.0069		
17	9.5077	0.0079	Ti	
20	9.5108	0.0107	Diameter (mm)	Roundness (mm)
21	9.5367	0.0147	9.5303	0.0693
24	9.5438	0.0198	9.5380	0.0084
27	9.5512	0.0104	9.5491	0.0155
30	9.5601	0.0191	9.5456	0.0091
33	9.5712	0.0188	9.5659	0.0091
36	9.5463	0.0066	9.5499	0.0091
39	9.5750	0.0180	9.5517	0.0084
40	9.5593	0.0147	9.5420	0.0081
41	9.5146	0.0137		
42	9.5164	0.0066		
44	9.5184	0.0038		
47	9.5194	0.0076		
50	9.5192	0.0081		
53	9.5131	0.0152		
56	9.5153	0.0175		
59	9.5187	0.0086	Ti	
60	9.5136	0.0140	Diameter (mm)	Roundness (mm)
61	9.5608	0.0297	9.5550	0.0061
62	9.5674	0.0381	9.5489	0.0038
63	9.5570	0.0239	9.5636	0.0069
64	9.5710	0.0378	9.5509	0.0038
67	9.5479	0.0274	9.5512	0.0041
70	9.5522	0.0295	9.5458	0.0038
71	9.5773	0.0246	9.5463	0.0048
73	9.5512	0.0264	9.5613	0.0025
76	9.5575	0.0198	9.5491	0.0086
79	9.5608	0.0310	9.5491	0.0196
80	9.5588	0.0302	9.5524	0.0076

APPENDIX C

Low Speed Experiment Type I WC (DC) Diameter and Roundness

		CFRP			
Hole #	Diameter (mm)	Roundness (mm)			
1	9.521952	0.007366			
4	9.5197	0.0079			
7	9.5181	0.0061			
10	9.5176	0.0076			
11	9.5184	0.0086			
14	9.5181	0.0091			
17	9.5179	0.0069	Ti		
20	9.5189	0.0086	Diameter (mm)	Roundness (mm)	
21	9.5395	0.0213	9.5489	0.0069	
24	9.5573	0.0272	9.5390	0.0028	
27	9.5664	0.0310	9.5418	0.0046	
30	9.5552	0.0259	9.5397	0.0028	
33	9.5644	0.0211	9.5489	0.0010	
36	9.5550	0.0198	9.5446	0.0094	
39	9.5613	0.0274	9.5489	0.0046	
40	9.5687	0.0173	9.5402	0.0071	
41	9.5166	0.0094			
44	9.5138	0.0081			
47	9.5153	0.0056			
50	9.5120	0.0104			
53	9.5100	0.0081			
56	9.5108	0.0061			
59	9.5131	0.0053	Ti		
60	9.5115	0.0071	Diameter (mm)	Roundness (mm)	
61	9.5448	0.0030	9.5613	0.0170	
64	9.5654	0.0384	9.5527	0.0084	
67	9.5758	0.0213	9.5433	0.0119	
70	9.5496	0.0221	9.5527	0.0099	
73	9.5646	0.0307	9.5453	0.0041	
76	9.5677	0.0279	9.5509	0.0079	
79	9.5537	0.0267	9.5433	0.0099	
80	9.5435	0.0292	9.5461	0.0099	

APPENDIX C

Low Speed Experiment Type I WC (DC5) Diameter and Roundness

CFRP				
Hole #	Diameter (mm)	Roundness (mm)		
1	9.5227	0.0051		
4	9.5187	0.0074		
7	9.5209	0.0081		
10	9.5171	0.0091		
11	9.5181	0.0066		
14	9.5179	0.0043		
17	9.5199	0.0028	Ti	
20	9.5199	0.0081	Diameter (mm)	Roundness (mm)
21	9.5646	0.0312	9.5573	0.0117
24	9.5601	0.0325	9.5585	0.0048
27	9.5512	0.0198	9.5659	0.0038
30	9.5443	0.0193	9.5682	0.0043
33	9.5608	0.0381	9.5486	0.0025
36	9.5598	0.0198	9.5529	0.0066
39	9.6009	0.0226	9.5529	0.0051
40	9.5748	0.0384	9.5423	0.0048
41	9.5204	0.0046		
44	9.5166	0.0079		
47	9.5174	0.0043		
50	9.5148	0.0038		
53	9.5181	0.0056		
56	9.5143	0.0051		
59	9.5128	0.0061	Ti	
60	9.5153	0.0051	Diameter (mm)	Roundness (mm)
61	9.5448	0.0236	9.5573	0.0041
64	9.5547	0.0323	9.5550	0.0046
67	9.5590	0.0338	9.5552	0.0069
70	9.5994	0.0401	9.5461	0.0114
73	9.5458	0.0290	9.5471	0.0272
76	9.5728	0.0361	9.5608	0.0086
79	9.5634	0.0399	9.5715	0.0107
80	9.5547	0.0368	9.5631	0.0053

APPENDIX C

Low Speed Experiment Type I PCD Diameter and Roundness

CFRP				
Hole #	Diameter (mm)	Roundness (mm)		
1	9.5199	0.0084		
4	9.5136	0.0046		
7	9.5133	0.0041		
10	9.5113	0.0061		
11	9.5118	0.0140		
14	9.5108	0.0066		
17	9.5110	0.0051	Ti	
20	9.5123	0.0071	Diameter (mm)	Roundness (mm)
21	9.5540	0.0351	9.5418	0.0041
24	9.5740	0.0224	9.5420	0.0036
27	9.5641	0.0152	9.5458	0.0028
30	9.5809	0.0384	9.5486	0.0043
33	9.5651	0.0175	9.5486	0.0036
36	9.5936	0.0229	9.5349	0.0145
39	9.5847	0.0358	9.5491	0.0152
40	9.5885	0.0277	9.5512	0.0038
41	9.5242	0.0061		
44	9.5174	0.0053		
47	9.5204	0.0033		
50	9.5174	0.0079		
53	9.5194	0.0076		
56	9.5184	0.0058		
59	9.5171	0.0069	Ti	
60	9.5171	0.0041	Diameter (mm)	Roundness (mm)
61	9.5834	0.0312	9.5397	0.0071
64	9.5733	0.0269	9.5514	0.0081
67	9.5758	0.0236	9.5369	0.0122
70	9.5860	0.0213	9.5458	0.0043
73	9.5979	0.0366	9.5522	0.0028
76	9.5870	0.0340	9.5466	0.0066
79	9.5512	0.0201	9.5618	0.0056
80	9.5659	0.0193	9.5484	0.0056

APPENDIX C

High Speed Experiment Type II WC (DC) Diameter and Roundness

Hole #	CFRP		Ti	
	Diameter (mm)	Roundness (mm)	Diameter (mm)	Roundness (mm)
1	9.4917	0.0683	9.5641	0.0269
2	9.5568	0.0559	9.5880	0.0038
3	9.5496	0.0721	9.5735	0.0157
4	9.4973	0.1168	9.5545	0.0234
5	9.5568	0.0381	9.5753	0.0180
6	9.5989	0.0170	9.5804	0.0180
7	9.7617	0.1930	9.5895	0.0089
8	9.6177	0.0198	9.5768	0.0274
9	9.5852	0.0348	9.5822	0.0178
10	9.6017	0.0262	9.5753	0.0188
11	9.5573	0.0130	9.5839	0.0135
14	9.6081	0.0089	9.5773	0.0678
17	9.6030	0.0081	9.5855	0.0521
20	9.6256	0.0203	9.5743	0.0505
21	9.5837	0.0262	9.5773	0.0610
24	9.5656	0.0201	9.5865	0.0246
27	9.5921	0.0132	9.5862	0.0320
30	9.5400	0.0132	9.5814	0.0170
31	9.5956	0.0117	9.5766	0.0450
34	9.5438	0.0117	9.5715	0.0300
37	9.5885	0.0170	9.5745	0.0142
39	9.5339	0.0102	9.5644	0.0160
40	9.5672	0.0114	9.5606	0.0208
41	9.5293	0.0079	9.5710	0.0122
44	9.5804	0.0150	9.5687	0.0198
47	9.5430	0.0137	9.5626	0.0104
50	9.5839	0.0211	9.5621	0.0241
51	9.5357	0.0109	9.5575	0.0140
54	9.5735	0.0145	9.5728	0.0399
57	9.5842	0.0119	9.5585	0.0462
60	9.5537	0.0127	9.5654	0.0079
61	9.5334	0.0109	9.5707	0.0175
64	9.5796	0.0363	9.5674	0.0081
67	9.5352	0.0213	9.5761	0.0150
70	9.5568	0.0371	9.5740	0.0109
73	9.5641	0.0173	9.5692	0.0127
76	9.5395	0.0216	9.5667	0.0127
79	9.5217	0.0058	9.5689	0.0124
80	9.5402	0.0058	9.5656	0.0046

APPENDIX C

High Speed Experiment Type II WC (DC5) Diameter and Roundness

Hole #	CFRP		Ti	
	Diameter (mm)	Roundness (mm)	Diameter (mm)	Roundness (mm)
1	9.5087	0.0531	9.5552	0.0376
2	9.6083	0.0569	9.5707	0.0338
3	9.6210	0.0353	9.5763	0.0366
4	9.6337	0.0251	9.5761	0.0188
5	9.6523	0.0384	9.5761	0.0183
6	9.6223	0.0361	9.5753	0.0229
7	9.5550	0.0165	9.5847	0.0163
8	9.6307	0.0165	9.5806	0.0102
9	9.8113	0.2621	9.5870	0.0432
10	9.8336	0.1953	9.5959	0.0419
13	9.6467	0.0422	9.6004	0.0417
16	9.5583	0.0201	9.6185	0.0152
19	9.5961	0.0264	9.5969	0.0173
20	9.6154	0.0333	9.5895	0.0173
21	9.6078	0.0246	9.5989	0.0155
24	9.5865	0.0302	9.5745	0.0201
27	9.6241	0.0277	9.5928	0.0142
30	9.5999	0.0239	9.5938	0.0224
33	9.6042	0.0378	9.6169	0.0231
36	9.6040	0.0297	9.5829	0.0193
39	9.5661	0.0185	9.5849	0.0089
40	9.5512	0.0160	9.5799	0.0066
41	9.5707	0.0262	9.5943	0.0109
44	9.5915	0.0305	9.5849	0.0107
47	9.5923	0.0297	9.5905	0.0191
50	9.6352	0.0292	9.5804	0.0216
53	9.6238	0.0302	9.5811	0.0300
56	9.6266	0.0335	9.5783	0.0203
59	9.6355	0.0561	9.5735	0.0353
60	9.6408	0.0254	9.5722	0.0188
61	9.5628	0.0302	9.5903	0.0152
64	9.5705	0.0264	9.5788	0.0155
67	9.5753	0.0472	9.5778	0.0188
70	9.5870	0.0394	9.5804	0.0168
73	9.5296	0.0163	9.5788	0.0094
76	9.5710	0.0218	9.5872	0.0061
79	9.6177	0.0373	9.5816	0.0099
80	9.6154	0.0480	9.5768	0.0135

APPENDIX C

Low Speed Experiment Type II WC (DC) Diameter and Roundness

Hole #	CFRP		Ti	
	Diameter (mm)	Roundness (mm)	Diameter (mm)	Roundness (mm)
1	9.5258	0.0409	9.5311	0.0094
4	9.5362	0.0378	9.5402	0.0064
7	9.5334	0.0328	9.5349	0.0071
10	9.5369	0.0269	9.5380	0.0076
13	9.5400	0.0132	9.5479	0.0117
16	9.5293	0.0287	9.5468	0.0061
19	9.5428	0.0175	9.5443	0.0048
20	9.5407	0.0142	9.5524	0.0043
21	9.5479	0.0117	9.5529	0.0061
24	9.5377	0.0119	9.5479	0.0043
27	9.5479	0.0102	9.5555	0.0028
30	9.5504	0.0224	9.5504	0.0030
33	9.5758	0.0211	9.5479	0.0036
36	9.5555	0.0081	9.5504	0.0043
39	9.5453	0.0140	9.5479	0.0023
40	9.5606	0.0157	9.5504	0.0061
41	9.5507	0.0196	9.5537	0.0094
44	9.5585	0.0292	9.5496	0.0127
47	9.5507	0.0183	9.5514	0.0152
50	9.5971	0.0213	9.5537	0.0079
51	9.5438	0.0201	9.5420	0.0084
54	9.5514	0.0218	9.5496	0.0107
57	9.5491	0.0279	9.5484	0.0036
60	9.5532	0.0160	9.5451	0.0071
61	9.5618	0.0274	9.5461	0.0036
64	9.5649	0.0386	9.5428	0.0114
67	9.5611	0.0274	9.5458	0.0041
70	9.5702	0.0318	9.5476	0.0069
73	9.5479	0.0290	9.5443	0.0071
76	9.5951	0.0597	9.5471	0.0160
79	9.5583	0.0384	9.5387	0.0127
80	9.5517	0.0391	9.5402	0.0041

APPENDIX C

Low Speed Experiment Type II WC (DC5) Diameter and Roundness

Hole #	CFRP		Ti	
	Diameter (mm)	Roundness (mm)	Diameter (mm)	Roundness (mm)
1	9.5463	0.0147	9.5453	0.0114
4	9.5390	0.0102	9.5413	0.0064
7	9.5598	0.0097	9.5481	0.0084
10	9.5504	0.0152	9.5448	0.0028
13	9.5484	0.0130	9.5418	0.0020
16	9.5446	0.0193	9.5453	0.0041
19	9.5489	0.0165	9.5415	0.0084
20	9.5631	0.0069	9.5372	0.0086
21	9.5453	0.0086	9.5504	0.0030
24	9.5580	0.0241	9.5479	0.0041
27	9.5529	0.0168	9.5504	0.0030
30	9.5529	0.0079	9.5555	0.0043
33	9.5656	0.0175	9.5555	0.0048
36	9.5580	0.0201	9.5504	0.0036
39	9.5961	0.0216	9.5580	0.0028
40	9.5809	0.0150	9.5555	0.0064
41	9.5684	0.0300	9.5611	0.0038
44	9.5628	0.0320	9.5509	0.0058
47	9.5621	0.0246	9.5458	0.0046
50	9.5590	0.0353	9.5390	0.0064
51	9.5682	0.0330	9.5527	0.0071
54	9.5679	0.0366	9.5501	0.0036
57	9.5659	0.0292	9.5458	0.0033
60	9.5667	0.0267	9.5499	0.0053
61	9.5613	0.0318	9.5486	0.0018
64	9.5667	0.0188	9.5456	0.0081
67	9.5626	0.0274	9.5573	0.0051
70	9.5852	0.0221	9.5593	0.0071
73	9.5621	0.0160	9.5550	0.0056
76	9.5710	0.0206	9.5585	0.0079
79	9.5695	0.0323	9.5509	0.0064
80	9.5646	0.0213	9.5674	0.0058

APPENDIX C

Low Speed Experiment Type II PCD Diameter and Roundness

Hole #	CFRP		Ti	
	Diameter (mm)	Roundness (mm)	Diameter (mm)	Roundness (mm)
1	9.5613	0.0155	9.5458	0.0094
4	9.5613	0.0155	9.5458	0.0094
7	9.5466	0.0086	9.5573	0.0084
10	9.5702	0.0241	9.5512	0.0069
13	9.5425	0.0127	9.5380	0.0137
16	9.5402	0.0117	9.5481	0.0150
19	9.5385	0.0112	9.5512	0.0094
20	9.5468	0.0102	9.5397	0.0071
21	9.5352	0.0142	9.5402	0.0130
24	9.5504	0.0099	9.5428	0.0066
27	9.5580	0.0198	9.5479	0.0041
30	9.5453	0.0089	9.5529	0.0124
33	9.5352	0.0081	9.5479	0.0071
36	9.5834	0.0071	9.5555	0.0058
39	9.5580	0.0155	9.5555	0.0020
40	9.5555	0.0163	9.5504	0.0061
41	9.5484	0.0147	9.5547	0.0086
44	9.5811	0.0193	9.5611	0.0218
47	9.5745	0.0267	9.5514	0.0069
50	9.5631	0.0140	9.5565	0.0079
51	9.5529	0.0112	9.5451	0.0302
54	9.5517	0.0150	9.5557	0.0061
57	9.5585	0.0257	9.5613	0.0097
60	9.5636	0.0140	9.5651	0.0135
61	9.5682	0.0376	9.5588	0.0051
64	9.5761	0.0310	9.5532	0.0079
67	9.5593	0.0330	9.5474	0.0013
70	9.5562	0.0274	9.5585	0.0038
73	9.5545	0.0160	9.5522	0.0020
76	9.5717	0.0196	9.5446	0.0053
79	9.5799	0.0142	9.5458	0.0064
80	9.5898	0.0145	9.5489	0.0066

APPENDIX D

APPENDIX D

Hole Surface Roughness

High Speed Experiment Type I WC (DC) CFRP

E1	CFRP						
test#	hole#	Ra	Rq	Rz	Rt	Rp	Rv
1	1	4.862	8.096	33.636	48.13	8.66	24.97
2	5	2.618	4.501	21.807	31.51	4.01	17.8
3	10	3.153	5.372	25.731	41	5.24	20.5
4	11	3.893	7.042	31.581	47.55	5.64	25.94
5	15	2.927	5.017	23.322	40.46	6.01	17.31
6	20	2.84	5.3	25.633	43.25	4.98	20.65
7	21	6.121	10.093	36.072	84.38	12.06	24.01
8	22	8.781	10.692	40.512	48.25	13.23	27.28
9	25	7.195	8.528	30.401	41.55	12.47	17.93
10	30	9.733	11.182	38.264	46.54	13.94	24.32
11	31	8.65	11.158	39.577	54.77	14.23	25.35
12	35	6.847	9.851	39.346	80.5	12.72	26.62
13	40	7.234	10.321	39.718	69.74	10.22	29.49
14	41	4.227	5.579	27.182	41.97	8.61	18.57
15	45	1.019	1.375	9.742	16.56	3.96	5.78
16	50	0.848	1.194	8.369	14.24	3.6	4.77
17	51	2.215	3.942	22.449	37.57	6.65	15.8
18	55	2.862	4.948	22.831	49.96	6.49	16.34
19	60	3.044	5.308	24.913	57.77	6.81	18.11
20	61	7.044	10.484	44.266	82.73	13.52	30.75
21	62	5.97	8.354	32.29	54.27	11.05	21.24
22	65	8.292	9.622	33.28	45.56	12.2	21.08
23	70	7.409	9.296	34.917	45.59	11.49	23.43
24	71	7.569	9.396	35.671	50.82	14.78	20.89
25	75	10.082	12.458	50.01	68.86	17.15	32.86
26	80	9.83	12.201	44.861	63.67	14.06	30.8
Average		5.5871	7.7427	31.399	50.277	9.7608	21.638

APPENDIX D

High Speed Experiment Type I WC (DC) Ti

E1	Ti							
test#	hole#	Ra	Rq	Rz	Rt	Rp	Rv	
1	21	0.431	0.609	2.628	4.19	1.41	1.21	
2	22	0.362	0.445	1.952	2.45	1.01	0.94	
3	25	0.908	1.223	5.259	7.85	3.18	2.08	
4	30	0.796	1.101	3.717	6.36	1.91	1.81	
5	31	0.705	0.897	3.764	5.31	1.87	1.89	
6	35	0.771	1.036	4.597	6.24	2.23	2.37	
7	40	0.423	0.565	2.562	4.11	1.44	1.12	
8	61	0.669	0.946	3.913	6.76	2.22	1.69	
9	62	0.626	0.907	3.36	7.24	1.78	1.58	
10	65	1.024	1.674	6.122	14.45	3.47	2.65	
11	70	0.437	0.552	2.497	3.83	1.47	1.03	
12	71	0.469	0.604	2.375	3.26	1.23	1.15	
13	75	0.45	0.56	2.271	2.9	1.11	1.16	
14	80	0.505	0.72	2.831	4.71	1.69	1.14	
Average		0.6126	0.8456	3.4177	5.69	1.8586	1.5586	

APPENDIX D

High Speed Experiment Type I PCD CFRP

G1		CFRP						
Test #	Hole #	Ra	Rq	Rz	Rt	Rp	Rv	
1	1	2.026	3.006	15.302	24.120	4.220	11.090	
2	5	2.414	4.064	15.893	38.010	4.370	11.520	
3	10	1.743	2.325	13.657	19.420	4.940	8.720	
4	15	1.676	2.179	11.373	14.700	3.540	7.830	
5	20	1.968	2.786	13.798	25.430	4.120	9.680	
6	21	2.346	3.568	15.661	31.430	5.290	10.370	
7	25	8.983	11.470	38.528	55.200	12.490	26.040	
8	30	6.477	9.111	32.993	64.650	10.660	22.340	
9	35	7.730	9.839	35.623	45.490	12.020	23.610	
10	40	9.828	11.142	38.760	57.460	12.800	25.960	
11	41	5.888	9.193	31.927	62.280	10.240	21.680	
12	45	1.407	2.185	15.862	28.960	6.700	9.160	
13	50	2.622	4.382	26.219	42.040	11.920	14.300	
14	51	3.272	5.714	27.554	52.380	10.010	17.540	
15	55	1.356	1.975	12.634	17.750	4.830	7.810	
16	60	3.587	6.887	28.185	68.190	6.780	21.430	
17	61	7.160	8.943	30.973	46.750	12.420	18.550	
18	65	5.190	7.194	24.155	45.480	7.890	16.270	
19	70	4.939	7.419	23.963	48.690	9.180	17.780	
20	75	5.121	6.998	26.653	37.340	7.970	18.680	
21	80	6.351	9.616	30.064	51.520	9.650	20.420	
Average		4.385	6.190	24.275	41.776	8.192	16.228	

APPENDIX D

High Speed Experiment Type II WC (DC) CFRP

E3	CFRP							
test#	hole#	Ra	Rq	Rz	Rt	Rp	Rv	
1	2	5.046	7.733	29.896	52.06	10.47	19.43	
2	5	5.259	6.628	28.615	40.73	10.73	17.88	
3	10	8.164	11.888	46.092	77.74	13.87	32.22	
4	11	4.882	6.8	28.404	55.74	9.42	18.98	
5	15	6.068	7.873	30.422	47.28	12.35	18.07	
6	20	6.016	8.681	35.256	57.19	10.57	24.69	
7	21	6.767	11.213	47.23	94.04	12.77	34.46	
8	25	7.633	11.144	42.436	74.63	12.35	30.08	
9	30	5.765	7.456	32.488	49.52	11.81	20.67	
10	31	6.786	9.917	40.728	63.81	11.42	29.31	
11	35	6.206	9.432	41.318	63.31	11.06	30.25	
12	40	4.218	5.844	23.156	37.2	8.15	15.01	
13	41	3.925	5.571	23.846	44.09	7.96	15.88	
14	45	9.326	13.618	53.365	72.37	15.53	37.84	
15	50	6.596	9.731	36.529	81.35	10.11	26.42	
16	51	4.85	6.825	31.211	46.57	9.18	22.03	
17	55	5.326	6.918	31.029	39.43	10.92	20.11	
18	60	5.294	8.095	34.676	60.26	9.42	25.25	
19	61	3.703	5.469	22.921	35.63	6.99	15.93	
20	65	5.895	9.894	34.537	90.24	16.2	18.34	
21	70	5.944	10.123	35.146	79.22	9.93	25.22	
22	71	4.318	7.142	28.5	46.26	8.22	20.28	
23	75	4.434	5.549	21.884	28.01	7.91	13.97	
24	80	7.558	10.726	43.878	63.16	12.87	31.01	
Average		5.8325	8.5113	34.315	58.327	10.842	23.472	
St Dev		1.3967	2.2389	8.3427	18.013	2.3574	6.6977	

APPENDIX D

High Speed Experiment Type II WC (DC) Ti

E3	Ti						
test#	hole#	Ra	Rq	Rz	Rt	Rp	Rv
1	2	0.441	0.552	2.603	3.38	1.39	1.21
2	5	0.692	0.889	3.343	4.54	1.79	1.55
3	10	1.32	1.783	6.527	9.31	3.6	2.92
4	11	0.811	1.23	4.854	10.6	2.27	2.59
5	15	0.803	1.002	3.493	6.26	1.85	1.65
6	20	0.697	0.887	3.493	5.8	1.96	1.53
7	21	0.536	0.666	2.691	4.12	1.52	1.17
8	25	0.915	1.246	4.792	7.78	2.98	1.82
9	30	0.921	1.153	4.397	6.09	2.43	1.97
10	31	0.611	0.748	2.796	3.53	1.64	1.16
11	35	0.713	0.958	3.998	6.89	1.85	2.14
12	40	0.981	1.352	4.928	8.61	2.67	2.26
13	41	0.663	0.834	3.13	5.27	1.51	1.62
14	45	0.734	0.959	3.912	5.08	2.1	1.81
15	50	0.488	0.613	2.751	3.51	1.48	1.27
16	51	0.971	1.275	4.894	6.73	2.5	2.39
17	55	0.889	1.279	4.967	9.39	2.08	2.89
18	60	0.79	1.022	3.85	6.12	1.99	1.86
19	61	0.721	0.915	3.51	5.83	1.84	1.67
20	65	1.378	2.037	7.143	12.46	3.84	3.31
21	70	0.588	0.788	3.065	4.85	1.97	1.1
22	71	0.707	0.893	3.229	4.72	1.66	1.57
23	75	0.66	0.794	2.955	4.49	1.41	1.55
24	80	0.687	0.873	3.407	4.22	1.95	1.46
Average		0.7799	1.0312	3.947	6.2325	2.095	1.8529
St Dev		0.2255	0.3479	1.1771	2.3786	0.6423	0.6026

APPENDIX D

Low Speed Experiment Type II WC (DC) CFRP

E4		CFRP						
test#	hole#	Ra	Rq	Rz	Rt	Rp	Rv	
1	1	4.873	7.673	29.164	42.17	7.06	22.11	
2*	4	5.14	6.472	21.628	37.89	7.96	13.67	
3	7	5.452	7.648	29.074	49.56	8.61	20.47	
4*	10	7.282	12.031	34.839	76.35	9.44	25.39	
5	13	6.357	8.53	32.793	45.2	11.42	21.37	
6	16	6.49	9.783	33.105	61.69	10.61	22.5	
7	19	8.333	12.717	49.199	78.02	11.94	37.26	
8	20	6.885	10.964	41.242	75.39	10.83	30.42	
9*	21	8.828	13.01	51.321	91.29	12.99	38.33	
10	24	4.86	6.663	27.767	48.01	10.15	17.61	
11	27	6.352	9.852	33.369	61.13	10.39	22.98	
12	30	9.669	12.458	44.096	53.29	13.21	30.89	
13	33	7.789	10.515	39.264	65.51	12.87	26.39	
14	36	6.724	9.873	45.718	51.41	12.18	33.54	
15	39	10.191	14.571	55.762	73.67	15.31	40.46	
16*	40	5.368	8.761	36.719	53.92	9	27.72	
17	41	7.992	12.352	46.768	80.17	14.23	32.54	
18	44	5.761	7.98	33.517	55.02	9.22	24.3	
19	47	6.445	9.652	44.246	64.16	11.96	32.29	
20	50	6.44	8.603	35.431	51.46	10.95	24.48	
21	51	6.802	9.803	40.235	62.47	11.75	28.48	
22	54	5.246	8.514	33.219	59.9	9.16	24.05	
23	57	6.668	9.801	38.474	55.65	11.33	27.15	
24	60	7.455	10.97	39.91	77.65	12.3	27.62	
Average		6.8084	9.9665	38.203	61.291	11.036	27.168	
St Dev		1.439	2.1048	8.1165	13.645	1.9978	6.4987	

* 2nd trial

APPENDIX D

Low Speed Experiment Type II WC (DC) Ti

E4	Ti							
test#	hole#	Ra	Rq	Rz	Rt	Rp	Rv	
1	1	0.856	1.139	4.457	6.98	2.58	1.88	
2	4	0.759	1.109	4.094	8.04	2.18	1.91	
3	7	0.409	0.579	2.683	4.87	1.65	1.03	
4	10	1.272	1.507	5.511	8.73	2.76	2.75	
5	13	0.562	0.7	2.388	3.18	1.28	1.11	
6	16	0.614	0.716	2.721	3.14	1.24	1.48	
7	19	0.304	0.406	1.822	3.17	1.08	0.75	
8	20	0.522	0.886	2.587	6.27	1.29	1.3	
9	21	0.72	0.859	3.408	4.14	1.59	1.82	
10	24	0.789	0.937	3.313	4.03	1.36	1.95	
11	27	0.333	0.434	2.192	3.44	0.88	1.31	
12	30	0.458	0.787	2.891	7.11	1.37	1.52	
13	33	1.066	1.187	3.759	3.99	2	1.75	
14	36	0.575	0.729	2.751	4.9	1.39	1.36	
15	39	0.452	0.614	2.484	3.83	1.51	0.97	
16	40	0.264	0.328	1.506	1.94	0.71	0.79	
17	41	0.883	1.072	4.255	4.77	2.24	2.01	
18	44	0.809	1.045	4.725	6.8	2.09	2.64	
19	47	0.611	0.884	3.04	6.4	1.35	1.69	
20	50	0.429	0.541	2.318	2.97	1.1	1.22	
21	51	0.512	0.789	3.712	8.51	1.92	1.79	
22	54	0.723	0.978	4.408	6.93	2.28	2.13	
23	57	0.522	0.707	2.937	3.88	1.51	1.42	
24	60	0.286	0.384	1.899	3.07	0.87	1.03	
Average		0.6138	0.8049	3.1609	5.0454	1.5929	1.5671	
St Dev		0.2506	0.2896	1.0194	1.9727	0.5494	0.5248	

APPENDIX D

Low Speed Experiment Type II PCD CFRP

G4	CFRP							
test#	hole#	Ra	Rq	Rz	Rt	Rp	Rv	
1	1	5.583	8.246	27.166	64.77	8.17	18.99	
2	4	7.24	9.627	35.864	50.54	12.4	23.46	
3	7	5.887	7.473	30.192	40.54	11.42	18.77	
4	10	6.543	9.665	36.409	61.86	10.89	25.52	
5*	13	6.796	9.299	32.837	49.07	11.27	21.57	
6	16	6.178	9.765	37.527	73.94	10.08	27.45	
7	19	9.362	12.811	48.036	69.66	12.88	35.16	
8	20	7.148	9.883	33.378	55.4	10.3	23.07	
9*	21	7.65	10.764	39.1	62.61	12.62	26.48	
10*	24	6.472	9.4	37.838	61	10.19	27.65	
11	27	6.148	10.239	36.694	73.88	11.43	25.26	
12	30	6.346	9.221	30.416	52.85	9.8	20.61	
13	33	9.692	13.103	48.928	78.26	14.9	34.02	
14	36	9.332	12.606	42.961	75.29	15.21	27.75	
15	39	6.85	9.257	35.026	58.45	11.65	23.37	
16	40	7.819	10.132	32.561	49.64	10.73	21.83	
17*	41	6.898	9.891	34.323	57.97	9.87	24.45	
18	44	7.424	10.169	40.678	62.53	12.03	28.65	
19	47	9.01	12.18	49.803	64.58	15.91	33.89	
20	50	6.669	9.937	40.316	72.95	10.7	29.61	
21	51	9.783	13.655	47.253	69.83	14.26	33	
22	54	6.54	9.758	39.807	79.5	11.19	28.62	
23	57	9.45	12.812	50.275	69.57	14.17	36.11	
24	60	7.369	10.675	41.144	72.55	12.19	28.96	
Average		7.4245	10.44	38.689	63.635	11.844	26.844	
St Dev		1.3051	1.5975	6.53	10.34	1.9224	5.0261	

* 2nd trial

APPENDIX D

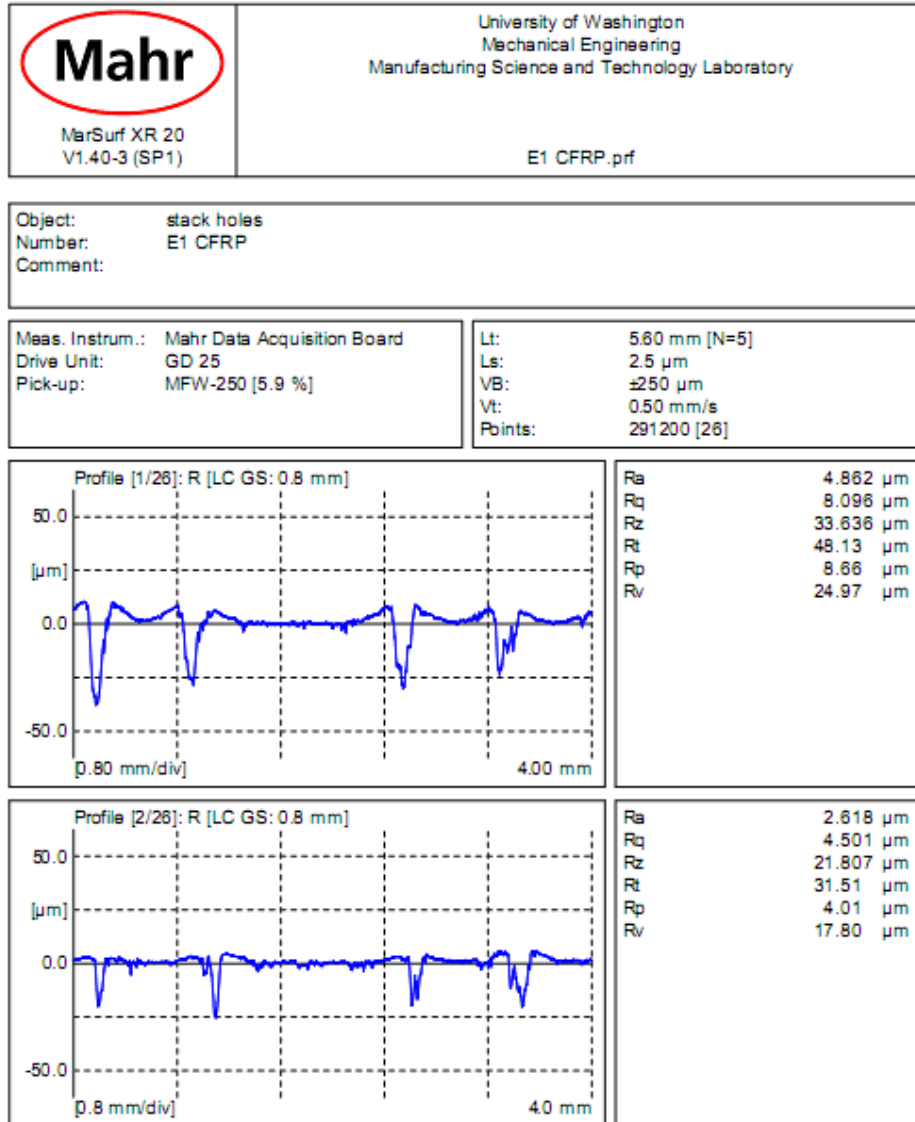
Low Speed Experiment Type II PCD Ti

G4	Ti							
test#	hole#	Ra	Rq	Rz	Rt	Rp	Rv	
1	1	1.221	1.513	5.853	8.01	2.74	3.11	
2	4	0.511	0.66	3.052	4.09	1.4	1.66	
3	7	0.274	0.358	1.599	2.08	0.83	0.77	
4	10	0.663	0.864	3.958	4.95	1.92	2.03	
5	13	0.348	0.55	2.668	5.08	1.22	1.44	
6	16	0.552	0.787	3.605	5.08	1.86	1.75	
7	19	0.75	0.962	3.836	5.64	1.98	1.86	
8	20	0.623	0.84	3.799	5.44	2.21	1.59	
9	21	0.743	1.055	4.836	7.47	2.36	2.47	
10	24	0.522	0.731	3.375	5.23	1.61	1.77	
11	27	0.707	0.942	3.932	6.27	1.86	2.07	
12	30	0.518	0.658	2.624	4.91	1.26	1.37	
13	33	0.498	0.716	2.764	5.29	1.25	1.52	
14	36	0.793	0.959	3.71	4.33	1.68	2.03	
15	39	0.579	0.762	3.567	5.49	1.81	1.76	
16	40	0.358	0.48	2.006	3.31	1.05	0.96	
17	41	0.679	0.94	3.908	6.75	2.16	1.75	
18	44	0.684	0.898	3.542	5.06	1.53	2.01	
19	47	0.836	1.216	4.675	8.06	2.47	2.21	
20	50	0.458	0.568	2.608	3.15	1.38	1.23	
21	51	0.501	0.707	2.649	5.01	0.97	1.68	
22	54	0.666	0.851	3.66	5.12	1.87	1.79	
23	57	0.716	1.024	4.401	6.65	1.87	2.53	
24	60	0.507	0.746	3.004	6.27	1.33	1.67	
average		0.6128	0.8245	3.4846	5.3642	1.6925	1.7929	
St Dev		0.194	0.2441	0.9369	1.4364	0.4905	0.4969	


APPENDIX D

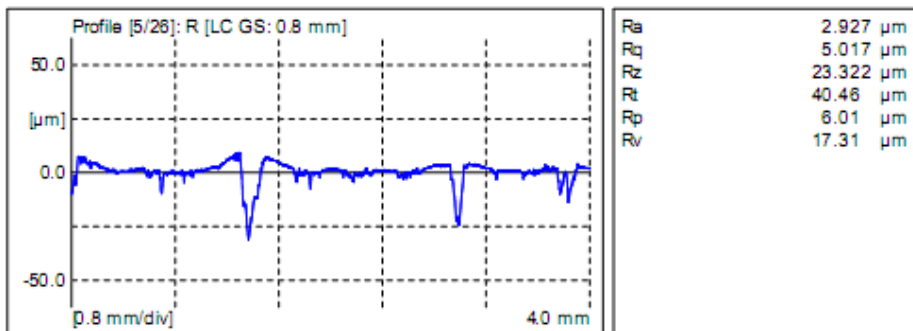
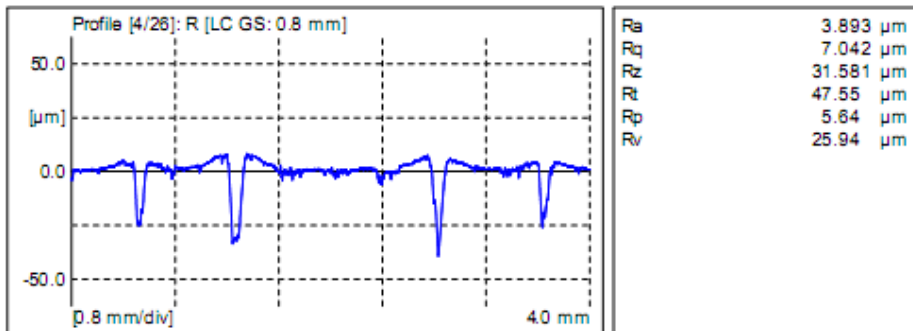
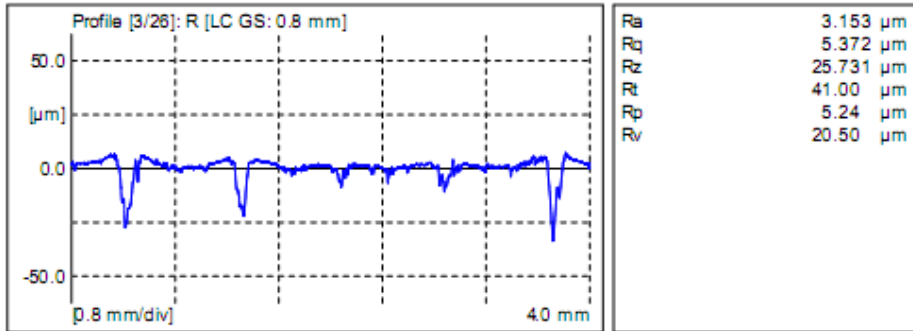
Surface Profiles

CFRP hole surface profiles: WC (DC) high speed Experiment Type I

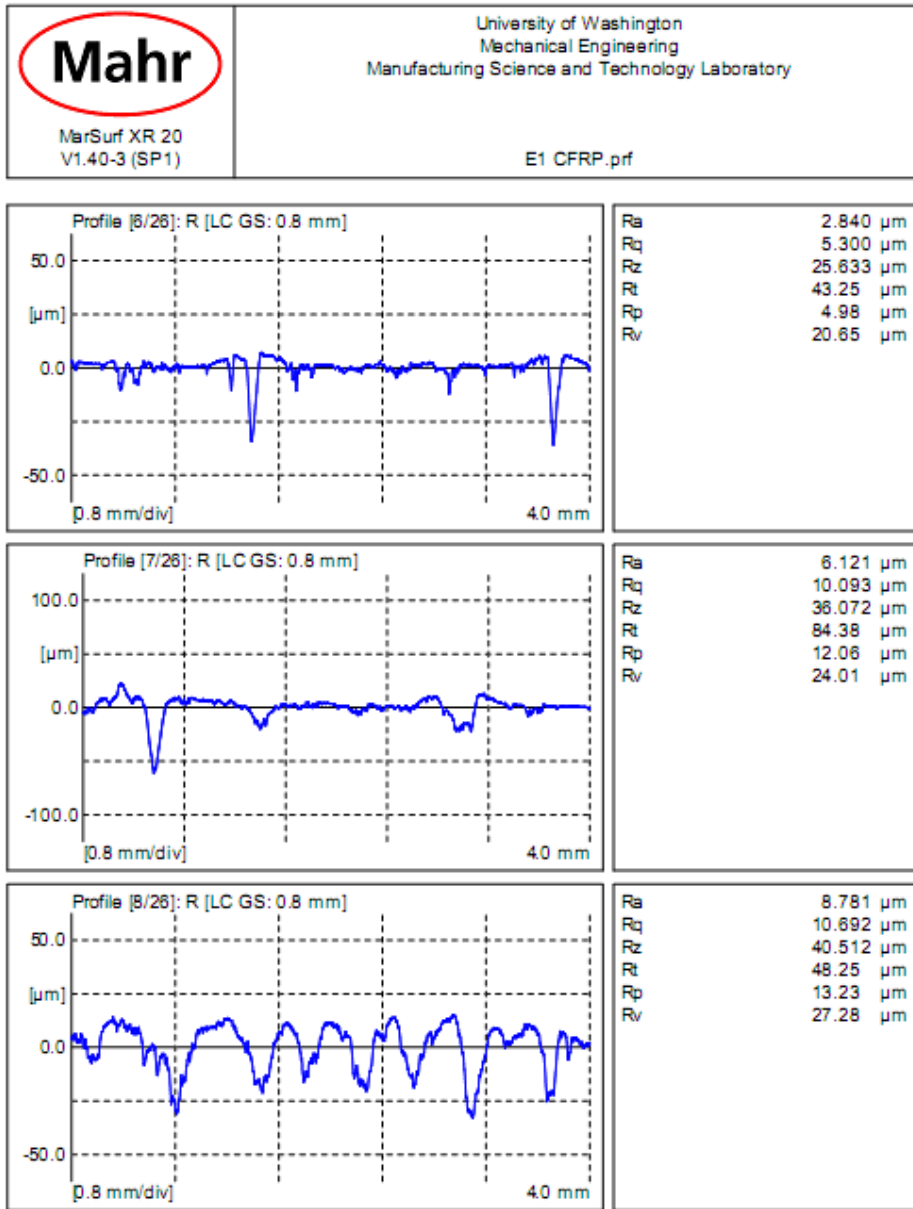


APPENDIX D

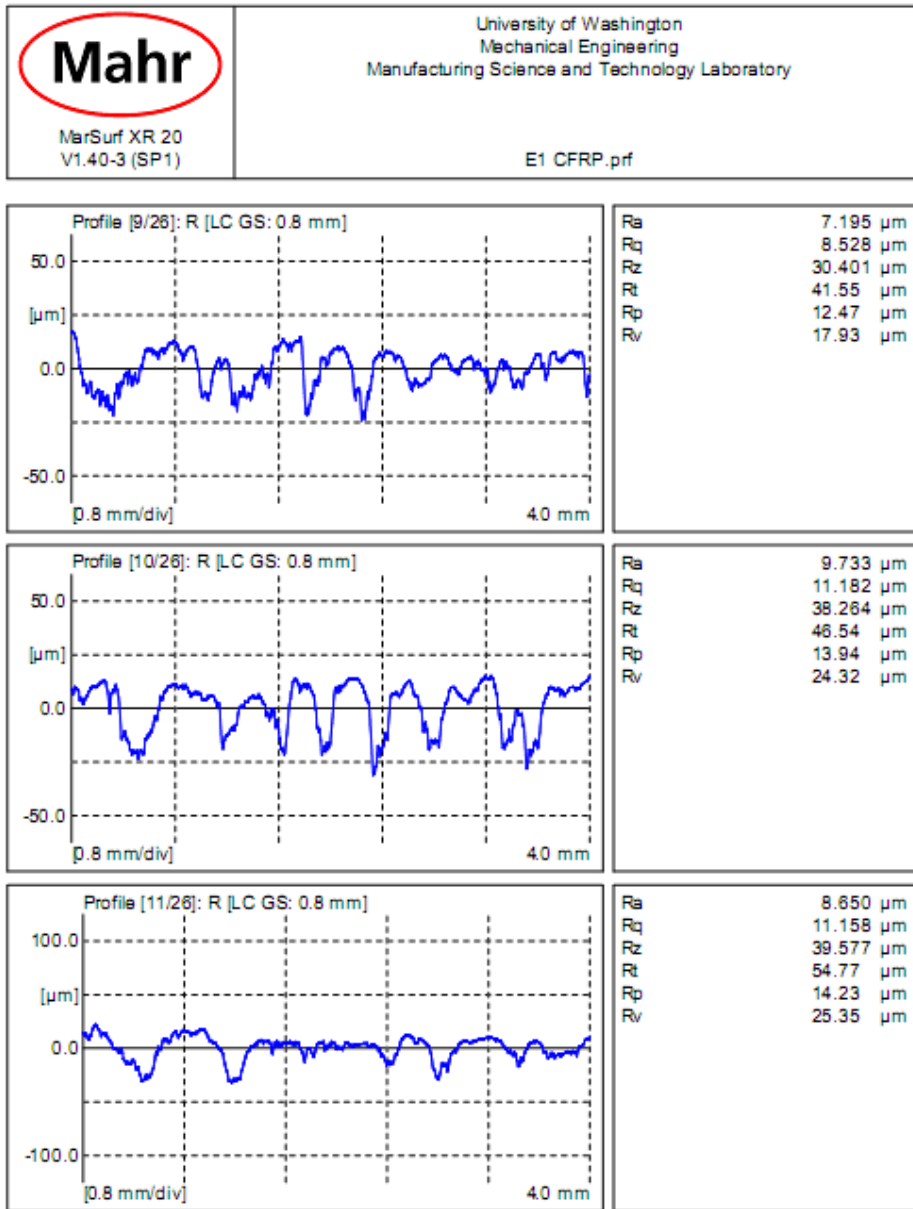
 <p>Mahr MarSurf XR 20 V1.40-3 (SP1)</p>	<p>University of Washington Mechanical Engineering Manufacturing Science and Technology Laboratory</p> <p>E1 CFRP.prf</p>
---	---



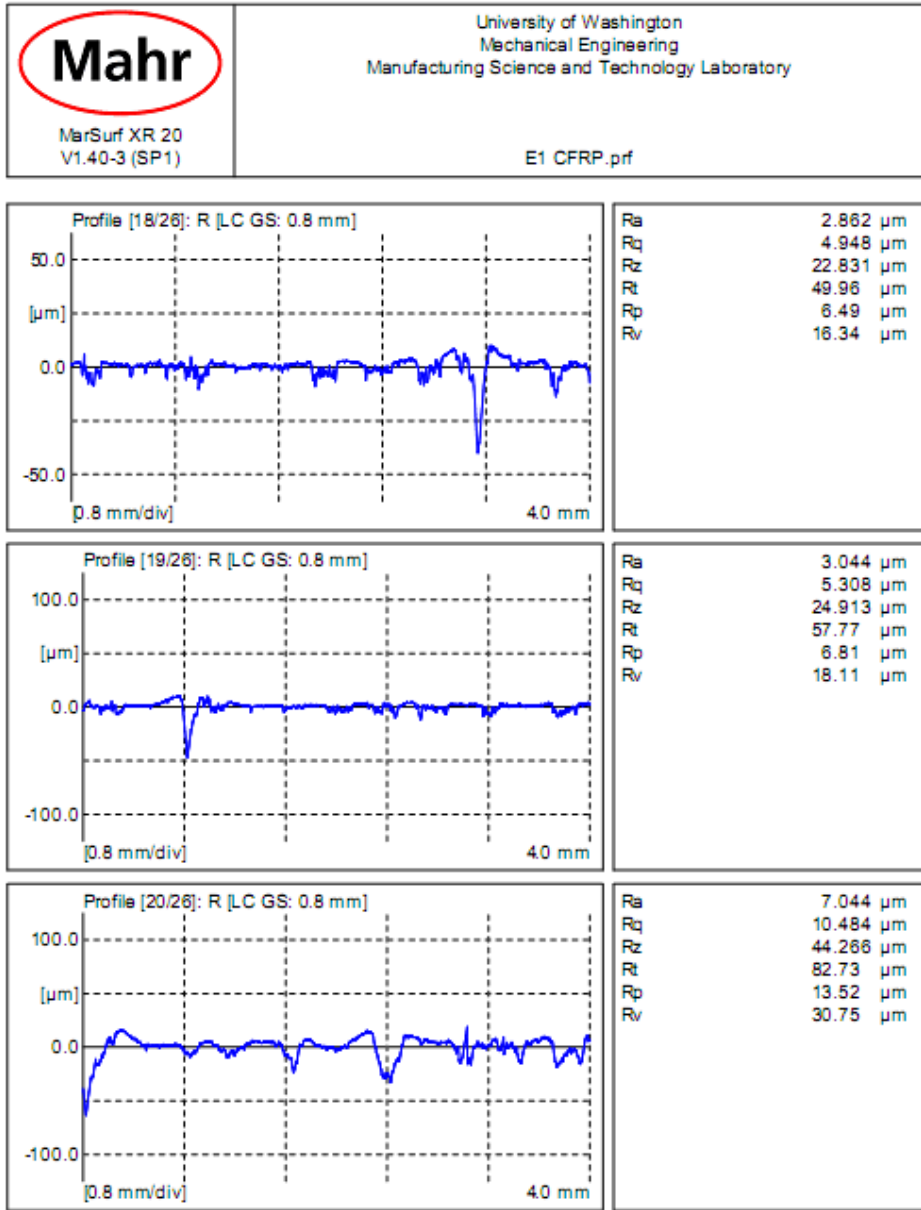
APPENDIX D




APPENDIX D

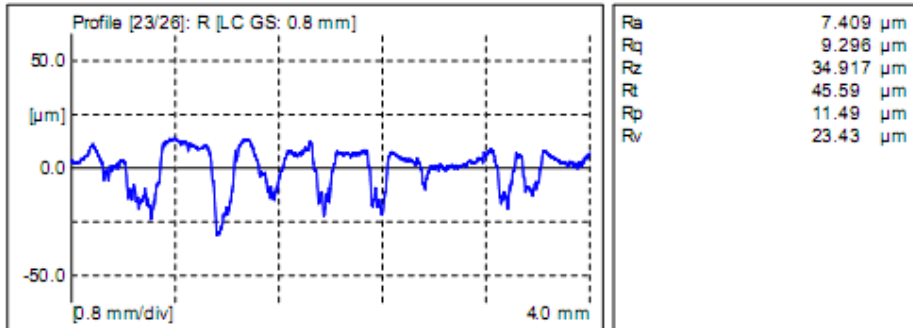
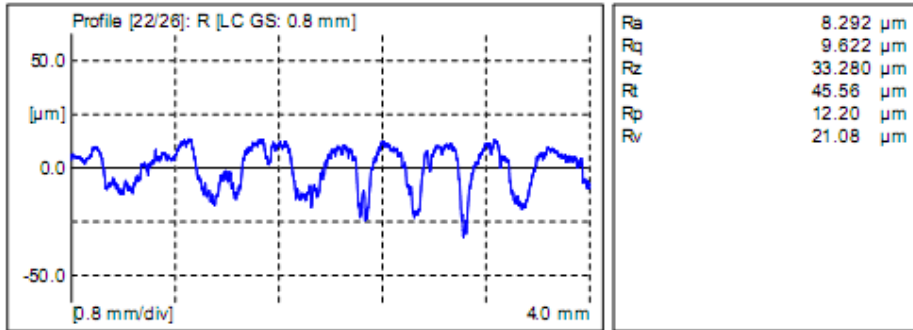
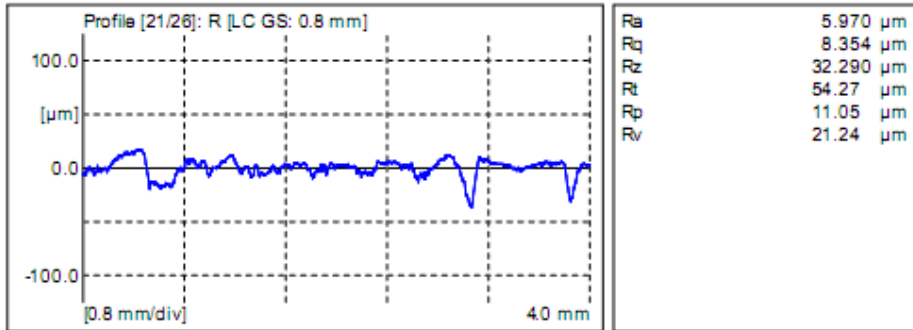


APPENDIX D




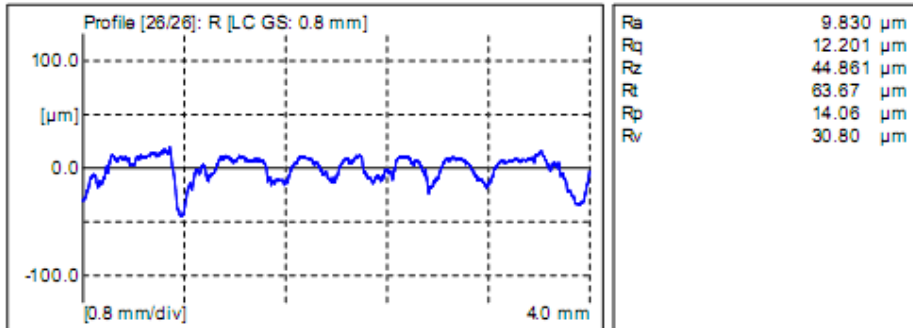
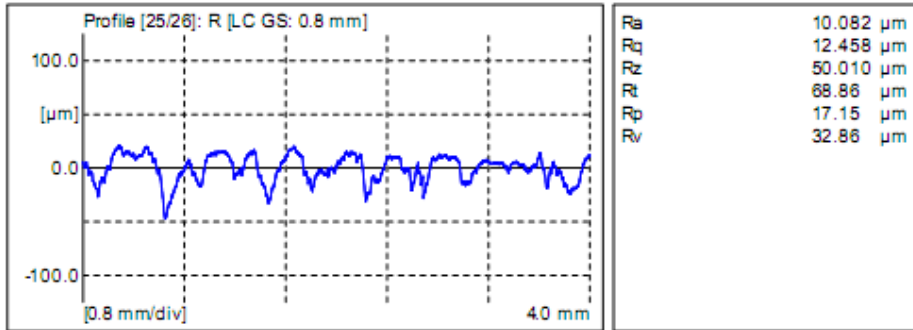
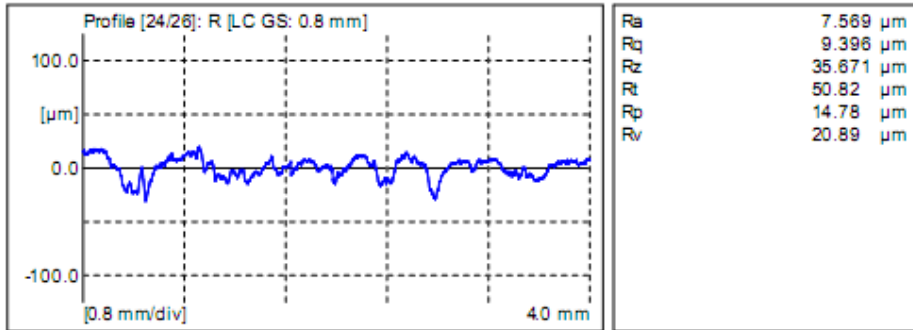
APPENDIX D

 <p style="font-size: small;">MarSurf XR 20 V1.40-3 (SP1)</p>	<p style="font-size: x-small;">University of Washington Mechanical Engineering Manufacturing Science and Technology Laboratory</p> <p style="font-size: x-small;">E1 CFRP.prf</p>
--	---



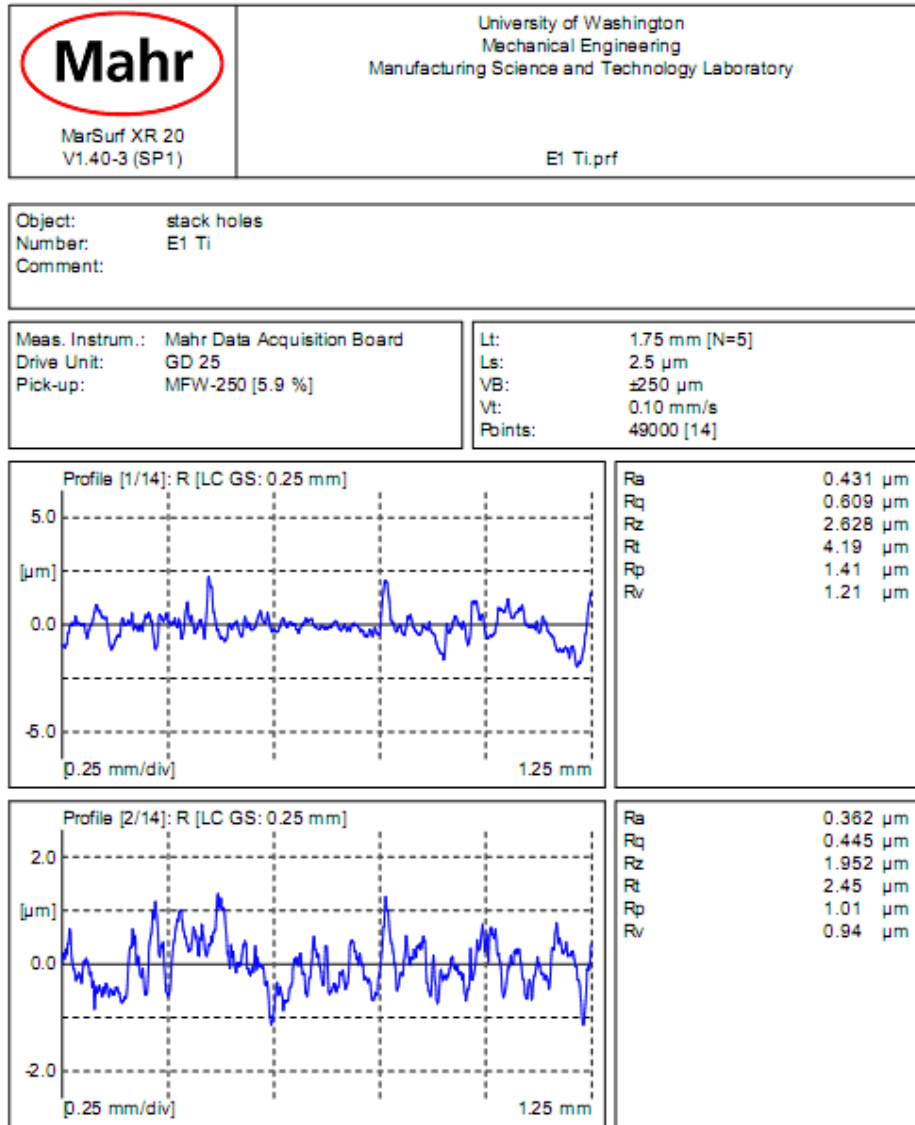
APPENDIX D

 <p style="margin: 0;">MarSurf XR 20 V1.40-3 (SP1)</p>	<p style="margin: 0;">University of Washington Mechanical Engineering Manufacturing Science and Technology Laboratory</p> <p style="margin: 0;">E1 CFRP.prf</p>
---	---




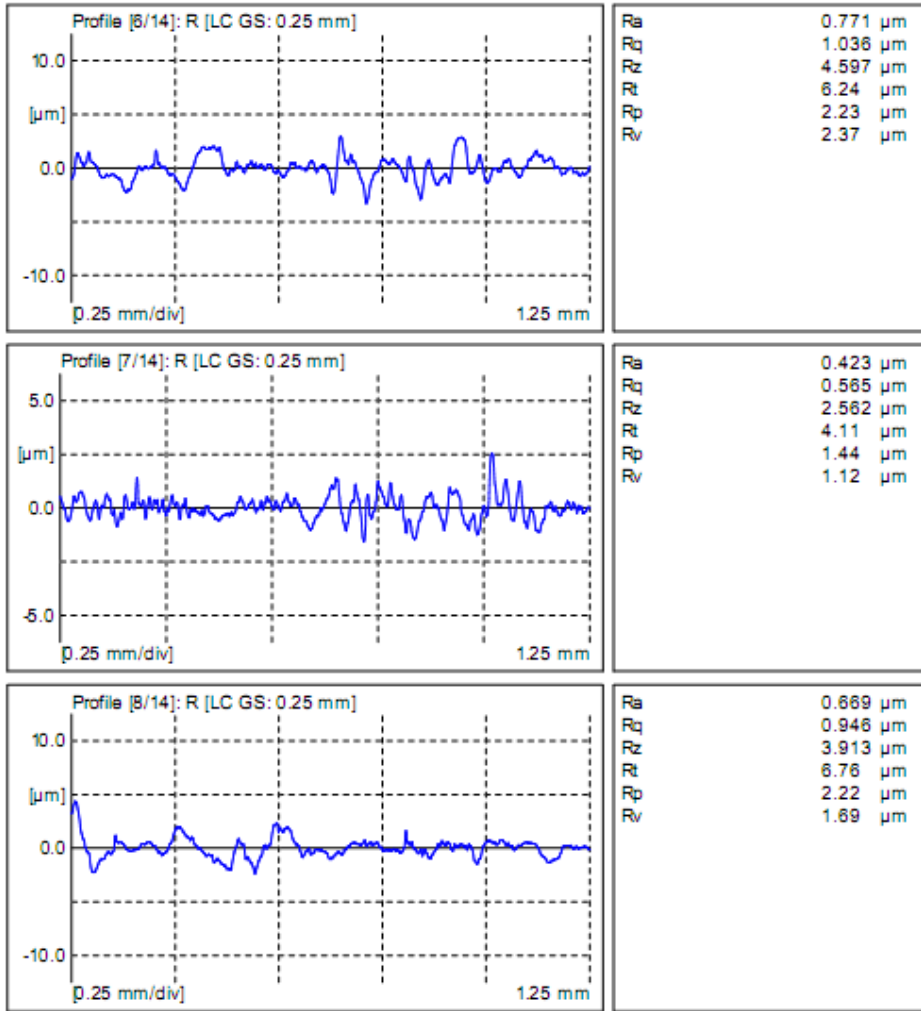
APPENDIX D

Titanium hole surface profiles: WC (DC) high speed Experiment Type I

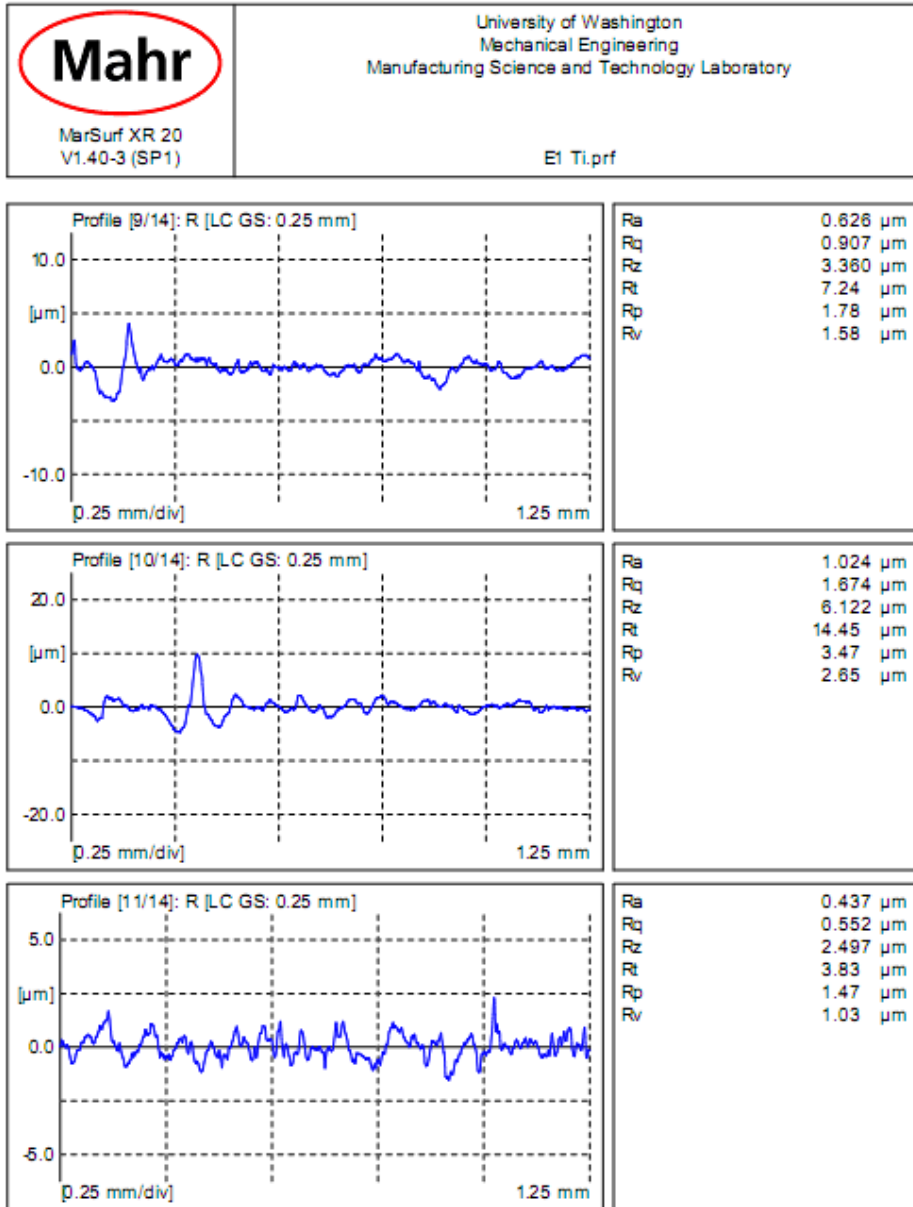


APPENDIX D


 <p>Mahr</p> <p>MarSurf XR 20 V1.40-3 (SP1)</p>	<p>University of Washington Mechanical Engineering Manufacturing Science and Technology Laboratory</p>
	<p>E1 Ti.prf</p>

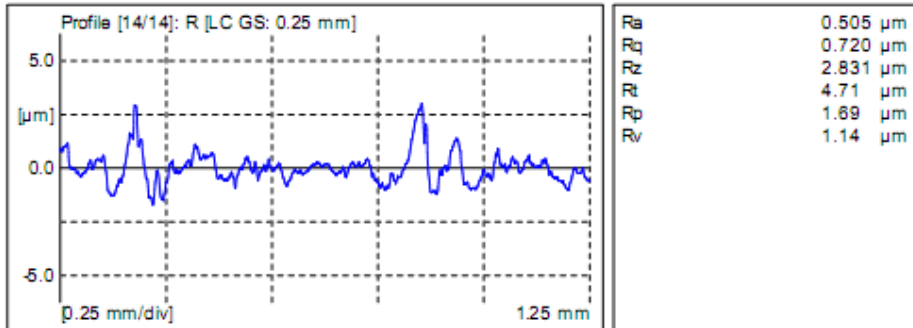
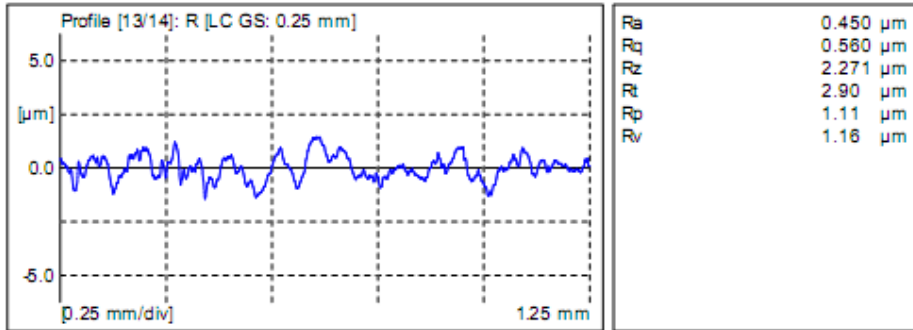
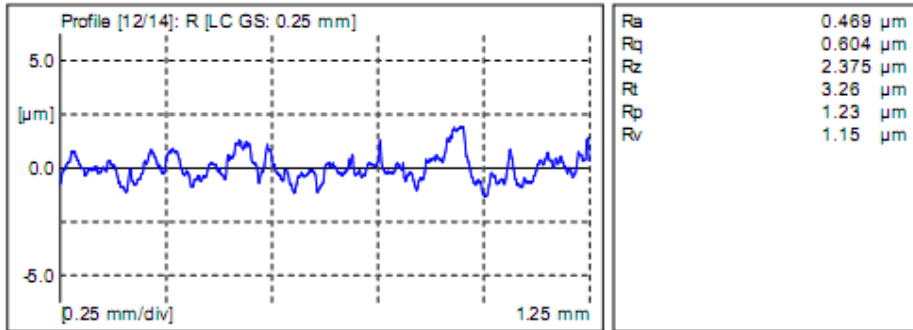


APPENDIX D




APPENDIX D

 <p>Mahr MarSurf XR 20 V1.40-3 (SP1)</p>	<p>University of Washington Mechanical Engineering Manufacturing Science and Technology Laboratory</p>
	<p>E1 Ti.prf</p>



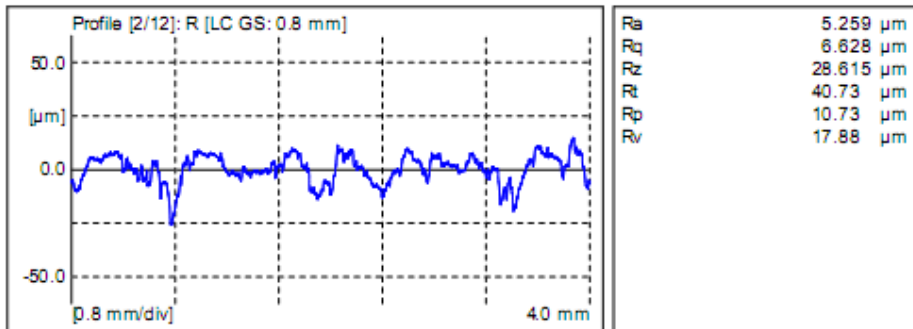
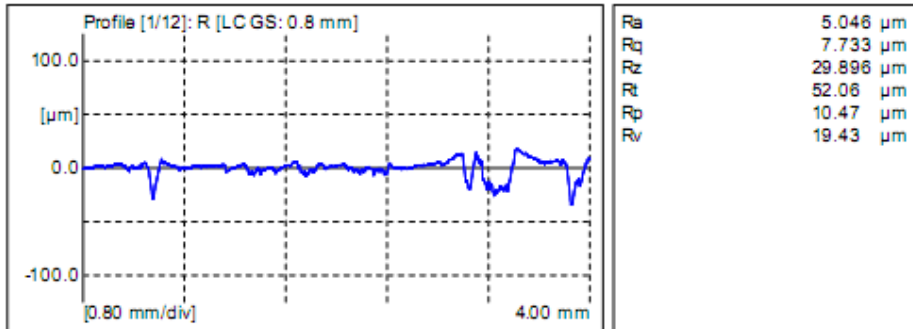
APPENDIX D

CFRP hole surface profiles: WC (DC) high speed Experiment Type II


 <p>Mahr</p> <p>MarSurf XR 20 V1.40-3 (SP1)</p>	<p>University of Washington Mechanical Engineering Manufacturing Science and Technology Laboratory</p> <p>20100212-161547.prf</p>
---	---

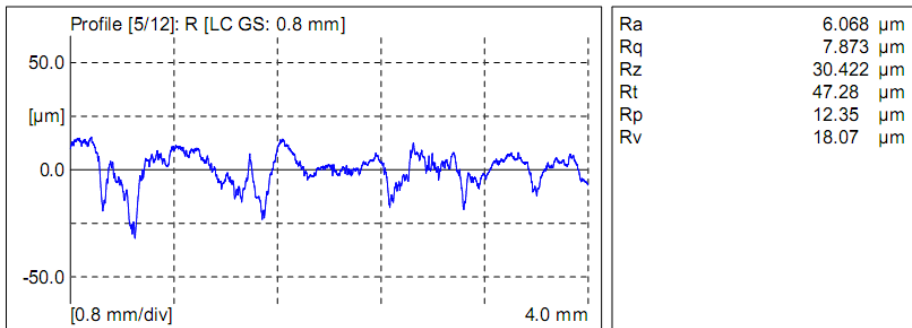
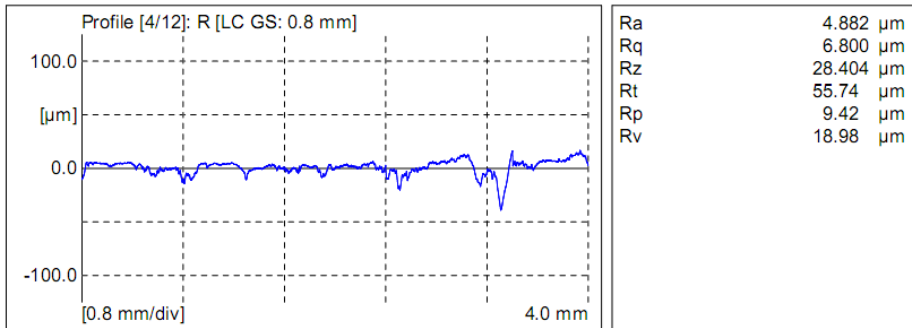
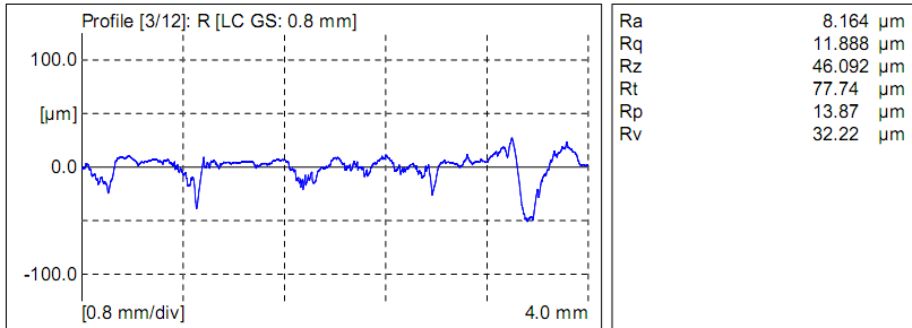
Object:	stack holes
Number:	E3 CFRP h1-40
Comment:	

Meas. Instrum.: Mahr Data Acquisition Board	Lt: 5.60 mm [N=5]
Drive Unit: GD 25	Ln: 2.5 μm
Pick-up: MFW-250 [5.9 %]	Vb: $\pm 250 \mu\text{m}$
	Vt: 0.50 mm/s
	Points: 134400 [12]




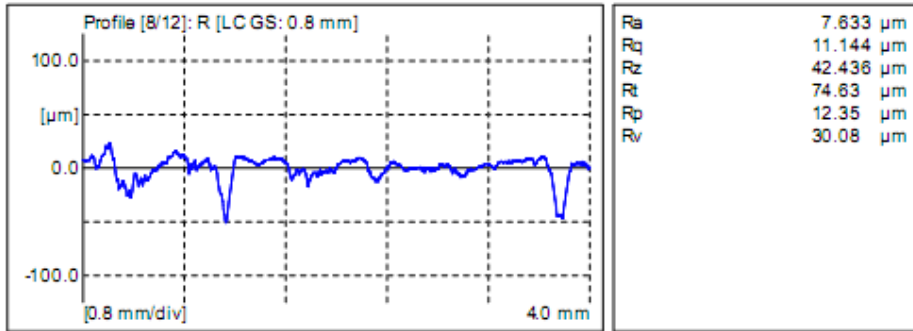
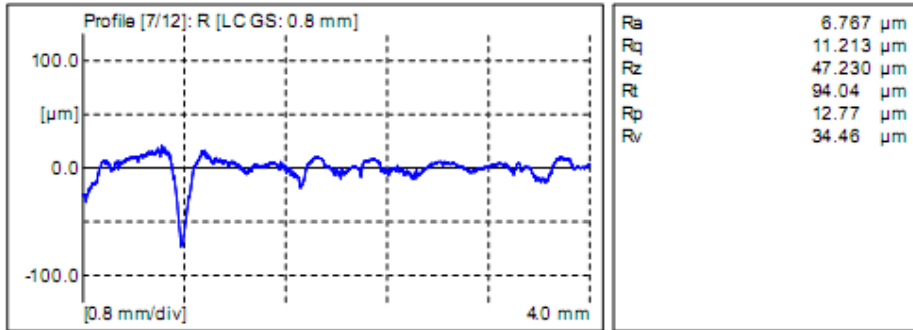
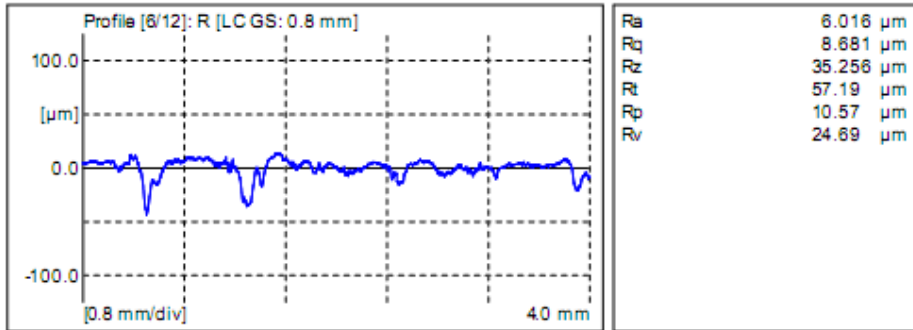
APPENDIX D

 <p style="margin: 0;">Mahr</p> <p style="margin: 0; font-size: small;">MarSurf XR 20 V1.40-3 (SP1)</p>	<p style="margin: 0; font-size: small;">University of Washington Mechanical Engineering Manufacturing Science and Technology Laboratory</p> <p style="margin: 0; font-size: small;">20100212-161547.pr1</p>
---	---




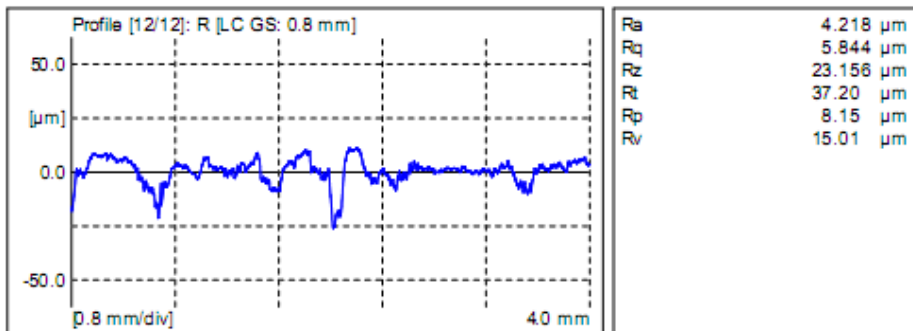
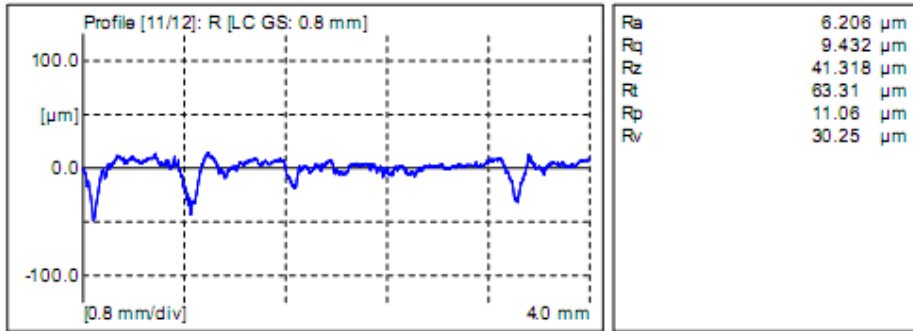
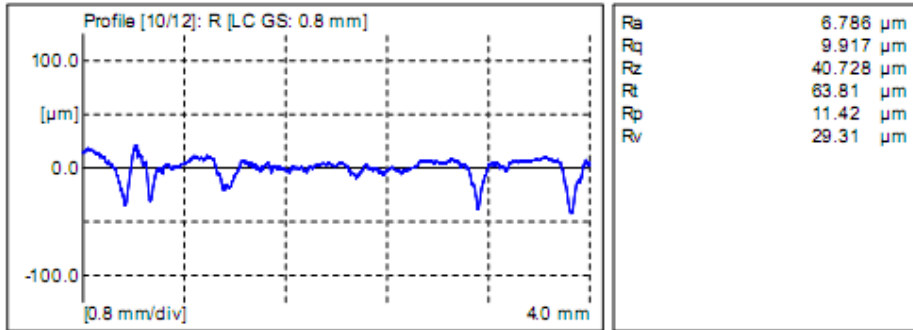
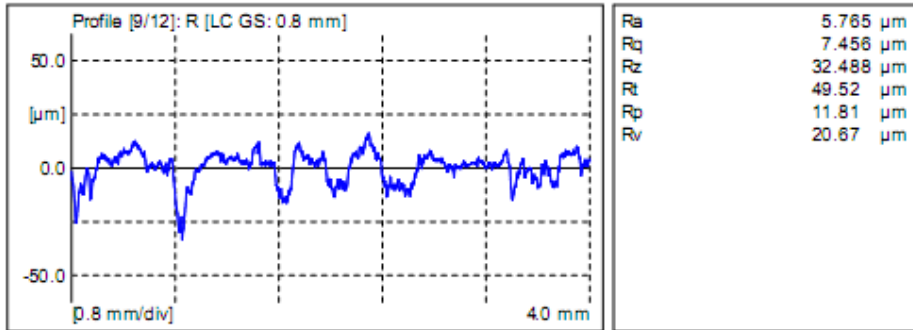
APPENDIX D

 <p>Mahr MarSurf XR 20 V1.40-3 (SP1)</p>	<p>University of Washington Mechanical Engineering Manufacturing Science and Technology Laboratory</p>
	<p>20100212-161547.prf</p>



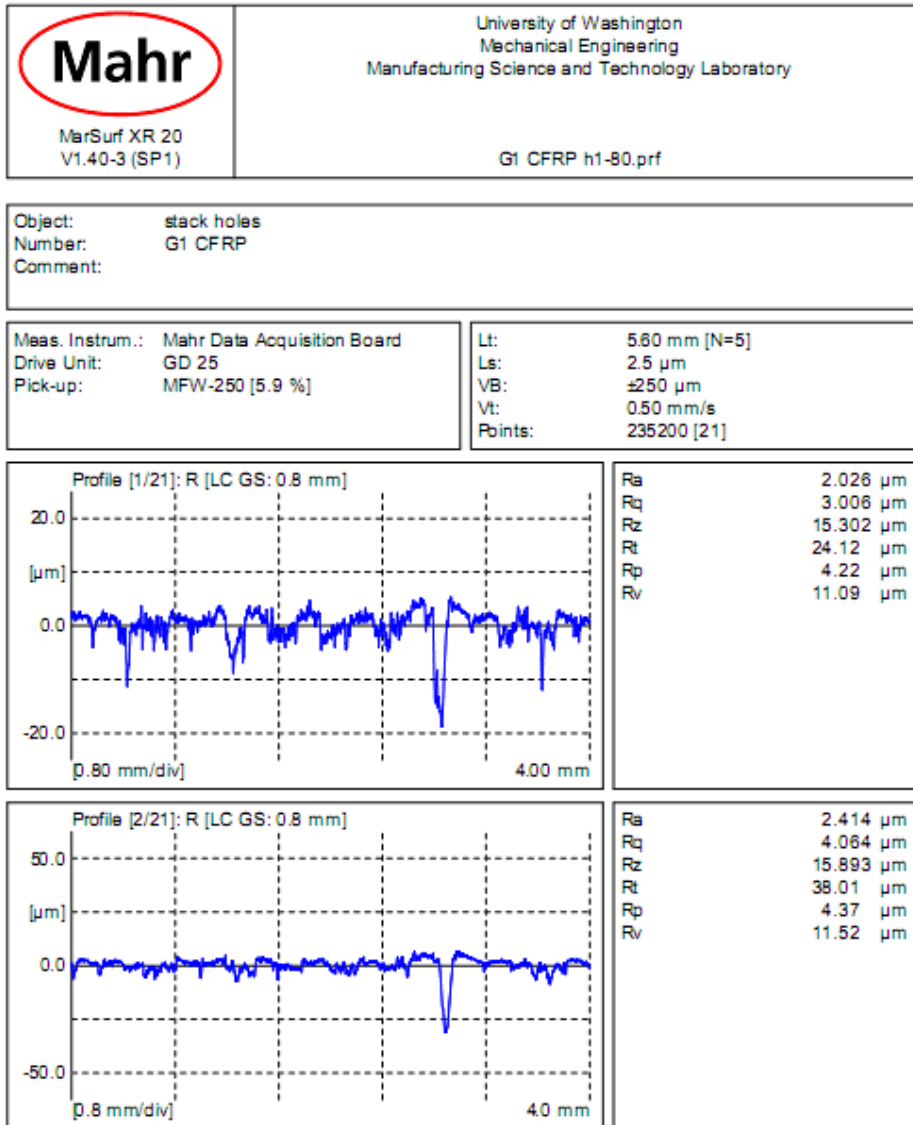
APPENDIX D

 <p>Mahr</p> <p>MarSurf XR 20 V1.40-3 (SP1)</p>	<p>University of Washington Mechanical Engineering Manufacturing Science and Technology Laboratory</p>
	<p>20100212-161547.prf</p>




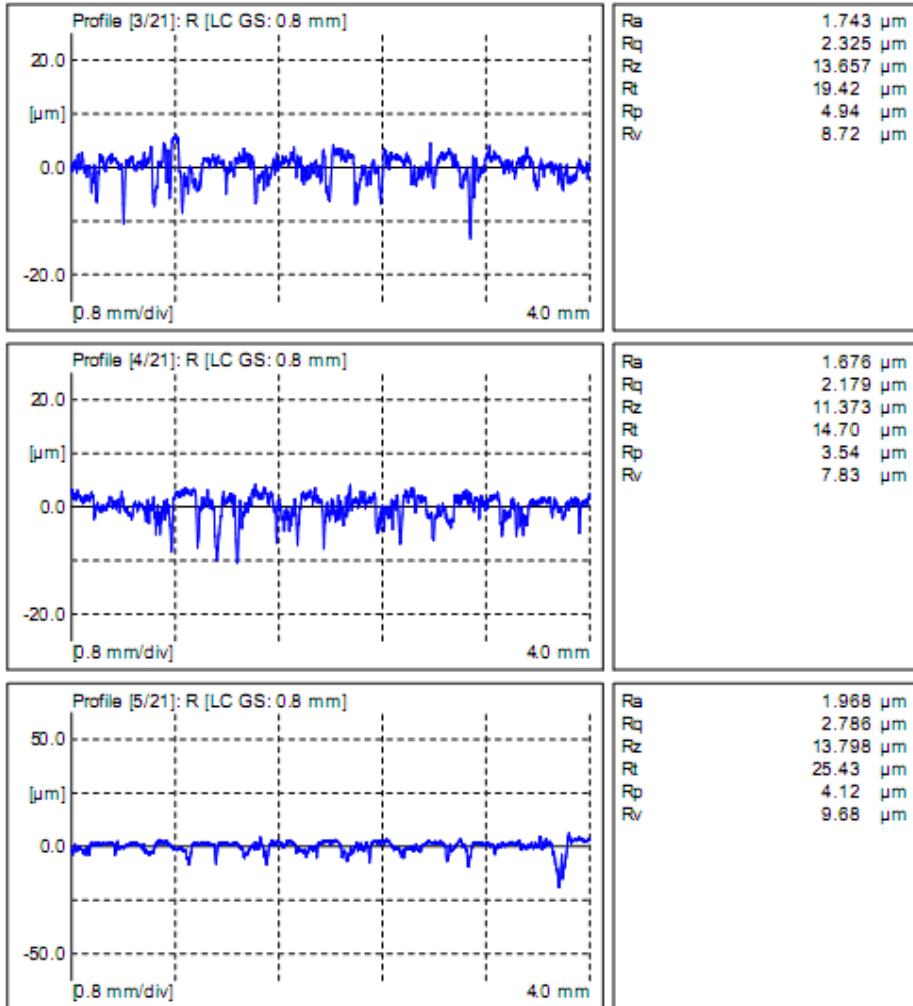
APPENDIX D

CFRP hole surface profiles: PCD high speed Experiment Type I

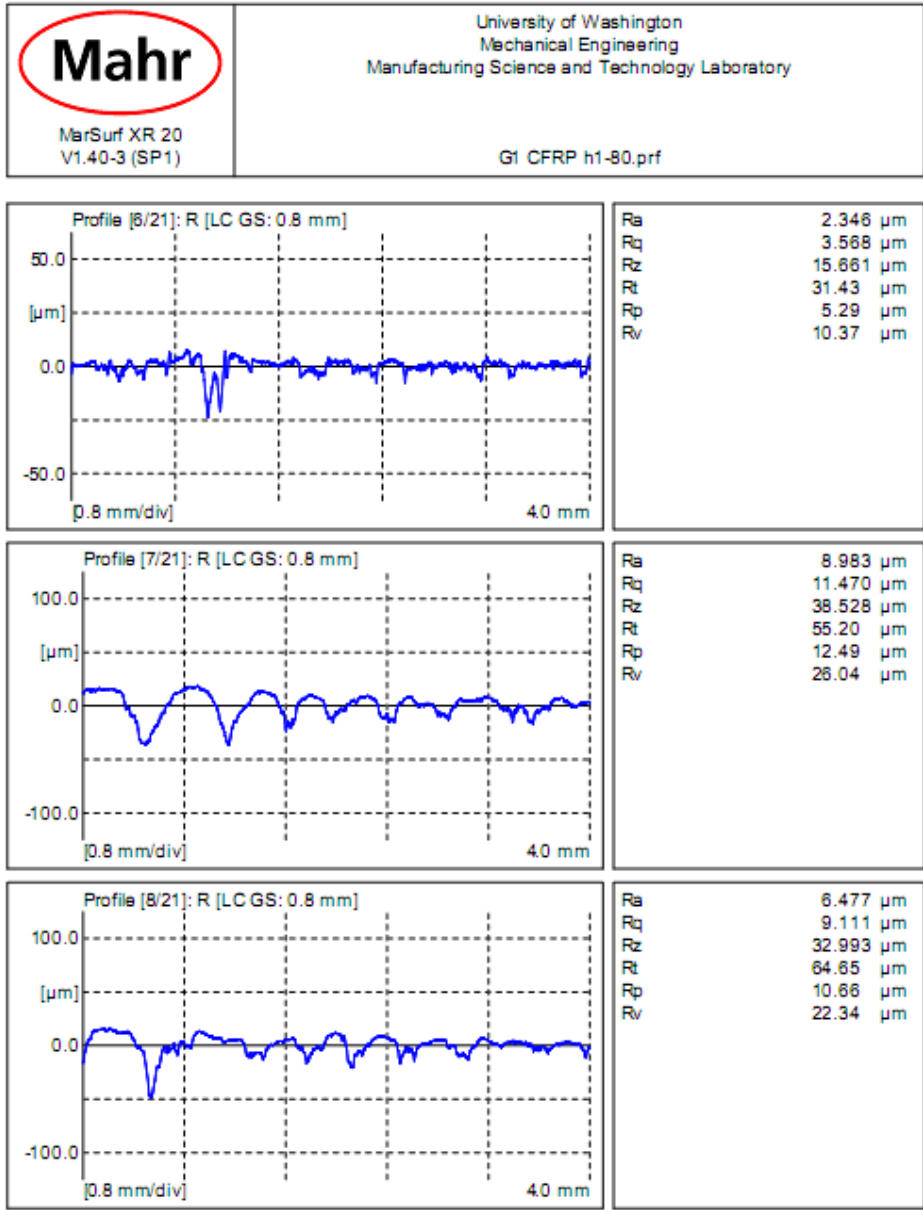


APPENDIX D


 <p style="margin: 0;">Mahr</p> <p style="margin: 0; font-size: small;">MarSurf XR 20 V1.40-3 (SP1)</p>	<p style="margin: 0; font-size: small;">University of Washington Mechanical Engineering Manufacturing Science and Technology Laboratory</p> <p style="margin: 0; font-size: small;">G1 CFRP h1-80.prf</p>
---	---

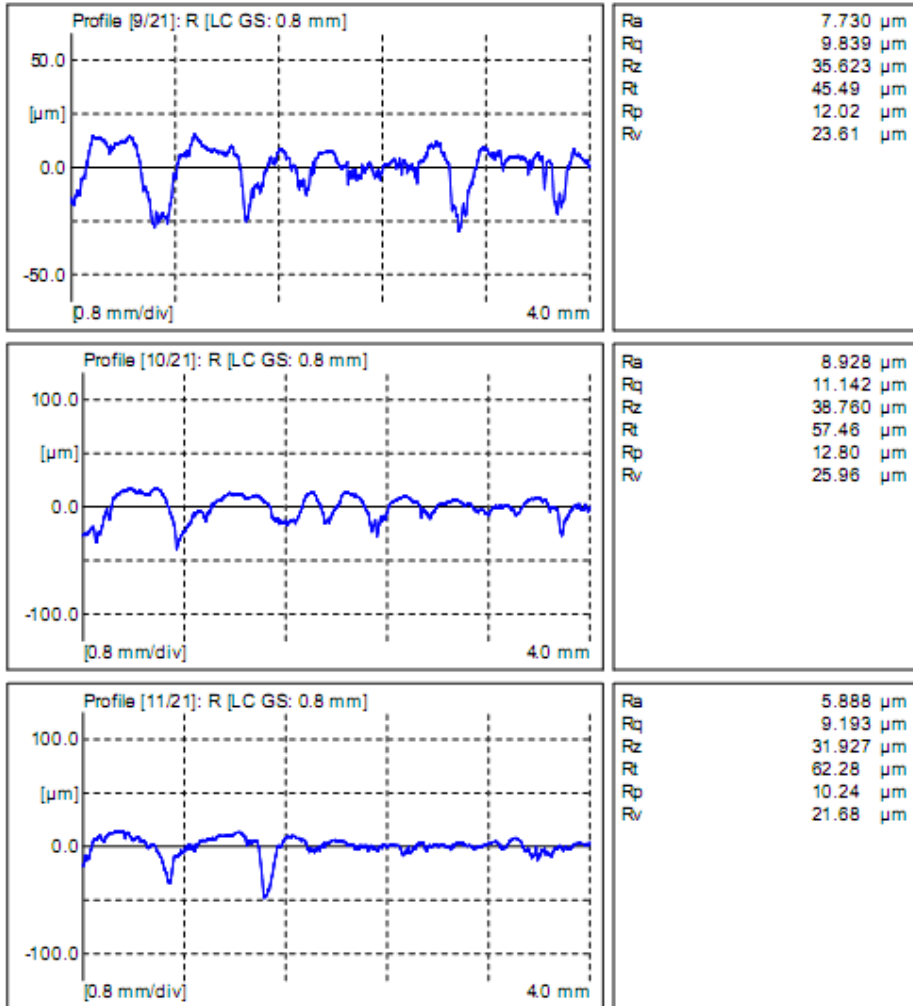


APPENDIX D




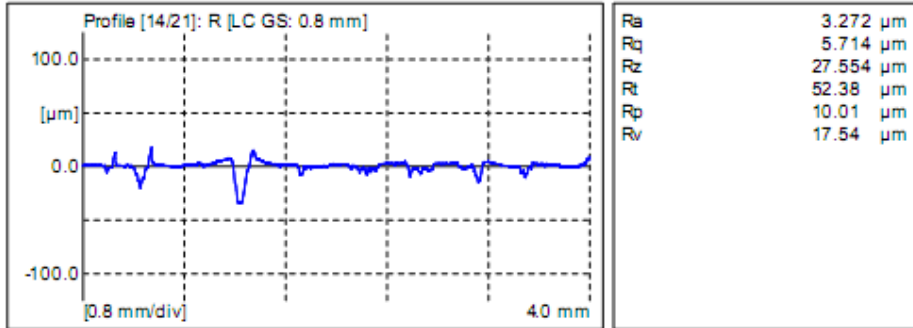
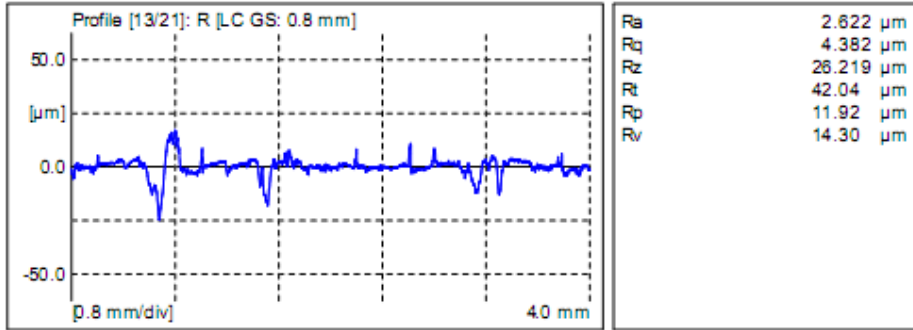
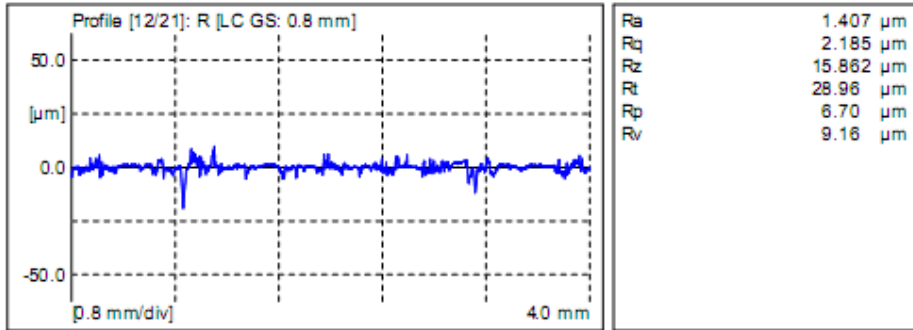
APPENDIX D

 <p style="margin: 0;">MarSurf XR 20 V1.40-3 (SP1)</p>	<p style="margin: 0;">University of Washington Mechanical Engineering Manufacturing Science and Technology Laboratory</p> <p style="margin: 0;">G1 CFRP h1-80.prf</p>
---	---




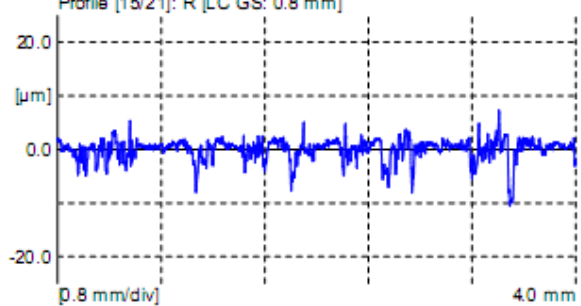
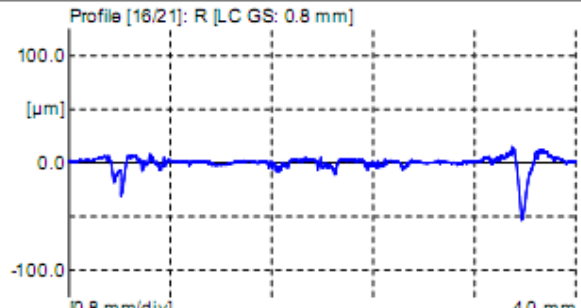
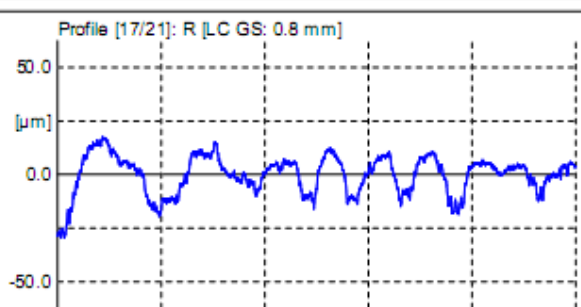
APPENDIX D

 <p>Mahr MarSurf XR 20 V1.40-3 (SP1)</p>	<p>University of Washington Mechanical Engineering Manufacturing Science and Technology Laboratory</p>
	<p>G1 CFRP h1-80.prf</p>

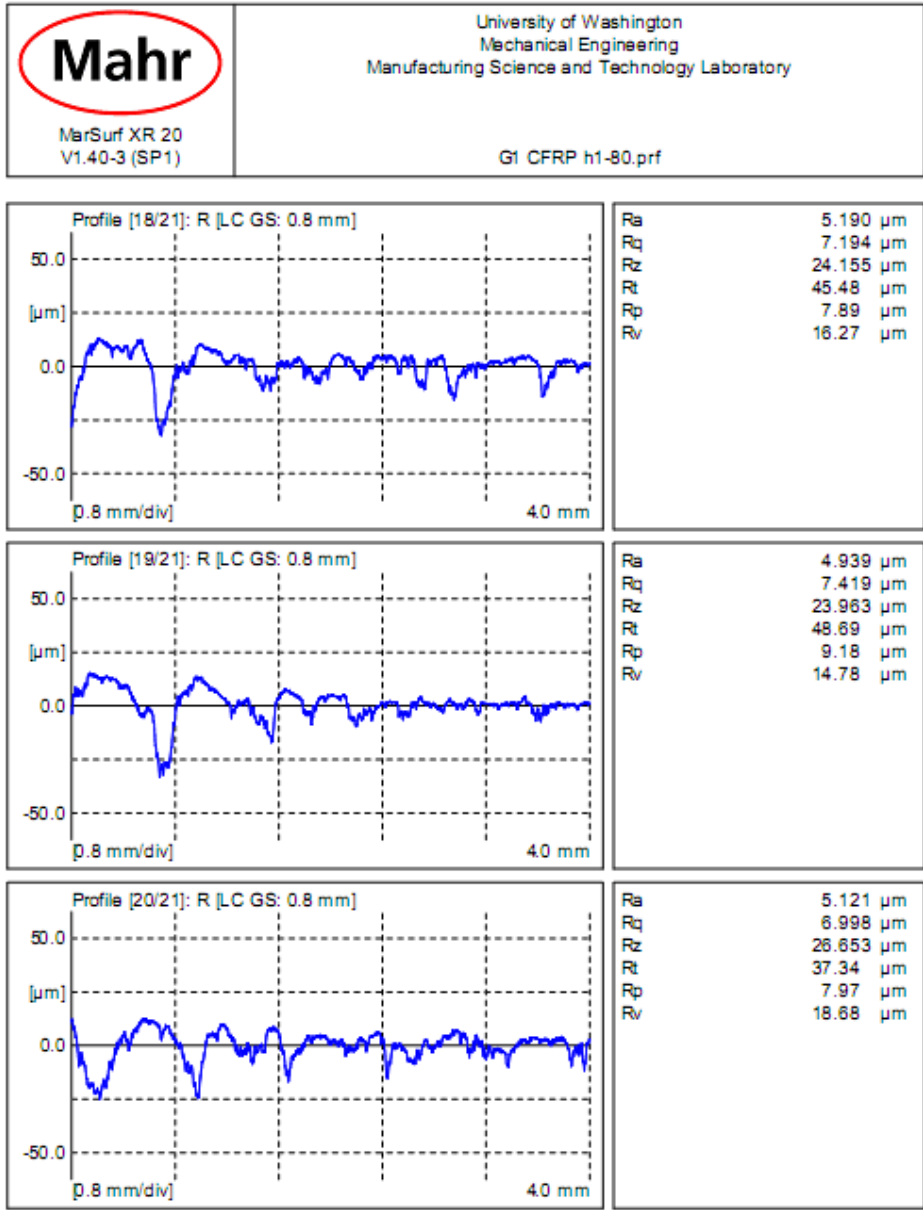


APPENDIX D


 <p>Mahr</p> <p>MarSurf XR 20 V1.40-3 (SP1)</p>	<p>University of Washington Mechanical Engineering Manufacturing Science and Technology Laboratory</p> <p>G1 CFRP h1-80.prf</p>
---	---

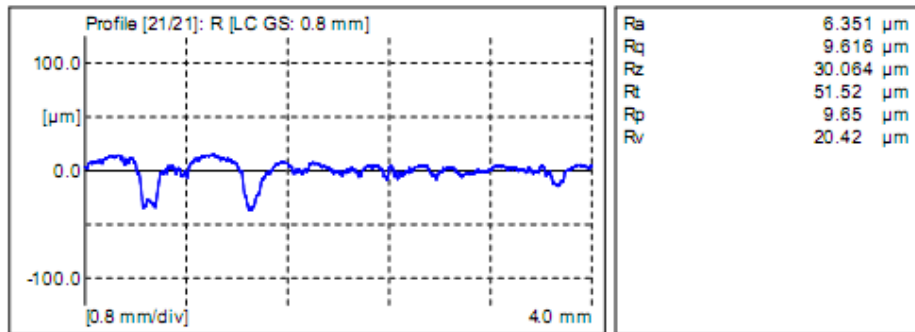
<p>Profile [15/21]: R [LC GS: 0.8 mm]</p>  <p>[µm]</p> <p>0.8 mm/div 4.0 mm</p>	<table style="width: 100%; border-collapse: collapse;"> <tr><td style="border-right: 1px solid black;">Ra</td><td style="text-align: right;">1.356 µm</td></tr> <tr><td style="border-right: 1px solid black;">Rq</td><td style="text-align: right;">1.975 µm</td></tr> <tr><td style="border-right: 1px solid black;">Rz</td><td style="text-align: right;">12.634 µm</td></tr> <tr><td style="border-right: 1px solid black;">Rt</td><td style="text-align: right;">17.75 µm</td></tr> <tr><td style="border-right: 1px solid black;">Rp</td><td style="text-align: right;">4.83 µm</td></tr> <tr><td style="border-right: 1px solid black;">Rv</td><td style="text-align: right;">7.81 µm</td></tr> </table>	Ra	1.356 µm	Rq	1.975 µm	Rz	12.634 µm	Rt	17.75 µm	Rp	4.83 µm	Rv	7.81 µm
Ra	1.356 µm												
Rq	1.975 µm												
Rz	12.634 µm												
Rt	17.75 µm												
Rp	4.83 µm												
Rv	7.81 µm												
<p>Profile [16/21]: R [LC GS: 0.8 mm]</p>  <p>[µm]</p> <p>0.8 mm/div 4.0 mm</p>	<table style="width: 100%; border-collapse: collapse;"> <tr><td style="border-right: 1px solid black;">Ra</td><td style="text-align: right;">3.587 µm</td></tr> <tr><td style="border-right: 1px solid black;">Rq</td><td style="text-align: right;">6.887 µm</td></tr> <tr><td style="border-right: 1px solid black;">Rz</td><td style="text-align: right;">28.185 µm</td></tr> <tr><td style="border-right: 1px solid black;">Rt</td><td style="text-align: right;">68.19 µm</td></tr> <tr><td style="border-right: 1px solid black;">Rp</td><td style="text-align: right;">6.76 µm</td></tr> <tr><td style="border-right: 1px solid black;">Rv</td><td style="text-align: right;">21.43 µm</td></tr> </table>	Ra	3.587 µm	Rq	6.887 µm	Rz	28.185 µm	Rt	68.19 µm	Rp	6.76 µm	Rv	21.43 µm
Ra	3.587 µm												
Rq	6.887 µm												
Rz	28.185 µm												
Rt	68.19 µm												
Rp	6.76 µm												
Rv	21.43 µm												
<p>Profile [17/21]: R [LC GS: 0.8 mm]</p>  <p>[µm]</p> <p>0.8 mm/div 4.0 mm</p>	<table style="width: 100%; border-collapse: collapse;"> <tr><td style="border-right: 1px solid black;">Ra</td><td style="text-align: right;">7.160 µm</td></tr> <tr><td style="border-right: 1px solid black;">Rq</td><td style="text-align: right;">8.943 µm</td></tr> <tr><td style="border-right: 1px solid black;">Rz</td><td style="text-align: right;">30.973 µm</td></tr> <tr><td style="border-right: 1px solid black;">Rt</td><td style="text-align: right;">46.75 µm</td></tr> <tr><td style="border-right: 1px solid black;">Rp</td><td style="text-align: right;">12.42 µm</td></tr> <tr><td style="border-right: 1px solid black;">Rv</td><td style="text-align: right;">18.55 µm</td></tr> </table>	Ra	7.160 µm	Rq	8.943 µm	Rz	30.973 µm	Rt	46.75 µm	Rp	12.42 µm	Rv	18.55 µm
Ra	7.160 µm												
Rq	8.943 µm												
Rz	30.973 µm												
Rt	46.75 µm												
Rp	12.42 µm												
Rv	18.55 µm												

APPENDIX D



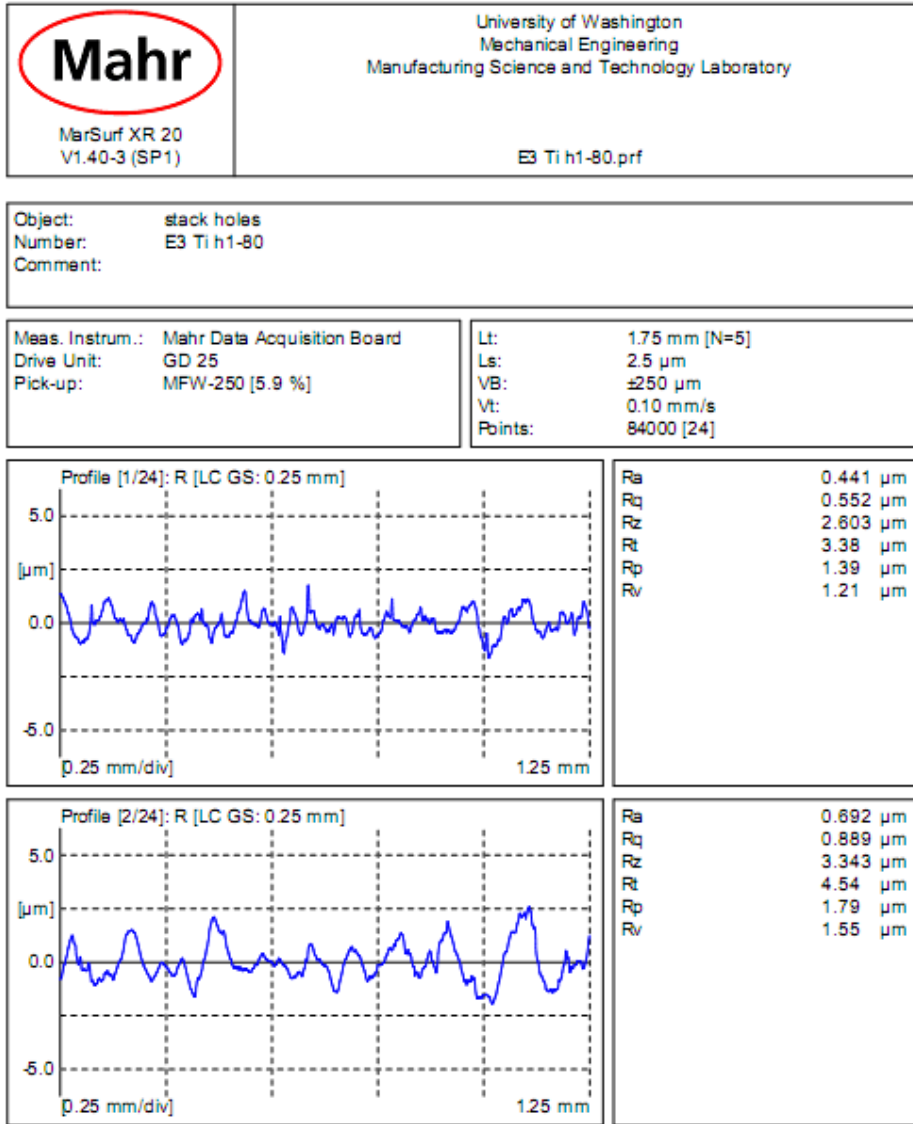
APPENDIX D

 MarSurf XR 20 V1.40-3 (SP1)	University of Washington Mechanical Engineering Manufacturing Science and Technology Laboratory G1 CFRP h1-80.prf
---	--

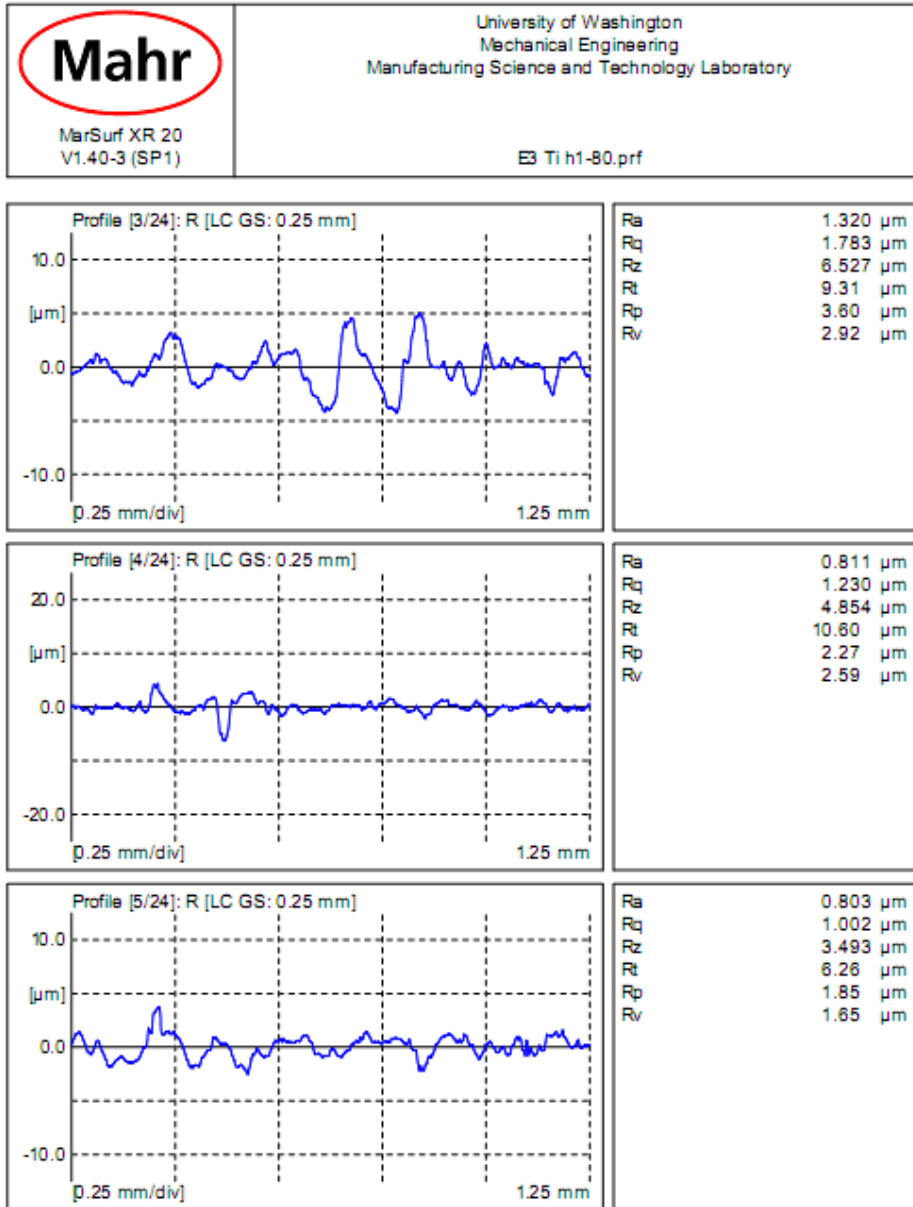


APPENDIX D


Titanium hole surface profiles: WC (DC) high speed Experiment Type II

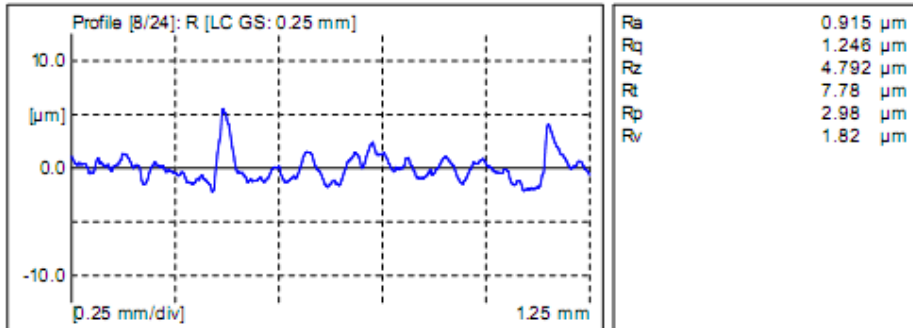
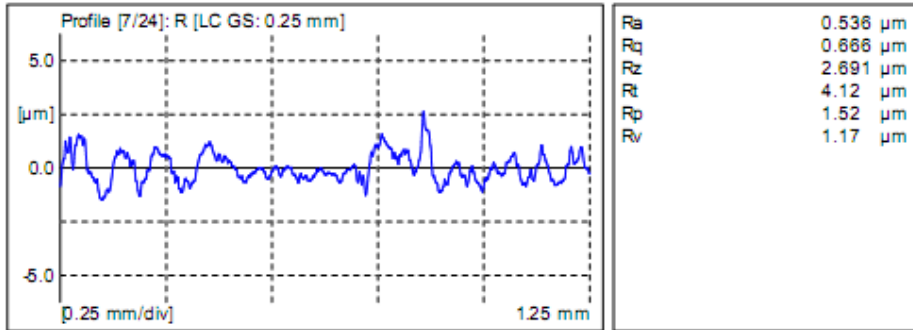
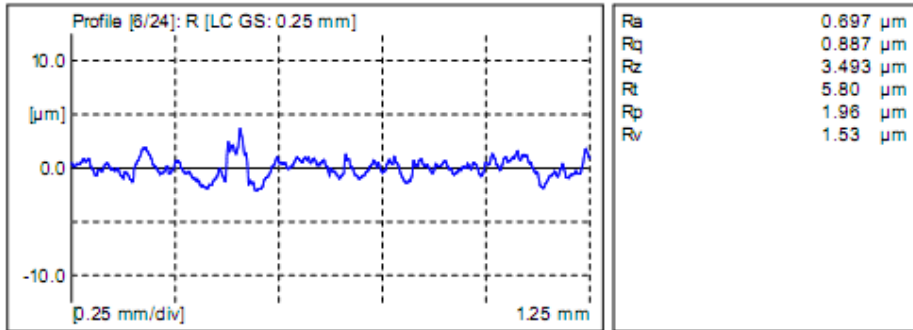


APPENDIX D




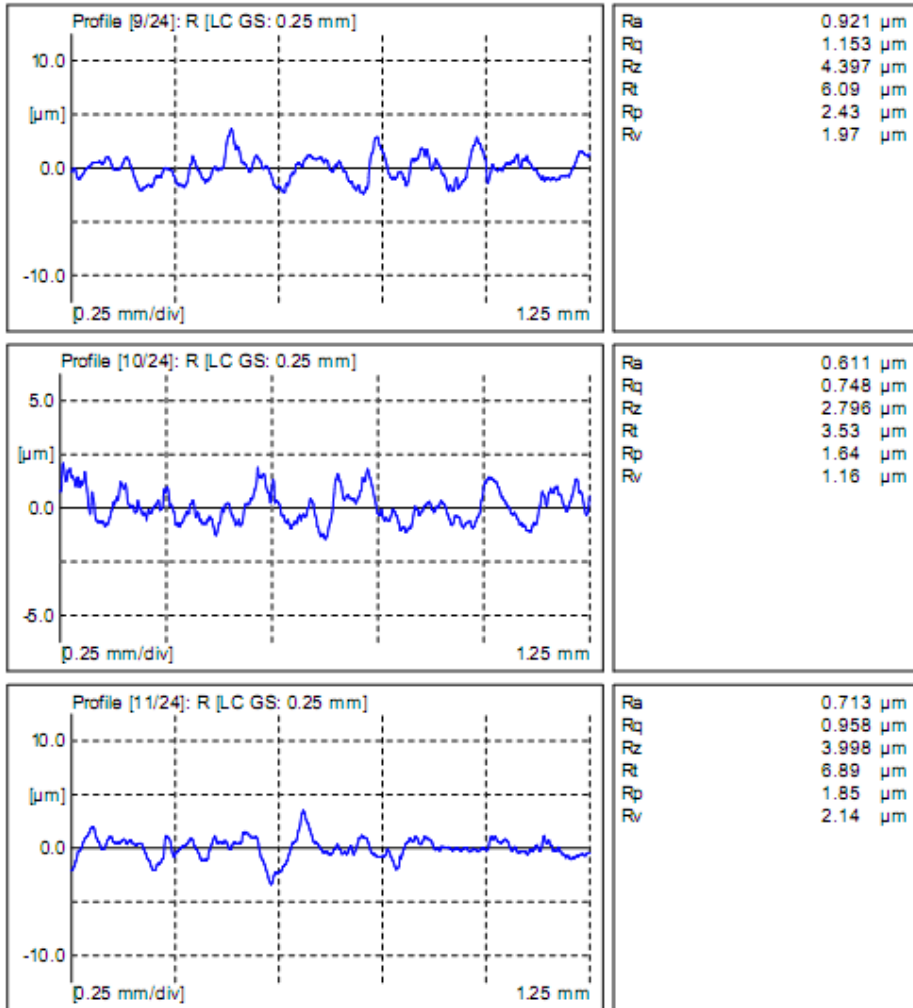
APPENDIX D

 <p>Mahr MarSurf XR 20 V1.40-3 (SP1)</p>	<p>University of Washington Mechanical Engineering Manufacturing Science and Technology Laboratory</p>
	<p>E3 Ti h1-80.prf</p>




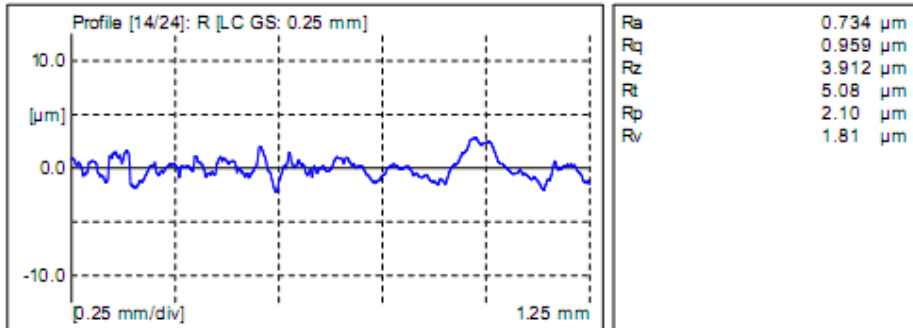
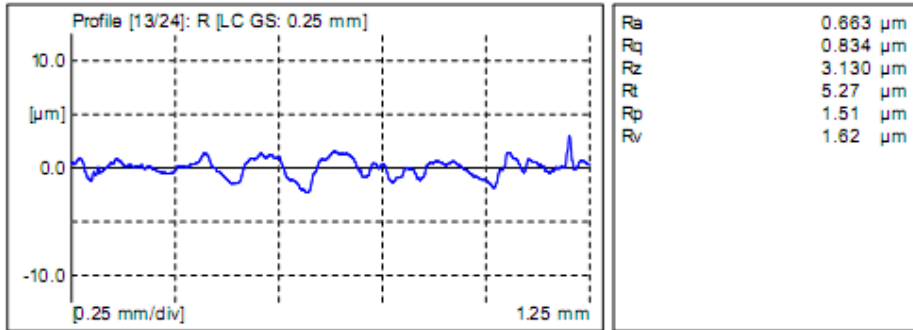
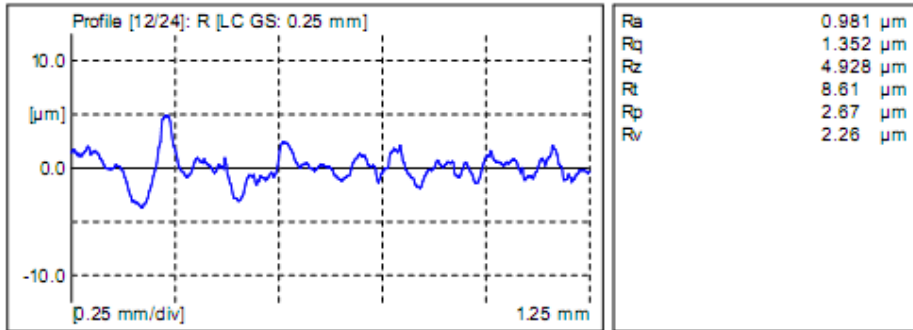
APPENDIX D

 <p style="margin: 0;">Mahr</p> <p style="margin: 0; font-size: small;">MarSurf XR 20 V1.40-3 (SP1)</p>	<p style="margin: 0; font-size: small;">University of Washington Mechanical Engineering Manufacturing Science and Technology Laboratory</p> <p style="margin: 0; font-size: small;">E3 Ti h1-80.prf</p>
---	---




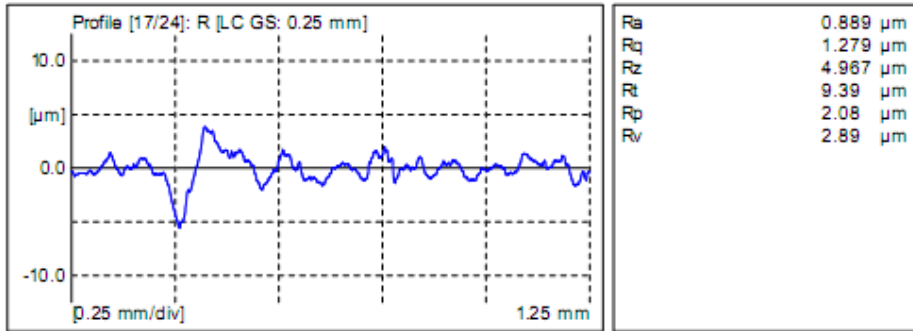
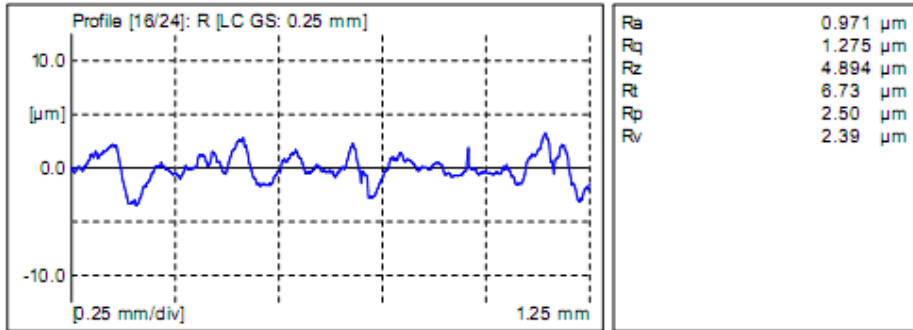
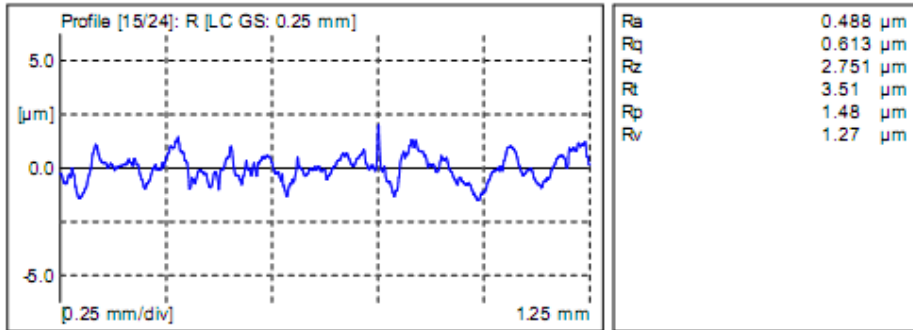
APPENDIX D

 <p style="font-size: small;">MarSurf XR 20 V1.40-3 (SP1)</p>	<p style="font-size: x-small;">University of Washington Mechanical Engineering Manufacturing Science and Technology Laboratory</p> <p style="font-size: x-small;">E3 Ti h1-80.prf</p>
--	---




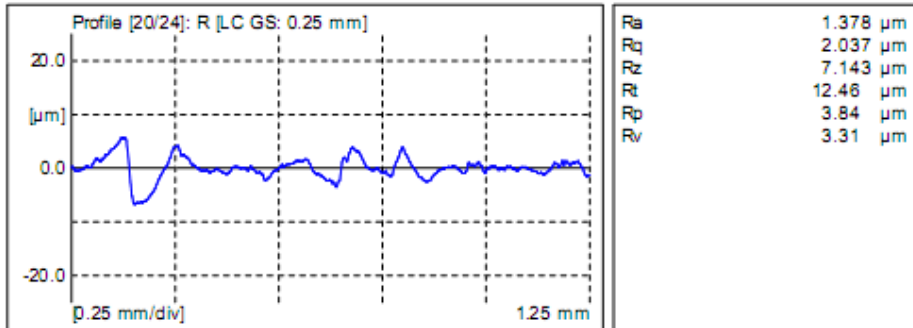
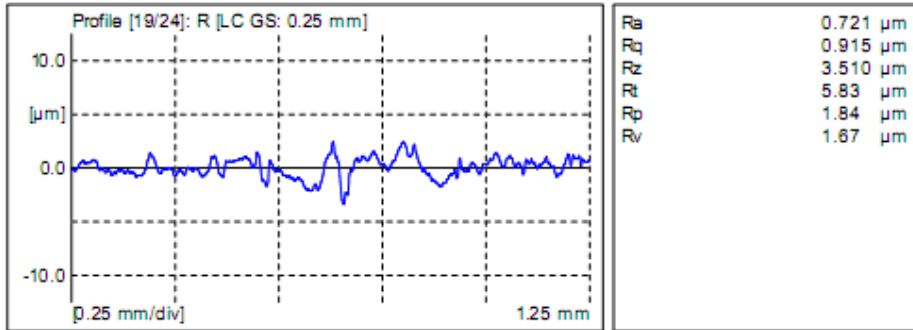
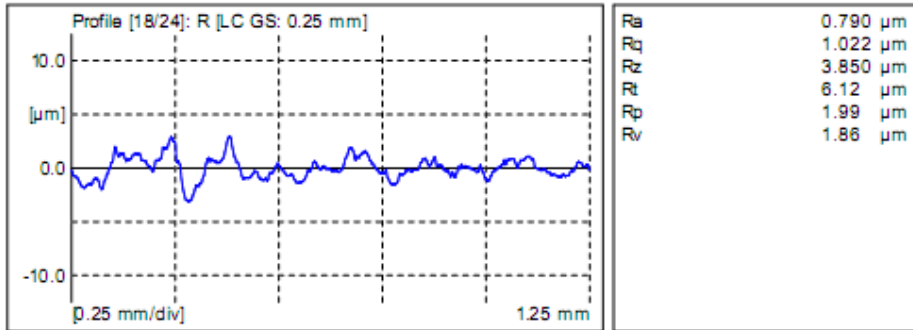
APPENDIX D

 <p style="margin: 0;">Mahr</p> <p style="margin: 0; font-size: small;">MarSurf XR 20 V1.40-3 (SP1)</p>	<p style="margin: 0; font-size: small;">University of Washington Mechanical Engineering Manufacturing Science and Technology Laboratory</p> <p style="margin: 0; font-size: small;">E3 Ti h1-80.prf</p>
---	---

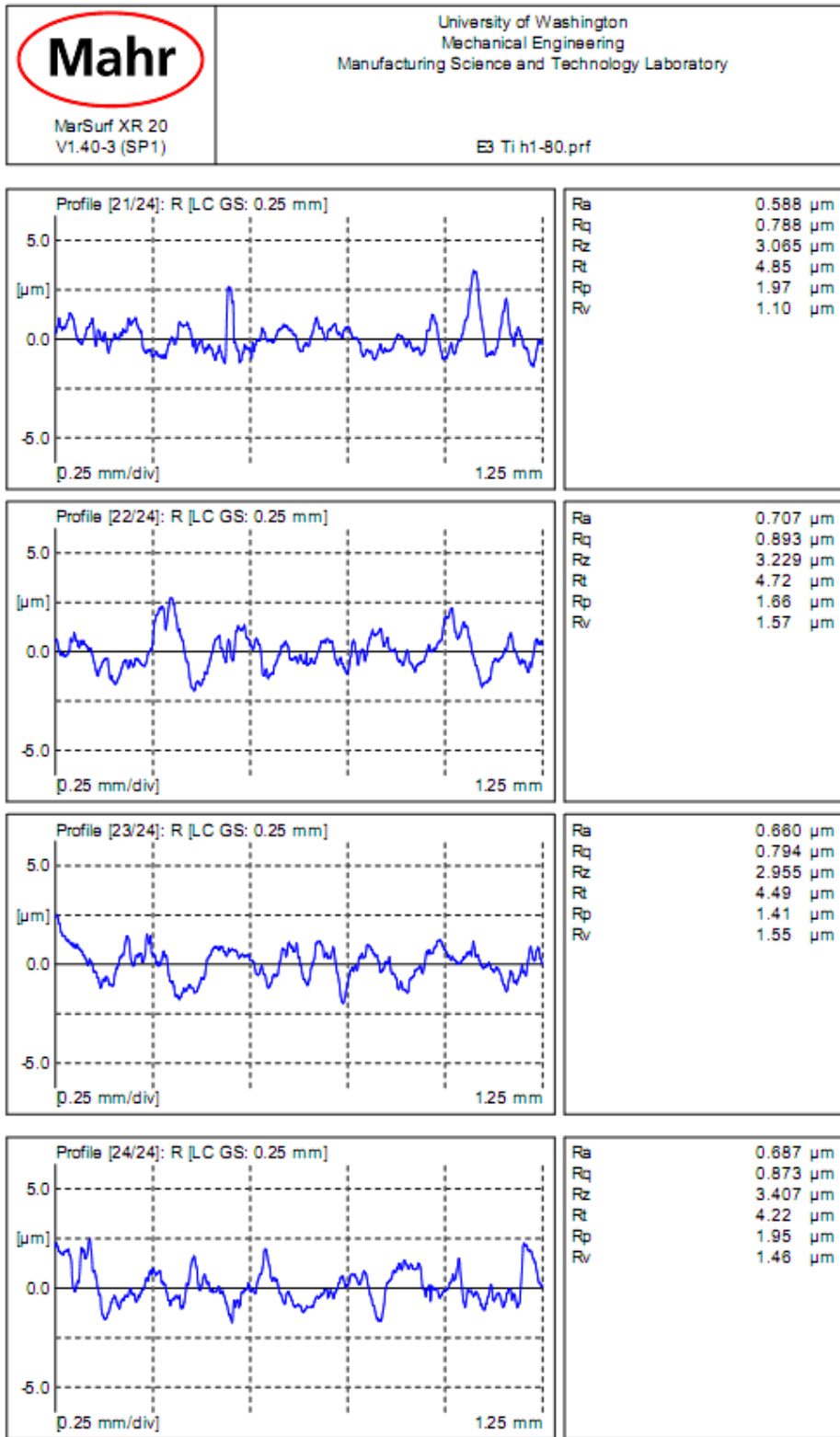


APPENDIX D

 <p>Mahr MarSurf XR 20 V1.40-3 (SP1)</p>	<p>University of Washington Mechanical Engineering Manufacturing Science and Technology Laboratory</p>
	<p>E3 Ti h1-80.prf</p>

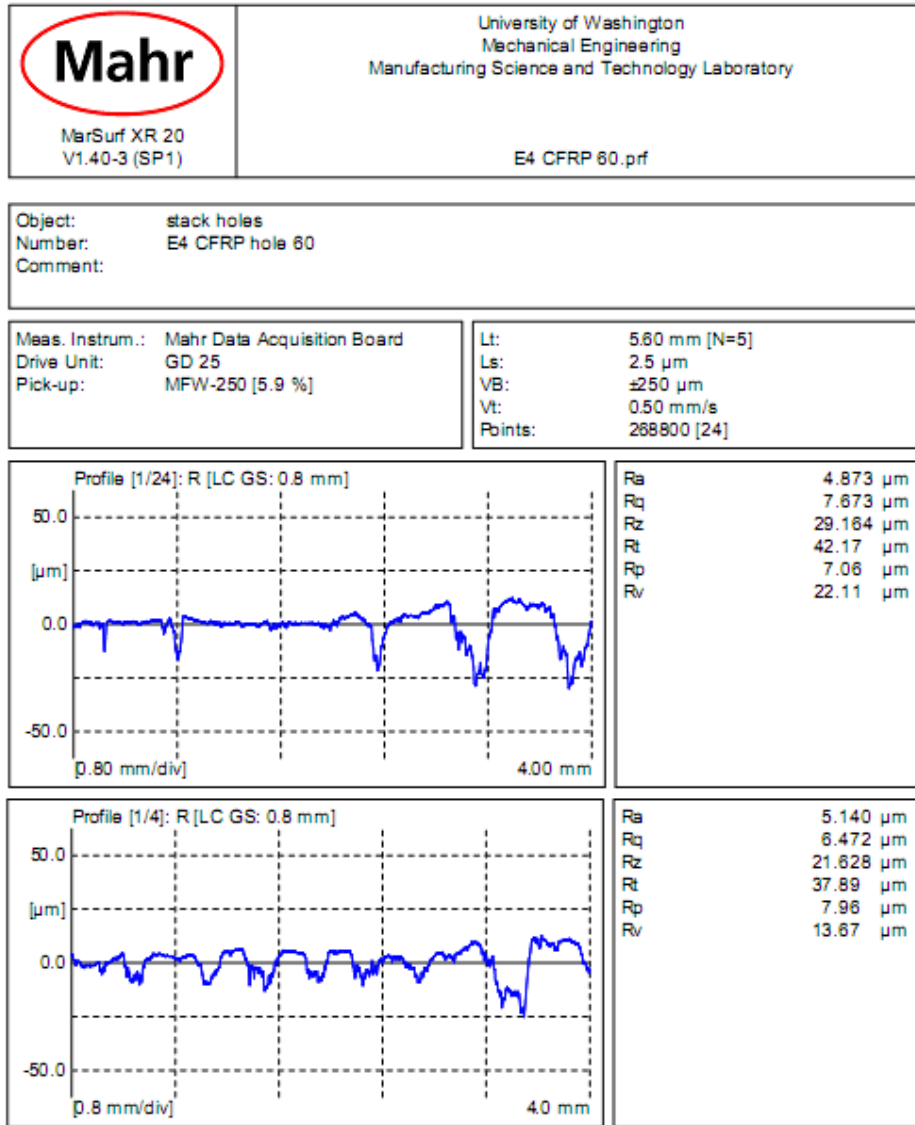


APPENDIX D




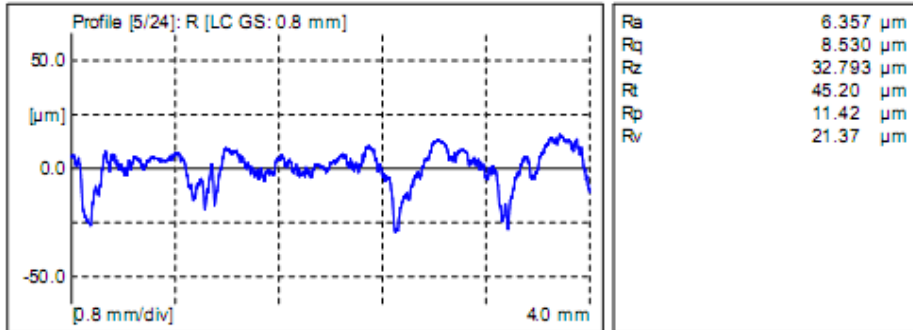
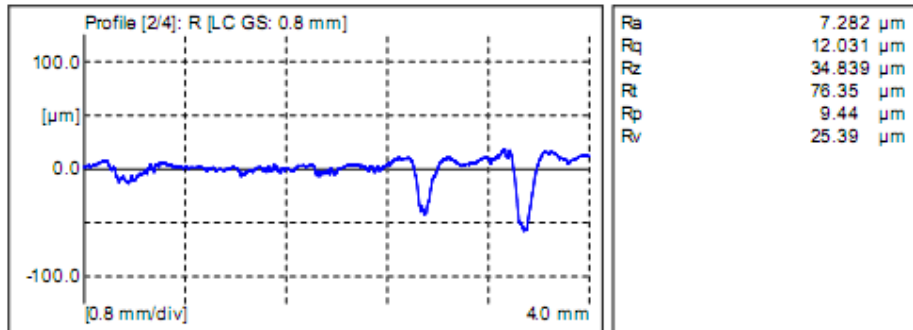
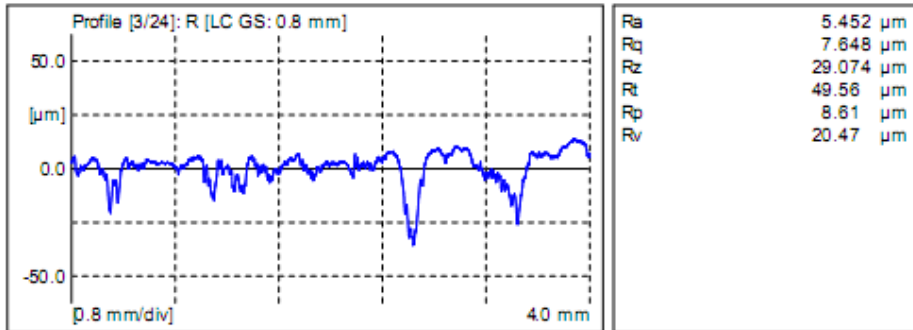
APPENDIX D

CFRP hole surface profiles: WC (DC) low speed Experiment Type II

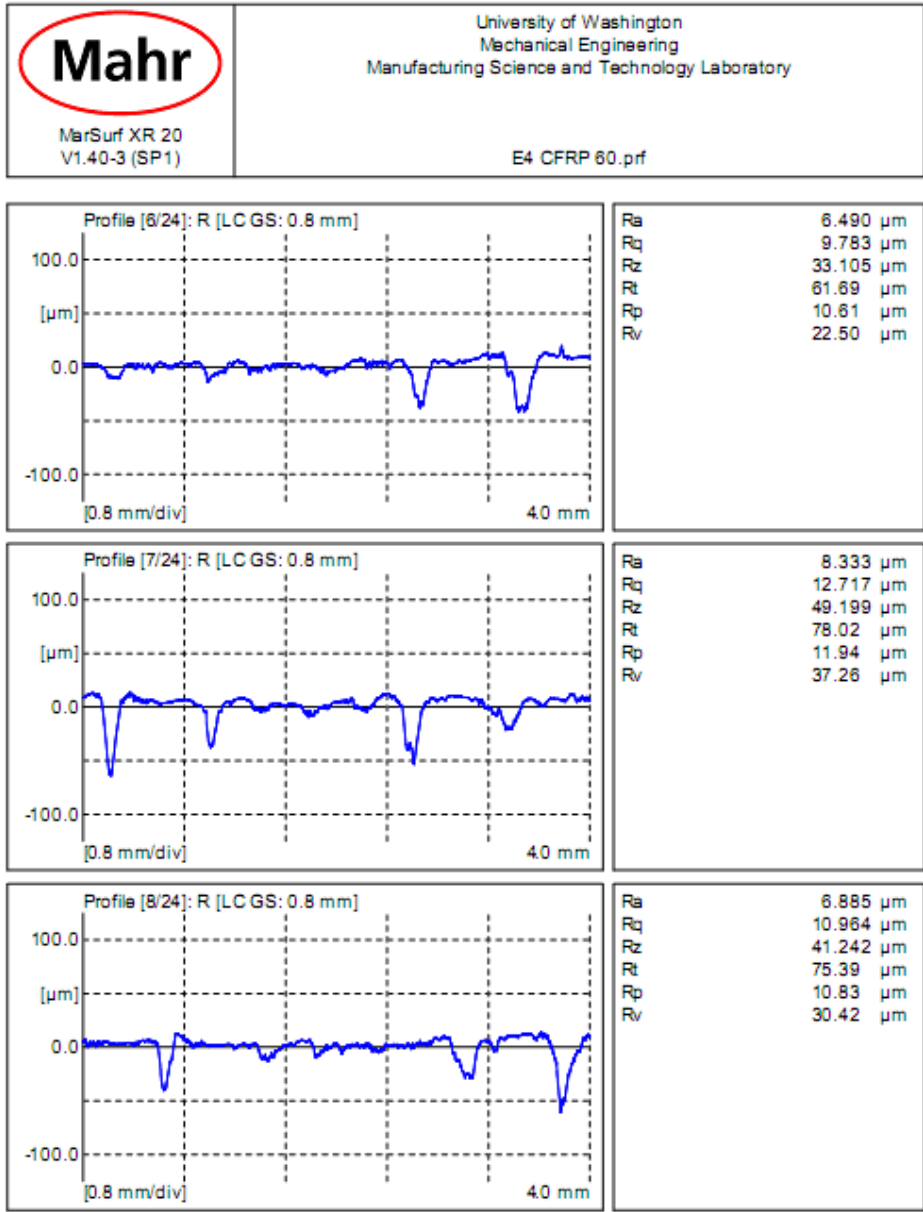


APPENDIX D


 <p>Mahr MarSurf XR 20 V1.40-3 (SP1)</p>	<p>University of Washington Mechanical Engineering Manufacturing Science and Technology Laboratory</p>
	<p>E4 CFRP 60.prf</p>

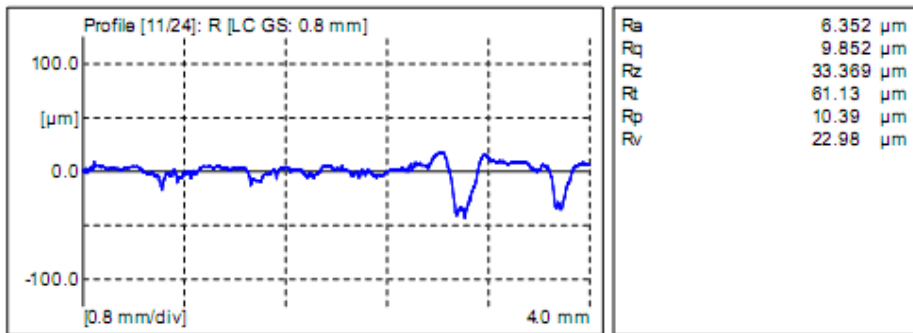
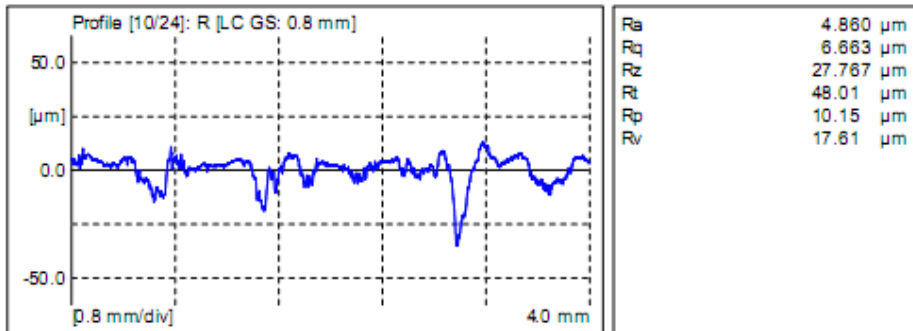
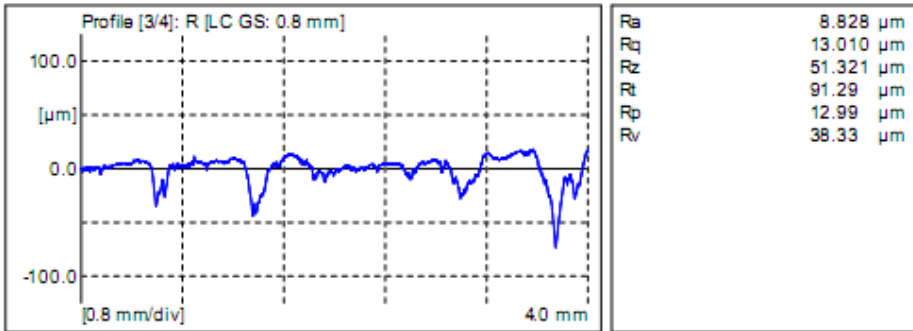


APPENDIX D




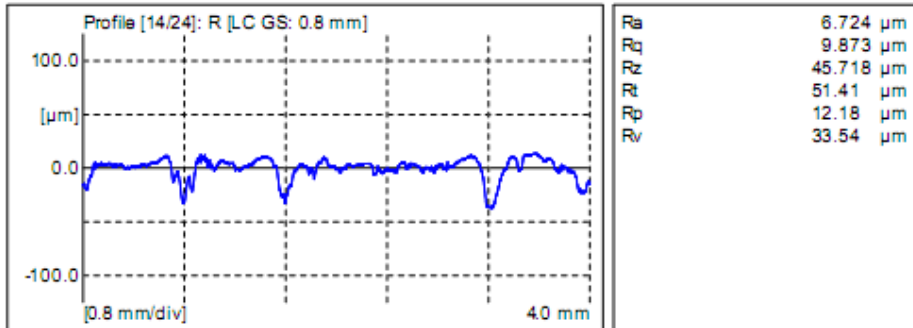
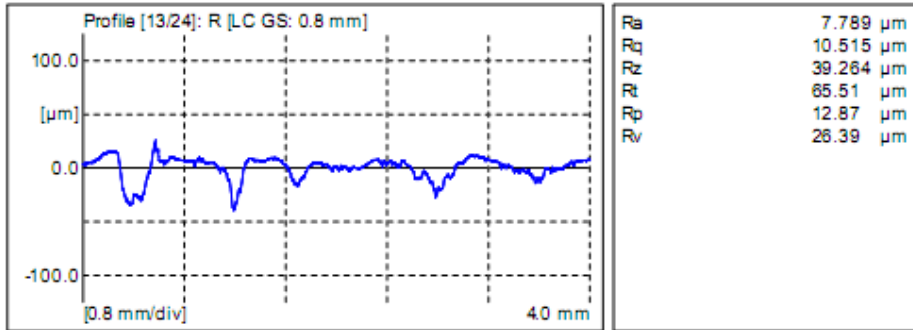
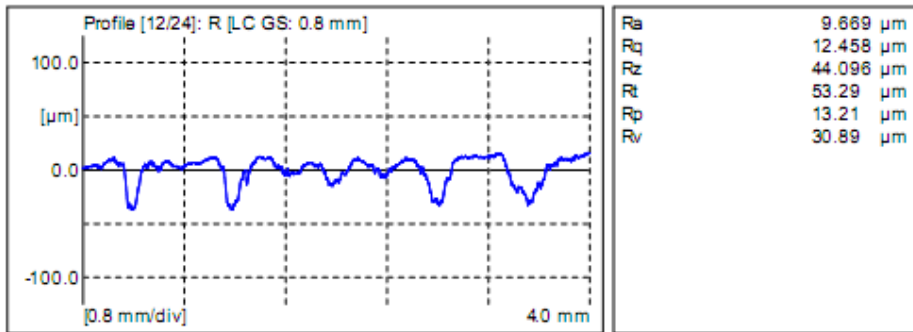
APPENDIX D

 <p>Mahr</p> <p>MarSurf XR 20 V1.40-3 (SP1)</p>	<p>University of Washington Mechanical Engineering Manufacturing Science and Technology Laboratory</p>
	<p>E4 CFRP 60.prf</p>




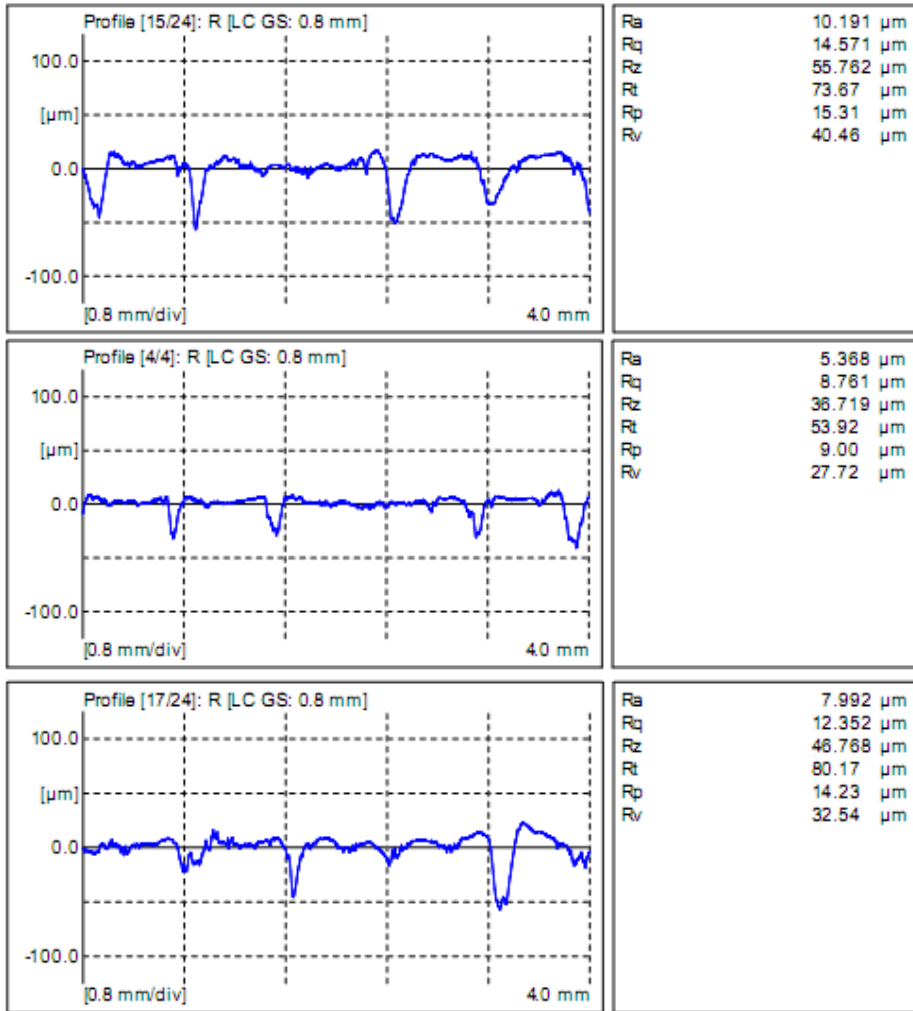
APPENDIX D

 <p>Mahr MarSurf XR 20 V1.40-3 (SP1)</p>	<p>University of Washington Mechanical Engineering Manufacturing Science and Technology Laboratory</p>
	<p>E4 CFRP 60.prf</p>




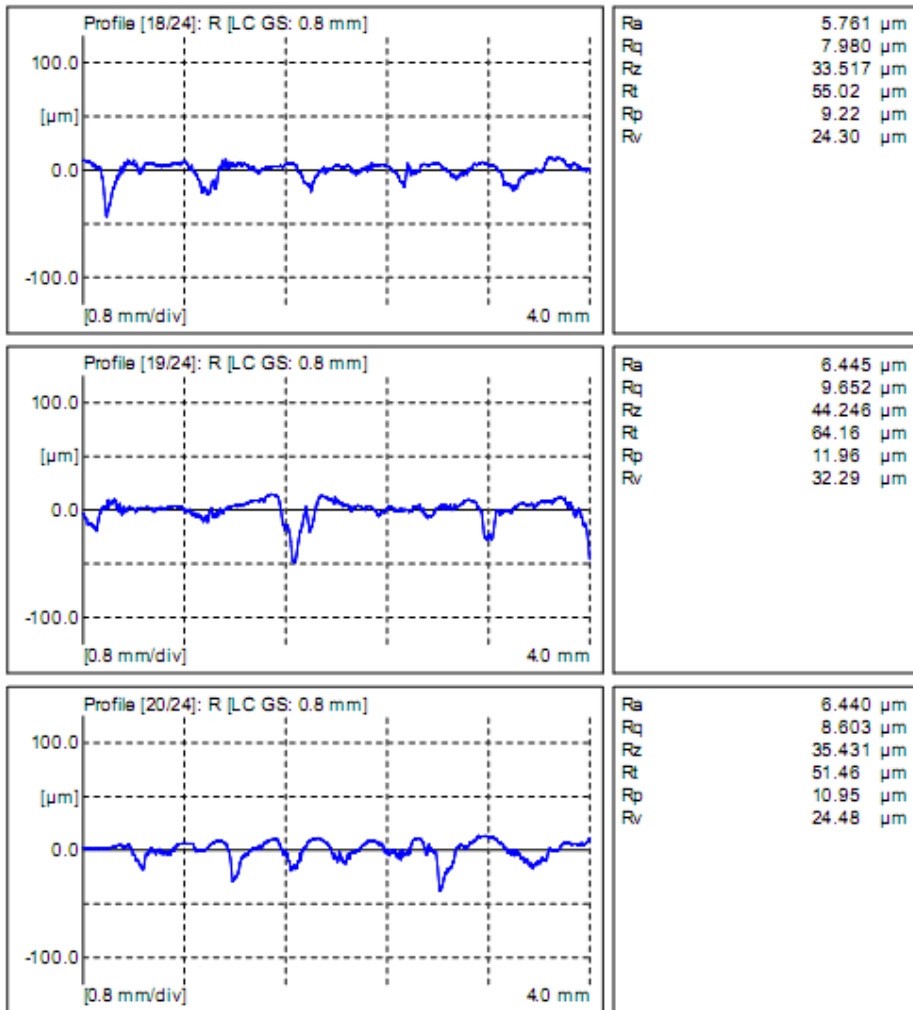
APPENDIX D

 <p style="font-size: small;">MarSurf XR 20 V1.40-3 (SP1)</p>	<p style="font-size: x-small;">University of Washington Mechanical Engineering Manufacturing Science and Technology Laboratory</p> <p style="font-size: x-small;">E4 CFRP 60.prf</p>
--	--




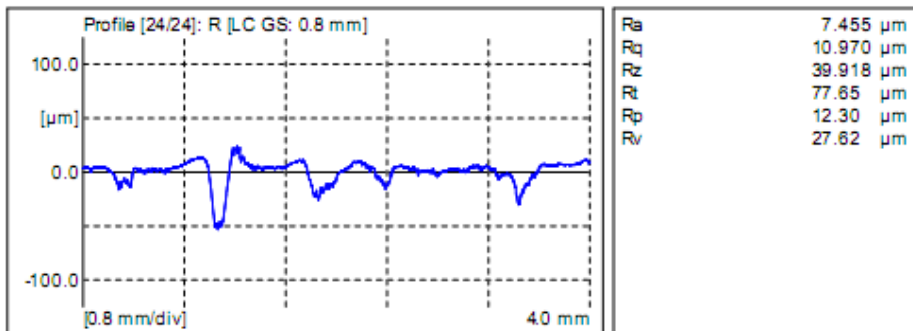
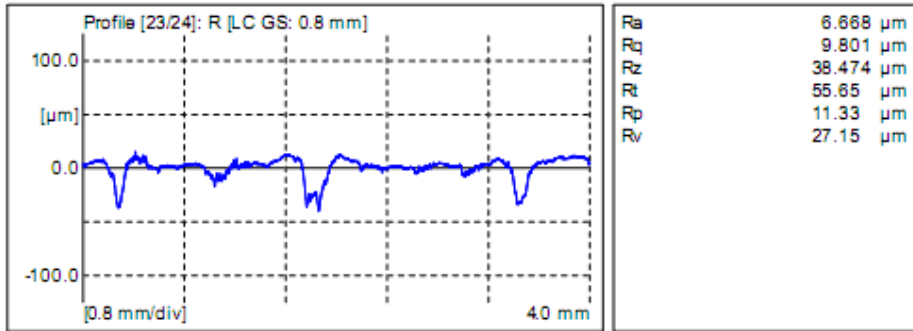
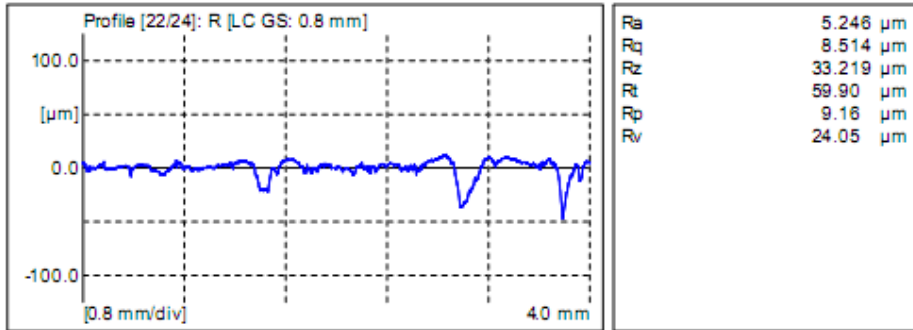
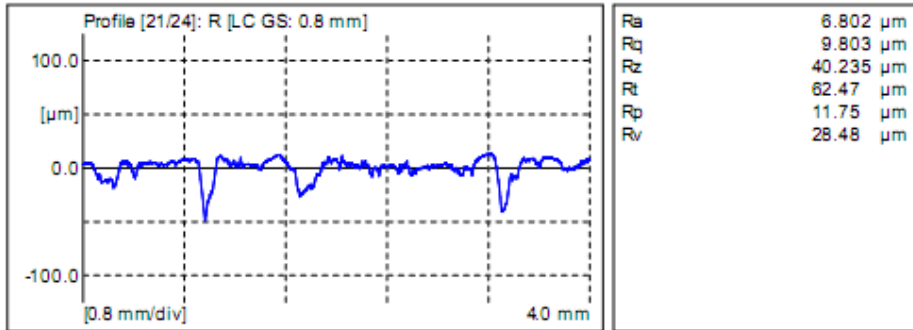
APPENDIX D

 <p style="margin: 0;">MarSurf XR 20 V1.40-3 (SP1)</p>	<p style="margin: 0;">University of Washington Mechanical Engineering Manufacturing Science and Technology Laboratory</p> <p style="margin: 0;">E4 CFRP 60.prf</p>
---	--



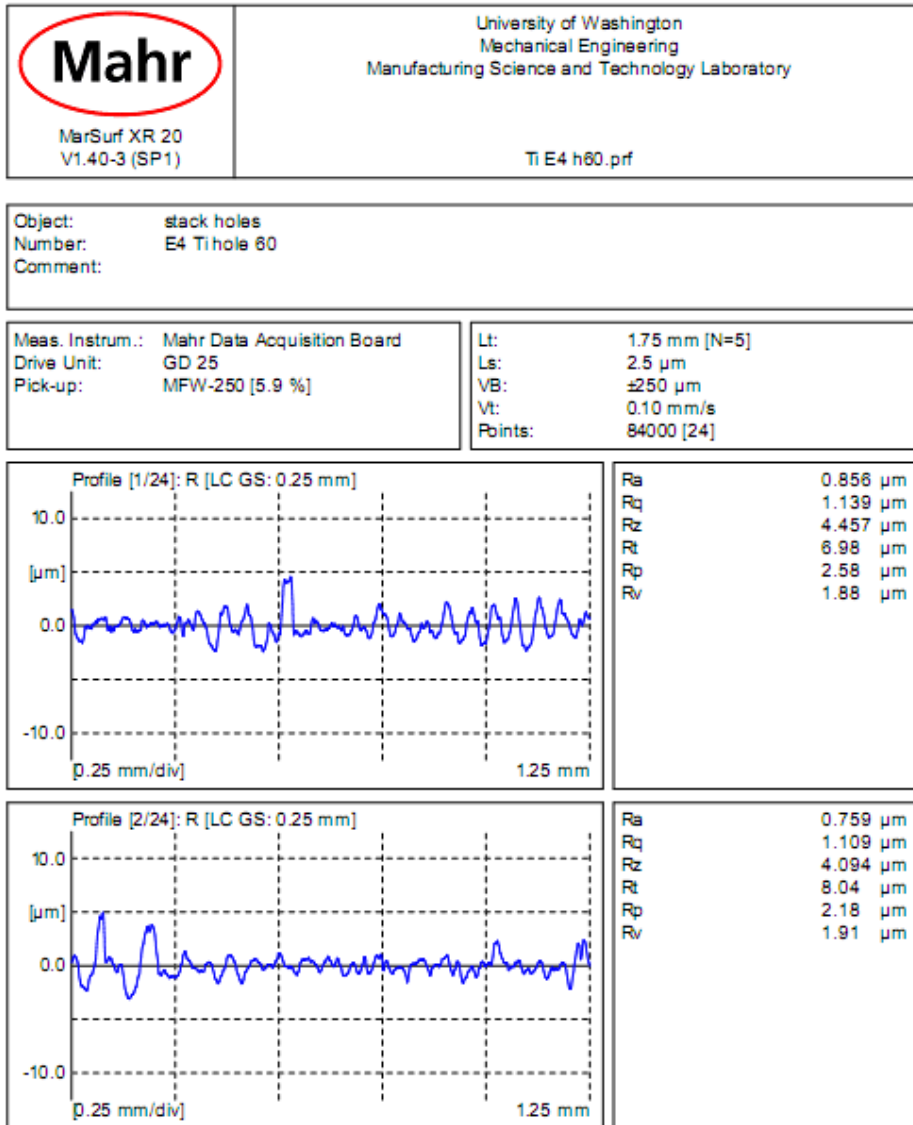
APPENDIX D

 <p style="margin: 0;">Mahr</p> <p style="margin: 0; font-size: small;">MarSurf XR 20 V1.40-3 (SP1)</p>	<p style="margin: 0; font-size: small;">University of Washington Mechanical Engineering Manufacturing Science and Technology Laboratory</p> <p style="margin: 0; font-size: small;">E4 CFRP 60.prf</p>
---	--




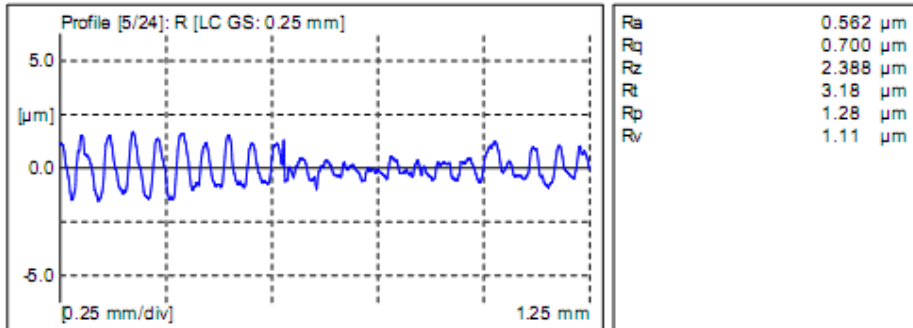
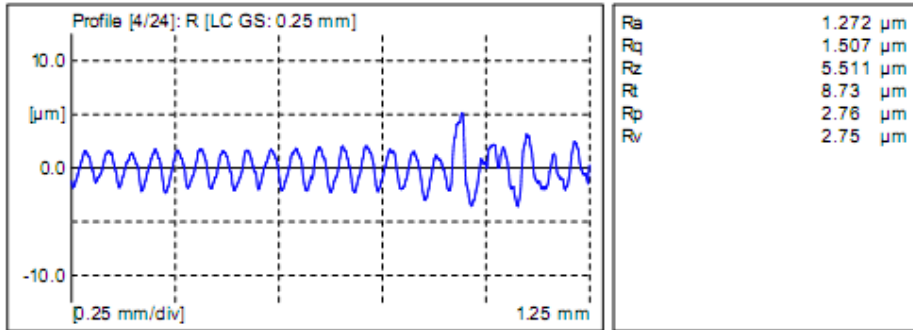
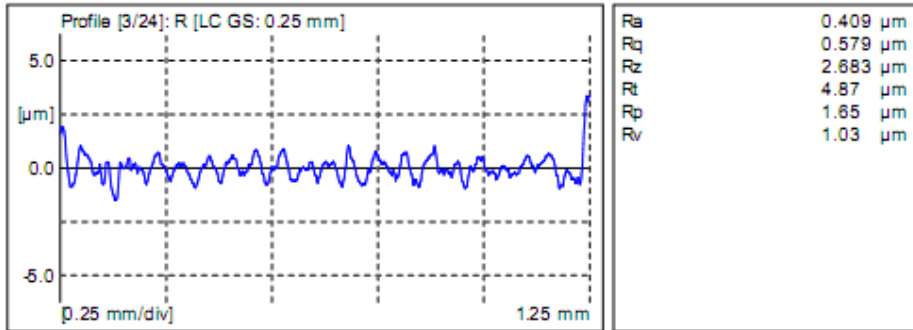
APPENDIX D

Titanium hole surface profiles: WC (DC) low speed Experiment Type II




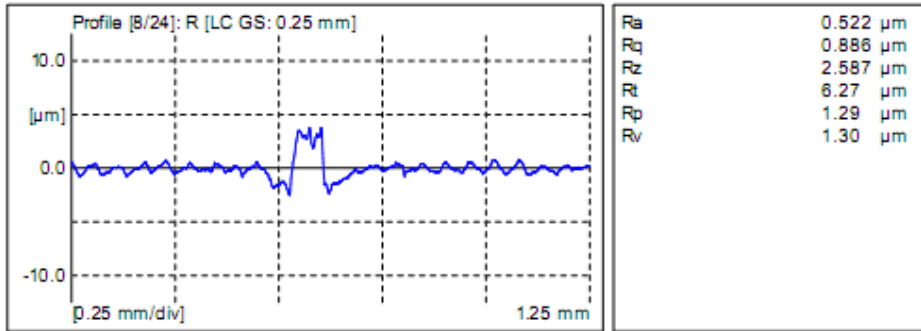
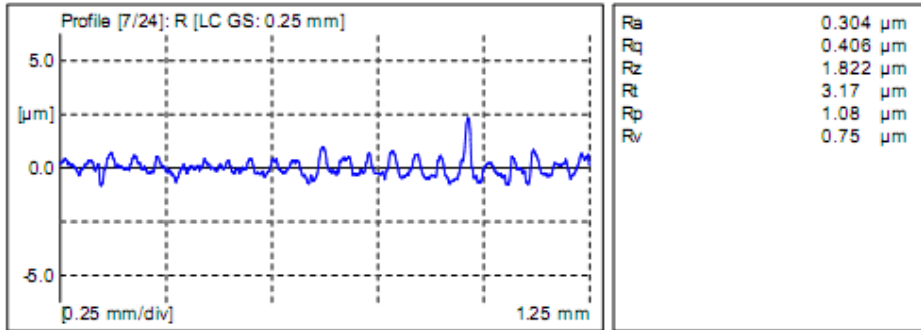
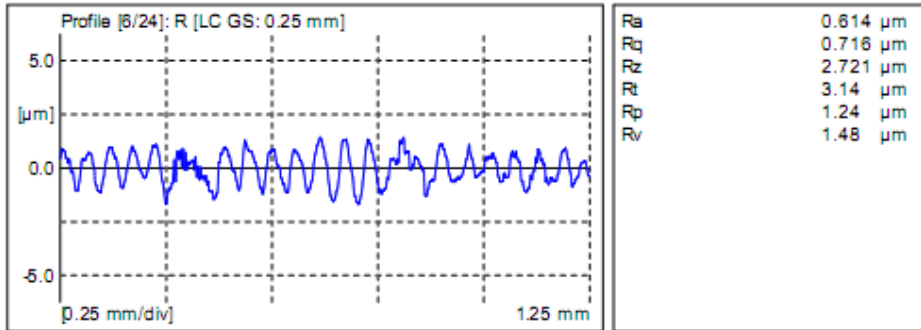
APPENDIX D

 <p>Mahr</p> <p>MarSurf XR 20 V1.40-3 (SP1)</p>	<p>University of Washington Mechanical Engineering Manufacturing Science and Technology Laboratory</p> <p>Ti E4 h60.prf</p>
---	---




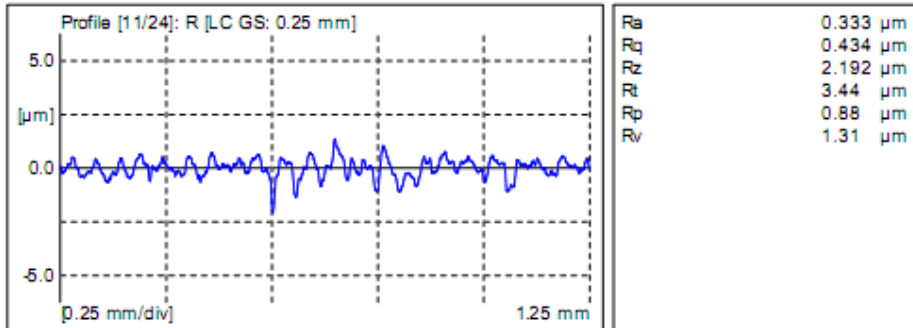
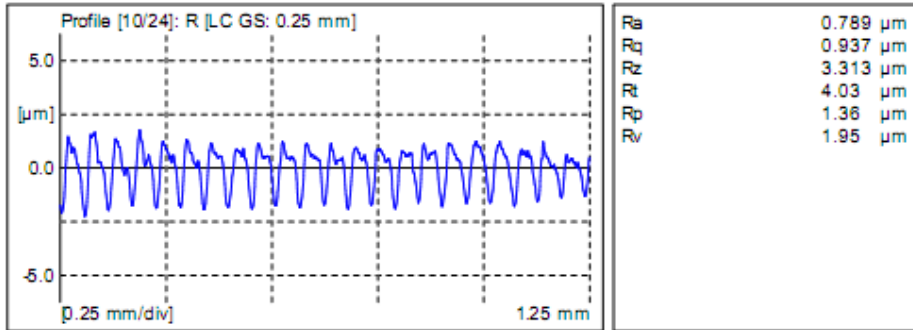
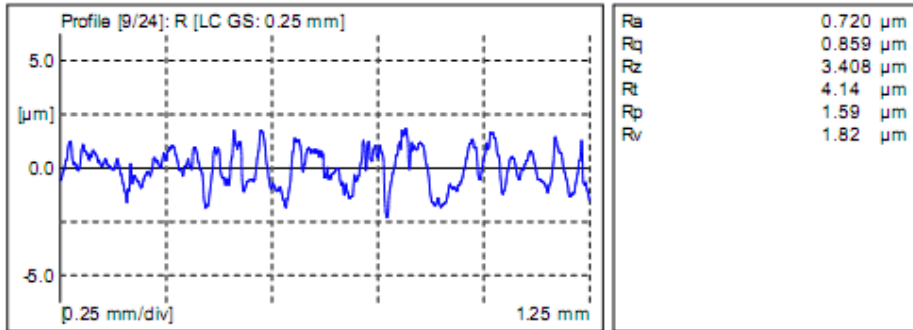
APPENDIX D

 <p>Mahr</p> <p>MarSurf XR 20 V1.40-3 (SP1)</p>	<p>University of Washington Mechanical Engineering Manufacturing Science and Technology Laboratory</p>
	<p>Ti E4 h60.prf</p>




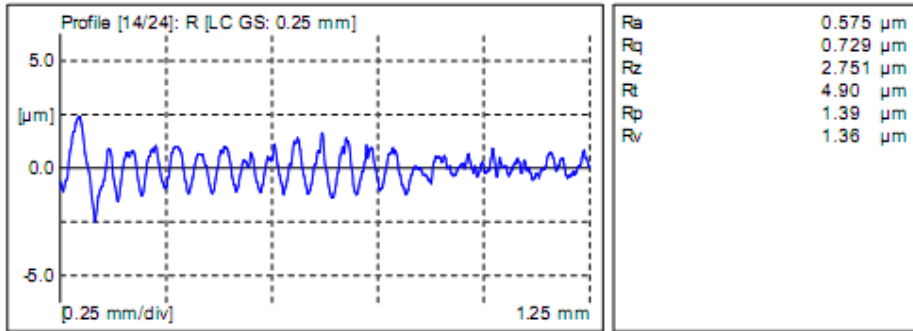
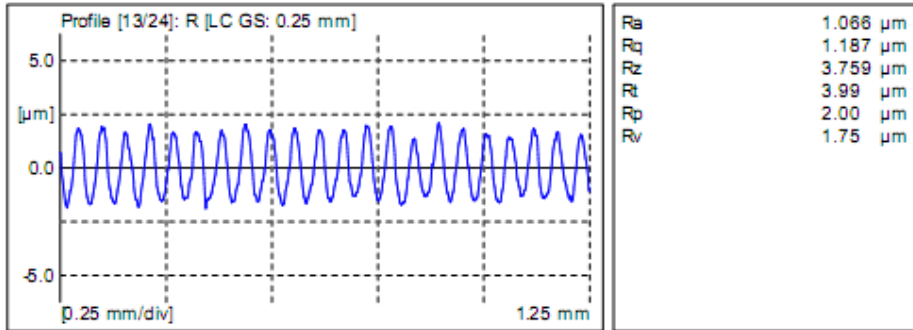
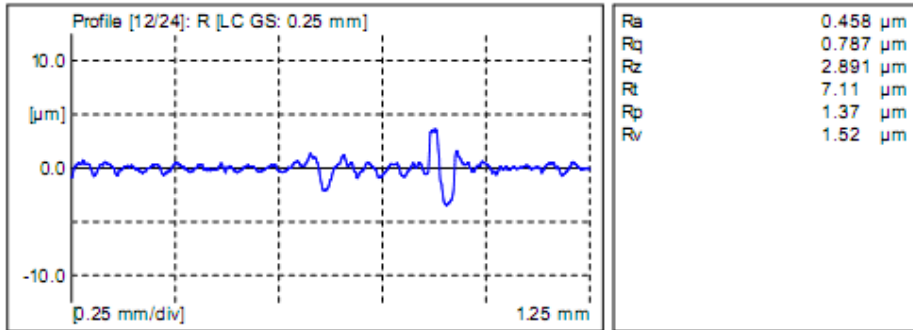
APPENDIX D

 <p style="margin: 0;">Mahr</p> <p style="margin: 0; font-size: small;">MarSurf XR 20 V1.40-3 (SP1)</p>	<p style="margin: 0; font-size: small;">University of Washington Mechanical Engineering Manufacturing Science and Technology Laboratory</p> <p style="margin: 0; font-size: small;">Ti E4 h60.prf</p>
---	---




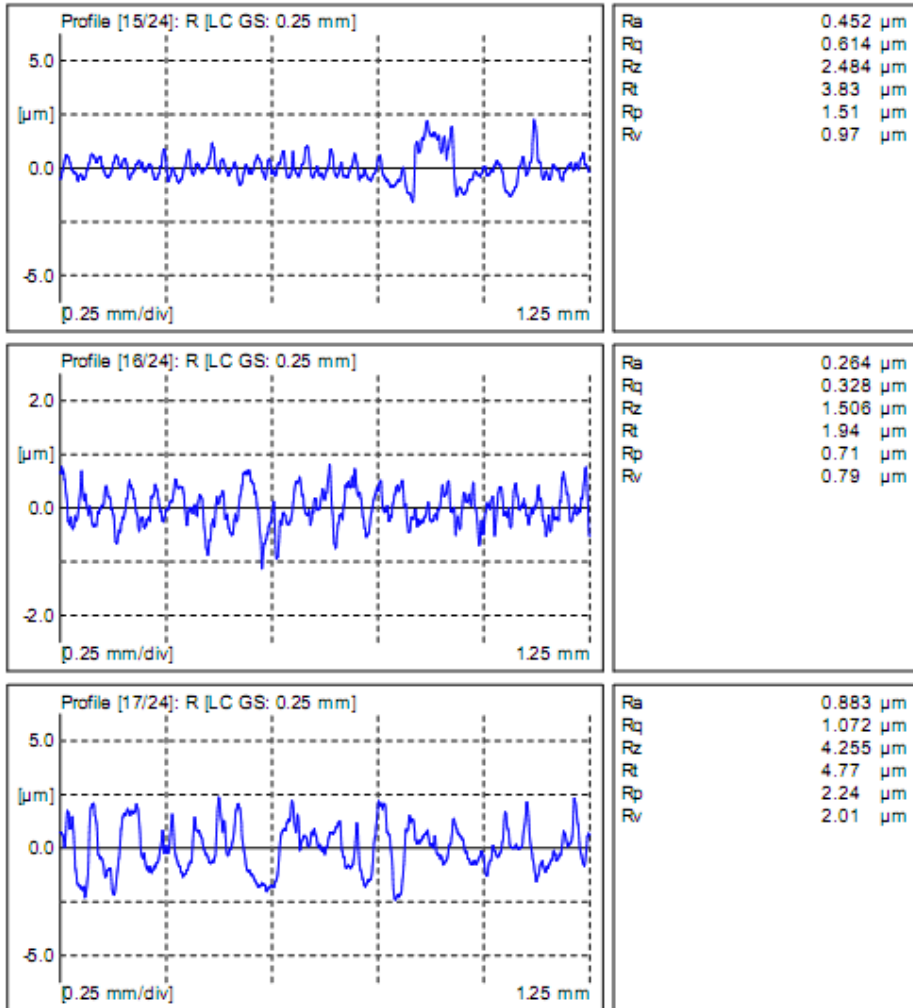
APPENDIX D

 <p style="font-size: small;">MarSurf XR 20 V1.40-3 (SP1)</p>	<p style="font-size: small;">University of Washington Mechanical Engineering Manufacturing Science and Technology Laboratory</p> <p style="font-size: small;">Ti E4 h60.prf</p>
--	---




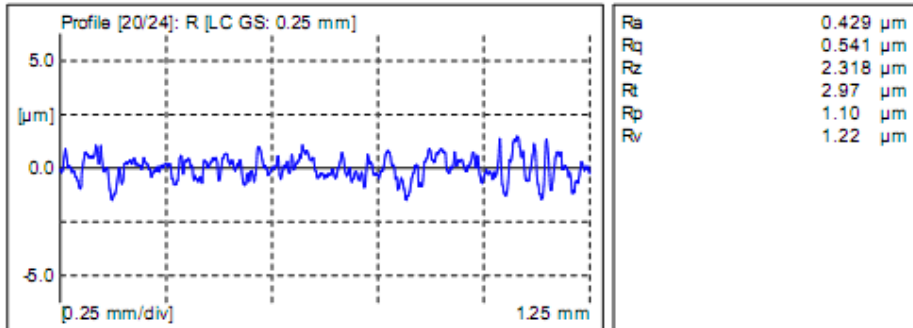
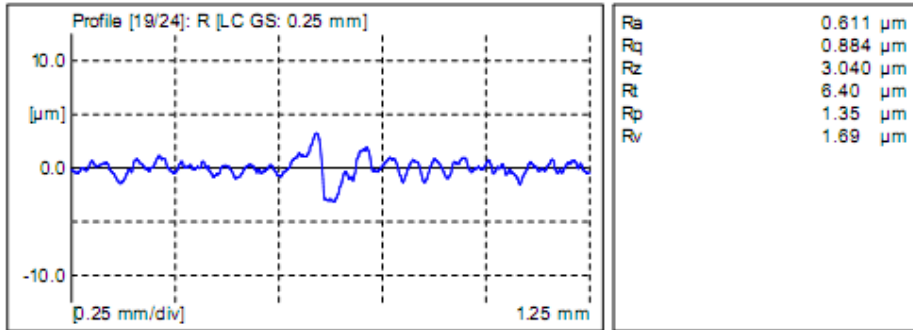
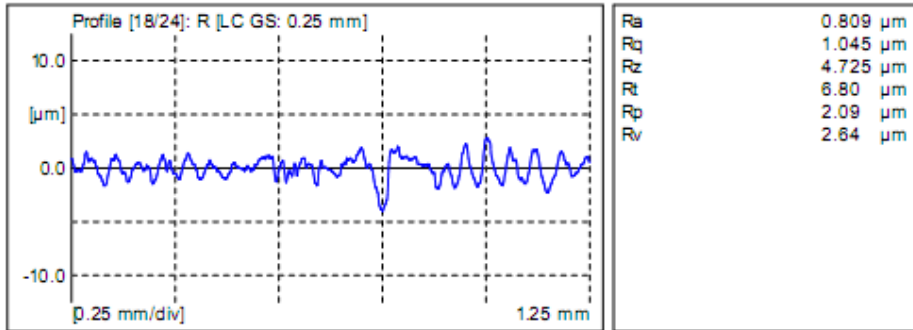
APPENDIX D

 <p style="margin: 0;">Mahr</p> <p style="margin: 0; font-size: small;">MarSurf XR 20 V1.40-3 (SP1)</p>	<p style="margin: 0; font-size: small;">University of Washington Mechanical Engineering Manufacturing Science and Technology Laboratory</p> <p style="margin: 0; font-size: small;">Ti E4 h60.prf</p>
---	---




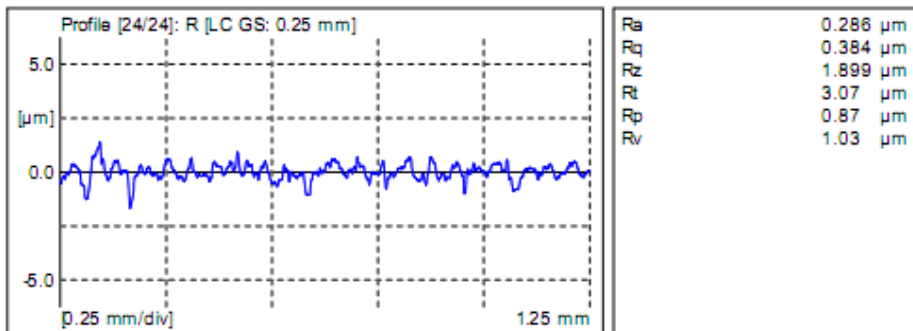
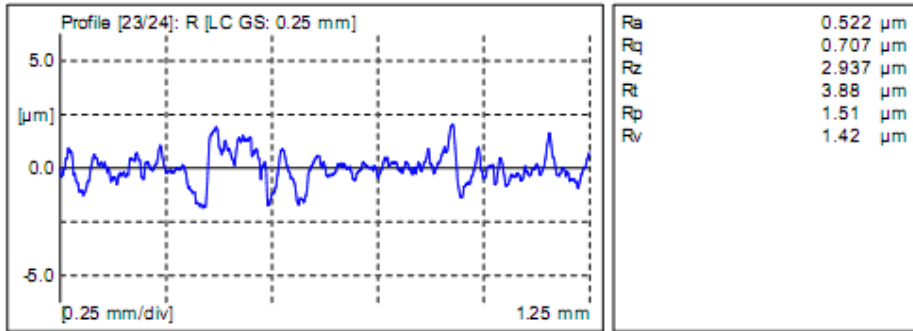
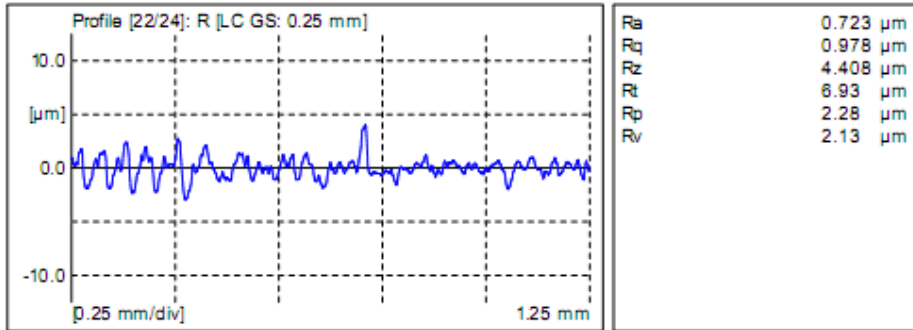
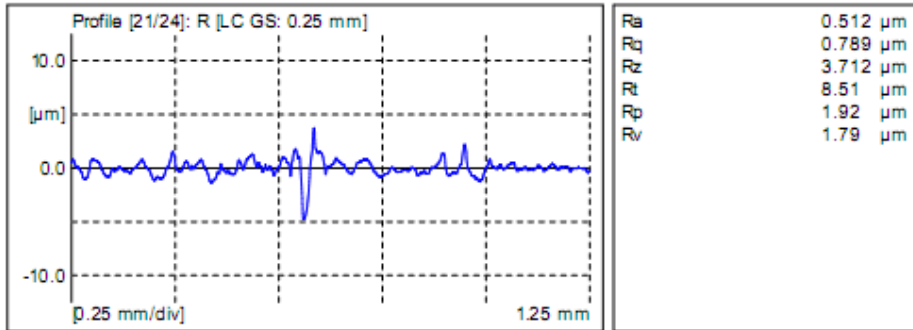
APPENDIX D

 <p>Mahr</p> <p>MarSurf XR 20 V1.40-3 (SP1)</p>	<p>University of Washington Mechanical Engineering Manufacturing Science and Technology Laboratory</p>
	<p>Ti E4 h60.prf</p>



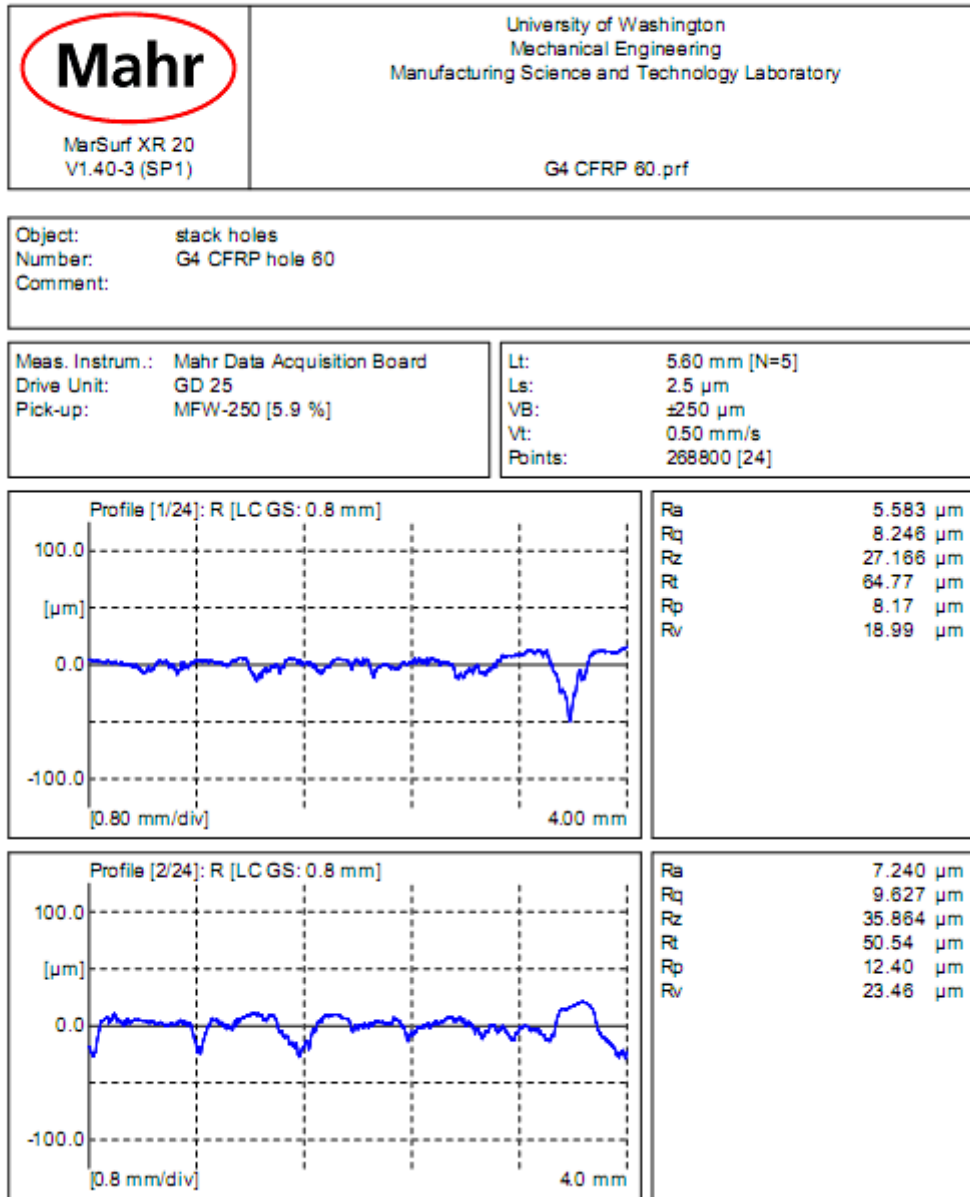
APPENDIX D

 <p style="margin: 0;">Mahr</p> <p style="margin: 0; font-size: small;">MarSurf XR 20 V1.40-3 (SP1)</p>	<p style="margin: 0; font-size: small;">University of Washington Mechanical Engineering Manufacturing Science and Technology Laboratory</p> <p style="margin: 0; font-size: small;">Ti E4 h80.prf</p>
---	---




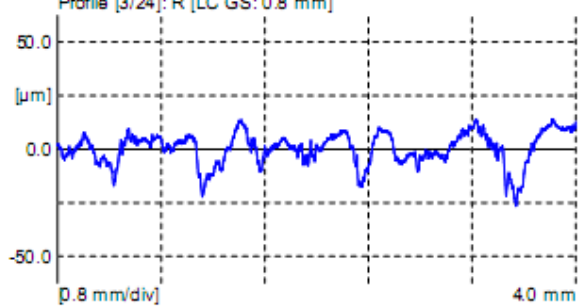
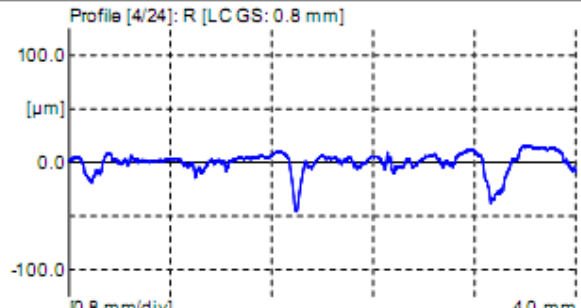
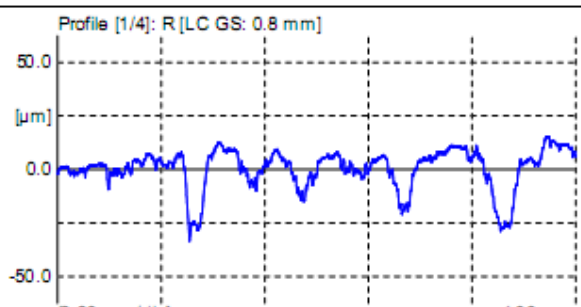
APPENDIX D

CFRP hole surface profiles: PCD low speed Experiment Type II

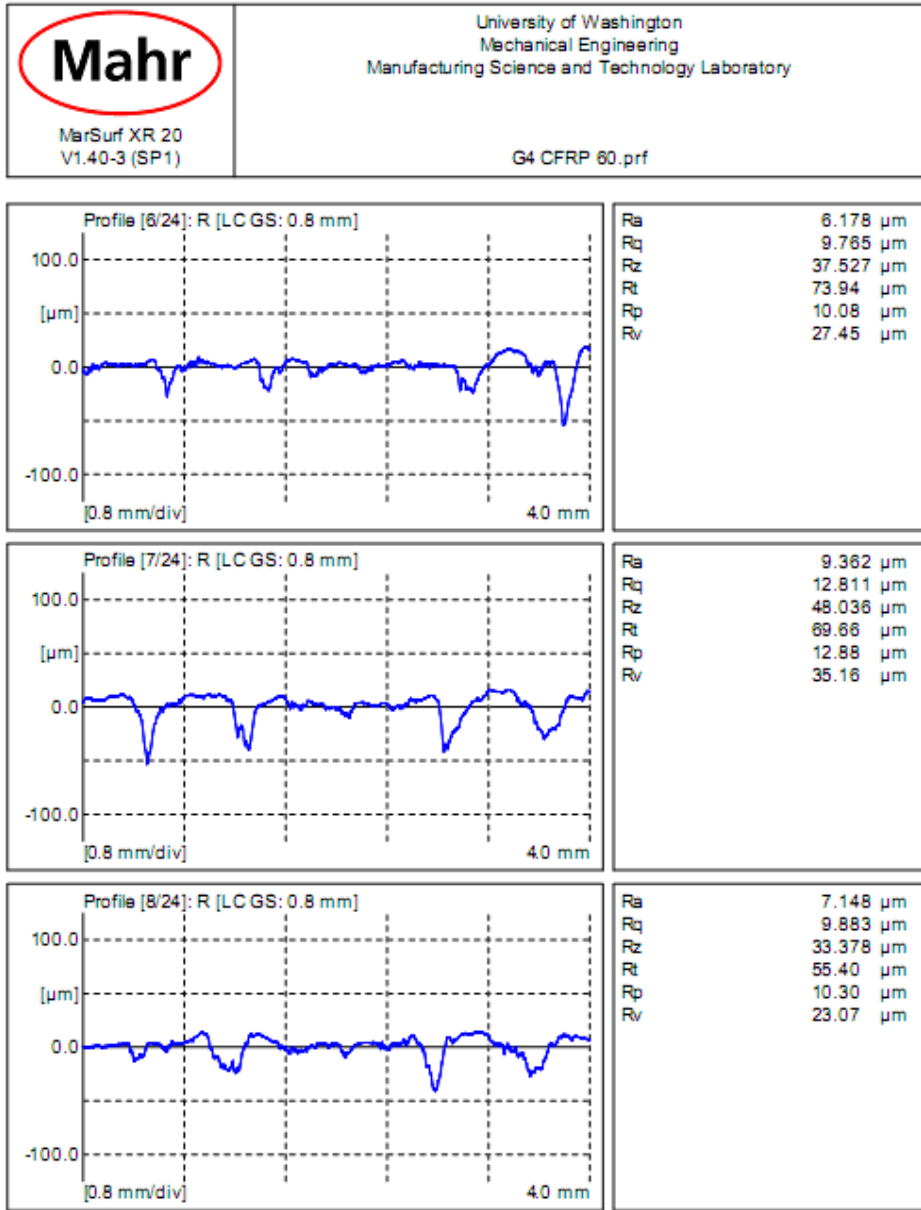


APPENDIX D

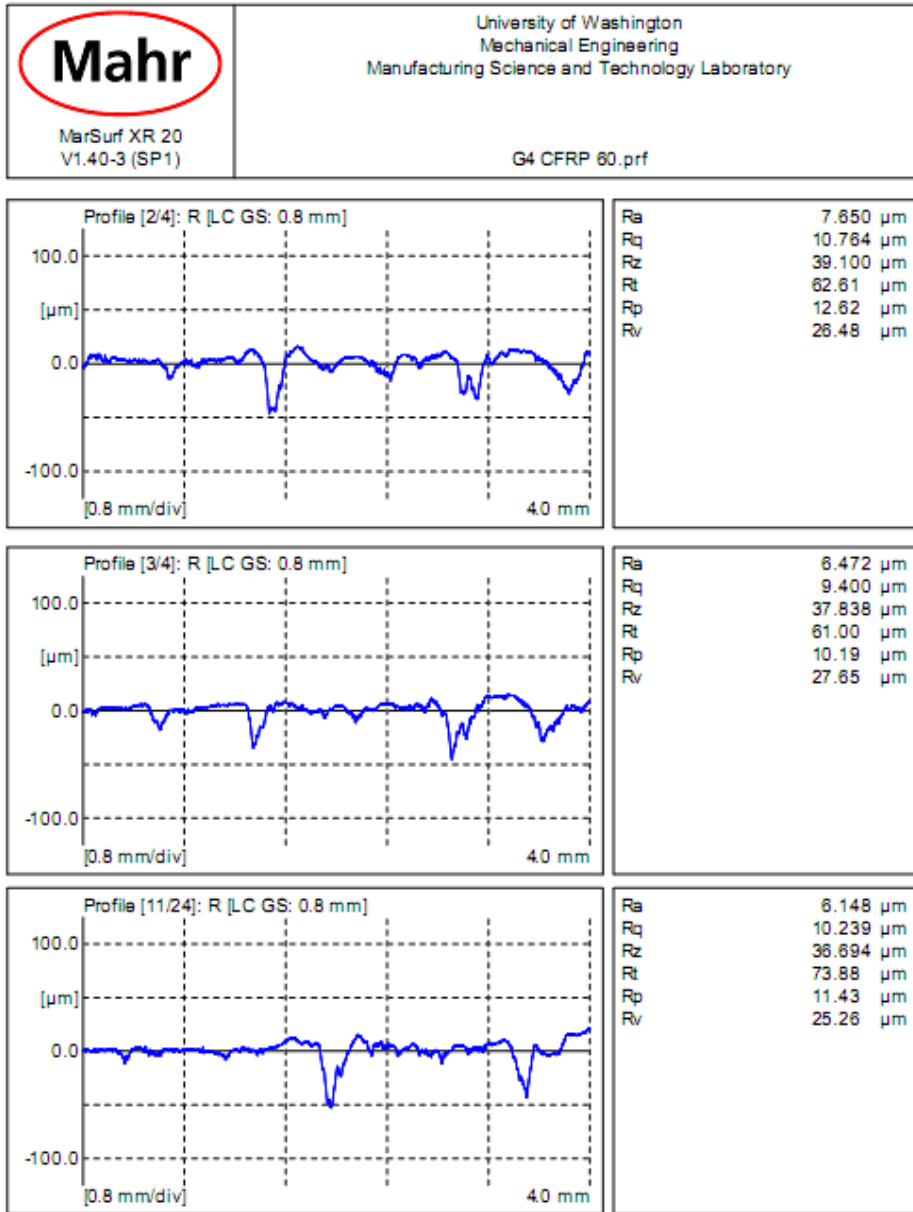
 <p>Mahr MarSurf XR 20 V1.40-3 (SP1)</p>	<p>University of Washington Mechanical Engineering Manufacturing Science and Technology Laboratory</p>
	<p>G4 CFRP 60.prf</p>

<p>Profile [3/24]: R [LC GS: 0.8 mm]</p> 	<table> <tr><td>Ra</td><td>5.887 μm</td></tr> <tr><td>Rq</td><td>7.473 μm</td></tr> <tr><td>Rz</td><td>30.192 μm</td></tr> <tr><td>Rt</td><td>40.54 μm</td></tr> <tr><td>Rp</td><td>11.42 μm</td></tr> <tr><td>Rv</td><td>18.77 μm</td></tr> </table>	Ra	5.887 μm	Rq	7.473 μm	Rz	30.192 μm	Rt	40.54 μm	Rp	11.42 μm	Rv	18.77 μm
Ra	5.887 μm												
Rq	7.473 μm												
Rz	30.192 μm												
Rt	40.54 μm												
Rp	11.42 μm												
Rv	18.77 μm												
<p>Profile [4/24]: R [LC GS: 0.8 mm]</p> 	<table> <tr><td>Ra</td><td>6.543 μm</td></tr> <tr><td>Rq</td><td>9.665 μm</td></tr> <tr><td>Rz</td><td>36.409 μm</td></tr> <tr><td>Rt</td><td>61.86 μm</td></tr> <tr><td>Rp</td><td>10.89 μm</td></tr> <tr><td>Rv</td><td>25.52 μm</td></tr> </table>	Ra	6.543 μm	Rq	9.665 μm	Rz	36.409 μm	Rt	61.86 μm	Rp	10.89 μm	Rv	25.52 μm
Ra	6.543 μm												
Rq	9.665 μm												
Rz	36.409 μm												
Rt	61.86 μm												
Rp	10.89 μm												
Rv	25.52 μm												
<p>Profile [1/4]: R [LC GS: 0.8 mm]</p> 	<table> <tr><td>Ra</td><td>6.796 μm</td></tr> <tr><td>Rq</td><td>9.299 μm</td></tr> <tr><td>Rz</td><td>32.837 μm</td></tr> <tr><td>Rt</td><td>49.07 μm</td></tr> <tr><td>Rp</td><td>11.27 μm</td></tr> <tr><td>Rv</td><td>21.57 μm</td></tr> </table>	Ra	6.796 μm	Rq	9.299 μm	Rz	32.837 μm	Rt	49.07 μm	Rp	11.27 μm	Rv	21.57 μm
Ra	6.796 μm												
Rq	9.299 μm												
Rz	32.837 μm												
Rt	49.07 μm												
Rp	11.27 μm												
Rv	21.57 μm												

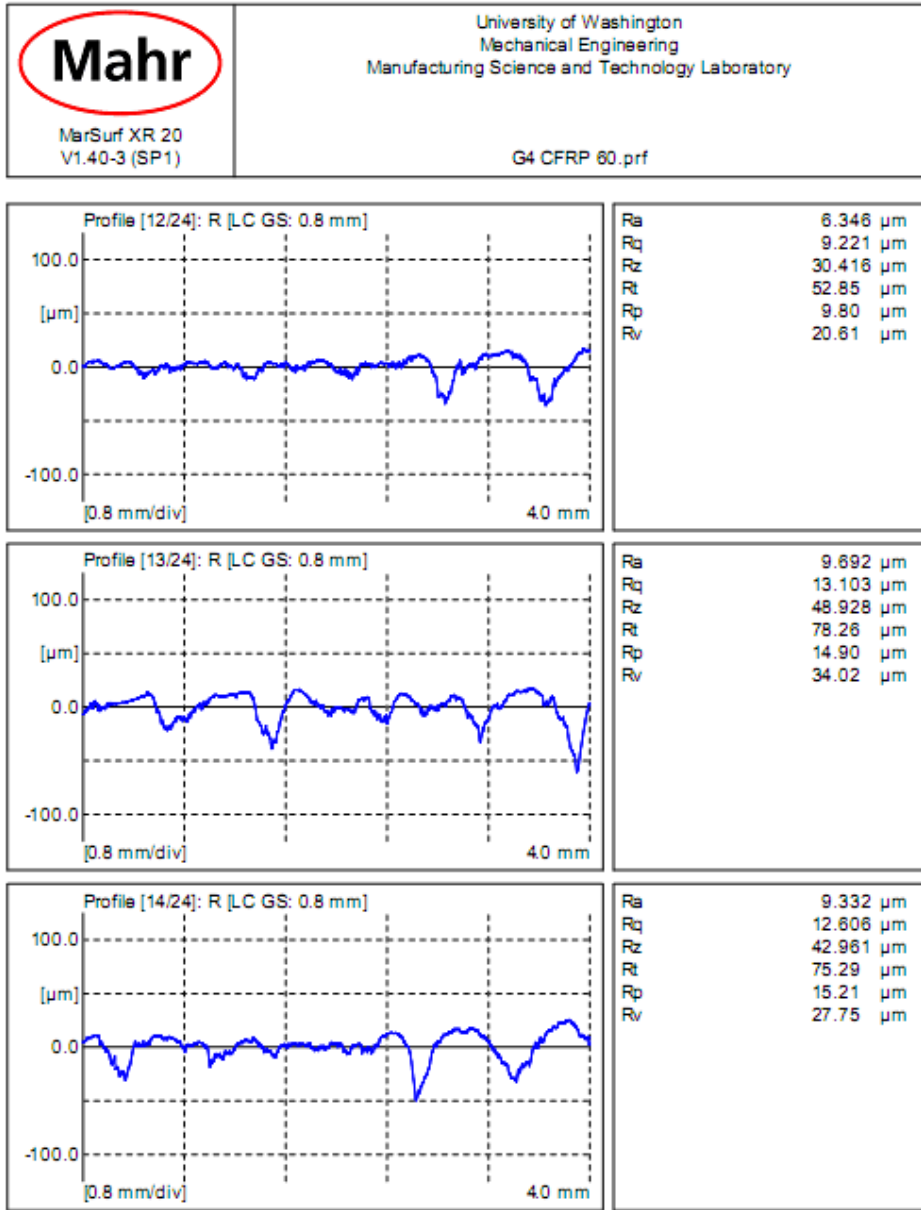
APPENDIX D




APPENDIX D

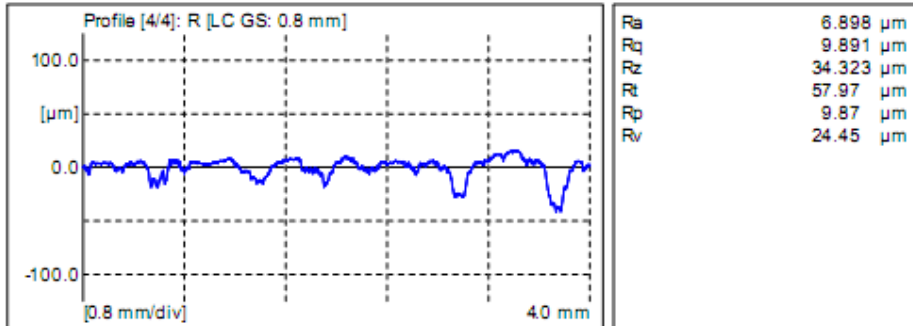
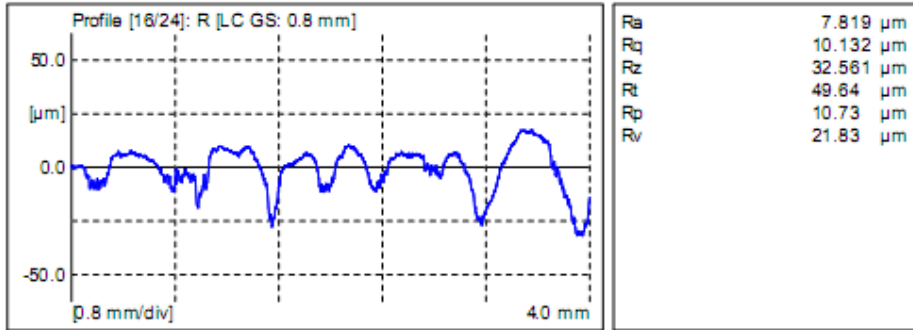
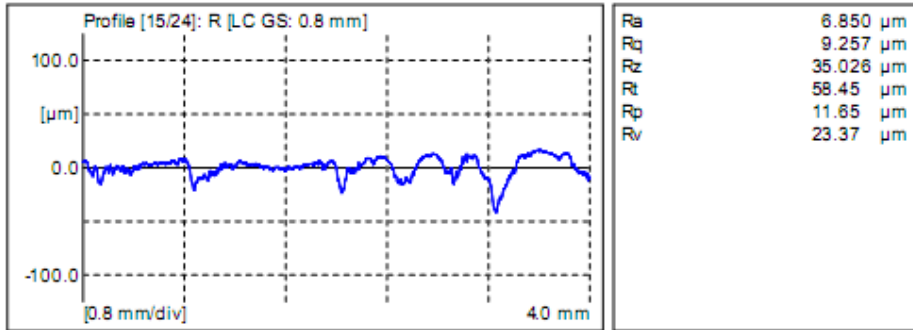


APPENDIX D

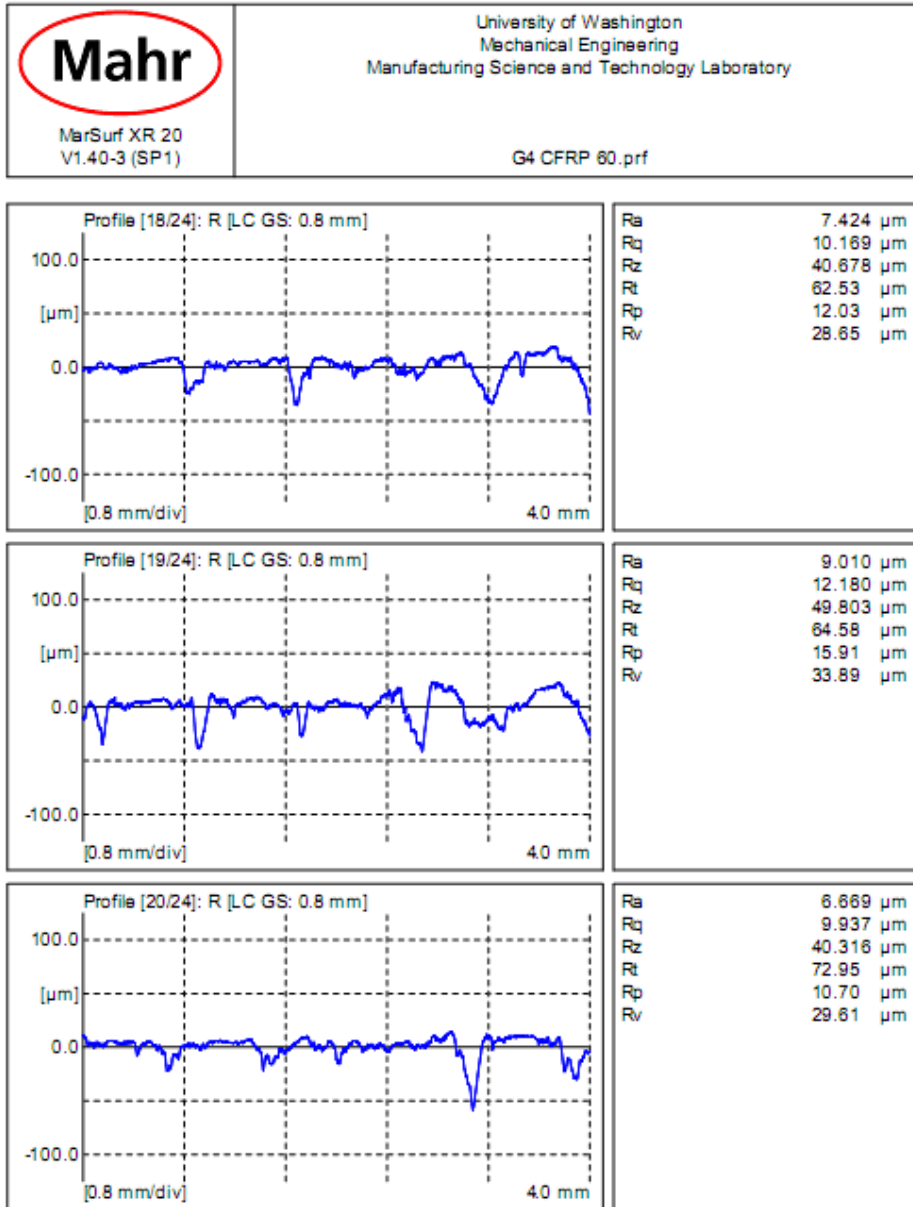


APPENDIX D


 <p>Mahr MarSurf XR 20 V1.40-3 (SP1)</p>	<p>University of Washington Mechanical Engineering Manufacturing Science and Technology Laboratory</p>
	<p>G4 CFRP 60.prf</p>

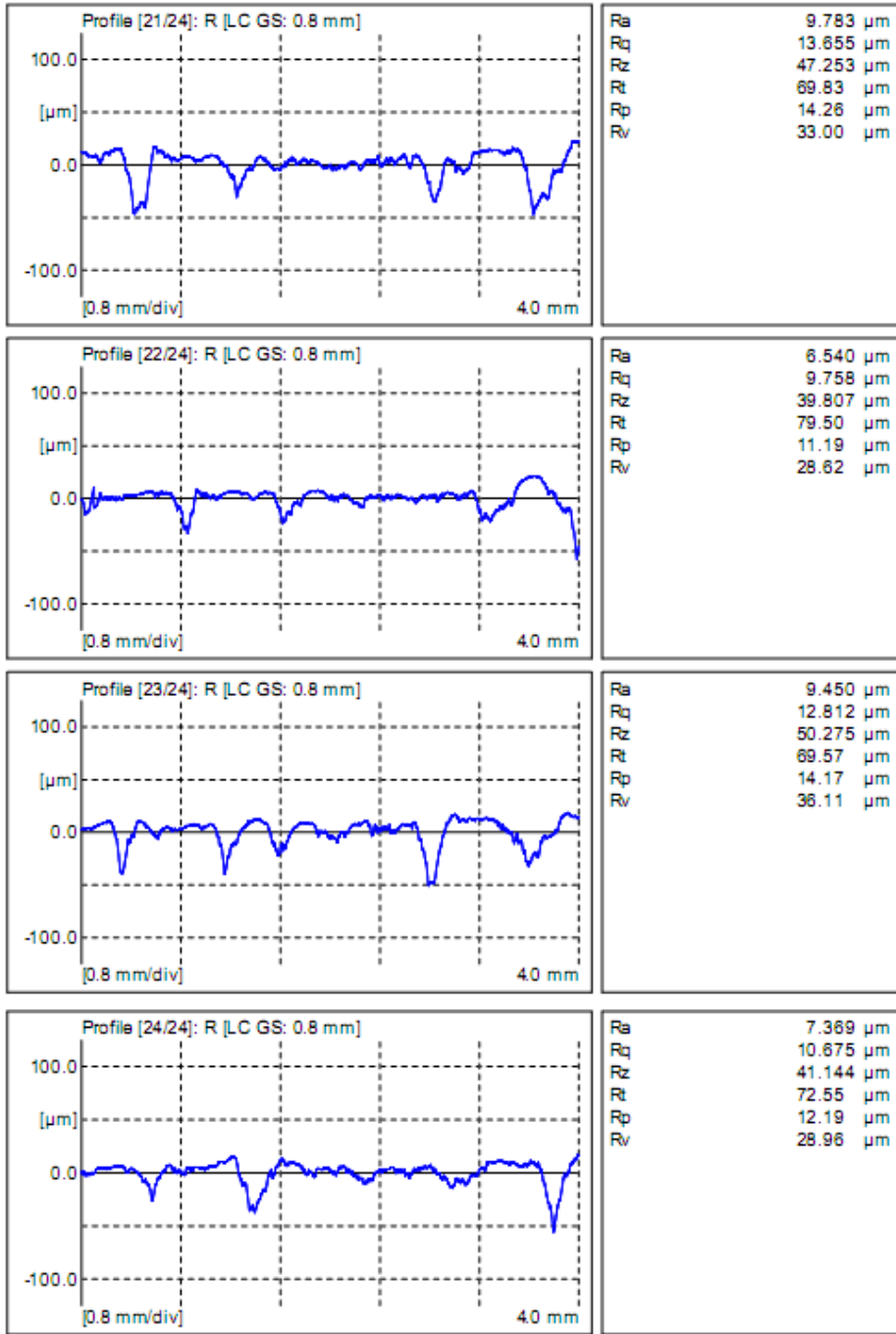


APPENDIX D




APPENDIX D

 <p style="margin: 0;">Mahr</p> <p style="margin: 0; font-size: small;">MarSurf XR 20 V1.40-3 (SP1)</p>	<p style="margin: 0; font-size: small;">University of Washington Mechanical Engineering Manufacturing Science and Technology Laboratory</p> <p style="margin: 0; font-size: small;">G4 CFRP 60.prf</p>
---	--



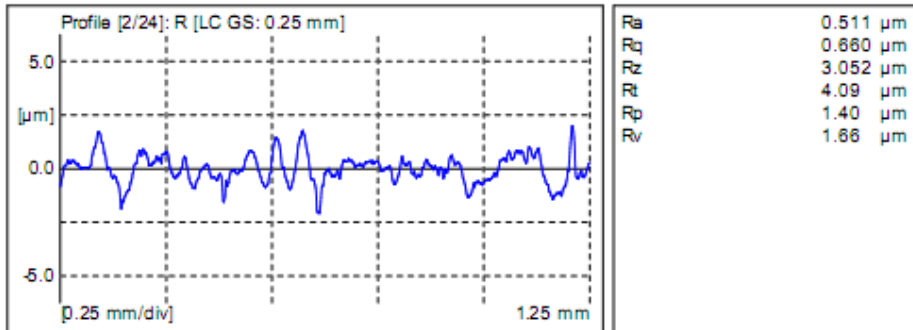
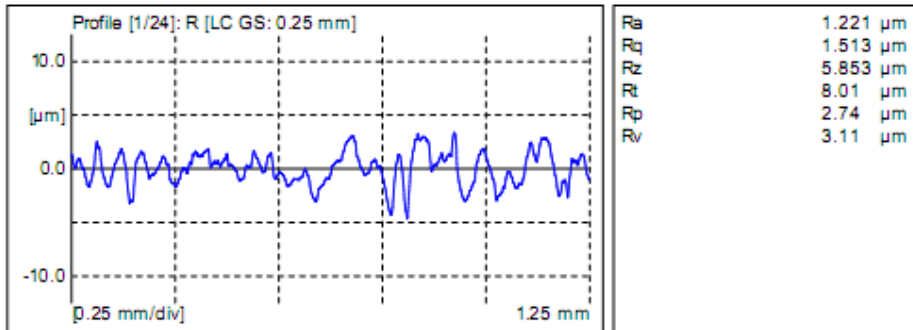
APPENDIX D

CFRP hole surface profiles: PCD low speed Experiment Type II


 MahrSurf XR 20 V1.40-3 (SP1)	University of Washington Mechanical Engineering Manufacturing Science and Technology Laboratory
	20100212-132426.prf

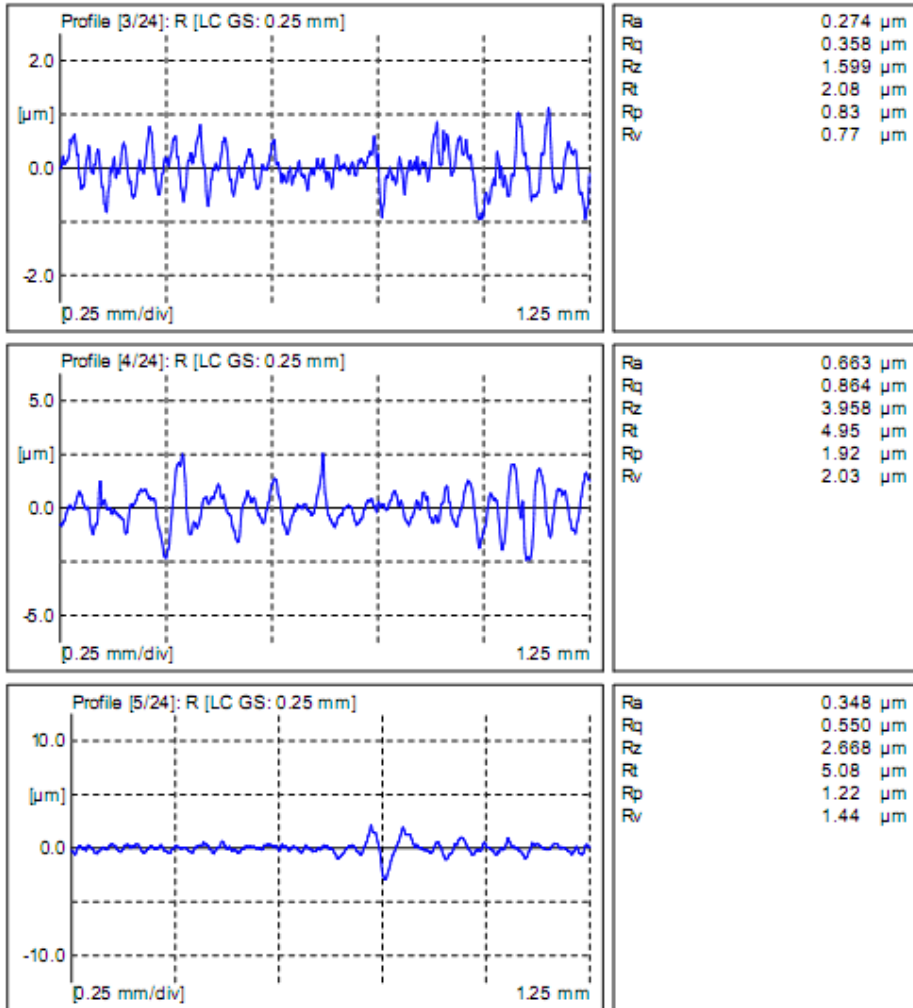
Object:	stack holes
Number:	G4 Ti hole 60
Comment:	

Meas. Instrum.:	Mahr Data Acquisition Board	Lt:	1.75 mm [N=5]
Drive Unit:	GD 25	Ls:	2.5 μm
Pick-up:	MFW-250 [5.9 %]	VB:	$\pm 250 \mu\text{m}$
		Vt:	0.10 mm/s
		Points:	84000 [24]




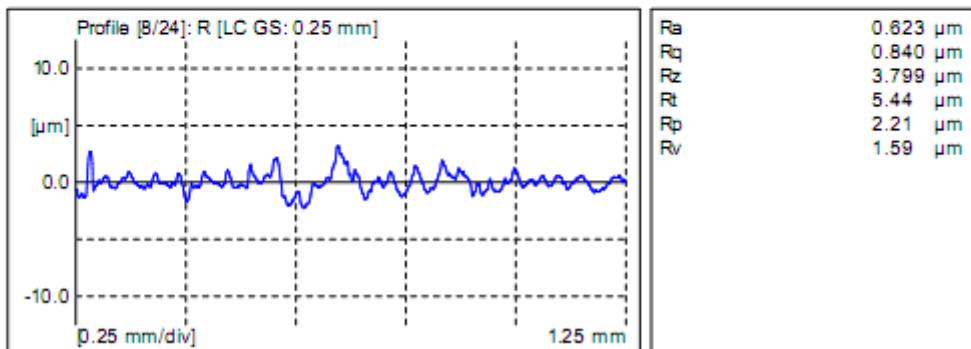
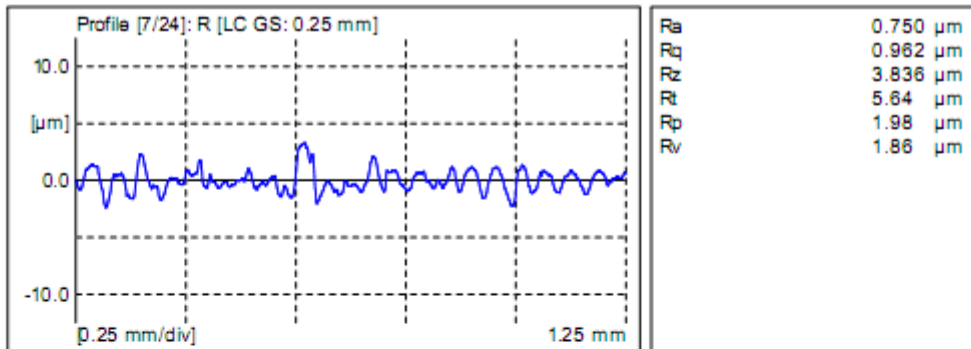
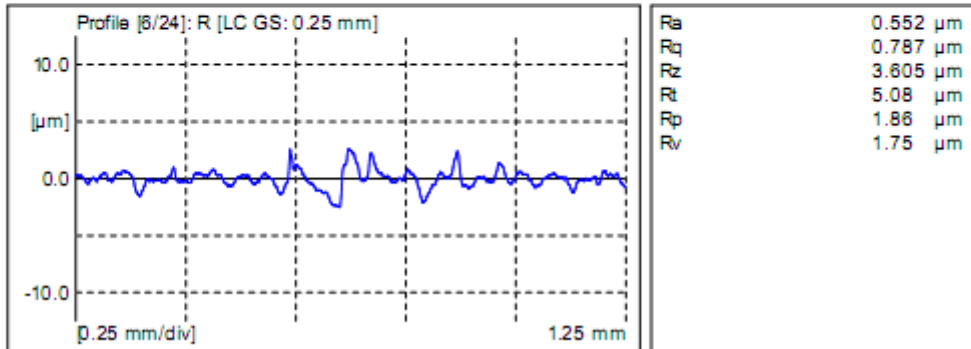
APPENDIX D

 <p>Mahr</p> <p>MarSurf XR 20 V1.40-3 (SP1)</p>	<p>University of Washington Mechanical Engineering Manufacturing Science and Technology Laboratory</p> <p>20100212-132426.prf</p>
---	---




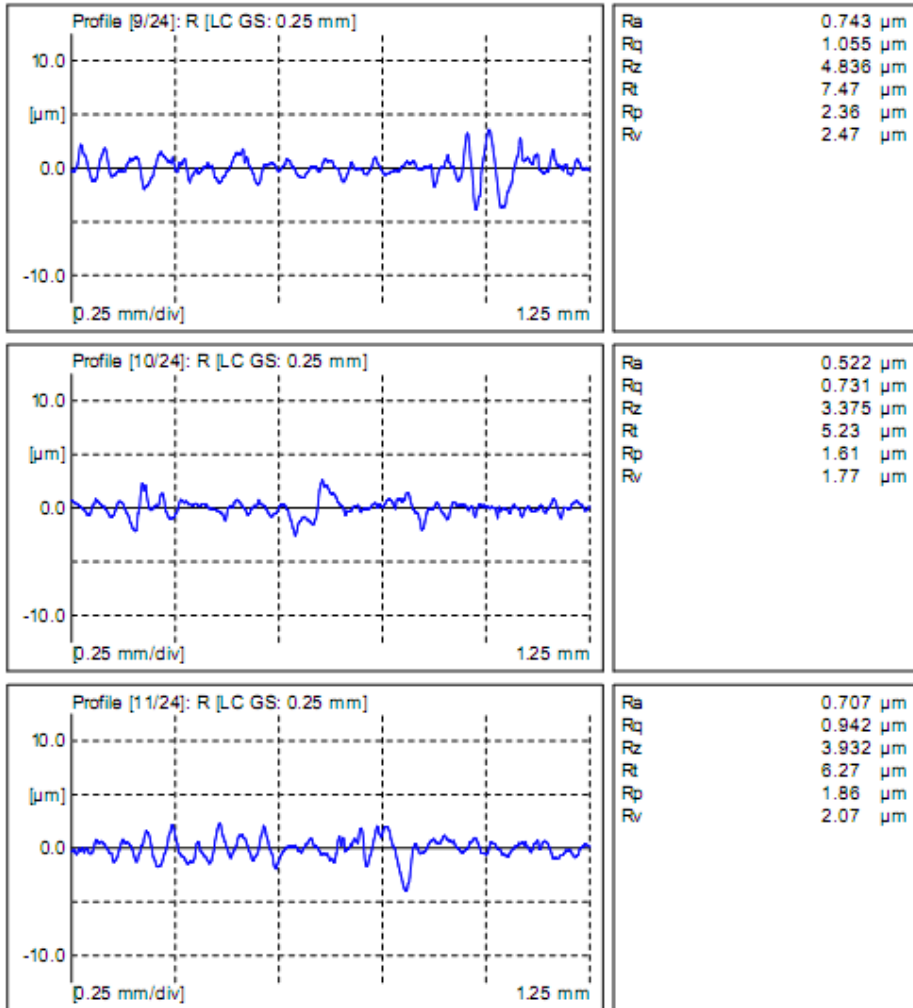
APPENDIX D

 MarSurf XR 20 V1.40-3 (SP1)	University of Washington Mechanical Engineering Manufacturing Science and Technology Laboratory
	20100212-132426.prf




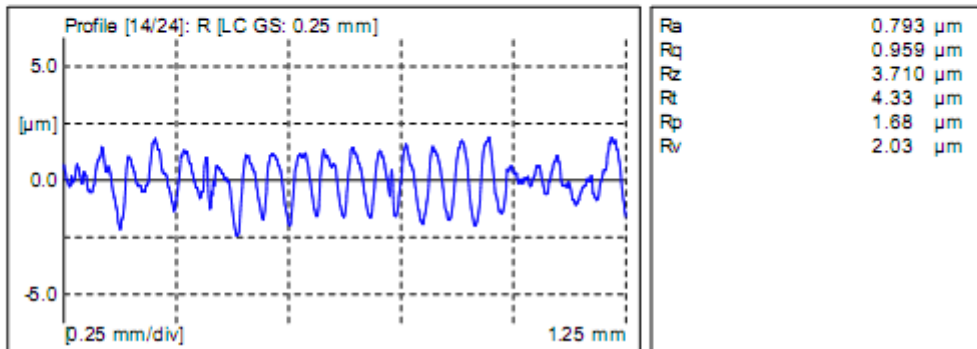
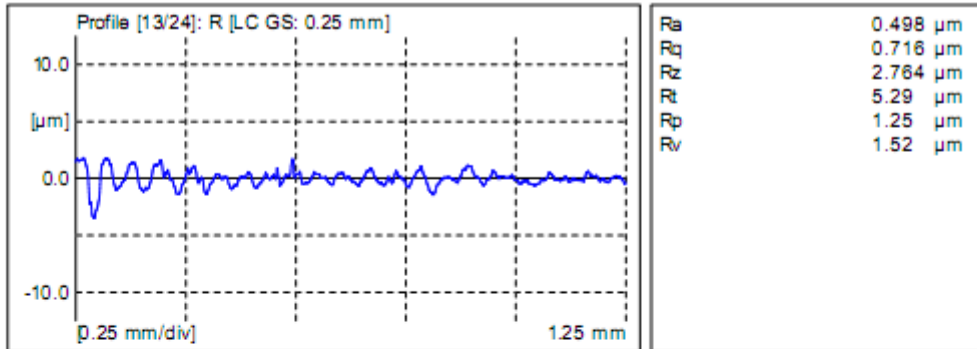
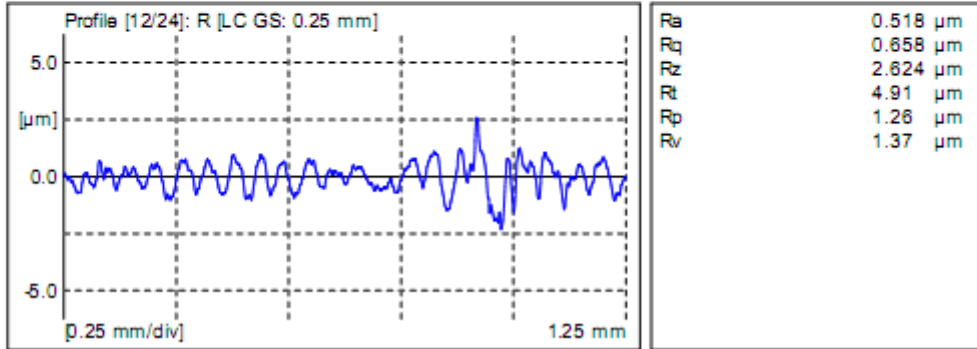
APPENDIX D

 <p>Mahr</p> <p>MarSurf XR 20 V1.40-3 (SP1)</p>	<p>University of Washington Mechanical Engineering Manufacturing Science and Technology Laboratory</p> <p>20100212-132426.prf</p>
---	---




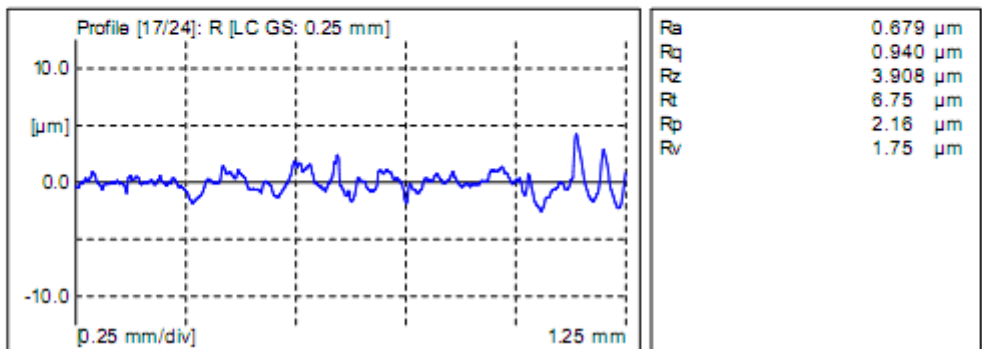
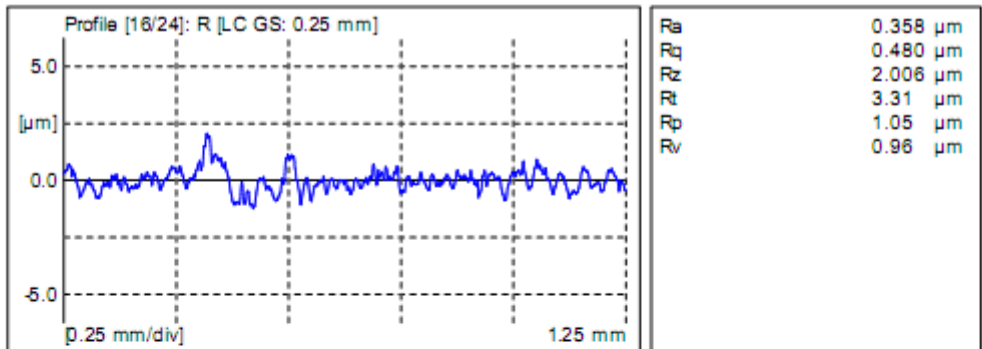
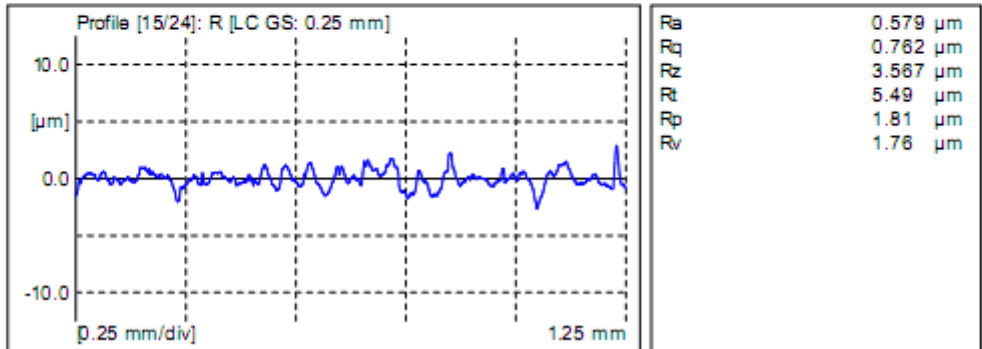
APPENDIX D

 MarSurf XR 20 V1.40-3 (SP1)	University of Washington Mechanical Engineering Manufacturing Science and Technology Laboratory
	20100212-132426.prf




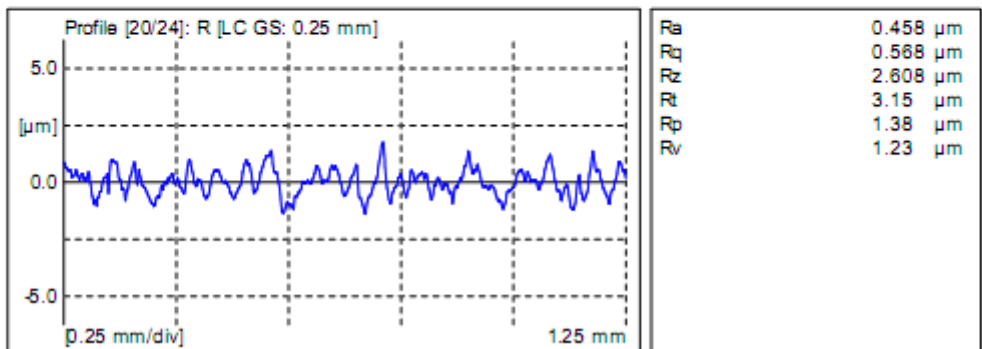
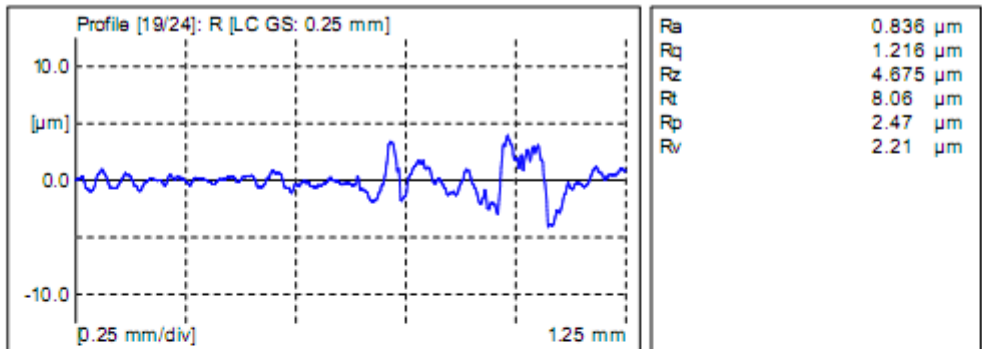
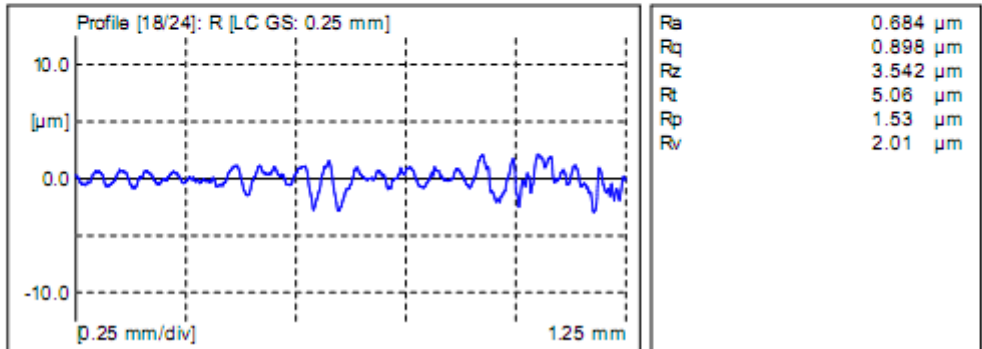
APPENDIX D

 MarSurf XR 20 V1.40-3 (SP1)	University of Washington Mechanical Engineering Manufacturing Science and Technology Laboratory
	20100212-132426.prf



APPENDIX D

 MarSurf XR 20 V1.40-3 (SP1)	University of Washington Mechanical Engineering Manufacturing Science and Technology Laboratory
	20100212-132426.prf



APPENDIX D

